

Electronic Thesis and Dissertation Repository

---

3-11-2011 12:00 AM

## Quantification of Pulmonary Ventilation using Hyperpolarized $^3\text{He}$ Magnetic Resonance Imaging

Lindsay Mathew  
*The University of Western Ontario*

Supervisor  
Dr. Grace Parraga  
*The University of Western Ontario*

Graduate Program in Medical Biophysics  
A thesis submitted in partial fulfillment of the requirements for the degree in Doctor of  
Philosophy  
© Lindsay Mathew 2011

Follow this and additional works at: <https://ir.lib.uwo.ca/etd>



Part of the [Medical Biophysics Commons](#)

---

### Recommended Citation

Mathew, Lindsay, "Quantification of Pulmonary Ventilation using Hyperpolarized  $^3\text{He}$  Magnetic Resonance Imaging" (2011). *Electronic Thesis and Dissertation Repository*. 103.  
<https://ir.lib.uwo.ca/etd/103>

This Dissertation/Thesis is brought to you for free and open access by Scholarship@Western. It has been accepted for inclusion in Electronic Thesis and Dissertation Repository by an authorized administrator of Scholarship@Western. For more information, please contact [wlsadmin@uwo.ca](mailto:wlsadmin@uwo.ca).

**QUANTIFICATION OF PULMONARY VENTILATION USING  
HYPERPOLARIZED  $^3\text{He}$  MAGNETIC RESONANCE IMAGING**

(Spine Title: Quantifying Ventilation using  $^3\text{He}$  MRI)

(Thesis Format: Integrated Article)

By

**Lindsay Mathew**

Graduate Program in Medical Biophysics

Submitted in partial fulfillment  
of the requirements for the degree of  
**Doctor of Philosophy**

The School of Graduate and Postdoctoral Studies  
The University of Western Ontario  
London, Ontario, Canada

© Lindsay Mathew 2011

# Certificate of Examination

## Supervisor

---

Grace Parraga, Ph.D.

## Supervisory Committee

---

Aaron Fenster, Ph.D.

---

George Rodrigues, M.D.

---

Roya Etemad-Rezai, M.D.

## Examiners

---

F. William Hersman, Ph.D.

---

Frank Prato, Ph.D.

---

Edward Yu, M.D.

---

Timothy Scholl, Ph.D.

The thesis by

**Lindsay Mathew**

entitled

Quantification of Pulmonary Ventilation using  
Hyperpolarized  $^3\text{He}$  Magnetic Resonance Imaging

is accepted in partial fulfilment of the  
requirements for the degree of  
Doctor of Philosophy

Date: March 11, 2011

---

Chair of Thesis Examination Board

# Abstract

Smoking-related lung diseases including chronic obstructive pulmonary disease (COPD) and lung cancer are projected to have claimed the lives of more than 30,000 Canadians in 2010. The poor prognosis and lack of new treatment options for lung diseases associated with smoking are largely due to the inadequacy of current techniques for evaluating lung function. Hyperpolarized  $^3\text{He}$  magnetic resonance imaging (MRI) is a relatively new technique, and quantitative measurements derived from these images, specifically the ventilation defect volume (VDV) and ventilation defect percent (VDP) have the potential to provide new sensitive measures of lung function. Here, we evaluate the reproducibility of VDV, and explore the sensitivity of these measurements in healthy young and elderly volunteers, and subjects with smoking-related lung disease (COPD and radiation-induced lung injury (RILI)). Our results show that  $^3\text{He}$  MRI measurements of ventilation have high short-term reproducibility in both healthy volunteers and subjects with COPD. Additionally, we report that these measurements are sensitive to age-related changes in lung function. Finally, in RILI we show that measurements of lung function derived from  $^3\text{He}$  MRI are sensitive to longitudinal changes in lung function following treatment, while in COPD we report that using VDP in conjunction with structural measurements of disease (using the apparent diffusion coefficient (ADC) derived from diffusion-weighted images) may provide a new method for phenotyping this smoking-related lung disease.

**Keywords:** Hyperpolarized  $^3\text{He}$  magnetic resonance imaging, functional lung imaging, ventilation defect, chronic obstructive pulmonary disease, lung cancer, radiation-induced lung injury

# Co-Authorship

The following thesis contains four manuscripts published in scientific journals, one manuscript published in a peer-reviewed conference proceeding and one manuscript submitted for publication. Chapter 2 is an original manuscript entitled, “Hyperpolarized  $^3\text{He}$  Magnetic Resonance Imaging of Chronic Obstructive Pulmonary Disease: Reproducibility at 3.0 Tesla”, and was published in the journal *Academic Radiology* in October 2008. The manuscript was coauthored by Lindsay Mathew, Andrea Evans, Alexei Ouriadov, Roya Etemad-Rezai, Robert Fogel, Giles Santyr, David G. McCormack and Grace Parraga. Chapter 3 is an original manuscript entitled “Hyperpolarized  $^3\text{He}$  Magnetic Resonance Imaging of Ventilation Defects in Healthy Elderly Volunteers: Initial Findings at 3.0T” and was published in the journal *Academic Radiology* in June 2008. The article was co-authored by Grace Parraga, Lindsay Mathew, Roya Etemad-Rezai, David G. McCormack and Giles E. Santyr. Chapter 4, entitled “Hyperpolarized  $^3\text{He}$  magnetic resonance imaging: Preliminary evaluation of phenotyping potential in chronic obstructive pulmonary disease” was published in the *European Journal of Radiology* (Epub ahead of print November 20, 2009). Co-authors on this paper were Lindsay Mathew, Miranda Kirby, Roya Etemad-Rezai, Andrew Wheatley, David G. McCormack and Grace Parraga. Chapter 5, a manuscript published in *Medical Physics* in January 2010, is entitled “Detection of longitudinal lung structural and functional changes after diagnosis of radiation-induced lung injury using hyperpolarized  $^3\text{He}$  magnetic resonance imaging” and was co-authored by Lindsay Mathew, Stewart Gaede, Andrew Wheatley, Roya Etemad-Rezai, George B. Rodrigues and Grace Parraga. Appendix A is an original manuscript published in the *Conference record on the Forty-second Asilomar Conference Signals, Systems and Computers, 2008*, co-authored by Lindsay Mathew, Andrew Wheatley, David G. McCormack and Grace Parraga, and entitled “Hyperpolarized  $^3\text{He}$  Magnetic Resonance Pulmonary Imaging: Image Processing Tools for Clinical Research”. Appendix B is an original case report co-authored by Lindsay Mathew, Miranda Kirby, Donald Farquhar, Christopher Liciskai, Roya Etemad-Rezai, David G. McCormack and Grace Parraga. This manuscript, entitled “Hyperpolarized  $^3\text{He}$  Magnetic Resonance Imaging Biomarkers of Bronchoscopic Airway Bypass in COPD”,

was submitted to the *Journal of Magnetic Resonance Imaging* in November 2010 (submission #JMRI-10-0886).

As the principal author and PhD candidate, Lindsay Mathew contributed to study design, wrote the protocol, UWO Health Sciences Research Ethics Board ethics submission, Health Canada ethics submissions, and London Regional Cancer Program Small Grants for Cancer Research grant to secure funding for ROB0016, entitled 'Predictors of Radiation-induced Lung Injury using Hyperpolarized  $^3\text{He}$  Magnetic Resonance Imaging'. Additionally, L.Mathew oversaw subject study visits, performed data analysis and statistical analysis, led interpretation of results, drafted manuscripts, and revised manuscripts for publication in response to reviews. Miranda Kirby provided assistance with data analysis, designed and wrote software for automated quantification of ventilation images, and contributed editorial assistance for the manuscripts in which she co-authored. Dr. Parraga, as the principal author's supervisor helped to determine the project objectives, provided mentorship, consulted on interpretation of results, provided editorial assistance and overall guidance. Dr. Roya Etemad-Rezai, Dr. David G. McCormack, Dr. Giles Santyr, Dr. Alexei Ouriadov, Dr. Robert Fogel and Dr. Stewart Gaede provided clinical and physics expertise and aided in interpretation of the results for the respective papers that they co-authored. Dr. George B. Rodrigues provided ongoing guidance, was instrumental in setting up the clinical studies and provided clinical expertise in reviewing the results and manuscripts.

Pulmonary function data acquisition was performed by Sandra Halko and Shayna McKay. Hyperpolarization of  $^3\text{He}$  was performed by Andrew Wheatley. MRI acquisition was performed by Cyndi Harper-Little and Trevor Szekeres.

*In Memory of my dad, Bruce Mathew; my inspiration...  
For your unconditional love, support and faith in me.*

# Acknowledgements

First and foremost, I would like to thank my supervisor Dr. Grace Parraga. I am grateful for the guidance, support and encouragement she has provided me over the past five years. Her belief in my abilities, our thought-provoking conversations and her emphasis on productivity have pushed me to excel. She is passionate about her research, which comes across daily in her dedication to her work, her staff and her students, and makes research in her lab exciting. Her mentorship has been invaluable to me during my time in her lab.

I would also like to thank the members of my advisory committee: Dr. Aaron Fenster, Dr. George Rodrigues, Dr. Roya Etemad-Rezai and Prof. Jake Van Dyk. I am most fortunate to have Dr. Fenster on my committee; he is the ultimate role model as a scientist, and his passion for, and dedication to imaging research are truly inspiring. Dr. Rodrigues has provided me new opportunities to pursue a research project in the area of Radiation oncology/biophysics; an area of research that I am passionate about, and has provided me with an unparalleled learning experience during my time at the cancer centre. His mentorship, expertise and guidance have greatly contributed to my research. Dr. Etemad-Rezai has been available to download and take me through countless chest x-rays and CTs. Her time in the lab on Tuesdays provided me with great learning opportunities both in the dark-room and during lab meetings. Her support and guidance during my time in the Parraga lab are most appreciated. Prof. Van Dyk has been an integral member of my advisory committee both during his time in London and during his time at the IAEA. Despite being half-way around the world and involved in a new high-level position, he still took the time to send me all of the latest articles he came across and felt were pertinent to my research.

I would also like to thank the staff of the Parraga lab, and many others at Western whose assistance has been crucial in my research and academic life. Members of the Parraga group have been supportive, knowledgeable and willing to provide assistance to make sure my projects in the lab have been successful. To Andrew Wheatley – thank you for always making sure my computer was running and had everything I needed to do my research, for your intellectual questions and witty comments in lab meeting, and for the



many bags of hyperpolarized  $^3\text{He}$  that always came out precisely on time. Sandra Halko has shared with me her expertise in running clinical studies, writing protocols and ethics submissions and spent countless hours with me looking up clinical data necessary for my clinical studies. I would like to thank both Sandra and Shayna McKay for their help in running study subject visits, for all the pulmonary function tests performed, and for time spent coaching research subjects in the MR. Thanks also to Trevor Szekeres and Cyndi Harper-Little for performing the many  $^3\text{He}$  MRI scans that made this research possible. I would also like to thank Laura Groom and Wendy Hough in Medical Biophysics for all of their hard work behind the scenes.

To my lab mates and friends at Robarts; you've made the last few years fun and enjoyable. I am thankful for the great friendship I've developed with Miranda Kirby, who allowed me to mentor her in her early years, and who now teaches me. Thanks Miranda for the afternoon chai latte breaks, some great memories at some amazing conferences and all the wonderful discussions that got me through the past few years! Thanks too to my other fellow lab mates past and present: Christianne Mallet for the coffee time chats and lunch breaks, Laura Wilson for many good laughs, Hassan Ahmed for his easy going, care-free outlook on life, to Amir Owrangi for the goofy smile he had on every time I walked to my desk and never failing to give me an 'Oh Really?!' just when I needed it, to Steven Choy, Steve Costella and Dan Buchanan for adding some male perspective to the lab group, and Jessica McCallum for the countless hours of company in the dark room.

A very special thank you to my husband, Sanjay, for your love, patience and understanding. Thanks too, to all of my family for all of their love and encouragement. Your support has meant a lot to me.

Finally, I am truly grateful for the financial support I received during my graduate studies that enabled me to completely focus my time and energy on my research. I acknowledge the funding I received from the Vanier Canadian Graduate Scholarship, the CIHR Strategic Training Program in Cancer Research and Technology Transfer, the Ontario Graduate Scholarship and the Schulich Graduate Scholarship.

# Table of Contents

Certificate of Examination.....	ii
Abstract.....	iii
Co-Authorship.....	iv
Acknowledgements.....	vii
Table of Contents.....	ix
List of Appendices.....	xiii
List of Tables.....	xiv
List of Figures.....	xv
List of Abbreviations.....	xvii
<b>CHAPTER 1: INTRODUCTION.....</b>	<b>1</b>
<b>1.1 Overview and Motivation.....</b>	<b>1</b>
<b>1.2 Lung Function: Delivery and Exchange of O<sub>2</sub> .....</b>	<b>2</b>
<b>1.3 Established Tests of Lung Function .....</b>	<b>3</b>
1.3.1 Pulmonary Function Tests .....	4
1.3.2 Clinical Measurements of Breathlessness.....	6
1.3.3 Inflammatory Markers .....	7
1.3.4 Other Tests .....	7
<b>1.4 Functional Decline of the Lung.....</b>	<b>8</b>
1.4.1 The Aging Lung: Normal Functional Decline .....	8
1.4.2 Chronic Obstructive Pulmonary Disease: Accelerated Functional Decline .	11
1.4.3 Lung Cancer.....	14
1.4.4 Radiation-induced lung injury .....	16
<b>1.5 Imaging Measurements of Lung Function .....</b>	<b>18</b>
1.5.1 Chest x-ray .....	19
1.5.2 X-ray Computed Tomography .....	21
1.5.3 Nuclear Medicine Methods.....	24
1.5.4 Magnetic Resonance Imaging.....	27
<b>1.6 Hyperpolarized Noble Gas MRI.....</b>	<b>29</b>
1.6.1 Development and Theory.....	29
1.6.2 Hyperpolarized <sup>3</sup> He MRI: Research Subject Studies.....	32
<b>1.7 Thesis Hypothesis and Objectives .....</b>	<b>34</b>
<b>1.8 References .....</b>	<b>36</b>

**CHAPTER 2: HYPERPOLARIZED <sup>3</sup>HE MAGNETIC RESONANCE IMAGING OF CHRONIC OBSTRUCTIVE PULMONARY DISEASE: REPRODUCIBILITY AT 3.0 TESLA..... 54**

**2.1 Introduction..... 54**

**2.2 Materials and Methods..... 56**

    2.2.1 Study Subjects..... 56

    2.2.2 Study Assessments..... 56

    2.2.3 Safety Monitoring and Hyperpolarized <sup>3</sup>He Administration ..... 57

    2.2.4 Imaging ..... 57

    2.2.5 Image Analysis..... 58

    2.2.6 Statistical Methods..... 59

**2.3 Results ..... 60**

    2.3.1 Study Subjects..... 60

    2.3.2 <sup>3</sup>He MRI Measurements..... 63

    2.3.3 <sup>3</sup>He Measurement Reproducibility..... 66

**2.4 Discussion..... 70**

**2.5 Conclusion ..... 75**

**2.6 References ..... 76**

**CHAPTER 3: HYPERPOLARIZED <sup>3</sup>HE MAGNETIC RESONANCE IMAGING OF VENTILATION DEFECTS IN HEALTHY ELDERLY VOLUNTEERS: INITIAL FINDINGS AT 3.0 TESLA ..... 79**

**3.1 Introduction..... 79**

**3.2 Methods..... 80**

    3.2.1 Study Population..... 80

    3.2.2 Spirometry..... 80

    3.2.3 Magnetic Resonance Imaging..... 80

    3.2.4 Image Analysis..... 81

**3.3 Results ..... 84**

    3.3.1 Study Subjects..... 84

    3.3.2 Ventilation Defects and Ventilation Defect Volume ..... 85

    3.3.3 Ventilation Defect Volume Interscan and Inter-observer Reproducibility... 86

**3.4 Discussion..... 89**

**3.5 Conclusion ..... 93**

**3.6 References ..... 94**

**CHAPTER 4: HYPERPOLARIZED <sup>3</sup>HE MAGNETIC RESONANCE IMAGING:  
PRELIMINARY EVALUATION OF PHENOTYPING POTENTIAL IN  
CHRONIC OBSTRUCTIVE PULMONARY DISEASE ..... 97**

<b>4.1</b>	<b>Introduction.....</b>	<b>97</b>
<b>4.2</b>	<b>Methods.....</b>	<b>99</b>
4.2.1	Subjects.....	99
4.2.2	Pulmonary Function Tests.....	99
4.2.3	Safety Monitoring and Hyperpolarized <sup>3</sup> He Administration.....	99
4.2.4	Imaging.....	100
4.2.5	Image Analysis.....	101
4.2.6	Statistical Methods.....	103
<b>4.3</b>	<b>Results.....</b>	<b>104</b>
4.3.1	Study Subjects.....	104
4.3.2	<sup>3</sup> He MRI Measurements.....	105
<b>4.4</b>	<b>Discussion.....</b>	<b>110</b>
<b>4.5</b>	<b>Conclusion.....</b>	<b>112</b>
<b>4.6</b>	<b>References.....</b>	<b>113</b>

**CHAPTER 5: DETECTION OF LONGITUDINAL STRUCTURAL AND  
FUNCTIONAL CHANGES AFTER DIAGNOSIS OF RADIATION-INDUCED  
LUNG INJURY USING HYPERPOLARIZED <sup>3</sup>HE MAGNETIC RESONANCE  
IMAGING..... 117**

<b>5.1</b>	<b>Introduction.....</b>	<b>117</b>
<b>5.2</b>	<b>Methods.....</b>	<b>118</b>
5.2.1	Study Subjects.....	118
5.2.2	Study Evaluations.....	118
5.2.3	Imaging.....	119
5.2.4	Image Analysis.....	120
5.2.5	<sup>3</sup> He – <sup>1</sup> H Image Registration.....	121
5.2.6	Statistical Analysis.....	121
<b>5.3</b>	<b>Results.....</b>	<b>122</b>
5.3.1	Study Subjects.....	122
5.3.2	<sup>3</sup> He MRI.....	124
5.3.3	Correlations.....	125
5.3.4	Image Registration.....	129
<b>5.4</b>	<b>Discussion.....</b>	<b>130</b>
<b>5.5</b>	<b>Conclusion.....</b>	<b>133</b>

<b>5.6</b>	<b>References .....</b>	<b>135</b>
<b>CHAPTER 6: CONCLUSIONS AND FUTURE DIRECTIONS.....</b>		<b>140</b>
<b>6.1</b>	<b>Overview and Summary .....</b>	<b>140</b>
<b>6.2</b>	<b>Summary of Conclusions.....</b>	<b>144</b>
<b>6.3</b>	<b>Limitations of Current Tools and Solutions.....</b>	<b>145</b>
6.3.1	Study Specific Limitations.....	145
6.3.2	General Limitations .....	148
<b>6.4</b>	<b>Roadmap for Future Studies.....</b>	<b>151</b>
6.4.1	Quantification of Lung Disease in Patients Diagnosed with Non-Resectable Lung Cancer using Hyperpolarized $^3\text{He}$ MRI.....	151
6.4.2	Ventilation Defect Etiology .....	154
6.4.3	Hyperpolarized Noble Gas MRI Phenotypes of COPD.....	155
6.4.4	Hyperpolarized $^{129}\text{Xe}$ MRI: Ventilation Defects in Health and Disease ....	156
<b>6.5</b>	<b>Impact and Significance .....</b>	<b>157</b>
<b>6.6</b>	<b>References .....</b>	<b>158</b>

# List of Appendices

<b>APPENDIX – A: HYPERPOLARIZED <sup>3</sup>HE MAGNETIC RESONANCE PULMONARY IMAGING: IMAGE PROCESSING TOOLS FOR CLINICAL RESEARCH .....</b>	<b>161</b>
<b>A.1 Introduction.....</b>	<b>161</b>
<b>A.2 Methods.....</b>	<b>164</b>
<b>A.3 Results .....</b>	<b>165</b>
A.3.1 Image Visualization .....	165
A.3.2 Image Registration .....	165
A.3.3 Signal Normalization .....	166
A.3.4 Image Subtraction .....	166
<b>A.4 Conclusion .....</b>	<b>167</b>
<b>A.5 References .....</b>	<b>169</b>
<b>APPENDIX – B: HYPERPOLARIZED <sup>3</sup>HE MAGNETIC RESONANCE IMAGING BIOMARKERS OF BRONCHOSCOPIC AIRWAY BYPASS IN COPD .....</b>	<b>171</b>
<b>B.1 Introduction.....</b>	<b>171</b>
<b>B.2 Case Report .....</b>	<b>171</b>
<b>B.3 Discussion.....</b>	<b>175</b>
<b>B.4 References .....</b>	<b>177</b>
<b>APPENDIX – C: PERMISSIONS FOR REPRODUCTION OF SCIENTIFIC ARTICLES .....</b>	<b>179</b>
<b>APPENDIX – D: HEALTH SCIENCE RESEARCH ETHICS BOARD APPROVAL NOTICES.....</b>	<b>185</b>
<b>CURRICULUM VITAE.....</b>	<b>187</b>

# List of Tables

## Chapter 2:

Table 2-1: Subject Demographics.....	62
Table 2-2: Same day and 7-day Rescan ADC and VDV Measurements.....	64
Table 2-3: Scan-Rescan Reproducibility. ....	67
Table 2-4: $^3\text{He}$ ADC and VDV Sample Size Calculations. ....	70

## Chapter 3:

Table 3-1: Study Subject Demographic Characteristics. ....	84
Table 3-2: Ventilation Defects in Healthy Elderly Volunteers.....	85
Table 3-3: Elderly Volunteer Ventilation Defect Volume Inter-observer Reproducibility. .....	87

## Chapter 4:

Table 4-1: Subject Demographics.....	104
Table 4-2: Whole Lung $^3\text{He}$ MRI ADC and Ventilation Measurements.....	106
Table 4-3: Whole lung $^3\text{He}$ MRI Correlations with Pulmonary Function. ....	107
Table 4-4: Center slice $^3\text{He}$ Measurement Contributions by Subject. ....	108

## Chapter 5:

Table 5-1: Subject Demographics.....	123
Table 5-2: Radiation Parameters.....	124
Table 5-3: $^3\text{He}$ MRI ADC and Ventilation Measurements. ....	127
Table 5-4: Longitudinal Differences.....	127

## Appendix B:

Table B-1: Pulmonary function test and $^3\text{He}$ MRI results pre- and post-AB. ....	173
---	-----

# List of Figures

## Chapter 1:

Figure 1-1: Lung Function.....	3
Figure 1-2: Pulmonary Function Testing.....	5
Figure 1-3: Normal Decline in Pulmonary Function with Age.....	10
Figure 1-4: COPD Pathology and Decline in Lung Function.....	13
Figure 1-5: Canadian Incidence and Mortality in Cancer for 2010.....	14
Figure 1-6: Stages of Radiation-induced lung injury.....	17
Figure 1-7: Chest x-ray of healthy volunteer, COPD and lung cancer.....	20
Figure 1-8: CT of Smoking-related lung disease.....	23
Figure 1-9: Proton MRI of the Lung.....	28
Figure 1-10: Hyperpolarized $^3\text{He}$ MRI in Health, COPD, Lung Cancer and RILI.....	33

## Chapter 2:

Figure 2-1: $^3\text{He}$ Apparent Diffusion Coefficient Maps and centre slice ADC results.....	61
Figure 2-2: $^3\text{He}$ MR Ventilation Images and Ventilation Defect Volume (VDV) Results. .....	65
Figure 2-3: Center Slice ADC and VDV Reproducibility.....	68
Figure 2-4: Center Slice $^3\text{He}$ VDV Reproducibility.....	69

## Chapter 3:

Figure 3-1: Hyperpolarized $^3\text{He}$ Magnetic Resonance Imaging Ventilation Defect Volume Segmentation Approach.....	83
Figure 3-2: Elderly Healthy Volunteers $^3\text{He}$ Magnetic Resonance Imaging.....	86
Figure 3-3: Middle-aged Healthy Volunteers $^3\text{He}$ Magnetic Resonance Imaging.....	87
Figure 3-4: Reproducibility of $^3\text{He}$ Ventilation in Healthy and Middle-aged Healthy Volunteers.....	88

## Chapter 4:

Figure 4-1: Schematic for $^3\text{He}$ MRI Ventilation Analysis.....	103
Figure 4-2: Linear Regression.....	105
Figure 4-3: $^3\text{He}$ MRI VDP and ADC% Contributions in COPD.....	107
Figure 4-4: $^3\text{He}$ MRI Classification by Thresholding.....	108
Figure 4-5: $^3\text{He}$ VDP and ADC Dominance.....	109

## Chapter 5:

Figure 5-1: Representative Baseline and Follow-up Hyperpolarized $^3\text{He}$ Ventilation Images, ADC Maps and ADC Histograms.....	123
Figure 5-2: Baseline and Follow-up Hyperpolarized $^3\text{He}$ MRI Measurements.....	125
Figure 5-3: Mean Longitudinal Differences in $^3\text{He}$ MRI and spirometry measurements. .....	126
Figure 5-4: $^3\text{He}$ MRI longitudinal changes compared to Radiation Parameters.....	128
Figure 5-5: Representative subjects showing $^3\text{He}$ – $^1\text{H}$ MR Image Registration.....	129



**Chapter 6:**

Figure 6-1: Representative  $^3\text{He}$  VDP dominant subjects ..... 153  
Figure 6-2: Representative  $^3\text{He}$  mixed subjects ..... 153

**Appendix A:**

Figure A-1: Clinical Hyperpolarized  $^3\text{He}$  Magnetic Resonance Imaging ..... 163  
Figure A-2: Ventilation Defect scoring of  $^3\text{He}$  MRI. .... 164  
Figure A-3: Ventilation Defect Evaluation: Estimation by Consensus. .... 165  
Figure A-4: Image Processing for a Subject with Stage III COPD. .... 168  
Figure A-5: Image Processing for a Subject with Radiation-induced lung injury..... 168

**Appendix B:**

Figure B-1:  $^3\text{He}$  MRI registered to  $^1\text{H}$  MRI Prior to Airway Bypass. .... 174  
Figure B-2:  $^3\text{He}$  MRI registered to  $^1\text{H}$  MRI Following Airway Bypass..... 175

# List of Abbreviations

2D	Two-dimensional
$^3\text{He}$	Helium-3
6MWD	Six minute walk distance
$^{99\text{m}}\text{Tc}$	Technetium-99m
$^{129}\text{Xe}$	Xenon-129
AB	Airway bypass
ADC	Apparent diffusion coefficient
ANOVA	Analysis of variance
ATS	American Thoracic Society
BAL	Bronchoalveolar lavage
BMI	Body mass index
BODE	<u>B</u> MI, <u>a</u> irflow <u>o</u> bstruction, <u>d</u> ypnea, <u>e</u> xercise capacity
BOLD	Burden of obstructive lung disease
BW	Bandwidth
CE	Centrilobular emphysema
COPD	Chronic obstructive lung disease
CPET	Cardiopulmonary exercise testing
CT	Computed tomography
COV	Coefficient of variation
$\text{DL}_{\text{CO}}$	Diffusing capacity of carbon monoxide
DWI	Diffusion-weighted imaging
ERV	Expiratory reserve volume
FDG	Fluorodeoxyglucose
$\text{FEV}_1$	Forced expiratory volume in one second
FGRE	Fast gradient recalled echo
FOV	Field of view
FRC	Functional residual capacity
FVC	Forced vital capacity
GEHC	General Electric Health Care
GOLD	Global initiative for obstructive lung disease
HIPAA	Health insurance portability and accountability act
HRCT	High resolution computed tomography
HU	Hounsfield units
IC	Inspiratory capacity
MAA	Macro-aggregated albumin
MLD	Mean lung dose
mMRC	modified Medical Research Council
MRI	Magnetic resonance imaging
NLST	National Lung Screening Trial
NSCLC	Non-small cell lung cancer
PET	Positron emission tomography
PFT	Pulmonary function test

PIPEDA	Personal information protection and electronic documents act
PTV	Planning target volume
PVV	Percent ventilated volume
RF	Radiofrequency
RILI	Radiation-induced lung injury
RV	Residual volume
SCLC	Small cell lung cancer
SGRQ	St. George's Respiratory Questionnaire
SNR	Signal-to-noise ratio
SPECT	Single photon emission computed tomography
SpO <sub>2</sub>	Oxygen saturation on pulse oximetry
T <sub>1</sub>	Longitudinal relaxation
TCV	Thoracic cavity volume
TE	Echo time
TLC	Total lung capacity
TNM	Tumour, node, metastasis
TR	Repetition time
TV	Tidal volume
VC	Vital capacity
VDP	Ventilation defect percent
VDS	Ventilation defects score
VDV	Ventilation defect volume
VV	Ventilation volume
WHO	World Health Organization
% <sub>pred</sub>	Percent of predicted value

# CHAPTER 1: INTRODUCTION

## 1.1 Overview and Motivation

More than 30,000 Canadians are projected to have died from smoking-related lung diseases in 2010<sup>1,2</sup>, which include both chronic obstructive pulmonary disease (COPD) and lung cancer. The staggering mortality rate for lung diseases that can be attributed to smoking continues to rise<sup>3</sup>, while current treatments remain largely unsuccessful and potential new treatments fail in clinical trials.<sup>4-7</sup> Currently, symptom management is the only available treatment option for COPD aside from smoking cessation<sup>3,8</sup>, while current treatments for lung cancer have a dismal 10-15% survival rate.<sup>9</sup> Moreover, radiation treatment for lung cancer causes further damage to the lung in more than 30% of patients, a condition known as radiation-induced lung injury (RILI).<sup>10-12</sup> These dismal mortality statistics and the lack of new treatment options are likely a consequence of the fundamental inadequacy of the current tools used to monitor and evaluate lung function. Spirometry is the current gold standard for measuring lung function and is also used as an intermediate endpoint for evaluation of new therapies in clinical trials, despite evidence that its measurements do not correlate well with patient outcomes.<sup>13</sup> Established measurements of lung function provide only global measures of largely regional diseases, cannot differentiate between true functional impairment and various underlying structural pathologies, and are largely insensitive to early disease-related changes, disease progression and response to therapy.<sup>14-16</sup> Thus, there is an urgent need for new tools that can provide sensitive measures of lung function, probing regional lung function independent of underlying pathology. Imaging tools have the potential to play a key role in the development of new sensitive measurements of lung function, though they are not yet fully developed.

This thesis focuses on the development and application of novel quantitative measurements of lung function derived from hyperpolarized helium-3 (<sup>3</sup>He) magnetic resonance imaging (MRI), and evaluates <sup>3</sup>He MRI measurements of lung function in healthy volunteers and subjects with smoking-related lung disease (COPD, lung cancer and RILI). In order to validate new metrics aimed at quantifying lung function the sensitivity and reproducibility of these measurements must first: 1) be characterized in

healthy individuals across a variety of ages, and, 2) be evaluated in the context of currently available tools. Finally, these measurements can then be extended to evaluate lung function in the context of COPD, lung cancer and RILI. To provide a foundation for these concepts, Chapter 1 addresses the current understanding of lung function in healthy young and elderly individuals. This chapter reviews the literature related to COPD, lung cancer and RILI, outlines the current tools and imaging methods for evaluating lung function, and describes hyperpolarized  $^3\text{He}$  MRI. Finally, an overview of the hypotheses tested in this thesis related to a novel metric for evaluating lung function in young and elderly healthy volunteers, as well COPD, lung cancer and RILI, derived from hyperpolarized  $^3\text{He}$  MRI are described.

## **1.2 Lung Function: Delivery and Exchange of $\text{O}_2$**

On average, a person takes a breath once every five seconds, breathing more than 8,600 L of air per day.<sup>17</sup> The act of breathing continually introduces oxygen into the body and expels carbon dioxide from the body. Thus, the continuous function of the respiratory system, which is responsible for breathing, is vital for human life. The respiratory system can be divided into two parts; the lung, the site of gas exchange, and the ventilatory pump, comprised of the components that facilitate breathing including the chest wall, diaphragm, inspiratory and expiratory muscles, the respiratory centres in the brain stem, and the neural connections between the brain and respiratory muscles.<sup>18</sup> The ventilatory pump works by a mechanical process to expand the lung, whereby the muscles of the thorax and abdomen work together under the control of the brain.<sup>19</sup> In order to increase the volume of the lungs the respiratory muscles must produce a pressure great enough to overcome the natural tendencies of the lung and chest wall to recoil.<sup>19</sup> When this pressure is achieved the lung expands, and the increase in lung volume creates a negative pressure within the lung relative to atmospheric pressure, resulting in an influx of air from the environment (Figure 1-1). Within the lung, air flows through many generations of airways, finally reaching alveoli; the site of gas exchange, where passive diffusion of oxygen and carbon dioxide across the blood-gas barrier occurs. The constant, synchronous functioning of the ventilatory pump and the lungs allows for gas delivery and gas exchange to occur.

The lung, as the site of gas exchange, has a unique structural design that maximizes its overall functional capacity. Normal lung function requires ventilation of the more than 300 million alveoli.<sup>20</sup> The architecture necessary for gas delivery and homogenous ventilation throughout the lungs is provided by over 2400 km of large and small airways, with more than 20 generations of dichotomous branching as shown in Figure 1-1.<sup>20</sup> Designed to maximize function, the dichotomous branching structure of the large airways, from the trachea to the terminal bronchioles, and small airways (<2mm in diameter) rapidly expand the total cross-sectional area of the airways, thereby providing a low-resistance path for airflow.<sup>20-22</sup> In total, the airway tree takes up a mere 3% of the total lung volume, minimizing the anatomic dead space in the lungs, and maximizing the volume available for gas exchange.<sup>23</sup>

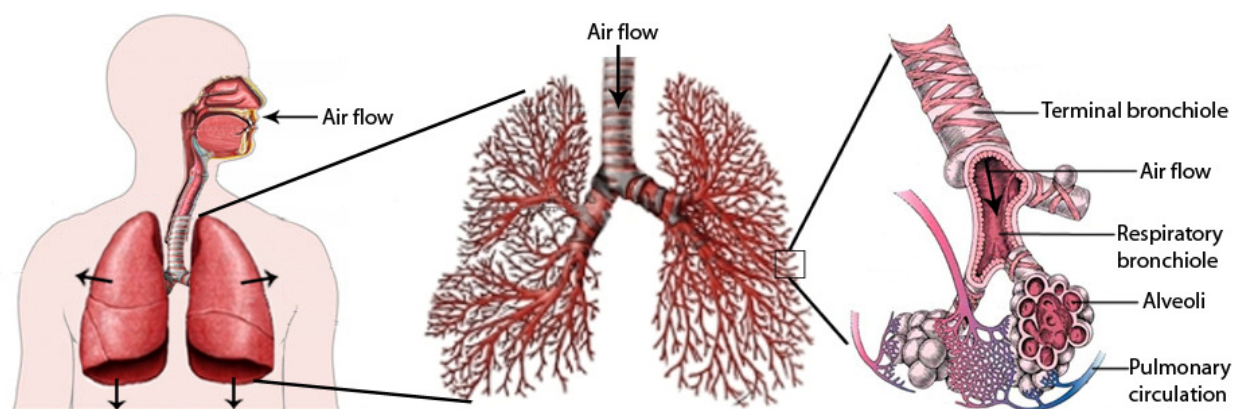


**Figure 1-1: Lung Function.**

In the young healthy adult lung, expansion of the lungs results in airflow through approximately 2400 km of large and small airways. The airways provide a pathway for ventilation of more than 300 million alveoli, where gas exchange across the blood-gas barrier occurs.

### 1.3 Established Tests of Lung Function

There are an array of methods for evaluating lung function; some are commonly used in the clinic, while others are more often performed in research studies as primary or secondary outcome measures. Methods for evaluating lung function include quantitative tests such as spirometry, plethysmography and diffusing capacity of carbon monoxide (DL<sub>CO</sub>), and qualitative tests such as the modified Medical Research Council (mMRC)

dyspnea scale. Despite the fact that these tests are either subjective or highly effort dependent, they are for the most part inexpensive and readily accessible making them ideal tools for clinical use. The various measurements of lung function that can be derived from these tests are described here.

### 1.3.1 Pulmonary Function Tests

Pulmonary function tests (PFT) directly measure overall lung function using three different sets of coached breathing maneuvers, which allow for the evaluation of, 1) dynamic flow rates, 2) static lung volumes, and 3) gas exchange. Spirometry, which measures flow rates using a spirometer (Figure 1-2A), is regarded as the gold standard for measuring lung function. Spirometry captures two specific measurements; the forced expiratory volume in one second ( $FEV_1$ ), the maximal volume of air that can be forcefully expired from the lungs in one second and the forced vital capacity (FVC), the total volume of air that can be forcefully expired from the lungs, as shown in Figure 1-2B. Static lung volumes can be measured using plethysmography (Figure 1-2C), which requires an individual to perform a series of breathing maneuvers in a closed system where pressure changes are measured, followed by the application of Boyle's Law to compute lung volumes. Lung volumes that can be measured are shown in Figure 1-2D, and include total lung capacity (TLC), the total volume of gas in the lungs following maximum inspiration; functional residual capacity (FRC), the lung volume at the end of normal expiration; inspiratory capacity (IC), the volume inspired from FRC; tidal volume (TV), the volume of gas inhaled and exhaled as during normal respiration; residual volume (RV), the volume of gas remaining in the lungs following maximum expiration; expiratory reserve volume (ERV), the volume of gas remaining in the lungs at the end of normal expiration that could be expired on maximum effort; and, vital capacity (VC), the maximum volume of gas inspired from RV. Both flow rates and lung volumes measured are commonly expressed as a percent predicted ( $\%_{pred}$ ) value that depends on age, height, gender and ethnicity.<sup>3,24</sup> Finally, diffusion of gases across the alveolar membrane can also be measured using  $DL_{CO}$ .  $DL_{CO}$  is measured during a breath-hold technique, whereby alveolar volume and alveolar concentrations of carbon monoxide are derived from measurements of the concentration of tracer gas in the inhaled and exhaled air and

the carbon monoxide concentration in the inspired gas.<sup>25</sup> Closing capacity is the lung volume at which the small airways in the dependent part of the lung close, and can be measured using a single-breath nitrogen wash-out test.<sup>29</sup>

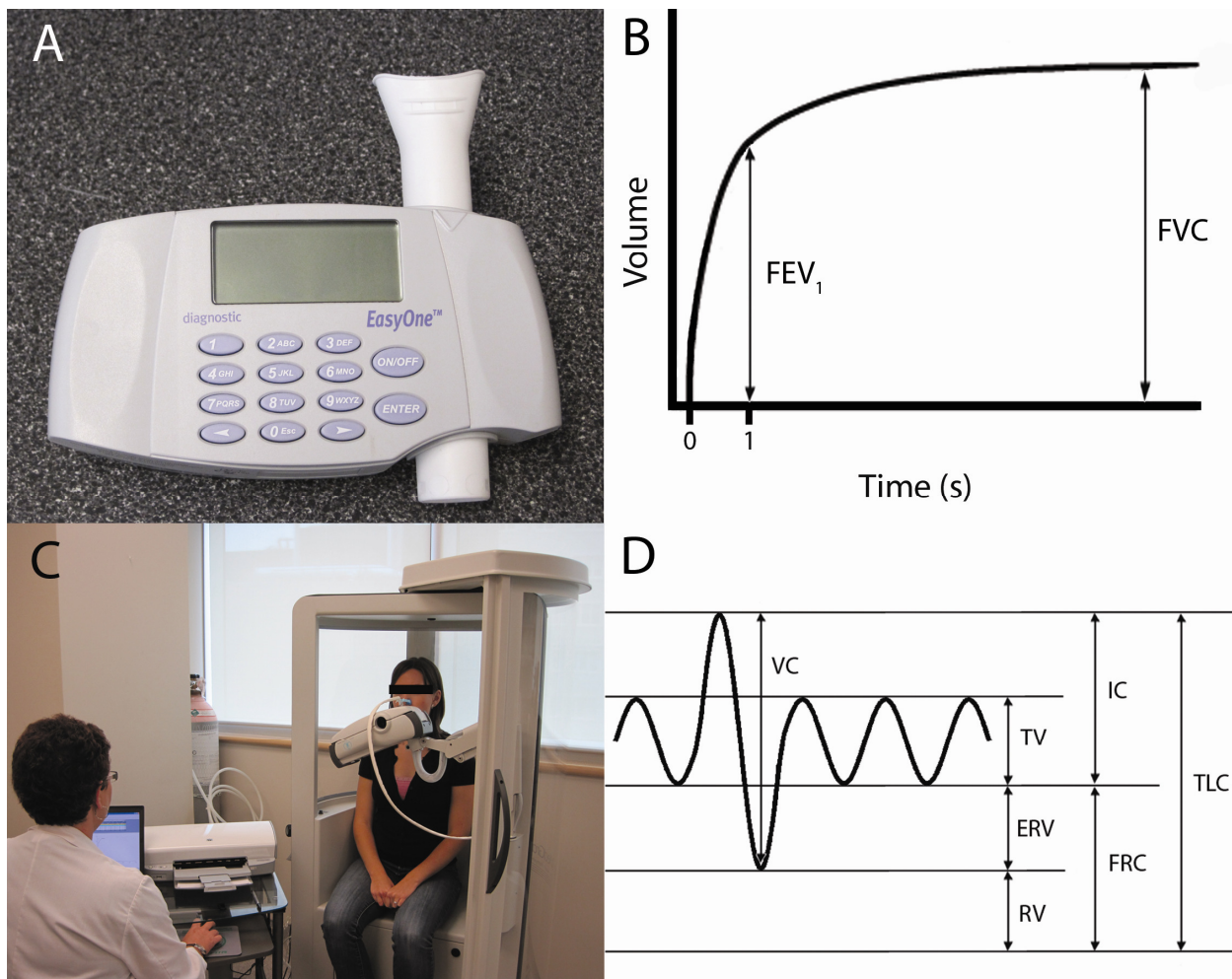


### Figure 1-2: Pulmonary Function Testing.

A hand-held spirometer is shown in (A) with a corresponding sample airflow curve in (B), depicting both the forced expiratory volume in one second and the forced vital capacity. (C) displays a subject in a plethysmography body box, where plethysmography and measurement of gas diffusion can be performed. Note that for plethysmography, the door of the body box is closed and sealed. Lung volumes that can be measured using plethysmography are shown in (D), and include vital capacity, tidal volume, expiratory reserve volume, residual volume, inspiratory capacity, functional residual capacity, and total lung capacity.

PFTs are the most commonly performed lung function tests in the clinic, largely due to the low cost associated with hand-held spirometers and their relative ease of use. Despite



the wide-spread use of PFTs, studies have shown they are highly effort dependent, may not be reproducible, and give a single global measurement of lung diseases that are thought to be highly regionally variable.<sup>16</sup> The variability in pulmonary function test results, primarily due to inconsistency in patient effort, have been found to be higher than for most other clinical laboratory tests.<sup>26</sup> The American Thoracic Society (ATS) has created acceptability and repeatability criteria to minimize the variability of these measurements, which dictates that a minimum of three technically acceptable spirometry maneuvers must be completed (free from artifacts and leaks, good start, acceptable exhalation), with the two largest FEV<sub>1</sub> and FVC measurements within 150mL of each other.<sup>27,28</sup> This criteria can be challenging for patients with lung disease, and many tests are often performed before the criteria is reached. Additionally, the ability to measure DL<sub>CO</sub> relies on the subjects' ability to perform a breath-hold ten seconds in duration, which is often not possible for patients with severe lung disease. Thus, pulmonary function testing, although inexpensive and easily accessible, can be difficult to execute properly, especially in patients with advanced lung disease. Furthermore, these tests do not provide specific measures of underlying disease in the lung parenchyma or airways.

### **1.3.2 Clinical Measurements of Breathlessness**

Clinical measurements of breathlessness aim to evaluate lung function by measuring dyspnea (shortness of breath) both qualitatively and quantitatively. The mMRC scale is a survey of respiratory symptoms that has been well validated in the literature.<sup>29</sup> This scale requires the subject to select one of five statements that best describes the type of physical task that usually leaves them feeling breathless, such as 'I get short of breath when hurrying on level ground or walking up a slight hill'.<sup>30</sup> Advancing on the mMRC's single component system, the St. George's Respiratory Questionnaire (SGRQ) addresses three areas of concern, including symptoms, activities that relate to breathlessness and disturbances to daily life.<sup>29</sup> This self-administered questionnaire includes 76 items weighted by the distress associated with each.<sup>29</sup> Another, more objective test used to evaluate breathlessness is the six minute walk distance (6MWD), whereby the distance that an individual can walk in six minutes on a hard flat surface is measured.<sup>31</sup> Results of the 6MWD test have been correlated to quality life and ability to complete daily

activities, and used to predict morbidity and mortality.<sup>31</sup> In fact, both mMRC and 6MWD have been shown to be better predictors of mortality in COPD than FEV<sub>1</sub>.<sup>32</sup> Overall, these tests are inexpensive, highly accessible, and despite their subjective nature appear to correlate well with disease outcomes.

### 1.3.3 Inflammatory Markers

Inflammation is heavily associated with the development of COPD, and subsequent decline in lung function. Inflammatory markers that may be related to COPD development and/or progression can be measured using bronchoalveolar lavage (BAL) and induced sputum measurements.<sup>31</sup> BAL is an invasive method using bronchoscopy to collect cells and proteins found in pulmonary secretions for evaluation.<sup>31</sup> While the patient is sedated a flexible bronchoscope is used for direct visualization and guidance through the airways to a location where the pulmonary secretion is sampled, generally at the level of the subsegmental bronchi (4<sup>th</sup>-6<sup>th</sup> generation).<sup>31</sup> At the location to be sampled, a saline solution is flushed into the airway, and then drawn back out for analysis. This technique allows for assessment of eosinophils, neutrophils, lymphocytes, mast cells, macrophages, histamine and subcellular protein components.<sup>31</sup>

Induced sputum measurements of inflammatory markers can also be made. In this procedure an individual inhales nebulized hypertonic saline that induces sputum production, specifically from the lower airways for sampling.<sup>31</sup> Due to the highly invasive nature of these procedures, coupled with the costs associated BAL, the widespread use of these techniques is limited.

### 1.3.4 Other Tests

Other tools have been developed to evaluate lung function, including the BODE index. This test combines four measures of lung function that have the strongest association with mortality – body mass index (BMI), airflow obstruction, dyspnea, and exercise capacity.<sup>33</sup> In this test measurements of these four parameters, BMI, post-bronchodilator FEV<sub>1</sub> %<sub>pred</sub> value, mMRC dypnea score and 6MWD, are each scored on a scale of zero to three (zero or one for BMI) and summed to compute a total BODE index score out of ten.<sup>33</sup>

Another approach to evaluate lung function is to evaluate exertional dyspnea. Cardiopulmonary exercise testing (CPET) allows for the simultaneous study of responses of the respiratory system to a known exercise stress through the measurement of gas exchange with the airway.<sup>34</sup> In addition to measuring gas exchange, oxygen uptake ( $\dot{V}O_{2\max}$ ), carbon dioxide output ( $\dot{V}CO_2$ ) and minute ventilation ( $\dot{V}_E$ ), electrocardiography, heart rate and blood pressure can also be measured.<sup>34,35</sup> There are a number of different protocols for CPET, using either a treadmill or cycle ergometer. Protocols are classified according to how the work rate is applied, and include 1) progressive incremental exercise, 2) a multi-stage exercise protocol, 3) a constant work rate protocol, and 4) a discontinuous protocol.<sup>35</sup>

## **1.4 Functional Decline of the Lung**

There is a natural decline in lung function that occurs due to aging and this decline occurs at an accelerated rate in individuals with lung disease. Accelerated functional decline occurs with smoking-related lung diseases, including COPD, lung cancer and RILI. Section 1.4 of this thesis provides an overview of the functional lung changes that occur with age, COPD, lung cancer, and RILI, as well as the underlying pathology thought to cause lung function impairment, and commonly presented symptoms that lead to COPD, lung cancer and RILI diagnosis.

### **1.4.1 The Aging Lung: Normal Functional Decline**

During the first two decades of life the lungs grow and mature, reaching maximal functional capacity at the age of approximately 20 for females and 25 for males.<sup>36</sup> Beyond this age, four basic physiological changes associated with aging begin to occur, including: 1) a decrease in the elastic recoil of the lung, 2) a decrease in compliance of the chest wall, 3) a decrease in strength of the respiratory muscles, and, 4) a change in shape and structure of the lung.<sup>36-38</sup> The decreases in static elastic recoil pressures that occur with age are most evident at high lung volumes (above 40-50% of TLC), which results in increased lung compliance (ability of the lungs to increase in volume with applied change in pressure) at these lung volumes.<sup>39</sup> The decline in lung elastic recoil can be attributed to changes in connective tissue; specifically elastin and collagen,

although conflicting evidence exists as to the exact changes that occur.<sup>39</sup> Stiffening of the chest wall occurs as its rigidity increases due to other age-related changes including decalcification of the ribs, costal cartilage calcification, changes in shape of the chest, and narrowing of the intervertebral disk spaces.<sup>39</sup> During normal breathing, the lung volume increase that results from rib cage expansion is 40% of the total volume increase. This drops by 10% to 30% in the elderly, while the energy required for chest wall movement is 70% of the total elastic work required to breathe, as compared to 40% in a 20 year-old.<sup>39</sup> Additionally, the diaphragm muscles have been shown to decline in strength in the elderly, which may be due to an overall decline in muscle mass with age.<sup>40</sup> With age, the lung changes shape due to the increase in kyphotic curvature of the spine and anteroposterior diameter of the chest wall.<sup>39</sup> The large airways are not generally affected by aging, other than calcification of the bronchial cartilage, which results in a slight increase in anatomic dead space.<sup>39</sup> In contrast, the small airways decrease in diameter due to a decrease in tethering, which would normally maintain patency at a given lung volume, leading to premature airway closure.<sup>39,40</sup> These changes in the small airways result in air-trapping and ventilation-perfusion mismatching.<sup>40</sup> There is an increase in distal airspace size with aging, resulting from loss of supporting tissue, along with a loss in the number of capillaries per alveolus.<sup>38,41</sup> Overall, the total alveolar surface area of the lung decreases by 0.27 m<sup>2</sup>/year, from 70m<sup>2</sup> at age 20 to 60 m<sup>2</sup> at age 70.<sup>39</sup> These age-related changes do not alter day-to-day lung function, as assessed by blood oxygenation and ventilation, although the respiratory system of elderly individuals has a diminished ventilatory response to hypercapnia, making them more vulnerable to respiratory failure and hypoxia when compromised (i.e. pneumonia).<sup>41,42</sup>

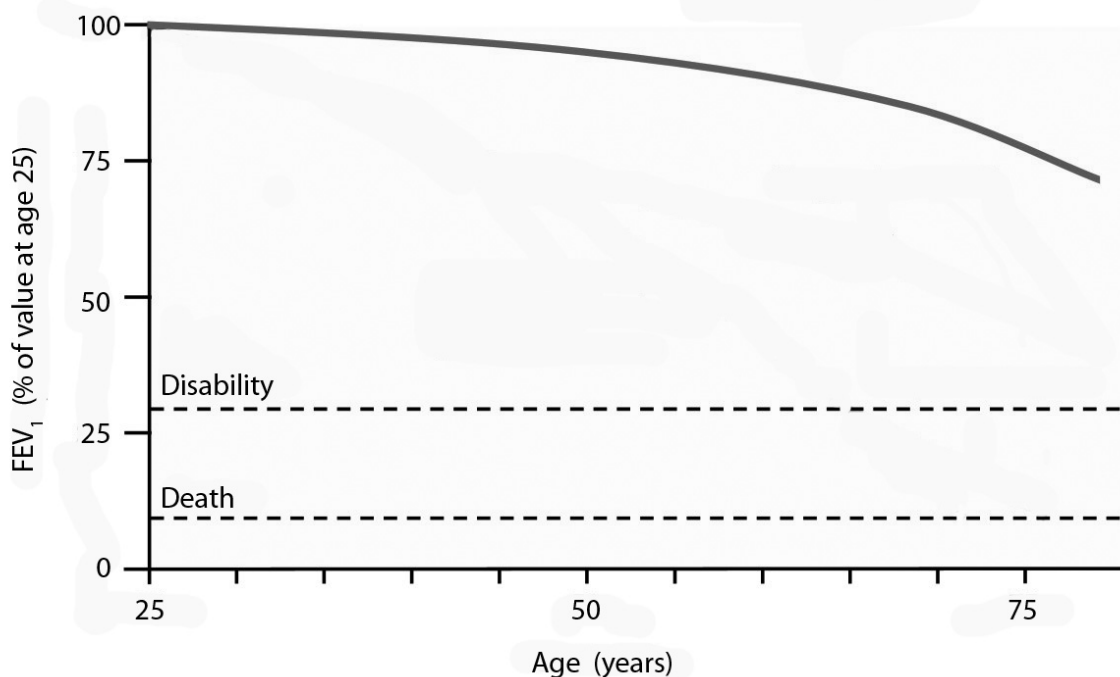


**Figure 1-3: Normal Decline in Pulmonary Function with Age.**

The functional decline of the healthy aging lung, as measured by FEV<sub>1</sub> is shown in this schematic. In the healthy elderly adult the decline in lung function does not amount into clinically relevant airflow obstruction. Adapted from reference (43).

The underlying physiological changes that occur in the lung with increasing age effect lung function, and the aging effect has been well characterized in cross-sectional studies using PFTs. The classic study by Fletcher and Peto in 1977 was the basis for our current understanding of functional lung decline that results from aging.<sup>43</sup> This study showed a continuous decline in FEV<sub>1</sub> beginning at the age of 25, at a rate of approximately 42 ml/year<sup>43</sup>, but this decline did not reach the threshold of clinically relevant airflow obstruction (Figure 1-3). The effects of age on lung function can also be detected with other PFT measurements, with results indicating that increased age is associated with an increase in RV, RV/TLC, and FRC (due to increased lung compliance), a decrease in FVC, and IC while TLC shows no change with age.<sup>36,38,41,44</sup> Additionally, VC declines by approximately 26mL/year in men and 21mL/year in women.<sup>39</sup> Interestingly, a longitudinal study using pulmonary function testing in fit, healthy elderly subjects (in

their sixth and seventh decades) showed that the longitudinal rate of change in VC, RV and FEV<sub>1</sub> is significantly greater than would be predicted from cross-sectional data.<sup>45</sup> The authors of this study hypothesized that the accelerated rate of decline reported in this longitudinal study may reflect non-linear changes in lung function in a subset of the population, which may be averaged out in cross-sectional studies.<sup>45</sup> Finally, the effects of age on gas diffusion across the blood-gas barrier have also been evaluated using the DL<sub>CO</sub>, with results indicating that there is a decline in DL<sub>CO</sub> with age, corrected for alveolar volume.<sup>46</sup> The reported decrease in DL<sub>CO</sub> correlates well with the decrease in internal surface area of the lung.<sup>39</sup>

Overall, physiological changes associated with aging can be quantified using PFTs, and these measurements show a decline in lung function in healthy adults as they age, with longitudinal studies showing that the rate of decline may be greater than previously thought.

#### **1.4.2 Chronic Obstructive Pulmonary Disease: Accelerated Functional Decline**

COPD is defined by the ATS as a preventable and treatable disease state characterized by airflow limitation that is not fully reversible, and usually progressive.<sup>47</sup> Airflow limitation in COPD is associated with an abnormal inflammatory response in the lungs to inhaled noxious particles or gases – most commonly cigarette smoke.<sup>3,8,47</sup> COPD is the fourth leading cause of death worldwide, with morbidity and mortality rates expected to increase in the coming years.<sup>8</sup> At least 750 000 Canadians are currently living with COPD, and as much as 10% of the population worldwide has the disease.<sup>48,49</sup> COPD results in thousands of hospitalizations in Canada every year, with the average hospital stay lasting 10 days and costing \$10,000.<sup>50,51</sup> Additionally, 18% of patients will be readmitted within the year.<sup>50,51</sup> Given that COPD is largely underdiagnosed, the true prevalence of this disease is not known.<sup>8</sup> Although current prevalence data is thought to largely underestimate the burden of COPD, historically the data has suggested that COPD occurs more commonly in men, but more recently the prevalence of COPD appears close to equal between the genders, with the latest data suggesting women may be more susceptible to developing COPD.<sup>49,52</sup>

COPD is caused by the inhalation of cigarette smoke and other toxic particles, which invoke a local and systemic inflammatory response.<sup>53</sup> In the subset of smokers that develop COPD this inflammatory response is persistent<sup>54</sup> and amplified.<sup>55</sup> The inflammatory reaction leads to pathological changes in four specific areas of the lung; the central airways, small airways, lung parenchyma and pulmonary vasculature<sup>47</sup> resulting in chronic bronchitis, small-airway obstruction, emphysematous destruction and pulmonary hypertension respectively.<sup>53</sup> Emphysema is characterized by the dilation and destruction of lung tissue beyond the terminal bronchioles (Figure 1-4A).<sup>22</sup> As shown in Figure 1-4B, chronic bronchitis is associated with inflammation in the central airways resulting in increased mucus production, defective mucociliary clearance and thickening of the bronchial walls<sup>22</sup>, while small-airway obstruction is associated with a remodeling of the airways leading to a thickening of all compartments of the airway wall and a malfunctioning of the mucociliary clearance apparatus resulting in an accumulation of inflammatory exudates in the airway lumen.<sup>22,56,57</sup> The occurrence of pulmonary hypertension in COPD is likely caused by hypoxic vasoconstriction.<sup>58</sup>

Spirometric measurements are used to diagnose COPD, as the disease is characterized by irreversible airflow limitation. The current ATS guidelines state that a post-bronchodilator  $FEV_1/FVC < 0.7$  dictates a diagnosis of COPD, with disease severity determined based on the  $FEV_1$  %<sub>pred</sub> values (stage I  $FEV_1 \geq 80\%$ <sub>pred</sub>, stage II  $50\%$ <sub>pred</sub>  $\leq FEV_1 < 80\%$ <sub>pred</sub>, stage III  $30\%$ <sub>pred</sub>  $\leq FEV_1 < 50\%$ <sub>pred</sub>, stage IV  $FEV_1 < 30\%$ <sub>pred</sub>).<sup>3</sup> The seminal cross-sectional study by Fletcher and Peto showed that the rate of decline in  $FEV_1$  in smokers with COPD is significantly greater than age-matched healthy volunteers, although smoking cessation slows the rate of decline to that of normal healthy aging (Figure 1-4).<sup>43</sup> COPD is also associated with increases in TLC due to loss of elastic recoil, RV due to the premature closing of narrowed airways at higher lung volumes, and RV/TLC, especially in advanced COPD.<sup>59</sup> A decrease in IC in COPD patients is indicative of hyperinflation.<sup>59</sup> A decline in  $DL_{CO}$  is measured in patients with COPD, reflective of the loss in alveolar surface area.<sup>60</sup>

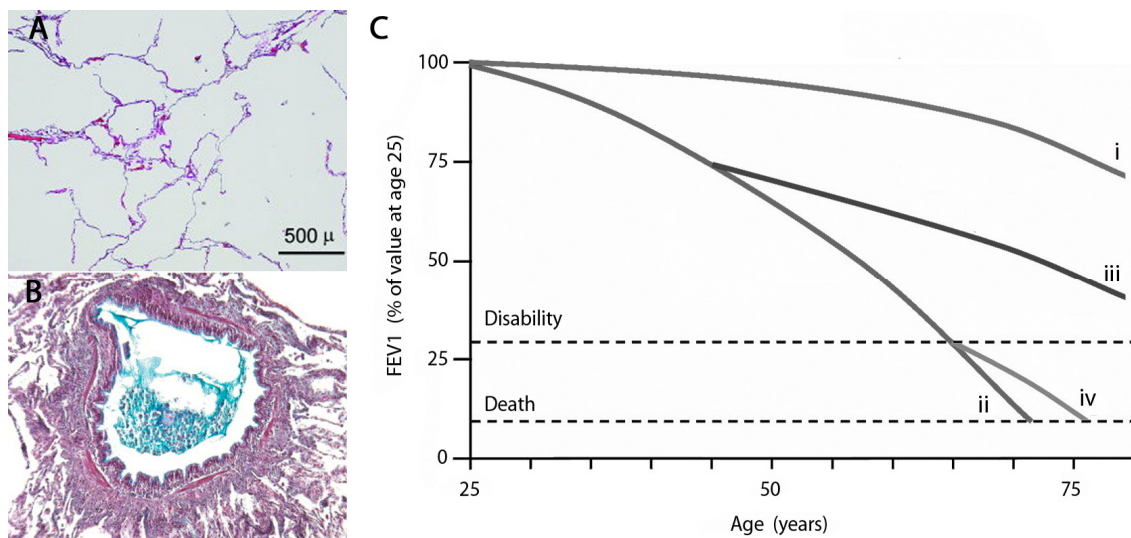


**Figure 1-4: COPD Pathology and Decline in Lung Function.**

Emphysematous destruction and chronic bronchitis are shown in A and B respectively. The functional decline of the lung likely related to these underlying conditions is shown in panel C, where Ci shows the natural decline in lung function due to age, Cii shows the decline associated with smokers susceptible to lung disease and Ciii and Civ show the decline in lung function associated with smoking cessation at 45 and 65 years respectively. Adapted from references (22), (43), and (212).

Those with COPD may experience a wide variety of symptoms including chronic cough, sputum production, dyspnea, wheezing, and chest tightness.<sup>3</sup> Generally, the first symptom to develop is coughing, followed by sputum production.<sup>8</sup> The primary reason medical attention is sought is for dyspnea, which is also the major cause of disability associated with COPD.<sup>3,8</sup> Symptoms are often related to smoking history as defined by pack-years; the number of years smoked multiplied by the number of packs smoked per day. These symptoms often result in a significant interference with normal activities of daily living and a decline in quality of life, which are assessed in research studies using quality of life metrics including the SGRQ<sup>61</sup>, the 6MWD<sup>62-64</sup>, mMRC<sup>65</sup> and the BODE index.<sup>33,66</sup> Quality of life measures including the mMRC scale, the 6MWD, and BMI are all better predictors of mortality than FEV<sub>1</sub>.<sup>32</sup> The BODE index predicts mortality in COPD patients better than any of its components taken independently.<sup>33</sup>

COPD is well described as a complex and heterogeneous disease in terms of clinical presentation, underlying pathology, physiology, imaging, response to therapy, decline in



lung function, and survival, which may be reflective of distinct underlying phenotypes.<sup>67</sup> The identification of elements that could be used to group COPD patients into clinically meaningful subgroups, providing prognostic information useful for guiding current treatments, and developing new therapies is necessary.<sup>67</sup> Although many studies have proposed potential COPD phenotypes<sup>68-71</sup>, large-scale longitudinal clinical studies aimed at identifying COPD phenotypes are needed to begin to enhance our understanding of the disease in this regard.<sup>67</sup> Studies of this nature, collecting clinical, physiological, radiological, biological and genetic data, aimed at evaluating COPD phenotypes are currently underway.<sup>14,72</sup>

### 1.4.3 Lung Cancer

Lung cancer is the leading cause of cancer related death, as shown in Figure 1-5, and responsible for more than 1 in 4 of all projected deaths from cancer.<sup>2</sup> In 2010 it is projected that 24,200 Canadians will have been newly diagnosed with lung cancer, an incidence rate second only to prostate cancer, and an additional 20,600 currently diagnosed Canadians will die from the disease.<sup>2</sup>

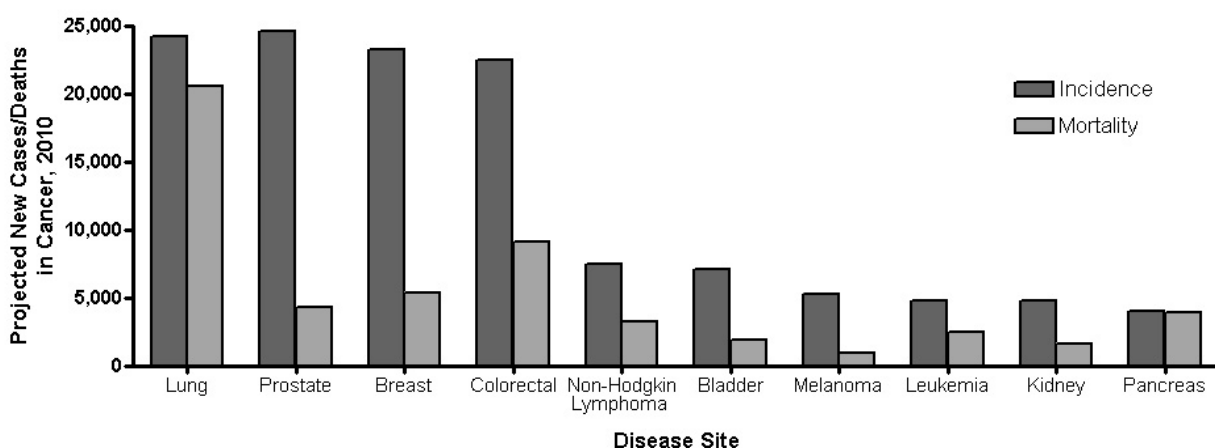


**Figure 1-5: Canadian Incidence and Mortality in Cancer for 2010.**

Projected incidence and mortality rates for cancer in Canada in 2010. Lung cancer is projected to be the second most commonly diagnosed cancer, and cause more than one in four of all cancer-related deaths. Adapted from reference (2).

The first classification system for lung cancer was proposed in 1924 by Marchesani and co-workers, and is the basis for World Health Organization (WHO) classification used today.<sup>9,73</sup> According to the current WHO classification, lung cancer can be divided up into four major histological subtypes; squamous cell carcinoma, adenocarcinoma, small-cell carcinoma and large-cell carcinoma.<sup>74,75</sup> Squamous cell carcinomas are generally larger than 4 cm in diameter, display cavitation, and are centrally located, often causing segmental or lobar collapse due to their location.<sup>9,76</sup> Adenocarcinoma on the other hand are usually located in peripheral regions of the lung, are typically less than 4 cm in diameter, and rarely cavitate.<sup>9,76</sup> Squamous cell and adenocarcinomas each comprise about 30% of all lung cancers seen in the clinic.<sup>75</sup> Small cell carcinomas are characterized by small tumour cells that are densely packed with limited cytoplasm and no nucleoli<sup>77</sup>, while large-cell lung cancers are usually poorly differentiated<sup>9</sup>, grow rapidly and metastasize quickly.<sup>78</sup> Squamous cell carcinoma, adenocarcinoma and large-cell lung cancer are frequently grouped into one category called non-small cell lung cancer (NSCLC) because of similar treatment options<sup>79</sup>, while small-cell lung cancer (SCLC) is treated with a different approach due to its chemosensitivity and mode of metastatic spread.

Lung cancer is treated according to the stage of the disease. Staging occurs according to the International System for Staging Lung Cancer; the T- primary tumour, N- regional lymph nodes, M- distant metastasis (TNM) classification. The primary tumour is classified on a scale of one to four according to its size (diameter) and location with respect to the chest wall, carina (ridge separating openings of right and left main bronchi), diaphragm, mediastinum and pericardium.<sup>80</sup> Regional lymph nodes are classified according to metastasis – either not present (0), present in the ipsilateral peribronchial and/or ipsilateral hilar nodes (1), present in the ipsilateral mediastinal and/or subcarinal lymph nodes (2), or metastasis mediastinal or supraclavicular lymph nodes (3).<sup>80</sup> Distant metastases are either not detected (0), or present (1).<sup>80</sup> The overall stage of a lung cancer is then determined by the combination of T, M and N stages. For example stage IIIA lung cancer can be any one of the following combinations: T3N1M0, T1N2M0, T2N2M0, or T3N2M0. Each overall stage has similar treatment options and survival expectancies.<sup>80</sup> Stage I and II (and occasionally IIIA) lung cancers are operable,

and surgery is performed as it has the highest long-term survival rates.<sup>75</sup> Stage III generally means that the tumour is non-resectable due to its location along the mediastinum and presence of positive nodes not having spread beyond the lung.<sup>81</sup> In this stage curative treatment combining chemotherapy and radiation therapy is the most common approach.<sup>75,79</sup> Stage IV lung cancer indicates that the tumour has metastasized beyond the lungs, and therefore in this late stage, palliative treatment is most commonly provided.<sup>75</sup>

Many lung tumours result in occlusion of the major airways causing breathlessness. Dyspnea is an early symptom in 60% of lung cancer cases, and accompanies other symptoms, including chronic cough and sputum production or hemoptysis.<sup>75,82</sup> Patients with lung cancer frequently have co-existing lung disease that adversely impacts lung function, and limits options for cancer therapy.<sup>82,83</sup> In a retrospective study of 294 newly diagnosed lung cancer patients with previously collected pulmonary function tests, findings revealed that 73% of men and 53% of women had airflow obstruction fitting the definition of COPD.<sup>84</sup> The prevalence of COPD in this study is potentially overestimated due to the impact of tumour burden of airflow measurements, and therefore highlights the difficulty in evaluating undiagnosed underlying lung disease in patients with lung cancer. Thus, the interaction between underlying lung disease, lung cancer onset, treatment, and survival outcomes are unclear.

#### **1.4.4 Radiation-induced lung injury**

Radiation treatment for lung cancer can be curative, but it can also be fatal. Damage to the lung can be incurred from radiation treatment leading to a significant decline in lung function accompanied by symptoms that degrade quality of life.<sup>10</sup> RILI is the major dose-limiting toxicity of lung cancer radiation. The lung is extremely sensitive to radiation, with RILI occurring in an estimated 5-35% of patients undergoing thoracic radiation, and the incidence of moderate to severe radiation injury between 10-20%.<sup>12</sup> With increasing severity, survival rates decrease dramatically, and studies show 3-year survival rates of 0% in subjects with severe injury.<sup>85</sup>

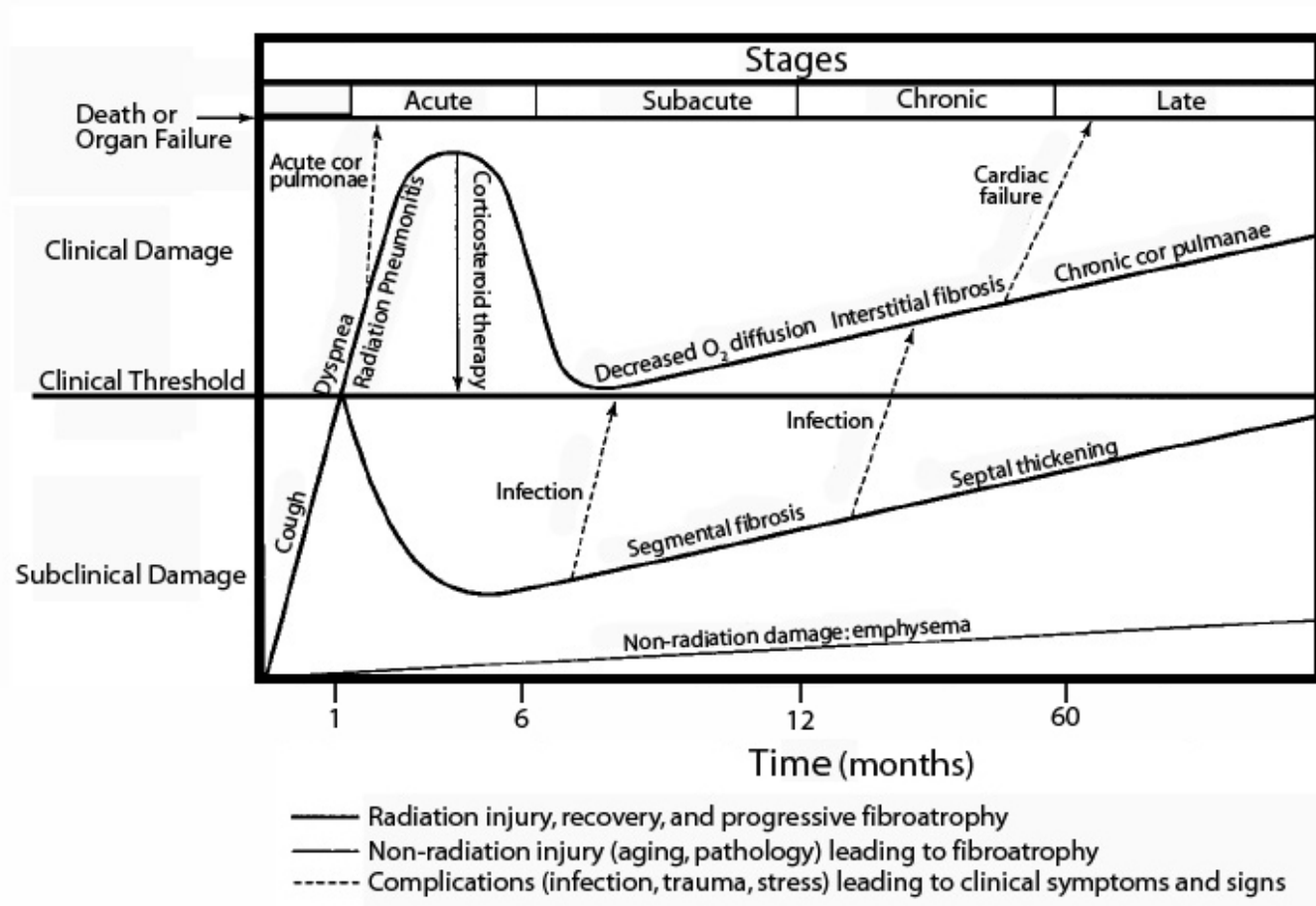


**Figure 1-6: Stages of Radiation-induced lung injury.**

The acute phase of radiation pneumonitis followed by the chronic late phases encompassing radiation fibrosis are shown in this schematic, along with the associated complications commonly arising in each phase. Adapted from reference (87).

RILI occurs in a series of stages, as depicted in Figure 1-6 - an early latent phase followed by an intermediate acute phase, a subacute phase, a late phase, and a chronic phase.<sup>86,87</sup> The intermediate acute phase – radiation pneumonitis, is marked by an inflammatory response during which leukocytes, plasma cells, macrophages, and fibroblasts invade the alveoli causing capillary obstruction and septal thickening.<sup>10,88</sup> Radiation fibrosis (late and chronic phases) is marked by further septal thickening and obliteration of the alveolar space.<sup>88</sup> This immune response is manifested in the form of clinical symptoms which include dyspnea and a productive or non-productive cough in the pneumonitis phase, and may develop into more severe dyspnea, reduced exercise tolerance, orthopnea (difficulty breathing when not upright), cyanosis (bluish colour of the skin due to insufficient oxygen), chronic cor pulmonale (a complication of pulmonary disease leading to enlargement of the right ventricle), and finger clubbing as the injury moves to the fibrotic stage.<sup>89</sup>

Many potential predictors of RILI have been examined including age, gender, histology, stage, tumour lobe, lung involved, performance status, weight loss, chemotherapy drugs, chemoradiation schedule, pulmonary function tests, radiation dose, daily dose delivered and volume irradiated, with the majority showing no significant relationship to RILI risk.<sup>11,90</sup> Robnett et al. indicated that low pre-treatment absolute FEV<sub>1</sub> was significantly associated with the development of severe radiation pneumonitis, and all patients in this study with severe RILI had a pre-treatment FEV<sub>1</sub> of less than 2.0 litres.<sup>91</sup> Recently, Rodrigues and co-workers have shown that elevated dose-volume parameters including the percentage of lung volume receiving greater than 20Gy and mean lung dose remain as the main correlation risk factors but with very low predictive value as an ensemble.<sup>11</sup>

## **1.5 Imaging Measurements of Lung Function**

Pulmonary imaging has evolved over many decades, with a large focus in recent years on structural techniques, specifically with the development of high resolution x-ray computed tomography (HRCT). Imaging techniques including nuclear medicine and MRI, aimed at evaluating lung function in COPD, lung cancer and RILI, have lagged behind structural lung imaging methods, and although in the last two decades some major

advances in functional lung imaging have been made, the clinical translation of these techniques has yet to be seen.

### 1.5.1 Chest x-ray

The chest radiograph (Figure 1-7) is the most commonly acquired image for the evaluation of the lung.<sup>92</sup> The standard method for acquiring chest x-rays is for the subject to stand with their back to the x-ray source and their hands placed on the posterior aspects of the hips with the elbows rolled forward such that the scapulae are not in the lung field, referred to as a postero-anterior (PA) x-ray.<sup>93</sup> The PA x-ray is acquired at full inspiration to capture the greatest possible area of lung structure. A lateral projection is often acquired in addition to the PA projection, with the median sagittal plane of the subject parallel to the film and the subjects arms folded across their head.<sup>93,94</sup> In a chest x-ray of a healthy young individual x-rays travel from the x-ray source on the posterior side, and through the lung parenchyma with relatively little attenuation or scatter, as compared to other bony thoracic structures such as the ribs or clavicles. The x-rays interact with the detector on the anterior side of the subject, generating an image in which the lung tissue appears predominantly black.<sup>95</sup> The branching of the pulmonary vessels can be seen; the fissures separating the lobes of the lungs may be visible; the trachea is centered; and the diaphragm appears as a smooth curve with acute and clearly defined costophrenic angles.<sup>93,95</sup> The radiation dose associated with a typical chest x-ray is 0.02mSv, which is equivalent to approximately three days background radiation.<sup>96</sup> This transmission-based imaging method is fast, widely available, and deposits relatively low radiation doses as compared to other lung imaging modalities used clinically.<sup>97</sup>

A longitudinal study of chest x-rays acquired in a group of healthy men initially  $48 \pm 13$  years, and followed for  $17 \pm 3$  years, showed a doubling in hyperinflation, increased markings, a three fold increase in the presence of enlarged pulmonary arteries and a dramatic increase in the presence of Kerley B lines (thickened interlobular septa visible in the subpleural region).<sup>98</sup> The width of the cardiac silhouette also increases with age.<sup>95</sup>

COPD can be difficult to detect on chest x-ray due to poor contrast of the two-dimensional (2D) projection image<sup>99</sup>, and detectability is related to overall severity of

COPD (stage III and IV are most easily detected), rather than specific underlying pathology such as emphysema or small airways disease.<sup>60,100</sup> Patients with COPD usually exhibit some degree of hyperinflation due to emphysema or airways disease, which presents as a flattened diaphragm, a large lucent retrosternal air space, a narrow vertical heart, and an overall increase in the anterior-posterior diameter of the chest (Figure 1-7B).<sup>60,100,101</sup> Focal areas that are hyper-lucent (darker than normal) within the lung parenchyma may be indicative of bullous disease.<sup>101</sup>

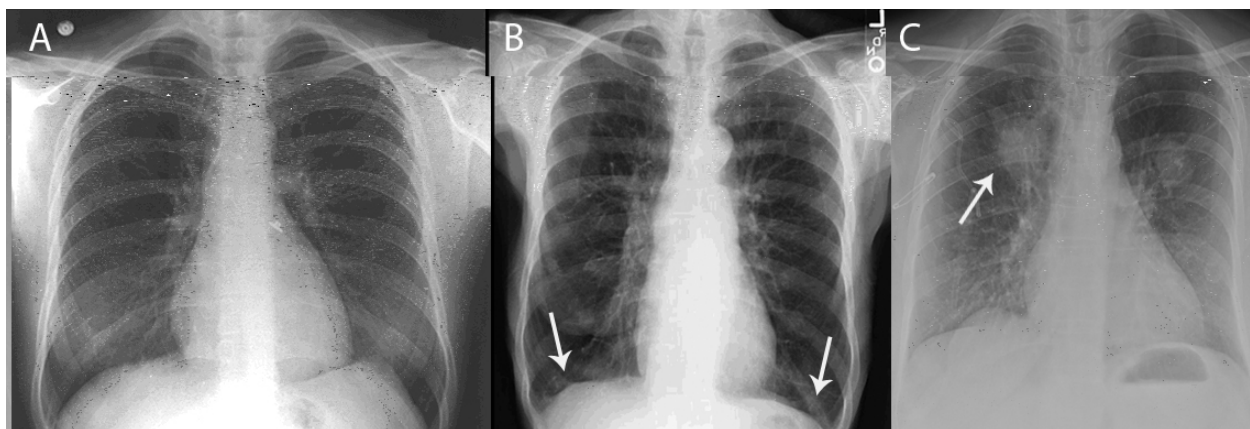


**Figure 1-7: Chest x-ray of healthy volunteer, COPD and lung cancer.**

Chest x-rays are shown for a healthy individual in A, a subject with COPD in B, and a subject with lung cancer in C. B displays hyperinflation and the presence of flattened diaphragm (as indicated by arrows) common on chest x-rays of COPD. The arrow in C points to a tumour in the right upper lung.

Chest x-rays continue to be the imaging modality used for the diagnosis of lung cancer (Figure 1-7C), despite their inaccuracy, largely due to the wide-spread availability and low cost relative to CT and MRI.<sup>102,103</sup> Chest x-ray is not a reliable method for detecting lung cancer, and many small tumours are missed.<sup>103,104</sup> Failure to detect lesions at favourable and even larger sizes can occur because the lesions can be obscured by the mediastinum and other aspects of the thorax.<sup>104</sup> In the context of lung radiotherapy, treatment plans were made using x-ray films until the 1980's.<sup>105</sup> These films provided only two-dimensional information with high levels of uncertainty surrounding precise tumour location, necessitating large planning target volume (PTV) margins (2-3cm in all directions) to account for this.<sup>105</sup>

Chest x-ray in RILI is critical for diagnosis, as symptoms are non-specific and pulmonary function tests are not routinely performed in follow-up evaluation. Changes in chest x-ray are usually first detected 2-3 months following radiation therapy, and include increased ground glass opacity, indistinctness of the usual pulmonary markings.<sup>89</sup> The appearance of acute radiation pneumonitis on chest x-ray widely varies, ranging from minimal changes (slight indistinctness of the pulmonary vasculature or slight increase in the thickening of the pleura) to complete consolidation of the irradiated area.<sup>106</sup> If fibrosis follows the pneumonitis phase, it commonly appears on chest x-ray as apical thickening, a slight retraction or elevation of a hemidiaphragm, minimal retraction or elevation of the hilum or minor fissure, linear strand-like densities in the area where pneumonitis was present.<sup>86,106</sup> Retraction secondary to radiation fibrosis follows the typical appearance of fibrosis of any other etiology.<sup>106</sup>

### **1.5.2 X-ray Computed Tomography**

In recent years, x-ray computed tomography (CT) has become the imaging modality of choice for evaluating the lung, providing highly detailed images with isotropic voxel size, all captured in a ten-second breath-hold.<sup>107,108</sup> The development of CT in the 1970's brought about many changes in terms of lung imaging. Through the acquisition and reconstruction of multiple projections of data, cross-sectional images of the body can be obtained.<sup>102</sup> Each image slice is a matrix of pixels representing a voxel of tissue, and specific to CT, each pixel is assigned a CT number based on the attenuation of signal in that pixel in relation to the attenuation of water.<sup>102</sup> CT is generally taken to be the best imaging modality for the evaluation of lung parenchyma, with HRCT providing morphological detail of the lung and generally accepted as the gold standard for structural assessment of the lung.<sup>109</sup> Despite the excellent morphological detail of the lung that thoracic CT provides, concerns remain regarding the radiation dose associated with these scans. A typical thoracic CT has an effective dose of 8 mSv, which is the equivalent of approximately 400 chest x-rays or 3.6 years of background radiation.<sup>96</sup>

Although CT is generally regarded as a structural imaging technique, recent research has evaluated the potential to extract functional information from inspiratory and expiratory CT and four-dimensional CT.<sup>110-112</sup> This emerging field of research has shown that



registration, thresholding and subtraction of pixel values at maximum inspiration and expiration may yield information regarding ventilation by evaluating density changes in registered pixels.<sup>110-112</sup> Research is continuing in this area, and studies aimed at evaluating the reproducibility, sensitivity, and correlates with currently accepted markers of lung function are required.

Cross-sectional CT studies of healthy young and elderly subjects have been performed to identify characteristics on CT that can be attributed to the normal aging process, in order to differentiate features associated with aging from those associated with potential disease. Findings suggest that in older healthy subjects there is a statistically significant increase in the prevalence of reticular pattern, cysts, bronchial dilation and bronchial wall thickening in elderly subjects, while no difference between ground glass opacity, interlobular septal thickening or centrilobular emphysema was found.<sup>113</sup> Another study examining age-related differences apparent on CT found that mean lung attenuation values decreased significantly with increasing age, while mean lung volumes showed no significant change with increasing age.<sup>114</sup>

CT imaging of COPD patients is routinely used to qualitatively detect emphysema, as shown in Figure 1-8A. Centrilobular emphysema (CE) is the most common form and strongly associated with cigarette smoking. CE is characterized by focal regions of decreased attenuation that are confined to the center of the secondary lobule, and is most commonly located in the upper lobes.<sup>109</sup> Two methods for quantifying emphysema from CT have been developed based on areas of low attenuation. The first is a threshold cutoff based on Hounsfield units (HU) to separate emphysematous tissue from normal tissue, with the most common threshold being -950 HU.<sup>108,115</sup> The second method uses a percentile point on the frequency distribution curve of attenuation values to compare subjects or groups of subjects.<sup>108</sup> The 15<sup>th</sup> percentile is most commonly used, and is the preferred method for longitudinal analysis.<sup>108,115</sup> Quantitative CT analysis of COPD patients commonly show an increase in low attenuation areas<sup>116-119</sup> and increases in airway wall area dimensions<sup>119-123</sup> reflective of emphysema and airways disease respectively. Although a number of algorithms exist to evaluate airway wall dimensions, the small airways cannot be well resolved on current resolution of CT.<sup>108</sup> Given that

these airways, <2mm in diameter, are the main site of airflow obstruction in COPD it is likely that current measurements of airways disease using CT largely underestimate the true burden of this underlying pathology in COPD.<sup>108</sup> Despite the limitations of CT airway measurements, Nakano and co-workers used measurements of emphysema and airways disease derived from CT in an effort to understand their relative contribution in COPD. They were the first to use CT as a tool for phenotyping COPD, and reported a single dominant phenotype in 40% of subjects.<sup>121</sup> A longitudinal study using CT by Ohara et.al. showed that surrogate measures of airways disease did not correlate with FEV<sub>1</sub> at baseline, but changes in airway measurements over four years were significantly inversely correlated to the change in FEV<sub>1</sub> over the same time period.<sup>123</sup> The change in percentage of low attenuation areas in this same study did not correlate with the decline in FEV<sub>1</sub>.<sup>123</sup>

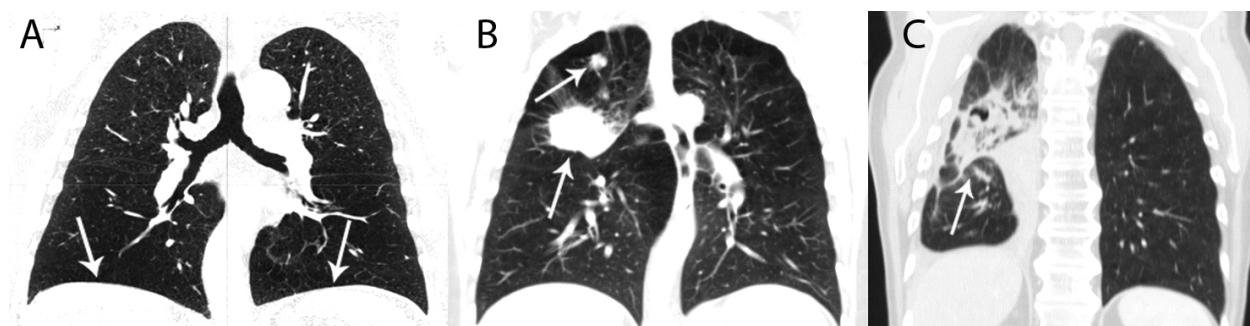


**Figure 1-8: CT of Smoking-related lung disease.**

COPD is identifiable on CT by the areas of decreased signal intensity and flattened diaphragm as indicated by the arrows in A. Arrows in B show stage III B lung cancer with the presence of underlying COPD, while the arrow in C points to RILI as evidenced by the marked increase in lung density in the irradiated portion of the lung.

CT is the modality of choice for evaluating lung cancer (Figure 1-8B), and is used for guidance of transthoracic needle biopsies of lung nodules.<sup>124</sup> Perhaps more importantly, CT is critical for staging lung cancer in terms of identifying tumour size, location, local extent of the primary tumour, including the presence or absence of atelectasis, pleural effusion, the status of the mediastinum, and lymph node abnormalities.<sup>125</sup> In recent years, given the dismal outcomes of the disease, the benefits of CT screening for lung cancer have been debated, amid concerns regarding radiation dose.<sup>126</sup> The National Lung

Screening Trial (NLST), a multi-centre randomized control trial, is evaluating spiral CT against standard chest x-ray for detection of lung cancer.<sup>126,127</sup> Results released in December 2010 from the NLST show a significant decrease of 20% in the number of deaths in the group screened with low-dose helical CT.<sup>128</sup> The appearance of thoracic tumours on chest radiography and CT differ based on the histological classification of the tumour. On chest radiography approximately half of all adenocarcinomas display mediastinal lymphadenopathy<sup>129</sup>, while on CT these tumours are characterized by either a localized ground glass opacity with a doubling time greater than one year, or a solid mass with a fast doubling time, less than one year.<sup>130</sup> In regard to radiation treatment planning, three-dimensional information for the purposes of target definition and treatment planning became widely available in the 1990's when CT largely replaced radiography<sup>105</sup>, and is now viewed as the minimum standard of care in the treatment of thoracic tumours.<sup>131</sup>

Radiographic evidence of RILI is frequently observed following radiotherapy, although only a fraction patients presenting with radiological evidence of RILI complain of symptoms.<sup>132</sup> CT evidence of RILI is shown in Figure 1-8C, and was described by Libshitz et al<sup>133</sup> as: 1) homogenous, with a slight increase in density uniformly involving the irradiated portions of the lung, 2) patchy consolidation contained within the irradiated lung, but not conforming to the shape of radiation portals, 3) discrete consolidation conforming to the shape of radiation portals, but non-uniformly, 4) solid consolidation conforming to and totally involving the irradiated portions of the lung. Radiation fibrosis has also been described on CT as well defined areas of atelectasis with parenchymal distortion, traction bronchiectasis, mediastinal shifting and pleural thickening.<sup>10,134,135</sup> In comparison to chest x-ray, CT is more sensitive to RILI-related changes in the lung and demonstrates changes sooner following treatment.<sup>133,136-138</sup>

### **1.5.3 Nuclear Medicine Methods**

Scintigraphy, single photon emission computed tomography (SPECT) and positron emission tomography (PET) have all been used in the context of functional lung imaging.<sup>139</sup> Planar scintigraphy images are still acquired clinically, however, research studies of lung function using nuclear medicine now focus on SPECT and PET

approaches.<sup>139</sup> Ventilation and perfusion are commonly imaged using these nuclear medicine techniques.

Ventilation images are generated using a gamma camera, which detects gamma rays released following radionuclide decay, with scintigraphy capturing a single 2D projection, and SPECT images reconstructed from multiple 2D projections.<sup>140,141</sup> Ventilation imaging using scintigraphy or SPECT can be performed with radioactive gases (<sup>133</sup>Xe, <sup>127</sup>Xe, <sup>81m</sup>Kr) or radiolabeled aerosols (i.e. Technegas).<sup>139</sup> Radioaerosols can be used as an alternative to radioactive gases, although their distribution is not always ideal.<sup>139,142</sup> When an aerosol such as Technegas is used, the deposition and distribution depend on its aerodynamic properties – primarily the particle size, with particles larger than 2µm tending to deposit in the large airways of the lung.<sup>143</sup> Ventilation patterns of the lung are studied using an array of protocols that largely depend on the half-life of the radioisotope used.<sup>144</sup> Ventilation can be evaluated during the wash-in phase of the gas, followed by the steady state and wash-out phases. This allows for analysis of lung volumes, regional clearance rate and gas trapping.<sup>144</sup> The effective radiation dose from these scans ranges from 0.1-0.6mSv. Ventilation images are often coupled with perfusion images, which allow for the evaluation of ventilation-perfusion matching. Perfusion images are commonly acquired following an injection of technetium-99m (<sup>99m</sup>Tc) labeled macro-aggregated albumin (MAA), which gives a measure of relative pulmonary arterial blood flow.<sup>144</sup> MAA has a diameter of 10-40µm, and therefore cannot pass through the terminal arterioles; a typical dose of 200 000 particles results in a blockage of less than 0.01% of the total number of arterioles.<sup>144</sup> The radiation dose associated with a perfusion scan is 1.0 mSv.<sup>144</sup>

PET provides structural and functional information using positron emitters that are physiologically and biochemically relevant to functional lung processes, including <sup>11</sup>C, <sup>13</sup>N, <sup>15</sup>O, <sup>18</sup>F, <sup>19</sup>Ne, and <sup>68</sup>Ga, with half-lives ranging from 17.4 seconds to 110 minutes.<sup>145</sup> These radionuclides decay via β+ decay, and a positron is emitted.<sup>146</sup> The positron quickly loses its kinetic energy, and combines with an electron in an annihilation event, simultaneously emitting two 511keV photons at 180 degrees from each other.<sup>146</sup> PET scanners localize the location of the annihilation event through coincidence

detection of photons in opposing detectors.<sup>146</sup> Functional measurements using PET commonly include regional ventilation using  $^{19}\text{Ne}$ , as well as the ventilation perfusion ratio using  $^{13}\text{N}$ .<sup>147,148</sup> The most common PET tracer is  $^{18}\text{F}$ - fluorodeoxyglucose (FDG), an analog of glucose is used as a marker of inflammation.<sup>145</sup> In the lung, it is suggested that the uptake of  $^{18}\text{F}$ -FDG is specific to neutrophilic infiltration.<sup>145</sup>

Limited studies evaluating the effect of aging on the distribution of ventilation using nuclear medicine techniques have been performed. A PET study using  $^{18}\text{F}$ -FDG-PET found that with increased age standard uptake values in the lung increase, which may relate to inflammation in the lung.<sup>114,145</sup>

Nuclear medicine has also been used to study COPD, more specifically to examine ventilation perfusion patterns in these subjects with airflow limitation. SPECT studies of COPD show two common findings in terms of ventilation; matched areas with defects in both ventilation and perfusion, and regions that are perfused but unventilated.<sup>149,150</sup> Ventilation studies using SPECT have also been found to correlate with FEV<sub>1</sub>.<sup>151</sup> In COPD, PET studies have shown there is a positive correlation between DL<sub>CO</sub> and perfusion, but a negative correlation with the ventilation-perfusion ratio.<sup>152</sup>

Nuclear medicine, and more specifically PET in combination with CT (PET/CT), has been heavily studied in recent years for its use in evaluating and staging lung cancer. Using  $^{18}\text{F}$ -FDG, PET studies have shown an increased specificity, sensitivity and negative predictive values in characterizing pulmonary nodules as benign or malignant as compared to conventional procedures (CT).<sup>153</sup> PET/CT also aids in staging, as it is useful for determining whether there is involvement of the thoracic wall.<sup>153</sup> Neither SPECT nor PET have been used to date to study the impact of lung cancer on regional pulmonary function.

Longitudinal nuclear medicine studies by Prato and co-workers using  $^{133}\text{Xe}$  ventilation scintigraphy and  $^{99\text{m}}\text{Tc}$ -MAA for evaluation of perfusion showed that the functional parameter in the lung most affected by radiation was blood flow, which was also affected the earliest.<sup>154</sup> They report that blood flow changes at 60 days-post radiation are predictive of perfusion values at 300 days, and therefore decreased perfusion as measured

by  $^{99m}\text{Tc}$ -MAA may be an indicator of patients that will go on to develop severe pulmonary complications.<sup>154</sup> Studies evaluating the ability of SPECT scans acquired pre-treatment to determine risk of developing radiation pneumonitis post-treatment have been performed, and to date these scans do not appear to have better predictive value than mean lung dose or PFTs.<sup>155</sup> One study did suggest that the presence of SPECT hypoperfusion adjacent to a central mediastinal mass might identify patients with improved  $\text{DL}_{\text{CO}}$  following radiation.<sup>156</sup> A study assessing the effects of radiation pneumonitis using PET showed increased  $^{18}\text{F}$ -FDG uptake in non-irradiated lung tissue of approximately 80% of patients following radiation treatment for lung cancer.<sup>157</sup>

### 1.5.4 Magnetic Resonance Imaging

Only recently, with advances in pulmonary MRI research, has MRI been used for lung imaging.<sup>158</sup> MRI utilizes the magnetic properties of certain nuclei, most commonly protons to create functional and structural images. Therefore, MRI has, until recently, had a limited use in visualization and functional assessment of the lung primarily due to the low water content (proton density) within the lung as visualized in Figure 1-9, as well as secondary factors that include image degradation by cardiac and respiratory motion, and high susceptibility artefacts at the alveolar interface.<sup>158-160</sup> New imaging techniques and hardware developed over the last decade have made it possible to use proton MRI to advance the knowledge of pulmonary function. Short echo times (TE) and single shot fast spin echo sequences have been used to probe pulmonary perfusion.<sup>160</sup> Additionally, oxygen-enhanced lung MRI, using inhaled molecular oxygen as a paramagnetic contrast agent, has been used for functional lung imaging.<sup>161-163</sup> This technique works by shortening the longitudinal relaxation ( $T_1$ ) time of protons in the blood, resulting in a reduction of measured  $T_1$  values of 7-14% depending on the exact approach used.<sup>163</sup> This decrease in  $T_1$  seen in normal lung tissue depends on three factors: 1) ventilation of the lung or region of interest within the lung, 2) diffusion of the oxygen from the alveoli into the capillaries, and 3) the perfusion of the lung tissue.<sup>161,164</sup> The functional changes measured with oxygen-enhanced MRI correlate with  $\text{FEV}_1$ <sup>165,166</sup>, and  $\text{DL}_{\text{CO}}$ .<sup>167</sup>

Proton MRI has been used to demonstrate changes in both the airways and parenchyma in subjects with COPD.<sup>168,169</sup> In emphysema the extent of tissue loss, decrease in blood

volume and degree of hyperinflation negatively correlate with MR signal.<sup>168,170</sup> Additionally, in regard to the lung parenchyma, it has been reported that the difference in parenchymal signal intensity between inspiration and expiration correlate with FEV<sub>1</sub>.<sup>171</sup> MRI has also been used to evaluate the airways, with an MRI study of COPD revealed bronchial wall thickening and mucus secretion.<sup>168</sup> Using oxygen-enhanced MRI methods, Ohno and co-workers showed that lifetime smoking exposure, FEV<sub>1</sub>/FVC, FEV<sub>1</sub> %<sub>pred</sub> correlate with quantitative measurements captured from this MRI technique.<sup>166</sup>



**Figure 1-9: Proton MRI of the Lung.**

Historically, proton MRI has not been used for lung imaging due to the low signal related to the lack of protons (water) within the lung. Characteristically, the lungs appear as a large regions of signal void on MRI.

MRI applications in lung cancer have focused on detection and classification of pulmonary nodules, as well as improvement of MR pulse sequences and contrast agents for prospective MR application in TNM staging.<sup>172</sup> In regard to functional lung imaging in lung cancer, MRI has been used to assess and quantify diaphragm motion in the first

second following maximum expiration and the total motion at end-expiration.<sup>173,174</sup> These measurements have been shown to correlate well with FEV<sub>1</sub>/FVC in healthy volunteers.<sup>173,174</sup> Differences between diaphragm motion in the ipsilateral and contralateral lungs exist in patients with stage IB tumours located in the middle and lower lung regions, but do not exist in patients with stage IA lung cancer.<sup>173,175</sup>

## 1.6 Hyperpolarized Noble Gas MRI

Using inhaled hyperpolarized gas as a contrast agent, research over the past two decades has demonstrated that MRI can be used a tool for functional imaging of the lung. This section will discuss the development of this technique, its application in imaging healthy young and elderly volunteers, and subjects with smoking-related lung disease. Findings that suggest this technique might provide a sensitive, non-invasive measurement of lung function will be discussed.

### 1.6.1 Development and Theory

An MR-detectable contrast agent that could be inhaled and imaged in vivo, providing high resolution functional lung images, would present an ideal alternative to standard proton MRI. In 1994, Albert and co-workers published the first-ever report showing that this was indeed possible, and reported that hyperpolarized Xenon-129 (<sup>129</sup>Xe) could be used as an inhaled contrast agent to produce MR images in an ex-vivo mouse model.<sup>176,177</sup> In order to produce these images, Albert and co-workers first faced the problem that <sup>129</sup>Xe gas on its own would not be sufficient to produce a detectable MR signal. Happer et al. had previously shown that noble gas nuclei can be hyperpolarized by optical pumping techniques; increasing the polarization of the gas, and thereby its MR detectability, by a factor of 100,000.<sup>177,178</sup> The optical pumping technique involves a glass cylinder filled with the noble gas and rubidium (Rb) vapour, which is illuminated by circularly polarized laser light.<sup>177,179</sup> The laser light is absorbed by the Rb vapour, causing high electronic polarization in the Rb atoms.<sup>179</sup> The polarized Rb atoms undergo collisions with the noble gas in the glass cell, resulting in a transfer of polarization between the atoms. This process takes 6-8 hours, and can result in polarizations of 10-25%.<sup>179</sup>



Hyperpolarized gas MRI applies specifically to the two non-radioactive noble gas isotopes with spin-1/2 nuclei;  $^3\text{He}$  and  $^{129}\text{Xe}$ . When comparing and contrasting these nuclei to select the most suitable agent for MRI use, it is noted that  $^3\text{He}$  has a gyromagnetic ratio ( $\gamma$ ) 2.7 times greater than that of  $^{129}\text{Xe}$ , and therefore yields a 2.7 times greater improvement in SNR<sup>177</sup> (given that signal scales with  $\gamma^2$  for hyperpolarized noble gas MRI<sup>180</sup>, and noise scales with  $\gamma$ ). In addition,  $^3\text{He}$  has been extensively used in the area of pulmonary function testing for the measurement of RV as well as other medical and non-medical uses<sup>181</sup>, and therefore well characterized and widely accepted as a safe agent for pulmonary imaging. For these reasons  $^3\text{He}$  has been the contrast agent of choice for much of the hyperpolarized noble gas MRI research performed to date, although supply of  $^3\text{He}$  is currently an issue.

Two years after the initial report of in vivo hyperpolarized noble gas MRI by Albert et al., the first ventilation images in humans were published.<sup>182,183</sup> Kauczor and co-workers showed homogenous signal intensity across the lungs of healthy volunteers, and regions of signal void in a subject with bronchogenic carcinoma and COPD.<sup>183</sup> Since this time, the technique has been widely applied in lung disease such as asthma<sup>184-190</sup>, cystic fibrosis<sup>191-195</sup>, and lung transplant cases.<sup>196-198</sup> Interest in this technique has grown since these first images were produced, as they provide complimentary and alternative information to standard x-ray and CT without the use of ionizing radiation. Furthermore, safety data on this method is positive as indicated in a retrospective analysis by Lutey and co-workers, who assessed the first 100 subjects (healthy and diseased) imaged using this technique at Washington University. They reported that the  $^3\text{He}$  MRI breath-hold technique had no effect on vital signs and that there was only a slight decrease in  $\text{SpO}_2$  in the first minute following breath-hold, thereby confirming the expected safety of this technique.<sup>199</sup>

Using hyperpolarized  $^3\text{He}$  MRI two different sets of images are commonly acquired; spin density images that provide high resolution functional information, and diffusion weighted images (DWI) that provide structural information. Standard spin density images produce functional images showing the location and density of  $^3\text{He}$  gas within the lung, thus yielding information on lung ventilation. The signal acquired in  $^3\text{He}$  MR

ventilation images is not always homogenous, and some regions of the lung do not fill with  $^3\text{He}$  gas at all, therefore appearing as regions of signal void. Regions of signal void are classified as ventilation defects, and are characterized as any well defined area of the lung showing no or low signal intensity compared with the remaining normal appearing ventilated lung, excluding signal loss appearing due to pulmonary vasculature, heart and mediastinum.<sup>188</sup> To date, ventilation defects have most commonly been characterized by radiologists using scoring methods<sup>187,188</sup> or by estimating the percentage of the lung occupied by ventilation defects<sup>193</sup>. One metric of quantifying lung function from  $^3\text{He}$  MRI reported in the literature is percent ventilated volume (PVV) and has been applied by the group in Sheffield.<sup>200</sup> This quantitative measurement normalizes the total volume of all reporting voxels appearing as ventilated in the  $^3\text{He}$  MR image by total volume of the thoracic cavity as determined by conventional  $^1\text{H}$  MRI.<sup>200</sup> Thus both ventilation defects and regions of signal void associated with pulmonary vasculature and other regions around the mediastinum both contribute to the PVV values of less than 100%. A study by Altes and co-workers directly compared functional images captured with  $^3\text{He}$  MRI to  $^{133}\text{Xe}$  scintigraphy using ventilation defect scoring methods. The signal from all  $^3\text{He}$  coronally acquired slices was summed for comparison purposes, and results showed that in more than 60% of the lung quadrants ventilation defects identified in both sets of images corresponded in size, conspicuity and location.<sup>201</sup> Dynamic  $^3\text{He}$  MR images have also been captured, allowing for visualization of  $^3\text{He}$  wash-in and wash-out in the lung, specifically allowing for visual assessment of airway function, although methods for quantifying these images are still under development.<sup>202-204</sup>

The second set of  $^3\text{He}$  MR images commonly acquired are DWI, which mean that in addition to high resolution functional lung images produced, the underlying structure of the lung can also be probed. Diffusion MR principles widely used in such areas as brain imaging can be applied to  $^3\text{He}$  or  $^{129}\text{Xe}$  MRI over short and long timescales, thereby allowing for the evaluation of acinar size.<sup>205-209</sup> The apparent diffusion coefficient (ADC), calculated from diffusion weighted images, is a measure of helium diffusivity (centimeters squared per second ( $\text{cm}^2/\text{s}$ )) in the lung and is highly reproducible<sup>210,211</sup>, and has been validated against histological<sup>212</sup> and CT<sup>213</sup> measurements.

### 1.6.2 Hyperpolarized $^3\text{He}$ MRI: Research Subject Studies

Static ventilation images of healthy volunteers have been acquired and evaluated at a handful of sites. Characteristically, as evident in Figure 1-10A, these images show homogenous signal throughout the lung, with a minimal number of ventilation defects observed in healthy subjects.<sup>214-216</sup> Lee and co-workers reported that ventilation defects observed in healthy volunteers were small; no larger than  $3\text{ cm}^2$ <sup>215</sup>, while Mata and co-workers reported that they occur in the posterior and anterior portions of the lung.<sup>216</sup> PVV was measured by Woodhouse et al. in middle-aged healthy volunteers (mean age = 51), and a mean PVV of 90% was reported.<sup>200</sup> Structural changes in lung microstructure occur over a lifetime in the healthy lung, and can be detected with  $^3\text{He}$  MRI. Post-natal lung development has been probed with  $^3\text{He}$  MRI, and in subjects aged four to 30 years, an increase of  $0.003\text{cm}^2/\text{s}/\text{y}$  was detected.<sup>217</sup> Once the lung reaches maturity, structural changes associated with aging occur and have been detected using  $^3\text{He}$  MRI, with results showing an annual increase in the ADC of  $0.0015\text{cm}^2/\text{s}$  for subjects between 20 and 70 years of age.<sup>218</sup>

$^3\text{He}$  MRI has been used to probe functional and structural changes in smokers with<sup>179,205,210,214,219-221</sup> and without<sup>200,222,223</sup> COPD. Subjects with COPD have an increased number of ventilation defects<sup>214</sup> as seen in Figure 1-10B, a reduced PVV<sup>200</sup>, and an increase in ADC<sup>219</sup> as compared to healthy age-matched volunteers. Kauczor et al. described the ventilation defects that occur in COPD as regions of patchy signal, or wedge shaped regions of signal void.<sup>224</sup> The ventilation defects that occur in subjects with COPD are predominantly in the upper lobes of the lung.<sup>225</sup> Measurements of PVV in smokers with and without COPD do not correlate with spirometry measurements.<sup>200</sup> Correlations have been reported between structural measurements of emphysema using  $^3\text{He}$  MRI derived ADC and  $\text{FEV}_1/\text{FVC}$ <sup>219,221</sup> and  $\text{DL}_{\text{CO}}$ .<sup>221</sup>

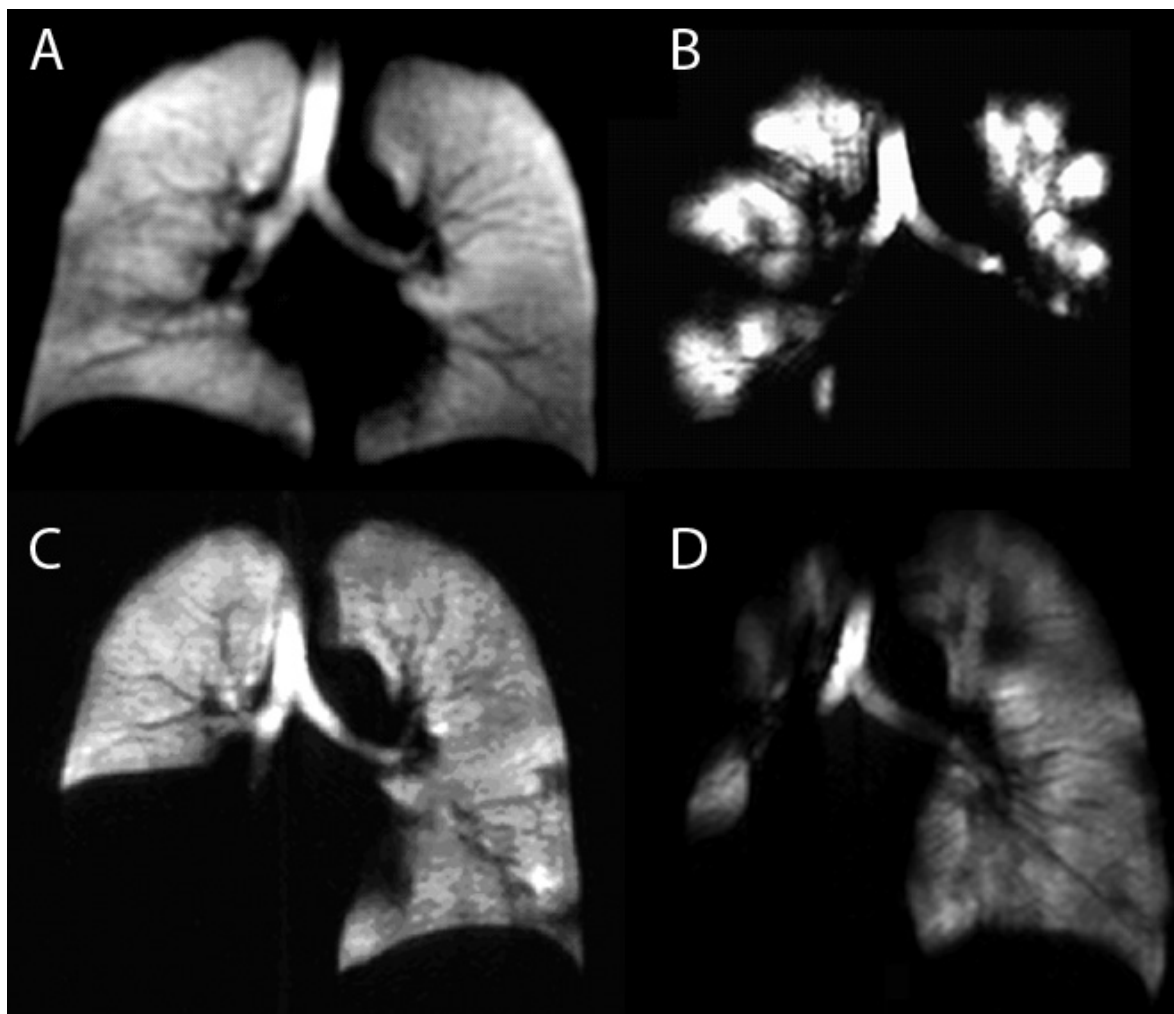


**Figure 1-10: Hyperpolarized  $^3\text{He}$  MRI in Health, COPD, Lung Cancer and RILI.**

Hyperpolarized  $^3\text{He}$  MRI are shown here for A. a young healthy volunteer, B. a subject with COPD, C. a subject with lung cancer obstructing ventilation of the right lower lobe, and D. a subject with RILI following radiation treatment for lung cancer. A homogenous signal is observed throughout the lungs in the healthy volunteer (A), while regions of signal void and heterogenous signal intensity are seen in smoking-related lung disease (B-D).

Limited clinical studies applying  $^3\text{He}$  MRI to lung cancer (Figure 1-10C) have been performed. Ireland and co-workers have shown that  $^3\text{He}$  MRI can be registered with CT scans for treatment planning purposes. This study showed, using simulated treatment plans, that both the functional and total lung volume receiving 20Gy or greater could be significantly reduced.<sup>226</sup> In a subsequent study, the same group showed that registration

accuracy of  $^3\text{He}$  MRI to CT in a group of patients with NSCLC could be improved using breath-hold CT as compared to free-breathing CT.<sup>227</sup>

## 1.7 Thesis Hypothesis and Objectives

The objective of this thesis was to develop an understanding of lung function in the context of hyperpolarized  $^3\text{He}$  MRI in healthy subjects and subjects with smoking-related lung disease, including COPD, lung cancer, and RILI. A method of quantifying ventilation defects in these images was developed, and evaluated here, in regard to its reproducibility and sensitivity in detecting disease-related changes in ventilation. The objectives and hypotheses tested in this thesis, specific to each chapter are described here.

We first evaluated the short-term reproducibility of ventilation defect volume (VDV) in both healthy subjects and subjects diagnosed with stage II and III COPD, and this is described in Chapter 2. Here we tested the hypothesis that VDV has high short-term reproducibility in healthy volunteers and COPD subjects. Eight age-matched healthy volunteers and 16 COPD subjects were evaluated twice in one day ( $7 \pm 2$  minutes) and again  $7 \pm 2$  days later using  $^3\text{He}$  MRI at 3.0 T.

We then evaluated VDV in the context of normal aging in Chapter 3, and tested the hypothesis that ventilation changes occurring with aging can be detected using quantitative measures of lung ventilation from  $^3\text{He}$  MRI. Twenty-four middle aged subjects and eight healthy elderly volunteers were imaged using  $^3\text{He}$  MRI, and VDV was used to quantify ventilation and evaluate differences between subject groups.

Chapter 4 of this thesis evaluates the potential for quantification of ventilation (ventilation defect percent (VDP)) in addition to structure (ADC) to classify subjects with COPD according to the proportion of underlying functional and structural disease. Twenty ex-smokers were evaluated at a single time point using both static ventilation imaging and diffusion-weighted imaging. We hypothesized that differences in ventilation patterns exist within subjects with COPD, and can be used for stratification purposes, and tested this hypothesis in Chapter 4.

In Chapter 5 subjects with clinically diagnosed RILI were evaluated twice within five months to evaluate functional and structural changes that occur post-RILI diagnosis. Seven subjects were scanned at baseline and four subjects returned for follow-up. Pulmonary function test data was also collected and compared to  $^3\text{He}$  MRI data. In this chapter we tested the hypothesis that lung damage occurring due to curative-intent radiation treatment results in long-term functional changes in ventilation that can be measured using  $^3\text{He}$  MRI.

The objective of Appendix A was to review the current state-of-the-art  $^3\text{He}$  MRI ventilation analysis, as described in the literature, and provide an overview of potential directions that these analysis methods might take in the future. Discussion of the current limitations and future requirements, specifically for ventilation analysis in serial or longitudinal image studies acquiring multiple  $^3\text{He}$  images from a single subject at multiple time-points, is described.

A case study of a single subject imaged twice prior to Airway Bypass, and twice following the procedure is presented in Appendix B. Here, we applied quantitative ventilation analysis to  $^3\text{He}$  images acquired over a four year period. While  $^3\text{He}$  MRI data was only available for a single subject, PFTs were also acquired at all four time-points and self-reported dyspnea scores were assessed. We hypothesized that changes in ventilation as quantified by  $^3\text{He}$  VDP would correspond to changes in mMRC.

The overarching hypothesis tested in this thesis is that VDV and VDP are sensitive measurements for evaluating differences in lung ventilation between subject groups and longitudinally. This hypothesis is tested in Chapters 2-5, in healthy volunteers and subjects with smoking-related lung disease. Chapter 6 of this thesis provides a summary of this work and highlights the conclusions drawn from these studies. New hypotheses generated based on the studies presented in this thesis are outlined in Chapter 6, and future directions for quantitative noble gas MRI ventilation analysis using VDV and VDP are described.

## 1.8 References

- (1) Chapman KR, Bourbeau J, Rance L. The burden of COPD in Canada: results from the Confronting COPD survey. *Respir Med.* 2003; 97 Suppl C:S23-S31.
- (2) Canadian Cancer Society, Statistics Canada, Public Health Agency of Canada. Canadian Cancer Statistics 2010. 2010.
- (3) Rabe KF, Hurd S, Anzueto A et al. Global strategy for the diagnosis, management, and prevention of chronic obstructive pulmonary disease: GOLD executive summary. *Am J Respir Crit Care Med.* 2007; 176(6):532-555.
- (4) Tashkin DP, Celli B, Senn S et al. A 4-year trial of tiotropium in chronic obstructive pulmonary disease. *N Engl J Med.* 2008; 359(15):1543-1554.
- (5) Calverley PM, Anderson JA, Celli B et al. Salmeterol and fluticasone propionate and survival in chronic obstructive pulmonary disease. *N Engl J Med.* 2007; 356(8):775-789.
- (6) Decramer M, Rutten-van Molken M, Dekhuijzen PN et al. Effects of N-acetylcysteine on outcomes in chronic obstructive pulmonary disease (Bronchitis Randomized on NAC Cost-Utility Study, BRONCUS): a randomised placebo-controlled trial. *Lancet.* 2005; 365(9470):1552-1560.
- (7) Pauwels RA, Lofdahl CG, Laitinen LA et al. Long-term treatment with inhaled budesonide in persons with mild chronic obstructive pulmonary disease who continue smoking. European Respiratory Society Study on Chronic Obstructive Pulmonary Disease. *N Engl J Med.* 1999; 340(25):1948-1953.
- (8) Pauwels RA, Buist AS, Calverley PM et al. Global strategy for the diagnosis, management, and prevention of chronic obstructive pulmonary disease. NHLBI/WHO Global Initiative for Chronic Obstructive Lung Disease (GOLD) Workshop summary. *Am J Respir Crit Care Med.* 2001; 163(5):1256-1276.
- (9) Beadsmoore CJ, Sreaton NJ. Classification, staging and prognosis of lung cancer. *Eur J Radiol.* 2003; 45(1):8-17.
- (10) Movsas B, Raffin TA, Epstein AH et al. Pulmonary radiation injury. *Chest.* 1997; 111(4):1061-1076.
- (11) Rodrigues G, Lock M, D'Souza D et al. Prediction of radiation pneumonitis by dose-volume histogram parameters in lung cancer--a systematic review. *Radiotherapy and Oncology.* 2004; 71(2):127-138.
- (12) Mehta V. Radiation pneumonitis and pulmonary fibrosis in non-small-cell lung cancer: Pulmonary function, prediction, and prevention. *Int J Radiat Oncol Biol Phys.* 2005; 63(1):5-24.

- (13) Jones PW, Kaplan RM. Methodological issues in evaluating measures of health as outcomes for COPD. *Eur Respir J Suppl.* 2003; 41:13s-18s.
- (14) Vestbo J, Anderson W, Coxson HO et al. Evaluation of COPD Longitudinally to Identify Predictive Surrogate End-points (ECLIPSE). *Eur Respir J.* 2008; 31(4):869-873.
- (15) Franciosi LG, Page CP, Celli BR et al. Markers of disease severity in chronic obstructive pulmonary disease. *Pulm Pharmacol Ther.* 2006; 19(3):189-199.
- (16) Reilly JJ. COPD and declining FEV1--time to divide and conquer? *N Engl J Med.* 2008; 359(15):1616-1618.
- (17) Lauralee Sherwood. *The Respiratory System. Fundamentals of Physiology.* Toronto: Thomson Nelson, 2010: 364-403.
- (18) Ward M, Macklem PT. The Act of Breathing and How It Fails. *Chest.* 1990; 97(3 Supplement):36S-39S.
- (19) Bates JHT. *Lung Mechanics: An Inverse Modeling Approach.* Cambridge University Press, 2009
- (20) Weibel ER, Gomez DM. Architecture of the Human Lung. *Science.* 1962; 137(3530):577-585.
- (21) *Respiratory Physiology. Human Physiology: The Mechanisms of Body Function.* McGraw Hill, 2004: 467-512.
- (22) Hogg JC. Pathophysiology of airflow limitation in chronic obstructive pulmonary disease. *Lancet.* 2004; 364(9435):709-721.
- (23) Sherwood L. *The Respiratory System. Fundamentals of Physiology.* Toronto: Thomson Nelson, 2006: 364-403.
- (24) Clayton N. Lung function made easy: assessing lung size. *Chron Respir Dis.* 2007; 4(3):151-157.
- (25) Light RW. Pulmonary Function Testing, Exercise Testing, and Disability Evaluation. In: George RB, editor. *Chest Medicine: Essentials of Pulmonary and Critical Care Medicine.* Lippincott Williams and Wilkins, 2005: 90-112.
- (26) Crapo RO. Pulmonary-Function Testing. *New England Journal of Medicine.* 1994; 331(1):25-30.
- (27) Standardization of Spirometry, 1994 Update. American Thoracic Society. *Am J Respir Crit Care Med.* 1995; 152(3):1107-1136.



- (28) Hancox B, Whyte K. Spirometry. Pocket Guide to Lung Function Tests. McGraw-Hill, 2006: 1-14.
- (29) Cotes JE, Chinn DJ, Miller MR. Respiratory Surveys. Lung Function: physiology, measurement and application in medicine. Wiley-Blackwell, 2006: 82-96.
- (30) Manning HL, Harver A, Mahler DA. Dyspnea in the Elderly Patient. In: Mahler DA, editor. Pulmonary Disease in the Elderly Patient. Marcel Dekker, Inc, 1993: 81-111.
- (31) Wilken LA, Joo MJ. Pulmonary Function and Related Tests. In: Lee M, editor. Basic Skills in Interpreting Laboratory Data. American Society of Health-System Pharmacists, Inc., 2009: 191-206.
- (32) Celli BR. Update on the management of COPD. *Chest*. 2008; 133(6):1451-1462.
- (33) Celli BR, Cote CG, Marin JM et al. The body-mass index, airflow obstruction, dyspnea, and exercise capacity index in chronic obstructive pulmonary disease. *N Engl J Med*. 2004; 350(10):1005-1012.
- (34) Wasserman K, Hansen JE, Sue DY et al. Exercise Testing and Interpretation: An Overview. Principles of Exercise Testing and Interpretation: Including Pathophysiology and Clinical Applications. Philadelphia: Lippincott Williams & Wilkins, 2005: 1-9.
- (35) ATS/ACCP Statement on cardiopulmonary exercise testing. *Am J Respir Crit Care Med*. 2003; 167(2):211-277.
- (36) Janssens JP, Pache JC, Nicod LP. Physiological changes in respiratory function associated with ageing. *European Respiratory Journal*. 1999; 13(1):197-205.
- (37) Wahba WM. Influence of Aging on Lung Function—Clinical Significance of Changes from Age Twenty. *Anesthesia & Analgesia*. 1983; 62(8):764-776.
- (38) Meyer KC. Aging. *Proc Am Thorac Soc*. 2005; 2(5):433-439.
- (39) Crapo RO. The Aging Lung. In: Mahler DA, editor. Pulmonary Disease in the Elderly Patient. Marcel Dekker, Inc, 1993: 1-25.
- (40) Mathur SK, Meyer KC. Lung Infections and Aging. In: Percival SL, editor. Microbiology and Aging. Humana Press, Springer, 2009: 95-112.
- (41) Sharma G, Goodwin J. Effect of aging on respiratory system physiology and immunology. *Clin Interv Aging*. 2006; 1(3):253-260.
- (42) Peterson DD, Pack AI, Silage DA et al. Effects of aging on ventilatory and occlusion pressure responses to hypoxia and hypercapnia. *Am Rev Respir Dis*. 1981; 124(4):387-391.

- (43) Fletcher C, Peto R. The natural history of chronic airflow obstruction. *British Medical Journal*. 1977; 1(6077):1645-1648.
- (44) Turner JM, Mead J, Wohl ME. Elasticity of human lungs in relation to age. *J Appl Physiol*. 1968; 25(6):664-671.
- (45) McClaran SR, Babcock MA, Pegelow DF et al. Longitudinal effects of aging on lung function at rest and exercise in healthy active fit elderly adults. *J Appl Physiol*. 1995; 78(5):1957-1968.
- (46) Stam H, Hrachovina V, Stijnen T et al. Diffusing capacity dependent on lung volume and age in normal subjects. *J Appl Physiol*. 1994; 76(6):2356-2363.
- (47) American Thoracic Society and European Respiratory Society. Standards for the Diagnosis and Management of Patients with COPD. <http://www.thoracic.org/clinical/copd-guidelines/resources/copddoc.pdf>. Accessed 13/12/2010
- (48) Halbert RJ, Isonaka S, George D et al. Interpreting COPD Prevalence Estimates\*. *Chest*. 2003; 123(5):1684-1692.
- (49) Buist AS, McBurnie MA, Vollmer WM et al. International variation in the prevalence of COPD (The BOLD Study): a population-based prevalence study. *The Lancet*. 2007; 370(9589):741-750.
- (50) Mittmann N, Kuramoto L, Seung SJ et al. The cost of moderate and severe COPD exacerbations to the Canadian healthcare system. *Respiratory Medicine*. 2008; 102(3):413-421.
- (51) Canadian Thoracic Society. The Human and Economic Burden of COPD: A Leading Cause of Hospital Admission in Canada. 2010.
- (52) Watson L, Vonk JM, L fdahl CG et al. Predictors of lung function and its decline in mild to moderate COPD in association with gender: Results from the Euroscop study. *Respiratory Medicine*. 2006; 100(4):746-753.
- (53) Hogg JC, Timens W. The pathology of chronic obstructive pulmonary disease. *Annu Rev Pathol*. 2009; 4:435-459.
- (54) Rutgers SR, Postma DS, ten Hacken NH et al. Ongoing airway inflammation in patients with COPD who Do not currently smoke. *Chest*. 2000; 117(5 Suppl 1):262S.
- (55) Retamales I, Elliott WM, Meshi B et al. Amplification of inflammation in emphysema and its association with latent adenoviral infection. *Am J Respir Crit Care Med*. 2001; 164(3):469-473.

- (56) Hogg JC, Chu F, Utokaparch S et al. The nature of small-airway obstruction in chronic obstructive pulmonary disease. *N Engl J Med.* 2004; 350(26):2645-2653.
- (57) Hogg JC. Lung structure and function in COPD. *Int J Tuberc Lung Dis.* 2008; 12(5):467-479.
- (58) Wright JL, Petty T, Thurlbeck WM. Analysis of the structure of the muscular pulmonary arteries in patients with pulmonary hypertension and COPD: National Institutes of Health nocturnal oxygen therapy trial. *Lung.* 1992; 170(2):109-124.
- (59) Celli BR. COPD: Clinical Presentation and Evaluation. In: Stockley RA, editor. *Chronic Obstructive Pulmonary Disease.* Wiley-Blackwell, 2007: 167-180.
- (60) Petty TL. Definitions, Clinical Assessments and Risk Factors. In: Petty TL, editor. *Chronic Obstructive Pulmonary Disease.* Marcel Dekker, Inc., 1985: 1-30.
- (61) Jones PW. Activity limitation and quality of life in COPD. *COPD.* 2007; 4(3):273-278.
- (62) Cote CG, Pinto-Plata V, Kasprzyk K et al. The 6-min walk distance, peak oxygen uptake, and mortality in COPD. *Chest.* 2007; 132(6):1778-1785.
- (63) Gerardi DA, Lovett L, Benoit-Connors ML et al. Variables related to increased mortality following out-patient pulmonary rehabilitation. *Eur Respir J.* 1996; 9(3):431-435.
- (64) Pinto-Plata VM, Cote C, Cabral H et al. The 6-min walk distance: change over time and value as a predictor of survival in severe COPD. *Eur Respir J.* 2004; 23(1):28-33.
- (65) Nishimura K, Izumi T, Tsukino M et al. Dyspnea is a better predictor of 5-year survival than airway obstruction in patients with COPD. *Chest.* 2002; 121(5):1434-1440.
- (66) Cote CG, Dordelly LJ, Celli BR. Impact of COPD exacerbations on patient-centered outcomes. *Chest.* 2007; 131(3):696-704.
- (67) Han MK, Agusti A, Calverley PM et al. Chronic Obstructive Pulmonary Disease Phenotypes: The Future of COPD. *Am J Respir Crit Care Med.* 2010; 182(5):598-604.
- (68) Kim WD, Ling SH, Coxson HO et al. The association between small airway obstruction and emphysema phenotypes in COPD. *Chest.* 2007; 131(5):1372-1378.
- (69) Marsh SE, Travers J, Weatherall M et al. Proportional classifications of COPD phenotypes. *Thorax.* 2008; 63(9):761-767.

- (70) Tashkin DP. Frequent exacerbations of chronic obstructive pulmonary disease--a distinct phenotype? *N Engl J Med.* 2010; 363(12):1183-1184.
- (71) Ley-Zaporozhan J, van Beek EJ. Imaging phenotypes of chronic obstructive pulmonary disease. *J Magn Reson Imaging.* 2010; 32(6):1340-1352.
- (72) Regan EA, Hokanson JE, Murphy JR et al. Genetic epidemiology of COPD (COPDGene) study design. *COPD.* 2010; 7(1):32-43.
- (73) Marchesani W. Ueber den primären bronchiekrebs. *Frankfurter Pathol.* 2010; 30:158.
- (74) The World Health Organization histological typing of lung tumours. Second edition. *Am J Clin Pathol.* 1982; 77(2):123-136.
- (75) Pretreatment evaluation of non-small-cell lung cancer. The American Thoracic Society and The European Respiratory Society. *Am J Respir Crit Care Med.* 1997; 156(1):320-332.
- (76) Chaudhuri MR. Primary pulmonary cavitating carcinomas. *Thorax.* 1973; 28(3):354-366.
- (77) Brambilla E, Travis WD, Colby TV et al. The new World Health Organization classification of lung tumours. *Eur Respir J.* 2001; 18(6):1059-1068.
- (78) Shin MS, Jackson LK, Shelton RW et al. Giant cell carcinoma of the lung. Clinical and roentgenographic manifestations. *Chest.* 1986; 89(3):366-369.
- (79) Stinchcombe TE, Socinski MA. Current treatments for advanced stage non-small cell lung cancer. *Proc Am Thorac Soc.* 2009; 6(2):233-241.
- (80) Mountain CF. Revisions in the International System for Staging Lung Cancer. *Chest.* 1997; 111(6):1710-1717.
- (81) Strauss GM. The Evolution of the Multimodality Approach to Regionally Advanced Non-small cell lung cancer. In: Weitberg AB, editor. *Cancer of the Lung.* Humana Press, Inc., 2002: 195-214.
- (82) Temel JS, Pirl WF, Lynch TJ. Comprehensive symptom management in patients with advanced-stage non-small-cell lung cancer. *Clin Lung Cancer.* 2006; 7(4):241-249.
- (83) Shannon VR. Role of pulmonary rehabilitation in the management of patients with lung cancer. *Curr Opin Pulm Med.* 2010; 16(4):334-339.
- (84) Loganathan RS, Stover DE, Shi W et al. Prevalence of COPD in women compared to men around the time of diagnosis of primary lung cancer. *Chest.* 2006; 129(5):1305-1312.

- (85) Inoue A, Kunitoh H, Sekine I et al. Radiation pneumonitis in lung cancer patients: a retrospective study of risk factors and the long-term prognosis. *International Journal of Radiation Oncology\*Biophysics*. 2001; 49(3):649-655.
- (86) Roswit B, White DC. Severe radiation injuries of the lung. *AJR Am J Roentgenol*. 1977; 129(1):127-136.
- (87) Rubin P, Casarett GW. Clinical radiation pathology as applied to curative radiotherapy. *Cancer*. 1968; 22(4):767-778.
- (88) Abratt RP, Morgan GW. Lung toxicity following chest irradiation in patients with lung cancer. *Lung Cancer*. 2002; 35(2):103-109.
- (89) Gross NJ. Pulmonary effects of radiation therapy. *Ann Intern Med*. 1977; 86(1):81-92.
- (90) Rancati T, Ceresoli GL, Gagliardi G et al. Factors predicting radiation pneumonitis in lung cancer patients: a retrospective study. *Radiotherapy and Oncology*. 2003; 67(3):275-283.
- (91) Robnett TJ, Machtay M, Vines EF et al. Factors predicting severe radiation pneumonitis in patients receiving definitive chemoradiation for lung cancer. *Int J Radiat Oncol Biol Phys*. 2000; 48(1):89-94.
- (92) Chiles C, Putnam CE. An Overview of Thoracic Imaging. In: Putnam CE, editor. *Diagnostic Imaging of the Lung*. New York: Marcel Dekker, Inc, 2010: 1-46.
- (93) The Normal Chest X-ray: An approach to interpretation. In: Joarder R, Crundwell N, editors. *Chest X-Ray in Clinical Practice*. Springer, 2009: 15-30.
- (94) Hartman TE. Basic principles of thoracic imaging. *Pulmonary Imaging*. 2007: 9-14.
- (95) Hofer M. Image Interpretation. In: Hofer M, Abanador N, editors. *The Chest X-Ray: A Systematic Teaching Atlas*. Thieme, 2007: 23-34.
- (96) Computed Tomography: Technical information. In: Joarder R, Crundwell N, editors. *Chest X-Ray in Clinical Practice*. Springer, 2009: 167-184.
- (97) Introduction to Medical Imaging. In: Bushberg JT, Seibert JA, Leidholdt EM et al, editors. *The Essential Physics of Medical Imaging*. Lippincott Williams & Wilkins, 2002: 3-15.
- (98) Ensor RE, Fleg JL, Kim YC et al. Longitudinal Chest X-ray Changes in Normal Men. *Journal of Gerontology*. 1983; 38(3):307-314.

- (99) Computed Tomography. In: Bushberg JT, Seibert JA, Leidholdt EM et al, editors. *The Essential Physics of Medical Imaging*. Lippincott Williams & Wilkins, 2002: 327-372.
- (100) McCleod TC, Muller NL. Chronic Diffuse Lung Disease. In: Putnam CE, editor. *Diagnostic Imaging of the Lung*. New York: Marcel Dekker, Inc, 1990: 443-490.
- (101) Kalra S., Levin D.L. Chronic Obstructive Pulmonary Disease. *Pulmonary Imaging*. Informa Healthcare, 2007: 135-144.
- (102) Chiles C, Putnam CE. An Overview of Thoracic Imaging. In: Putnam CE, editor. *Diagnostic Imaging of the Lung*. New York: Marcel Dekker, Inc, 1990: 1-46.
- (103) Gutman HA. Diagnostic Tools and Interacting with your Physician. *Lung Cancer and Mesothelioma*. Xlibris, 2009: 125.
- (104) Smith R, Duffy S, Brawley O. Cancer Screening and Early Detection. In: Hong WK, Bast Jr RC, Hait WN et al, editors. *Cancer Medicine*. BC Dekker, 2009: 419-445.
- (105) Haasbeek CJ, Slotman BJ, Senan S. Radiotherapy for lung cancer: clinical impact of recent technical advances. *Lung Cancer*. 2009; 64(1):1-8.
- (106) Libshitz HI, Southard ME. Complications of radiation therapy: the thorax. *Semin Roentgenol*. 1974; 9(1):41-49.
- (107) Turner MO, Mayo JR, Muller NL et al. The value of thoracic computed tomography scans in clinical diagnosis: a prospective study. *Can Respir J*. 2006; 13(6):311-316.
- (108) Coxson HO, Mayo J, Lam S et al. New and Current Clinical Imaging Techniques To Study Chronic Obstructive Pulmonary Disease. *Am J Respir Crit Care Med*. 2009.
- (109) Verschakelen JA, DeWeaver W. *Computed Tomography of the Lung: A Pattern Approach*. Springer, 2007
- (110) Guerrero T, Sanders K, Noyola-Martinez J et al. Quantification of regional ventilation from treatment planning CT. *Int J Radiat Oncol Biol Phys*. 2005; 62(3):630-634.
- (111) Guerrero T, Sanders K, Castillo E et al. Dynamic ventilation imaging from four-dimensional computed tomography. *Phys Med Biol*. 2006; 51(4):777-791.
- (112) Castillo R, Castillo E, Martinez J et al. Ventilation from four-dimensional computed tomography: density versus Jacobian methods. *Phys Med Biol*. 2010; 55(16):4661-4685.

- (113) Copley SJ, Wells AU, Hawtin KE et al. Lung Morphology in the Elderly: Comparative CT Study of Subjects over 75 Years Old versus Those under 55 Years Old1. *Radiology*. 2009; 251(2):566-573.
- (114) Well DS, Meier JM, Mahne A et al. Detection of age-related changes in thoracic structure and function by computed tomography, magnetic resonance imaging, and positron emission tomography. *Semin Nucl Med*. 2007; 37(2):103-119.
- (115) Coxson HO, Rogers RM. Quantitative computed tomography of chronic obstructive pulmonary disease. *Acad Radiol*. 2005; 12(11):1457-1463.
- (116) Bankier AA, de M, V, Keyzer C et al. Pulmonary emphysema: subjective visual grading versus objective quantification with macroscopic morphometry and thin-section CT densitometry. *Radiology*. 1999; 211(3):851-858.
- (117) Bankier AA, Madani A, Gevenois PA. CT quantification of pulmonary emphysema: assessment of lung structure and function. *Crit Rev Comput Tomogr*. 2002; 43(6):399-417.
- (118) Madani A, Van Muylem A, Gevenois PA. Pulmonary emphysema: effect of lung volume on objective quantification at thin-section CT. *Radiology*. 2010; 257(1):260-268.
- (119) Kim WJ, Silverman EK, Hoffman E et al. CT metrics of airway disease and emphysema in severe COPD. *Chest*. 2009; 136(2):396-404.
- (120) Nakano Y, Muro S, Sakai H et al. Computed tomographic measurements of airway dimensions and emphysema in smokers. Correlation with lung function. *Am J Respir Crit Care Med*. 2000; 162(3 Pt 1):1102-1108.
- (121) Nakano Y, Muller NL, King GG et al. Quantitative assessment of airway remodeling using high-resolution CT. *Chest*. 2002; 122(6 Suppl):271S-275S.
- (122) Nakano Y, Wong JC, de Jong PA et al. The prediction of small airway dimensions using computed tomography. *Am J Respir Crit Care Med*. 2005; 171(2):142-146.
- (123) Ohara T, Hirai T, Sato S et al. Longitudinal study of airway dimensions in chronic obstructive pulmonary disease using computed tomography. *Respirology*. 2008; 13(3):372-378.
- (124) Yankelevitz DF, Shaham D, Vazquez M et al. Transthoracic Needle Biopsy of Lung Nodules. In: Schoepf UJ, editor. *Multidetector-Row CT of the Thorax*. Springer, 2005: 185-202.
- (125) Mountain CF, Hermes KE. The Role of Imaging in Lung Cancer. In: Hayat MA, editor. *Cancer Imaging: Lung and breast carcinomas*. Academic Press, 2007: 163-170.

- (126) Jacobson FL. MDCT Screening for Lung Cancer: Current Controversies. In: Schoepf UJ, editor. Multidetector-Row CT of the Thorax. Springer, 2005: 145-183.
- (127) The National Lung Screening Trial: Overview and Study Design. *Radiology*. 2010.
- (128) National Cancer Institute. Lung cancer trial results show mortality benefit with low-dose CT. <http://www.cancer.gov/newscenter/pressreleases/NLSTresultsRelease>. Accessed 20/12/2010
- (129) Woodring JH, Stelling CB. Adenocarcinoma of the lung: a tumor with a changing pleomorphic character. *Am J Roentgenol*. 1983; 140(4):657-664.
- (130) Aoki T, Nakata H, Watanabe H et al. Evolution of Peripheral Lung Adenocarcinomas: CT Findings Correlated with Histology and Tumor Doubling Time. *Am J Roentgenol*. 2000; 174(3):763-768.
- (131) Senan S, De Ruyscher D, Giraud P et al. Literature-based recommendations for treatment planning and execution in high-dose radiotherapy for lung cancer. *Radiother Oncol*. 2004; 71(2):139-146.
- (132) Marks LB, Fan M, Clough R et al. Radiation-induced pulmonary injury: symptomatic versus subclinical endpoints. *Int J Radiat Biol*. 2000; 76(4):469-475.
- (133) Libshitz HI, Shuman LS. Radiation-induced pulmonary change: CT findings. *J Comput Assist Tomogr*. 1984; 8(1):15-19.
- (134) Davis SD, Yankelevitz DF, Henschke CI. Radiation effects on the lung: clinical features, pathology, and imaging findings. *AJR Am J Roentgenol*. 1992; 159(6):1157-1164.
- (135) Fennessy JJ. Irradiation damage to the lung. *J Thorac Imaging*. 1987; 2(3):68-79.
- (136) Ikezoe J, Takashima S, Morimoto S et al. CT appearance of acute radiation-induced injury in the lung. *AJR Am J Roentgenol*. 1988; 150(4):765-770.
- (137) Mah K, Poon PY, Van Dyk J et al. Assessment of acute radiation-induced pulmonary changes using computed tomography. *J Comput Assist Tomogr*. 1986; 10(5):736-743.
- (138) Bell J, McGivern D, Bullimore J et al. Diagnostic imaging of post-irradiation changes in the chest. *Clin Radiol*. 1988; 39(2):109-119.
- (139) Bajc M, Jonson B, Steinert HC. Lung. In: Biersack H-J, Freeman LM, editors. Clinical Nuclear Medicine. Springer, 2007: 118-146.



- (140) Sharp PF, Goatman KA. Nuclear Medicine Imaging. In: Sharp PF, Gemmell HG, Murray AD, editors. Practical Nuclear Medicine. Springer, 2005: 1-19.
- (141) Gemmell HG, Staff RT. Single Photon Emission Computed Tomography (SPECT). In: Sharp PF, Gemmell HG, Murray AD, editors. Practical Nuclear Medicine. Springer, 2005: 21-33.
- (142) Jogi J, Jonson B, Ekberg M et al. Ventilation-Perfusion SPECT with <sup>99m</sup>Tc-DTPA Versus Technegas: A Head-to-Head Study in Obstructive and Nonobstructive Disease. *J Nucl Med.* 2010; 51(5):735-741.
- (143) Bajc M, Neilly JB, Miniati M et al. EANM guidelines for ventilation/perfusion scintigraphy : Part 1. Pulmonary imaging with ventilation/perfusion single photon emission tomography. *Eur J Nucl Med Mol Imaging.* 2009; 36(8):1356-1370.
- (144) Gray HW. The Lung. In: Sharp PF, Gemmell HG, Murray AD, editors. Practical Nuclear Medicine. Springer, 2005: 179-204.
- (145) Harris RS, Schuster DP. Visualizing lung function with positron emission tomography. *J Appl Physiol.* 2007; 102(1):448-458.
- (146) Positron Emission Tomography. In: Cherry SR, Sorrenson JA, Phelps ME, editors. The Physics of Nuclear Medicine. Saunders, 2003.
- (147) Rhodes CG, Hughes JM. Pulmonary studies using positron emission tomography. *Eur Respir J.* 1995; 8(6):1001-1017.
- (148) Schuster DP. Assessment of Pulmonary Function by PET. In: Valk PE, Bailey DL, editors. Positron Emission Tomography: Basic Science and Clinical Practice. Springer, 2003: 465-480.
- (149) Gottschalk A, Sostman HD, Coleman RE et al. Ventilation-perfusion scintigraphy in the PIOPED study. Part II. Evaluation of the scintigraphic criteria and interpretations. *J Nucl Med.* 1993; 34(7):1119-1126.
- (150) Chapman CN, Sziklas JJ, Spencer RP et al. Pulmonary perfusion "without ventilation". *J Nucl Med.* 1983; 24(12):1149-1150.
- (151) Garg A, Gopinath PG, Pande JN et al. Role of radio-aerosol and perfusion lung imaging in early detection of chronic obstructive lung disease. *Eur J Nucl Med.* 1983; 8(4):167-171.
- (152) Brudin LH, Rhodes CG, Valind SO et al. Regional structure-function correlations in chronic obstructive lung disease measured with positron emission tomography. *Thorax.* 1992; 47(11):914-921.

- (153) Rigo P, Hustinx R, Bury T. PET and PET/CT imaging in Lung Cancer. In: Valk PE, Delbeke D, Bailey DL, editors. *Positron Emission Tomography: Clinical Practice*. Springer, 2006: 89-106.
- (154) Prato FS, Kurdyak R, Saibil EA et al. Physiological and Radiographic Assessment During the Development of Pulmonary Radiation Fibrosis. *Radiology*. 1977; 122(2):389-397.
- (155) Kocak Z, Borst GR, Zeng J et al. Prospective assessment of dosimetric/physiologic-based models for predicting radiation pneumonitis. *International Journal of Radiation Oncology\*Biological\*Physics*. 2007; 67(1):178-186.
- (156) Marks LB, Hollis D, Munley M et al. The role of lung perfusion imaging in predicting the direction of radiation-induced changes in pulmonary function tests. *Cancer*. 2000; 88(9):2135-2141.
- (157) Hassaballa HA, Cohen ES, Khan AJ et al. Positron Emission Tomography Demonstrates Radiation-Induced Changes to Nonirradiated Lungs in Lung Cancer Patients Treated With Radiation and Chemotherapy. *Chest*. 2005; 128(3):1448-1452.
- (158) Eichinger M, Tetzlaff R, Puderbach M et al. Proton magnetic resonance imaging for assessment of lung function and respiratory dynamics. *Eur J Radiol*. 2007; 64(3):329-334.
- (159) Hopkins SR, Levin DL, Emami K et al. Advances in magnetic resonance imaging of lung physiology. *J Appl Physiol*. 2007; 102(3):1244-1254.
- (160) Togao O, Tsuji R, Ohno Y et al. Ultrashort echo time (UTE) MRI of the lung: assessment of tissue density in the lung parenchyma. *Magn Reson Med*. 2010; 64(5):1491-1498.
- (161) Edelman RR, Hatabu H, Tadamura E et al. Noninvasive assessment of regional ventilation in the human lung using oxygen-enhanced magnetic resonance imaging. *Nat Med*. 1996; 2(11):1236-1239.
- (162) Chen Q, Jakob PM, Griswold MA et al. Oxygen enhanced MR ventilation imaging of the lung. *MAGMA*. 1998; 7(3):153-161.
- (163) Dietrich O. MRI of Pulmonary Ventilation. In: Kauczor HU, editor. *MRI of the Lung*. Springer, 2008: 75-90.
- (164) Loffler R, Muller CJ, Peller M et al. Optimization and evaluation of the signal intensity change in multisection oxygen-enhanced MR lung imaging. *Magn Reson Med*. 2000; 43(6):860-866.

- (165) Ohno Y, Hatabu H, Takenaka D et al. Oxygen-enhanced MR ventilation imaging of the lung: preliminary clinical experience in 25 subjects. *AJR Am J Roentgenol*. 2001; 177(1):185-194.
- (166) Ohno Y, Iwasawa T, Seo JB et al. Oxygen-enhanced magnetic resonance imaging versus computed tomography: multicenter study for clinical stage classification of smoking-related chronic obstructive pulmonary disease. *Am J Respir Crit Care Med*. 2008; 177(10):1095-1102.
- (167) Ohno Y, Hatabu H, Takenaka D et al. Dynamic oxygen-enhanced MRI reflects diffusing capacity of the lung. *Magn Reson Med*. 2002; 47(6):1139-1144.
- (168) Ley-Zaporozhan J, Ley S, Kauczor HU. Proton MRI in COPD. *COPD*. 2007; 4(1):55-65.
- (169) Bankier AA, O'Donnell CR, Mai VM et al. Impact of lung volume on MR signal intensity changes of the lung parenchyma. *J Magn Reson Imaging*. 2004; 20(6):961-966.
- (170) Bankier AA, O'Donnell CR, Mai VM et al. Impact of lung volume on MR signal intensity changes of the lung parenchyma. *J Magn Reson Imaging*. 2004; 20(6):961-966.
- (171) Iwasawa T, Takahashi H, Ogura T. Correlation of lung parenchymal MR signal intensity with pulmonary function tests and quantitative computed tomography (CT): a pilot study. *J Magn Reson Imaging*. 2007; 26:1530-1536.
- (172) Ohno Y, Koyama H, Dinkel J et al. Lung Cancer. In: Kauczor HU, editor. *MRI of the Lung*. Springer, 2009: 179-216.
- (173) Plathow C, Fink C, Sandner A et al. Comparison of relative forced expiratory volume of one second with dynamic magnetic resonance imaging parameters in healthy subjects and patients with lung cancer. *J Magn Reson Imaging*. 2005; 21(3):212-218.
- (174) Plathow C, Ley S, Fink C et al. Evaluation of chest motion and volumetry during the breathing cycle by dynamic MRI in healthy subjects: comparison with pulmonary function tests. *Invest Radiol*. 2004; 39(4):202-209.
- (175) Plathow C, Fink C, Ley S et al. Measurement of diaphragmatic length during the breathing cycle by dynamic MRI: comparison between healthy adults and patients with an intrathoracic tumor. *Eur Radiol*. 2004; 14(8):1392-1399.
- (176) Albert MS, Cates GD, Driehuys B et al. Biological magnetic resonance imaging using laser-polarized  $^{129}\text{Xe}$ . *Nature*. 1994; 370(6486):199-201.
- (177) Albert MS, Balamore D. Development of hyperpolarized noble gas MRI. *Nucl Instrum Methods Phys Res A*. 1998; 402:441-453.

- (178) Happer W, Miron E, Schaefer S et al. Polarization of the nuclear spins of noble-gas atoms by spin exchange with optically pumped alkali-metal atoms. *Phys Rev A*. 1984; 29(6):3092-3110.
- (179) de Lange EE, Mugler JP, III, Brookeman JR et al. Lung air spaces: MR imaging evaluation with hyperpolarized <sup>3</sup>He gas. *Radiology*. 1999; 210(3):851-857.
- (180) Middleton H, Black RD, Saam B et al. MR imaging with hyperpolarized <sup>3</sup>He gas. *Magn Reson Med*. 1995; 33(2):271-275.
- (181) Kauczor HU, Eberle B. Elucidation of structure-function relationships in the lung: contributions from hyperpolarized <sup>3</sup>helium MRI. *Clin Physiol Funct Imaging*. 2002; 22(6):361-369.
- (182) Ebert M, Grossmann T, Heil W et al. Nuclear magnetic resonance imaging with hyperpolarised helium-3. *Lancet*. 1996; 347(9011):1297-1299.
- (183) Kauczor HU, Hofmann D, Kreitner KF et al. Normal and abnormal pulmonary ventilation: visualization at hyperpolarized He-3 MR imaging. *Radiology*. 1996; 201(2):564-568.
- (184) Altes TA, Powers PL, Knight-Scott J et al. Hyperpolarized <sup>3</sup>He MR lung ventilation imaging in asthmatics: preliminary findings. *J Magn Reson Imaging*. 2001; 13(3):378-384.
- (185) Samee S, Altes T, Powers P et al. Imaging the lungs in asthmatic patients by using hyperpolarized helium-3 magnetic resonance: assessment of response to methacholine and exercise challenge. *J Allergy Clin Immunol*. 2003; 111(6):1205-1211.
- (186) Koumellis P, van Beek EJ, Woodhouse N et al. Quantitative analysis of regional airways obstruction using dynamic hyperpolarized <sup>3</sup>He MRI-preliminary results in children with cystic fibrosis. *J Magn Reson Imaging*. 2005; 22(3):420-426.
- (187) de Lange EE, Altes TA, Patrie JT et al. Evaluation of asthma with hyperpolarized helium-3 MRI: correlation with clinical severity and spirometry. *Chest*. 2006; 130(4):1055-1062.
- (188) de Lange EE, Altes TA, Patrie JT et al. The variability of regional airflow obstruction within the lungs of patients with asthma: assessment with hyperpolarized helium-3 magnetic resonance imaging. *J Allergy Clin Immunol*. 2007; 119(5):1072-1078.
- (189) Tzeng YS, Lutchen KR, Albert MS. The Difference in Ventilation Heterogeneity between Asthmatic and Healthy Subjects Quantified using Hyperpolarized <sup>3</sup>He MRI. *J Appl Physiol*. 2008.

- (190) Wang C, Altes TA, Mugler JP, III et al. Assessment of the lung microstructure in patients with asthma using hyperpolarized  $^3\text{He}$  diffusion MRI at two time scales: comparison with healthy subjects and patients with COPD. *J Magn Reson Imaging*. 2008; 28(1):80-88.
- (191) Donnelly LF, MacFall JR, McAdams HP et al. Cystic fibrosis: combined hyperpolarized  $^3\text{He}$ -enhanced and conventional proton MR imaging in the lung--preliminary observations. *Radiology*. 1999; 212(3):885-889.
- (192) McMahan CJ, Dodd JD, Hill C et al. Hyperpolarized  $^3\text{He}$  magnetic resonance ventilation imaging of the lung in cystic fibrosis: comparison with high resolution CT and spirometry. *Eur Radiol*. 2006; 16(11):2483-2490.
- (193) van Beek EJ, Hill C, Woodhouse N et al. Assessment of lung disease in children with cystic fibrosis using hyperpolarized  $^3\text{-Helium}$  MRI: comparison with Shwachman score, Crispin-Norman score and spirometry. *Eur Radiol*. 2007; 17(4):1018-1024.
- (194) Altes TA, Eichinger M, Puderbach M. Magnetic resonance imaging of the lung in cystic fibrosis. *Proc Am Thorac Soc*. 2007; 4(4):321-327.
- (195) Woodhouse N, Wild JM, van Beek EJR et al. Assessment of hyperpolarized  $^3\text{He}$  lung MRI for regional evaluation of interventional therapy: A pilot study in pediatric cystic fibrosis. *J Magn Reson Imaging*. 2009; 30(5):981-988.
- (196) McAdams HP, Palmer SM, Donnelly LF et al. Hyperpolarized  $^3\text{He}$ -enhanced MR imaging of lung transplant recipients: preliminary results. *AJR Am J Roentgenol*. 1999; 173(4):955-959.
- (197) Gast KK, Puderbach MU, Rodriguez I et al. Distribution of ventilation in lung transplant recipients: evaluation by dynamic  $^3\text{He}$ -MRI with lung motion correction. *Invest Radiol*. 2003; 38(6):341-348.
- (198) Zaporozhan J, Ley S, Gast KK et al. Functional analysis in single-lung transplant recipients: a comparative study of high-resolution CT,  $^3\text{He}$ -MRI, and pulmonary function tests. *Chest*. 2004; 125(1):173-181.
- (199) Lutey BA, Lefrak SS, Woods JC et al. Hyperpolarized  $^3\text{He}$  MR imaging: physiologic monitoring observations and safety considerations in 100 consecutive subjects. *Radiology*. 2008; 248(2):655-661.
- (200) Woodhouse N, Wild JM, Paley MN et al. Combined helium-3/proton magnetic resonance imaging measurement of ventilated lung volumes in smokers compared to never-smokers. *J Magn Reson Imaging*. 2005; 21(4):365-369.
- (201) Altes TA, Rehm PK, Harrell F et al. Ventilation imaging of the lung: comparison of hyperpolarized helium-3 MR imaging with Xe-133 scintigraphy. *Acad Radiol*. 2004; 11(7):729-734.

- (202) Tooker AC, Hong KS, McKinstry EL et al. Distal airways in humans: dynamic hyperpolarized  $^3\text{He}$  MR imaging--feasibility. *Radiology*. 2003; 227(2):575-579.
- (203) Dupuich D, Berthezene Y, Clouet PL et al. Dynamic  $^3\text{He}$  imaging for quantification of regional lung ventilation parameters. *Magn Reson Med*. 2003; 50(4):777-783.
- (204) Salerno M, Altes TA, Mugler JP, III et al. Hyperpolarized noble gas MR imaging of the lung: potential clinical applications. *Eur J Radiol*. 2001; 40(1):33-44.
- (205) Saam BT, Yablonskiy DA, Kodibagkar VD et al. MR imaging of diffusion of  $(^3\text{He})$  gas in healthy and diseased lungs. *Magn Reson Med*. 2000; 44(2):174-179.
- (206) Yablonskiy DA, Sukstanskii AL, Leawoods JC et al. Quantitative in vivo assessment of lung microstructure at the alveolar level with hyperpolarized  $^3\text{He}$  diffusion MRI. *Proc Natl Acad Sci U S A*. 2002; 99(5):3111-3116.
- (207) Wang C, Altes TA, Mugler JP, III et al. Assessment of the lung microstructure in patients with asthma using hyperpolarized  $^3\text{He}$  diffusion MRI at two time scales: comparison with healthy subjects and patients with COPD. *J Magn Reson Imaging*. 2008; 28(1):80-88.
- (208) Wang C, Miller GW, Altes TA et al. Time dependence of  $^3\text{He}$  diffusion in the human lung: measurement in the long-time regime using stimulated echoes. *Magn Reson Med*. 2006; 56(2):296-309.
- (209) Conradi MS, Yablonskiy DA, Woods JC et al.  $^3\text{He}$  diffusion MRI of the lung. *Acad Radiol*. 2005; 12(11):1406-1413.
- (210) Morbach AE, Gast KK, Schmiedeskamp J et al. Diffusion-weighted MRI of the lung with hyperpolarized helium-3: a study of reproducibility. *J Magn Reson Imaging*. 2005; 21(6):765-774.
- (211) Diaz S, Casselbrant I, Piitulainen E et al. Hyperpolarized  $^3\text{He}$  apparent diffusion coefficient MRI of the lung: reproducibility and volume dependency in healthy volunteers and patients with emphysema. *J Magn Reson Imaging*. 2008; 27(4):763-770.
- (212) Woods JC, Choong CK, Yablonskiy DA et al. Hyperpolarized  $^3\text{He}$  diffusion MRI and histology in pulmonary emphysema. *Magn Reson Med*. 2006; 56(6):1293-1300.
- (213) Tanoli TS, Woods JC, Conradi MS et al. In vivo lung morphometry with hyperpolarized  $^3\text{He}$  diffusion MRI in canines with induced emphysema: disease progression and comparison with computed tomography. *J Appl Physiol*. 2007; 102(1):477-484.

- (214) Parraga G, Ouriadov A, Evans A et al. Hyperpolarized  $^3\text{He}$  ventilation defects and apparent diffusion coefficients in chronic obstructive pulmonary disease: preliminary results at 3.0 Tesla. *Invest Radiol.* 2007; 42(6):384-391.
- (215) Lee EY, Sun Y, Zurakowski D et al. Hyperpolarized  $^3\text{He}$  MR imaging of the lung: normal range of ventilation defects and PFT correlation in young adults. *J Thorac Imaging.* 2009; 24(2):110-114.
- (216) Mata J, Altes T, Knake J et al. Hyperpolarized  $^3\text{He}$  MR imaging of the lung: effect of subject immobilization on the occurrence of ventilation defects. *Acad Radiol.* 2008; 15(2):260-264.
- (217) Altes TA, Mata J, de Lange EE et al. Assessment of lung development using hyperpolarized helium-3 diffusion MR imaging. *J Magn Reson Imaging.* 2006; 24(6):1277-1283.
- (218) Fain SB, Altes TA, Panth SR et al. Detection of age-dependent changes in healthy adult lungs with diffusion-weighted  $^3\text{He}$  MRI. *Acad Radiol.* 2005; 12(11):1385-1393.
- (219) Salerno M, de Lange EE, Altes TA et al. Emphysema: hyperpolarized helium 3 diffusion MR imaging of the lungs compared with spirometric indexes--initial experience. *Radiology.* 2002; 222(1):252-260.
- (220) Stavngaard T, Sogaard LV, Mortensen J et al. Hyperpolarized  $^3\text{He}$  MRI and  $^{81}\text{mKr}$  SPECT in chronic obstructive pulmonary disease. *Eur J Nucl Med Mol Imaging.* 2005; 32(4):448-457.
- (221) van Beek EJ, Dahmen AM, Stavngaard T et al. Hyperpolarised  $^3\text{-He}$  MRI vs HRCT in COPD and normal volunteers - PHIL trial. *Eur Respir J.* 2009.
- (222) Fain SB, Panth SR, Evans MD et al. Early emphysematous changes in asymptomatic smokers: detection with  $^3\text{He}$  MR imaging. *Radiology.* 2006; 239(3):875-883.
- (223) Swift AJ, Wild JM, FICHELE S et al. Emphysematous changes and normal variation in smokers and COPD patients using diffusion  $^3\text{He}$  MRI. *Eur J Radiol.* 2005; 54(3):352-358.
- (224) Kauczor HU, Ebert M, Kreitner KF et al. Imaging of the lungs using  $^3\text{He}$  MRI: preliminary clinical experience in 18 patients with and without lung disease. *J Magn Reson Imaging.* 1997; 7(3):538-543.
- (225) Gierada DS, Saam B, Yablonskiy D et al. Dynamic echo planar MR imaging of lung ventilation with hyperpolarized ( $^3\text{He}$ ) in normal subjects and patients with severe emphysema. *NMR Biomed.* 2000; 13(4):176-181.

- (226) Ireland RH, Bragg CM, McJury M et al. Feasibility of image registration and intensity-modulated radiotherapy planning with hyperpolarized helium-3 magnetic resonance imaging for non-small-cell lung cancer. *Int J Radiat Oncol Biol Phys.* 2007; 68(1):273-281.
- (227) Ireland RH, Woodhouse N, Hoggard N et al. An image acquisition and registration strategy for the fusion of hyperpolarized helium-3 MRI and x-ray CT images of the lung. *Phys Med Biol.* 2008; 53(21):6055-6063.



## CHAPTER 2: HYPERPOLARIZED $^3\text{He}$ MAGNETIC RESONANCE IMAGING OF CHRONIC OBSTRUCTIVE PULMONARY DISEASE: REPRODUCIBILITY AT 3.0 TESLA

The work presented in this chapter has been previously published in *Academic Radiology* as indicated below, and is reproduced here with permission (Appendix C).

L. Mathew, A. Evans, A. Ouriadov, R. Etemad-Rezai, R. Fogel, G. Santyr, D.G. McCormack, G. Parraga. "Hyperpolarized  $^3\text{He}$  Magnetic Resonance Imaging of Chronic Obstructive Pulmonary Disease at 3.0 Tesla: Reproducibility at 3.0 Tesla" *Acad Radiol.* 2008 Oct;15(10):1298-311

### 2.1 Introduction

Chronic obstructive pulmonary disease (COPD) is the fourth leading cause of death worldwide and continues to increase in incidence, morbidity and mortality rates, as well as direct and indirect costs.<sup>1</sup> The increasing prevalence and economic burden related to COPD is motivating the assessment of new ways to provide earlier diagnosis, better patient risk assessment, and improved patient monitoring of disease progression and treatment. While both pulmonary function tests and high resolution computed tomography (HRCT) have been well-established as non-invasive diagnostic tools and biomarkers in clinical studies of COPD, some of the limitations of these approaches are driving the development of new imaging tools that are sensitive to disease changes, that provide regional information, and that have the appropriate specificity and precision for use in clinical research.

Hyperpolarized  $^3\text{He}$  magnetic resonance imaging (MRI) has emerged as a radiological research method for the evaluation of the regional distribution of anatomical and functional lung changes associated with COPD.<sup>2-5</sup> In particular, the measurement of the  $^3\text{He}$  apparent diffusion coefficient (ADC)<sup>6</sup> has been exploited to probe the lung microstructure in patients with COPD<sup>2,3,5-7</sup> and in *ex vivo* explanted lungs.<sup>8</sup> Same-day scanning reproducibility has also been assessed.<sup>9</sup> Increases in ADC are consistent with expected increases in acinar size due to destruction of alveoli accompanying emphysema<sup>5,7,10</sup>. Furthermore, increases in ADC have been shown to correlate with histological measurements of disease<sup>11,12</sup> and also have been shown to correlate positively with age.<sup>13</sup> Parenchymal focal ventilation defects in  $^3\text{He}$  images also appear to

be sensitive to lung ventilation changes that accompany COPD.<sup>10,14-16</sup> The  $^3\text{He}$  ventilation defect score correlates with both age<sup>17</sup> and disease status providing radiologists and respirologists with a new measurement tool for clinical studies of the spatial and temporal changes in the lung that accompany COPD. The percent ventilation volume<sup>18</sup> as well as ADC measurements<sup>16</sup> derived from  $^3\text{He}$  images have been shown to be altered in otherwise asymptomatic smokers with normal pulmonary function values, suggesting that these measures are sensitive to early lung changes in smokers. Finally, safety and tolerability have been shown to be excellent across a variety of healthy and respiratory compromised patients.<sup>19,20</sup>

While these studies have assessed the sensitivity of  $^3\text{He}$  MRI to lung differences in COPD, the development of  $^3\text{He}$  MRI for clinical studies also requires the evaluation of measurement precision, which is a critical consideration for clinical study design. For example, in longitudinal clinical studies that aim to utilize  $^3\text{He}$  MRI measurements of disease, it will be critical to understand variability that can be attributed to: 1) image acquisition methods including those related to the scanner (field-strength, coils used) and subject compliance (breath-hold, motion), 2) image analysis methods that are observer-dependent or computationally driven, 3) center- or site-specific methodologies including gas delivery methods, 4) potential variability differences among different disease states including healthy age-matched control subjects, and, 5) potential physiological and/or radiological changes that occur over short periods of time. Accordingly, the goal of this study was to assess subjects with stage II and stage III COPD as well as age-matched healthy volunteers at a single center using  $^3\text{He}$  MRI at 3T and the reproducibility of  $^3\text{He}$  MRI measurements during repeated scanning visits. We present same-day and 7-day reproducibility of  $^3\text{He}$  ADC and ventilation defect volume (VDV). Reproducibility measurements also allowed for the calculation of sample sizes that may aid in the design of clinical studies of COPD utilizing  $^3\text{He}$  ADC and VDV.

## 2.2 Materials and Methods

### 2.2.1 Study Subjects

Twenty-four subjects were enrolled from the general population of the tertiary health care center as well as directly from the COPD clinics at the local three teaching hospitals. All subjects provided written informed consent to the study protocol approved by the local research ethics board and Health Canada and the study was compliant with the Personal Information Protection and Electronic Documents Act ((PIPEDA) Canada). COPD subjects required a disease diagnosis of at least one year, having had a smoking history of at least 10-pack-years and fewer than three COPD exacerbations within the last 12 months. Healthy subjects were included if they had no history of chronic respiratory disease, less than one pack-year smoking history, forced expiratory volume in 1 s ((FEV<sub>1</sub>) greater than 80% predicted, FEV<sub>1</sub> divided by the forced vital capacity (FVC) or FEV<sub>1</sub>/FVC greater than 70%, and no current diagnosis or history of cardiovascular disease. Throughout the duration of the study, COPD subjects were to be withdrawn from the study if they had experienced a COPD exacerbation or if they experienced a drop in arterial oxygen levels as monitored using pulse oximetry below 80% for 15 continuous seconds during MRI procedures. COPD and healthy subjects were categorized according to GOLD criteria.<sup>21</sup>

### 2.2.2 Study Assessments

After subjects provided written informed consent, they were screened for MRI and coil compatibility and underwent a physical exam, plethysmography and spirometry. Spirometry and plethysmography were performed in the morning after patients delayed inhaled bronchodilators and corticosteroids for approximately 12 hours as previously described.<sup>14</sup> Briefly, spirometry was performed at screening and at each MRI visit using an *ndd EasyOne* spirometer (ndd Medizintechnik AG, Zurich, CH) reporting forced expiratory volume in 1 s ((FEV<sub>1</sub>) absolute and percent predicted) and forced vital capacity (FVC). COPD subjects performed spirometry at a pre-MRI screening visit (pre- and post-bronchodilator) and were enrolled based on the post-bronchodilator FEV<sub>1</sub> measurement that was furthermore required to be within 3% of pre-bronchodilator FEV<sub>1</sub>,

which eliminated any potential subjects with underlying lung disease responsive to bronchodilators such as asthmatics. Whole body plethysmography (SensorMedics VIASYS Healthcare Inc. Yorba Linda, CA USA) was also performed at the pulmonary function laboratory at University Hospital (London Health Sciences Centre, London, Canada) for the measurement of total lung capacity (TLC), inspiratory capacity (IC) residual volume (RV), and functional residual capacity (FRC).

### **2.2.3 Safety Monitoring and Hyperpolarized $^3\text{He}$ Administration**

On both MRI visit dates, subject supine vital signs and arterial  $\text{O}_2$  levels were recorded before pre-MRI spirometry and subjects were administered a practice dose of mixed  $^4\text{He}$ -nitrogen while seated outside the scanner. Digital pulse oximetry was used to monitor arterial blood oxygenation levels during MR scanning and all breath-hold maneuvers. Hyperpolarized  $^3\text{He}$  gas was provided by a turn-key, spin-exchange polarizer system (HeliSpin<sup>TM</sup>, GEHC, Durham, NC). In a typical study this system provided 30% polarization in 12 hours. Doses (5 mL/kg) were delivered in 1 L plastic bags (Tedlar®, Jensen Inert Products, Coral Springs, FL) diluted with ultrahigh purity, medical grade nitrogen (Spectra Gases, Alpha, NJ). Polarization of the diluted dose was quantified by a polarimetry station (GEHC, Durham, NC).  $^3\text{He}$  MR scans were acquired during an inhalation breath-hold after inspiration from tidal volume of a 1L 5 ml/kg dose of  $^3\text{He}$  mixed with  $\text{N}_2$ . Post-MRI spirometry was also performed for all subjects.

### **2.2.4 Imaging**

Magnetic resonance imaging was performed on a whole body 3.0 Tesla Excite 12.0 MRI system (GEHC, Milwaukee, WI USA) with broadband imaging capability as previously described.<sup>14</sup> All helium imaging employed a whole body gradient set with maximum gradient amplitude of 19.4 mT/m and a single channel, rigid elliptical transmit/receive chest coil (RAPID Biomedical GmbH, Wuerzburg Germany). The basis frequency of the coil was 97.3 MHz and excitation power was 3.2 kW using an AMT 3T90 RF power amplifier (GEHC, Milwaukee WI USA).

The time-frame between  $^3\text{He}$  MRI scans was within  $7 \pm 2$  minutes and again  $7 \pm 2$  days later. A one-week period between scanning sessions was selected to minimize subject

inconvenience, and to model typical sources of variability stemming from the acquisition of the images over time due to technologist changes, coil positioning, subject motion and positioning changes and potential physiological changes. Repeat spirometry at the second MR visit (pre- and post-MRI) was performed to screen for exacerbations or global disease changes that may have occurred during the one-week scanning period.

$^1\text{H}$  scans were acquired prior to the  $^3\text{He}$  imaging with subjects scanned during breath-hold at the top of tidal volume using a whole body radiofrequency (RF) coil and again after  $^3\text{He}$  imaging using a 4-channel torso array coil (GEHC, Milwaukee, WI) and a fast spoiled gradient recalled echo sequence (256x256 matrix, FOV 40x 40cm, TR= 2.7, TE=1.3, flip angle=8 degrees).

$^3\text{He}$  multislice images were obtained in the coronal plane using a fast gradient-recalled echo (FGRE) method with centric k-space sampling.<sup>16</sup> Two interleaved images (TE = 3.7 ms, TR = 7.6 ms, 128 x 128, 7 slices, 30 mm slice thickness, FOV = 40cm x 40cm) without and with additional diffusion sensitization ( $G = 19.4 \text{ mT/m}$ , rise and fall time = 0.5 ms, duration = 0.46 ms,  $b$  value =  $1.6 \text{ s/cm}^2$ ) were acquired for each slice. The first image served as a map of ventilation, while the combination of the two images was used to compute ADC maps. All scanning was completed within approximately 10 minutes of first lying in the scanner.

### 2.2.5 Image Analysis

A single expert observer analyzed images for center slice ADC and another single observer analyzed images for center slice VDV. Two observers were used to minimize the potential for observer bias. The ADC images were analyzed by a single trained observer in an image visualization environment (digital copy) with room lighting levels equivalently established for all image analysis sessions. Mean ADC and ADC maps were processed using in-house software programmed in the IDL Virtual Machine platform (Research Systems Inc., Denver, CO) as previously described<sup>14</sup> with  $b = 1.6 \text{ s/cm}^2$ .

The non-diffusion weighted images were examined in the same image visualization environment by a single trained observer for analysis of ventilation defects in the center coronal slice, which was defined as the slice including the carina. Three observers, in

consensus determined the total number and location of ventilation defects at baseline scan, same-day rescan and 7-day rescan. Images were reviewed such that all three  $^3\text{He}$  images were visible on a digital workstation monitor system (consisting of identical 19 inch flat panel monitors). A ventilation defect was defined as previously described<sup>22</sup> as any well-defined area of the lung showing no signal intensity compared with the remaining ventilated lung. Areas of absent signal associated with the pulmonary vascular structures, heart, hilum and mediastinum were not considered to be ventilation defects. Ventilation defect volume was manually segmented without the aid of a quantitative signal-to-noise or spin density threshold. After scoring ventilation defects, manual segmentation of the defects was performed by a single observer (one of the three consensus observers) using the non-diffusion weighted images of the center coronal slice with the observer blinded to subject identity, disease status and scan time-point. Images were randomized (subject and scan time) and the 32 bit image slices were imported into a 3D image visualization platform developed in our laboratory<sup>23,24</sup> for MR and ultrasound applications as previously described.<sup>25</sup> Segmentation was performed using this image visualization software which also provided a method for 2-dimensional rigid image overlay or registration (of the center slice  $^1\text{H}$  image and the center slice  $^3\text{He}$  image), facilitating the manual segmentation of center-slice ventilation defect volume. Ventilation defect volume, as segmented from center slice  $^3\text{He}$  images, was computed as the area of the segmented defect multiplied by the slice thickness (30mm).

## 2.2.6 Statistical Methods

Means for ADC, ADC standard deviation of center slice and whole lung as well as ventilation defect volume of center slice were calculated. The difference in center slice ADC values and VDV between time points was computed for every subject, and the mean and standard deviations of these differences reported. Comparison of ADC and VDV means was performed using the one-way analysis of variance (ANOVA) in SPSS 14.00 (LEAD Technologies, Inc., Chicago, IL). Intraclass correlation coefficients (ICC) and Lin's concordance correlation coefficients (CCC)<sup>26</sup>, were calculated using SPSS. The ICC provides a way to quantify the reproducibility of the relative rankings of each subject's repeated scans and the CCC provides a way to show the reproducibility of both

the relative rankings and agreement of repeated scanning results. The sample size (N) required to detect specific volumetric changes or differences ( $\delta$ ) in ADC and VDV was also calculated for power  $\beta = 0.80$ , with  $\alpha = 0.05$ ; accordingly,  $Z_\alpha = 1.96$ , and  $Z_\beta = 0.80$  and N is calculated as<sup>27</sup>:

$$N = \frac{2(Z_\alpha + Z_\beta)^2 SD^2}{\delta^2}$$

## 2.3 Results

### 2.3.1 Study Subjects

Baseline demographic characteristics are provided in Table 2-1 for the 24 subjects enrolled (15 male) with very similar mean ages and age ranges for each subgroup. Mean body mass index (BMI) and BMI range for each subject subgroup was also very similar. As the COPD subjects and healthy volunteers were enrolled based upon FEV<sub>1</sub> and FEV<sub>1</sub>/FVC according to GOLD criteria<sup>21</sup>, the mean values for FEV<sub>1</sub> and FEV<sub>1</sub>/FVC for each subject subgroup reflect the GOLD criteria categorization. In addition to the expected and significantly decreased FEV<sub>1</sub> and FEV<sub>1</sub>/FVC for the COPD subgroups as compared to the healthy volunteers (p<.01), baseline FRC was also significantly increased for both COPD subject groups (p<.01) and TLC was also significantly increased for the stage III COPD subgroup (p<.001), both findings consistent with lung hyperinflation.

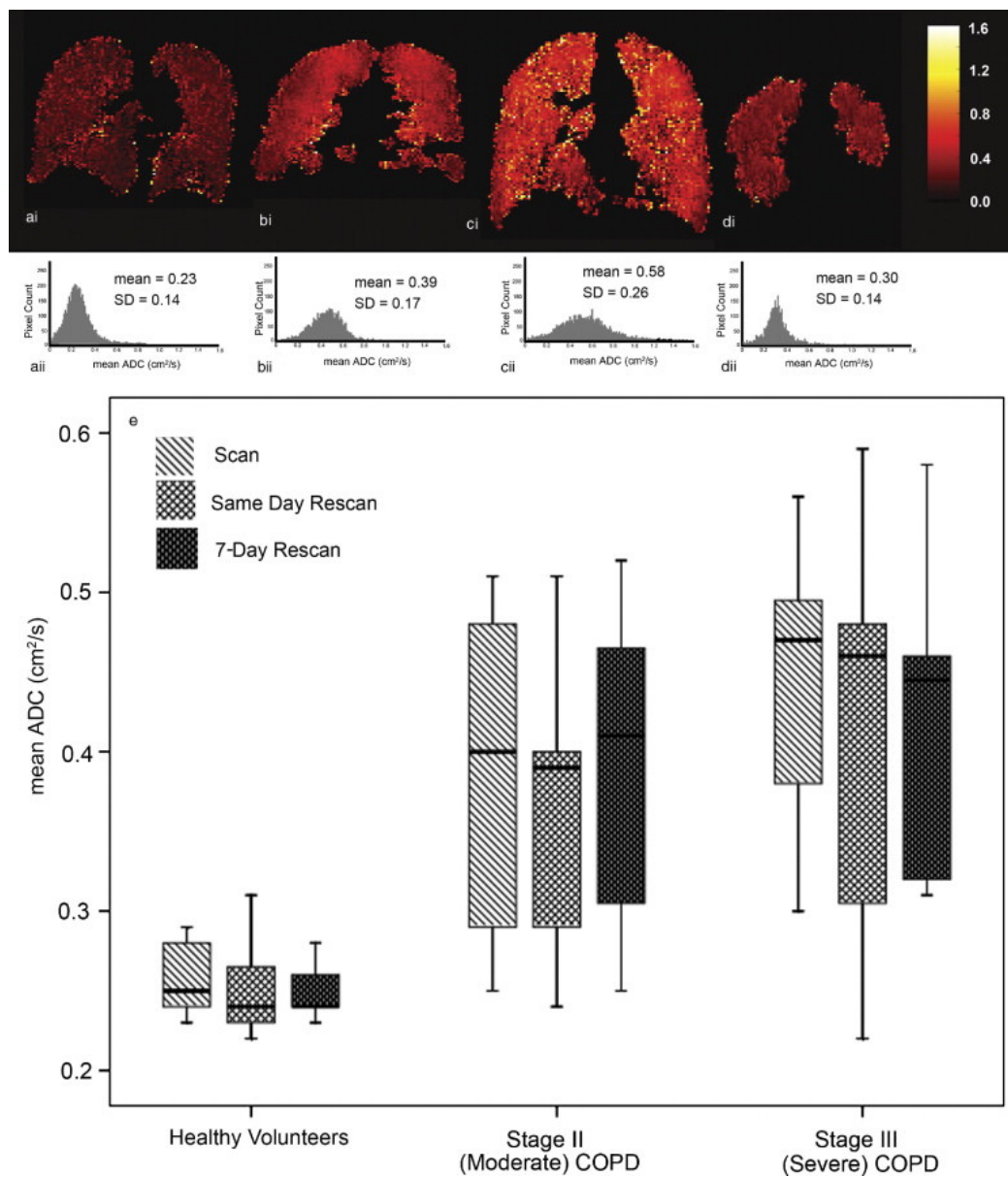


**Figure 2-1: <sup>3</sup>He Apparent Diffusion Coefficient Maps and centre slice ADC results.**

i) ADC Maps ii) Corresponding ADC Histograms

A) Healthy Volunteer (male, age = 63 yrs, FEV<sub>1</sub> = 92% predicted)

B) Stage II COPD (male, age = 72 yrs, FEV<sub>1</sub> = 62% predicted)

C) Stage III COPD (male, age = 52 yrs, FEV<sub>1</sub> = 49% predicted)

D) Stage III COPD (male, age = 72 yrs, FEV<sub>1</sub> = 49% predicted)

E) Box and Whisker plots for subject subgroups at scan, same day rescan and 7-day rescan. Boxes represent the interquartile range (25<sup>th</sup> to 75<sup>th</sup> percentile), the whiskers represent the minimum and maximum values and the solid line represents the median value. Healthy volunteers n=8 (7 at 7-day rescan), stage II COPD n=9 (8 at 7-day rescan), stage III COPD n=7 (6 at same-day rescan).



Two subjects did not return for the second MR visit: 1) a single healthy volunteer (male, age 72 years) did not return due to claustrophobia, and 2) a single subject with stage II COPD (female, age 72 years), who was hospitalized due to an exacerbation of her disease. However, both of these subjects completed both scans during their first visit, allowing for same-day reproducibility analysis. All subjects with stage III COPD returned for the second MR visit, however as previously described <sup>14</sup>, for a single subject (the first scanned at our site with stage III COPD ) the MR images for same-day rescan could not be evaluated. This was due to the subject's high respiratory rate which made the inhalation maneuver difficult. This resulted in a <sup>3</sup>He image with low SNR (<10). Thus in total 24 subjects were evaluable at baseline scan, 23 subjects at same-day rescan and 22 subjects at 7-day rescan. There was a single subject with stage II COPD who experienced three episodes of mild and transient (all < 5 seconds in duration) hypoxemia (SpO<sub>2</sub> dropped below 88%) sporadically before (once) and after (twice) MR scanning. All of these episodes resolved spontaneously, and all were asymptomatic (no clinical symptoms). The same subject experienced shoulder pain due to restriction of her shoulder in the rigid MR coil perhaps due to her size and shape (subject BMI=38). There were no other scanning- or breath-hold-related adverse events reported in the study, and no serious or severe adverse events reported related to any protocol procedure.

**Table 2-1: Subject Demographics.**

	Healthy Volunteers n=8	Stage II COPD n=9	Stage III COPD n=7
Age yrs (±SD) [range]	67 (6) [58-74]	68 (6) [59-74]	67 (8) [52-75]
Male Sex	5	4	6
Body Mass Index (±SD) [range]	27 (4) [24-35]	28 (5) [21-38]	27 (4) [22-34]
FEV <sub>1</sub> %* (±SD)	106 (19)	63 (8)**	42 (7)**
FEV <sub>1</sub> /FVC % (±SD)	77 (5)	54 (11)**	38 (10)**
IC %* (±SD)	111 (16)	99 (18)	78 (17)
RV %* (±SD)	97 (10)	142 (20)	188 (55)
FRC %* (±SD)	95 (14)	116 (14)**	152 (37)**
TLC %* (±SD)	104 (19)	108 (9)	115(23)***

\*Percent predicted, FEV<sub>1</sub> = Forced Expiratory Volume in 1s, FVC= Forced Vital Capacity  
FRC= Functional Residual Capacity, TLC= Total Lung Capacity

\*\*significantly different than healthy volunteers (p<0.01), \*\*\* significantly different than healthy volunteers (p<0.001)

### 2.3.2 $^3\text{He}$ MRI Measurements

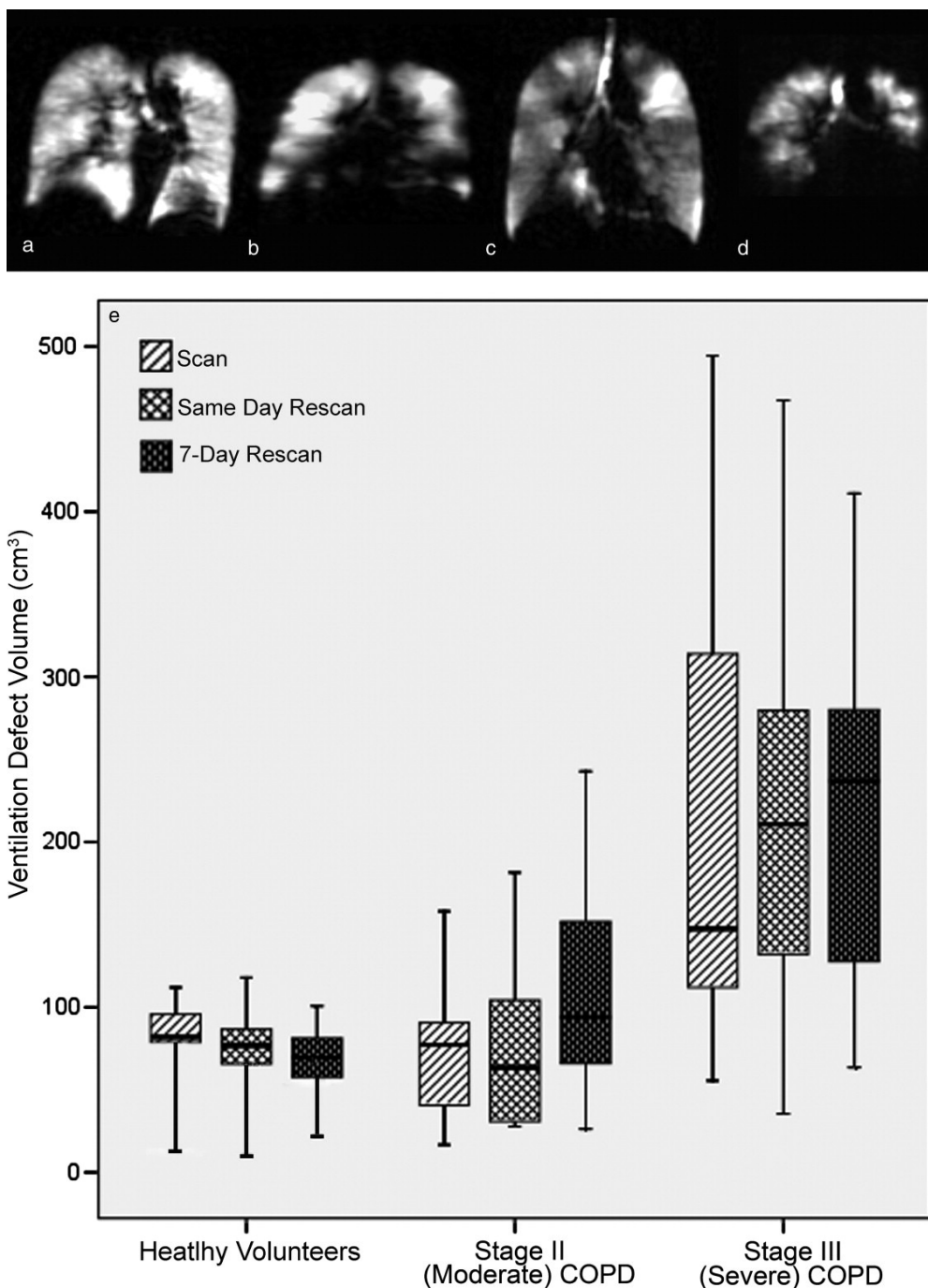
Representative center slice ADC maps and corresponding ADC histograms are provided for a healthy volunteer (Figure 2-1A), a subject with stage II COPD (Figure 2-1B) and two subjects with stage III COPD, (Figure 2-1C and 2-1D). Mean ADC and mean ADC standard deviations (SD) for all the representative subjects is provided in Figure 2-1(ii) and in Figure 2-1E, a box and whisker plot shows the mean center slice ADC values for each subgroup and scan time point (Scan, same day rescan and 7-day rescan). In Figure 2-2, the non-diffusion-weighted images of the diffusion-weighted pair are provided for the same representative subjects (Figures 2-2A-D). In Figure 2-2E, a box and whisker plot shows the mean center slice VDV values for each subgroup and scan time point (scan, same day rescan and 7-day rescan).

Table 2-2 shows mean whole lung ADC, whole lung SD, center slice ADC, center slice SD as well as center slice VDV for all subgroups and scan time-points. The difference in both whole lung and center slice mean ADC between healthy volunteers and subjects with stage II COPD was significant ( $p < .05$ ) as was the difference between healthy volunteers and subjects with stage III COPD ( $p < .01$ ) at all time points. There was no significant difference for whole lung ADC SD between any subject subgroup at any time-point but there was a significant difference for center slice ADC SD between subjects with stage III COPD and healthy volunteers and subjects with stage II COPD ( $p < .01$ ) at all time-points. For mean ventilation defect volume, there was no significant difference between healthy volunteers and subjects with stage II COPD at any time point. However, there was a significant difference between subject with stage III COPD and both healthy volunteers and subjects with stage II COPD ( $p < .01$ ) at all time-points.

**Table 2-2: Same day and 7-day Rescan ADC and VDV Measurements.**

	Healthy Volunteers n=8	Stage II COPD n=9	Stage III COPD n=7
Whole Lung Mean ADC ( $\pm$ SD) $\text{cm}^2/\text{s}$			
Scan	0.27 (0.02)	0.38 (0.09)	0.44 (0.09)
Same-day Rescan	0.26 (0.02)	0.36 (0.09)	0.42 (0.09)*
7-day Rescan	0.26 (0.02)**	0.39 (0.08)***	0.43 (0.09)
Whole Lung ADC SD ( $\pm$ SD) $\text{cm}^2/\text{s}$			
Scan	0.18 (0.03)	0.24 (0.07)	0.24 (0.04)
Same-day Rescan	0.19 (0.05)	0.22 (0.08)	0.24 (0.04)*
7-day Rescan	0.16 (0.02)**	0.25 (0.08)***	0.24 (0.04)
Center Slice Mean ADC ( $\pm$ SD) $\text{cm}^2/\text{s}$			
Scan	0.26 (0.02)	0.38 (0.10)	0.47 (0.10)
Same-day Rescan	0.25 (0.03)	0.36 (0.09)	0.46 (0.11)*
7-day Rescan	0.24 (0.02)**	0.39 (0.10)***	0.46 (0.10)
Center Slice ADC SD ( $\pm$ SD) $\text{cm}^2/\text{s}$			
Scan	0.15 (0.03)	0.19 (0.06)	0.26 (0.07)
Same-day Rescan	0.14 (0.04)	0.15 (0.03)	0.24 (0.06)*
7-day Rescan	0.12 (0.03)**	0.19 (0.04)***	0.29 (0.15)
Center Slice Ventilation Defect Volume ( $\pm$ SD) $\text{cm}^3$			
Scan	80 (30)	70 (40)	220 (160)
Same-day Rescan	70 (30)	80 (50)	220 (150)*
7-day Rescan	70 (30)**	110 (70)***	220 (110)

\*(n=6) \*\*(n=7) \*\*\*(n=8)



**Figure 2-2:  $^3\text{He}$  MR Ventilation Images and Ventilation Defect Volume (VDV) Results.**

- A) Healthy Volunteer (male, age = 63 yrs,  $\text{FEV}_1 = 92\%$  predicted)  
 B) Stage II COPD (male, age = 72 yrs,  $\text{FEV}_1 = 62\%$  predicted)  
 C) Stage III COPD (male, age = 52 yrs,  $\text{FEV}_1 = 49\%$  predicted)  
 D) Stage III COPD (male, age = 72 yrs,  $\text{FEV}_1 = 49\%$  predicted)  
 E) Box and Whisker plot for mean VDV for subject subgroups at scan, same day rescan and 7-day Rescan. Boxes represent the interquartile range (25<sup>th</sup> to 75<sup>th</sup> percentile), the whiskers represent the minimum and maximum values and the solid line represents the median value.

### 2.3.3 <sup>3</sup>He Measurement Reproducibility

As a reference for the measurement of <sup>3</sup>He MRI reproducibility, repeated spirometry at the second scanning visit showed no change for any subject or subject subgroup in FEV<sub>1</sub> or FEV<sub>1</sub>/FVC within the 7 ± 2 days rescan period. Scan-rescan <sup>3</sup>He MRI reproducibility was assessed using linear regression as shown in Figure 2-3 as well as the ICC and CCC as shown in Table 2-3. In Figure 2-3, same-day ( $R^2 = 0.934$ ) and 7-day rescan ( $R^2 = 0.960$ ) linear regression for center slice ADC was high and not significantly different and furthermore not significantly different from same-day rescan mean VDV ( $R^2 = 0.941$ ). 7-day rescan VDV was lower and significantly different ( $R^2 = 0.576$ ,  $p < .001$ ). The corresponding Pearson correlations were also high for same-day and 7-day rescan mean ADC ( $r = 0.959$  and  $r = 0.980$  respectively) as well as same-day rescan mean VDV ( $r = 0.970$ ) with 7-day rescan mean VDV somewhat lower ( $r = 0.759$ ).

Table 2-3 provides a comparison of same-day and 7-day ICC and CCC for FEV<sub>1</sub>, center slice ADC and center slice VDV. ICC and CCC were both high for FEV<sub>1</sub> and not significantly different for same-day and 7-day repeated spirometry, or between subject subgroups. Center slice mean ADC for all subjects pooled together was highly reproducible for both same-day and 7-day rescan (ICC and CCC 0.96 and 0.98 respectively). When reproducibility of mean ADC is considered for subject subgroups, ICC and CCC was highest for subjects with stage III COPD. For center slice VDV, ICC and CCC were high for same-day rescan for all subject subgroups and for all subjects pooled together (ICC and CCC 0.97 and 0.98 respectively) and not significantly different from same-day ADC reproducibility. However, 7-day rescan ICC and CCC was significantly lower ( $p < .01$ ) than same-day rescan for all subject subgroups and for all subjects pooled together.

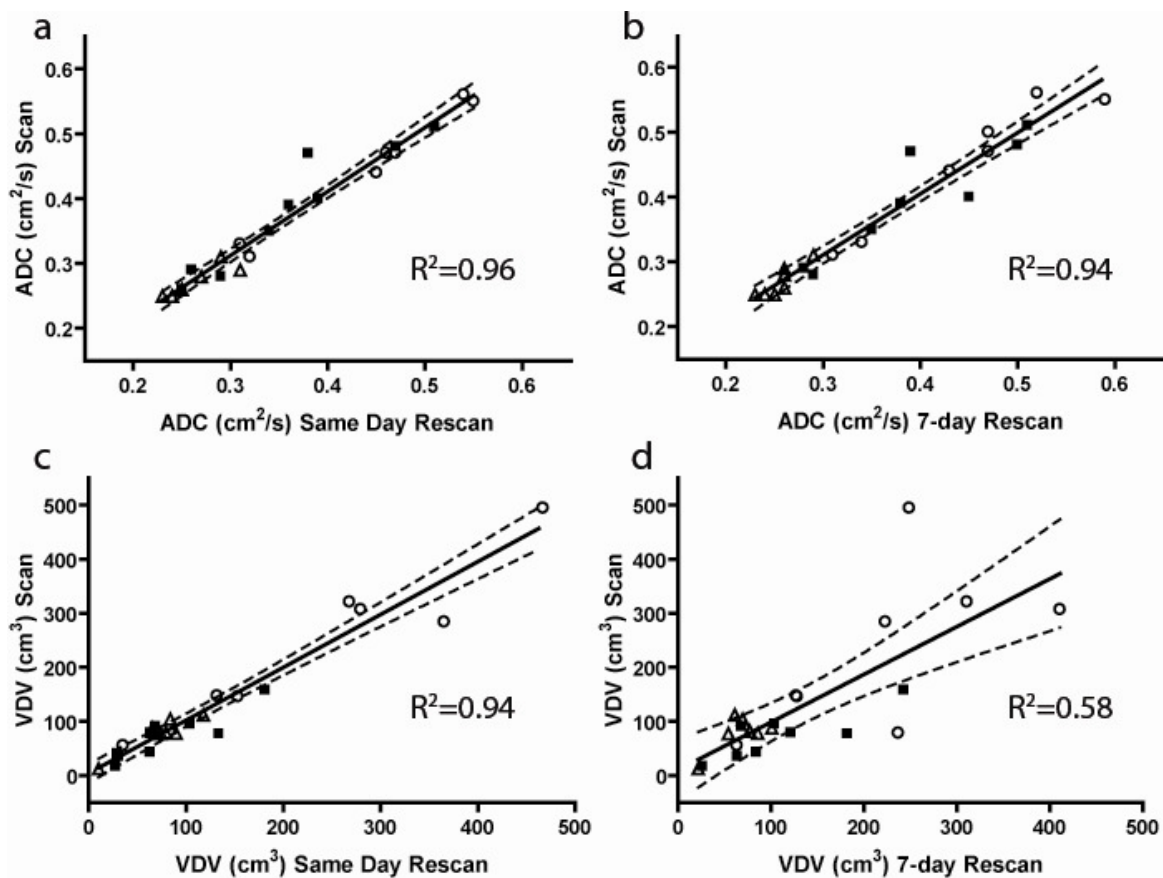
In Figure 2-4, <sup>3</sup>He images are provided to show visual evidence of the location, number and size of ventilation defects at scan (Figure 2-4i) same-day rescan (Figure 2-4ii) and 7-day rescan (Figure 2-4iii). In Figure 2-4A and 2-4B, <sup>3</sup>He images for two representative healthy volunteers are shown, in Figure 2-4C and Figure 2-4D, <sup>3</sup>He images for two representative subjects with stage II COPD and in Figures 2-4E and 2-4F, <sup>3</sup>He images for two representative subjects with stage III COPD are provided.

Table 2-4 provides sample sizes that would be required to measure ADC and VDV ( $\alpha = 0.05$ ,  $\beta = 0.80$ ) derived from the observed 7-day rescan differences. The 7-day rescan differences were selected because they provide the most conservative estimate (based on the fact that variability is higher at 7-days) and because for clinical trials designed to detect disease changes, repeated scans over longer periods of time would be utilized. The sample size required to measure a 1% / 5% / 10% change in ADC in healthy volunteers (0.0025 / 0.0125 / 0.025 cm<sup>2</sup>/s, respectively) was 975 / 39 / 10 subjects, and in subjects with stage III COPD (0.0047 / 0.0235 / 0.047 cm<sup>2</sup>/s) this was reduced to 69 / 3 / 1 subjects. Sample sizes calculated related to the use of VDV as an intermediate endpoint required to measure a 5% to 10% change would be 331 to 83 healthy volunteers, 882-220 subjects with stage II COPD and 1089-272 subjects with stage III COPD.

**Table 2-3: Scan-Rescan Reproducibility.**

	Healthy Volunteers n=8		Stage II COPD n=9		Stage III COPD n=7		All Subjects n= 24	
	ICC	CCC	ICC	CCC	ICC	CCC	ICC	CCC
Center Slice Mean ADC (cm <sup>2</sup> /s)								
Same day Rescan	0.83	0.85	0.91	0.91	0.98	0.93	0.96	0.96
7-day Rescan	0.17	0.24	0.97	0.96	0.99	0.98	0.98	0.98
Center Slice VDV (cm <sup>3</sup> )								
Same day Rescan	0.91	0.90	0.94	0.94	0.96	0.96	0.97	0.98
7-day Rescan	0.56	0.57	0.59	0.62	0.63	0.58	0.74	0.75
FEV <sub>1</sub> (%predicted)								
Same Day Spirometry	0.98	0.98	0.97	0.97	0.94	0.94	0.99	0.99
7-day Spirometry	0.99	0.99	0.94	0.94	0.97	0.96	0.99	0.99

ICC is Intraclass Correlation Coefficient and CCC is Lin's Concordance Correlation Coefficient. Correlation coefficients represent reproducibility between baseline scan and either same-day rescan or 7-day rescan.



**Figure 2-3: Center Slice ADC and VDV Reproducibility.**

Hollow triangles represent healthy volunteers, solid squares represent subjects with stage II COPD, and hollow circles represent subjects with stage III COPD. Dashed line represents 95% confidence interval of regression (solid line).

A. Scan - Same day Rescan ADC linear regression:  $y = 0.99x + 0.016$  ( $p < .001$ ) Pearson  $r = 0.96$

B. Scan - 7-day Rescan ADC linear regression:  $y = 0.94x + 0.028$  ( $p < .001$ ) Pearson  $r = 0.97$

C. Scan - Same-day Rescan VDV linear regression:  $y = 0.98x + 4.12$  ( $p < .001$ ) Pearson  $r = 0.97$

D. Scan - 7-day Rescan VDV. Linear regression:  $y = 0.88x + 9.94$  ( $p < .001$ ) Pearson  $r = 0.76$

ADC:  $R^2$  Same Day Rescan versus  $R^2$  7-day Rescan,  $p = \text{NS}$

VDV:  $R^2$  Same Day Rescan versus  $R^2$  7-day Rescan,  $p < 0.001$

ADC and VDV: ADC  $R^2$  Same Day Rescan vs. VDV  $R^2$  Same Day Rescan :  $p = \text{NS}$

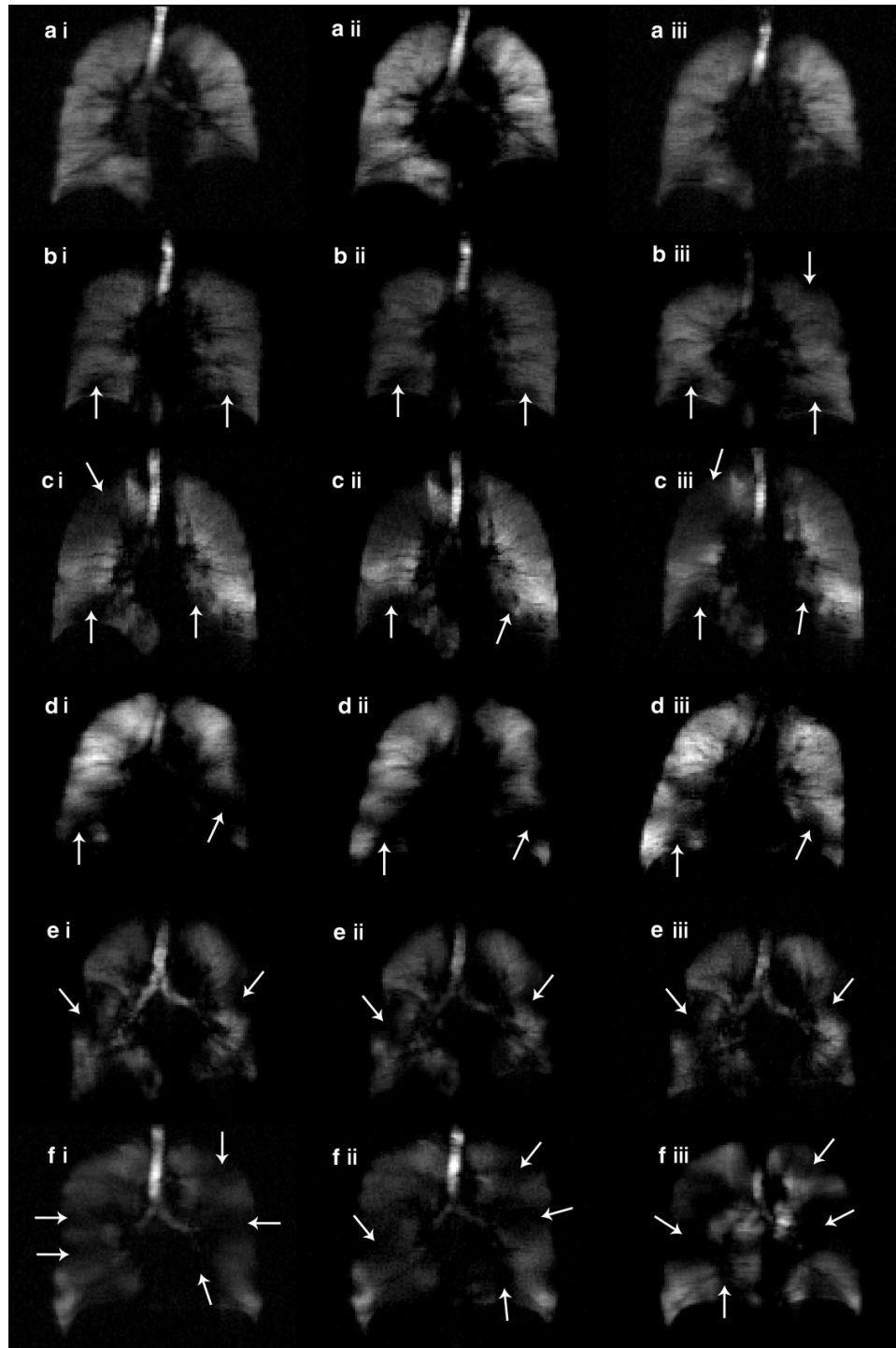


**Figure 2-4: Center Slice  $^3\text{He}$  VDV Reproducibility**

A) and B) Healthy volunteers at Scan (i), Same-day Rescan (ii) and 7-day Rescan (iii)

C) and D) Subjects with Stage II COPD at Scan (i), Same-day Rescan (ii) and 7-day Rescan (iii)

E) and F) Subjects with Stage III COPD at Scan (i), Same-day Rescan (ii) and 7-day Rescan (iii).



**Table 2-4:  $^3\text{He}$  ADC and VDV Sample Size Calculations.**

	Healthy Volunteers n= 8	Stage II COPD n= 9	Stage III COPD n= 7
<b><i>ADC (Center Slice)</i></b>			
Seven Day (N)	7	8	7
Mean (BL and 7-day) $\text{cm}^2/\text{s}$	0.25	0.39	0.47
Difference ( $\text{SD}_{\text{diff}}$ ) $\text{cm}^2/\text{s}$	0.02	0.01	0.01
Sample Size 1%/5%/10% change (n)	975 / 39 / 10	100 / 4 / 1	69 / 3 / 1
<b><i>VDV (Center Slice)</i></b>			
Seven Day (N)	7	8	7
Mean (BL and 7-day) $\text{cm}^3$	73	92	220
$\text{SD}_{\text{diff}}$ $\text{cm}^3$	17	35	93
Sample Size 5%/10% change (n)	331 / 83	882 / 220	1089 / 272

## 2.4 Discussion

In order to assess the feasibility of  $^3\text{He}$  MRI at 3T for use in clinical research studies of COPD, we prospectively assessed 24 age-matched subjects, including 15 subjects with stage II or stage III COPD. We directly assessed and compared same-day and 7-day measurements of  $^3\text{He}$  MRI ADC and  $^3\text{He}$  ventilation defect volume. Here we provide the quantitative results of this study performed at 3T and show: 1) high reproducibility of  $^3\text{He}$  ADC that was not significantly different between same-day rescan and 7-day rescan, 2) high reproducibility of  $^3\text{He}$  VDV that was significantly higher at same-day rescan as compared to 7-day rescan, 3) significant differences in  $^3\text{He}$  ADC between healthy subjects and those with COPD, and, 4) significant differences in  $^3\text{He}$  center slice VDV between subjects with stage III COPD and those subjects with stage II COPD and healthy volunteers.

The study was designed primarily to assess the reproducibility of these measurements at 3T and to compare measurement precision by assessing repeated scanning measurements over a few minutes and over a one week period. It is worth noting that repeated spirometry at the second scanning visit also showed no change for any subject or subject subgroup in  $\text{FEV}_1$  or  $\text{FEV}_1/\text{FVC}$ , suggesting that no global changes in respiratory

function had occurred during this time-frame. For ADC, same-day reproducibility measured using linear regression ( $R^2 = 0.934$ ), ICC and CCC was high (as previously reported<sup>9</sup>) and similar to 7-day rescan measurements of ADC reproducibility and also to same-day rescan mean VDV ( $R^2 = 0.941$ ), suggesting that these measurements are not sensitive to changes in subject positioning or any scanner-coil interactions that might change over short periods of time. However, 7-day rescan reproducibility for VDV was lower and significantly different ( $R^2 = 0.576$ ,  $p < .001$ ). Some explanation for this may be derived from the fact that the measurement of VDV itself was performed by manual segmentation and center slice VDV was represented by very small volumes in the healthy volunteers and stage II subjects. Accordingly, the differences in VDV measured at same-day rescan and 7-day rescan as shown in Figure 2-4 were not large, with the majority of defects having the same location and similar size in all scans. Nevertheless, the possibility exists that the differences measured, though small, were due to physiological changes that occurred over a one week period. This would suggest that VDV sensitively quantified ventilation changes resultant from airway narrowing or closure that occurred without changes in global disease measurements such as  $FEV_1$  and  $FEV_1/FVC$  or in the  $^3\text{He}$  ADC measurements. In addition it suggests that it is possible to measure physiological changes that occur over short periods of time in some subjects and such changes cannot be detected by spirometry. Sample sizes required to measure changes in ADC and in VDV over time reflected the increased variability of the VDV measurement as compared to ADC. It is difficult to provide an appropriate context for the potential changes in ADC and VDV that may occur over time as a function of disease progression, normal aging processes or COPD exacerbations. The sample size calculations may be viewed as a guide to assist in the design of studies sensitive to morphological changes in the lung parenchyma or airways using ADC, or studies sensitive to dynamic processes using VDV such as those aimed at assessing ventilation changes that are dependent on airway patency to provide gas into the lung parenchyma. Thus, overall, if direct measurement of airway or alveolar size changes is required, a smaller group of subjects would be adequate, whereas precise measurement of more dynamic processes such as those involving mucus plugging and other ventilation changes would require a larger patient group.

In this study we made a number of other observations that are relevant to the potential clinical research use of  $^3\text{He}$  MRI. First, the use of  $^3\text{He}$  MRI at 3T in elderly healthy volunteers and subjects with stage II and stage III COPD was well-tolerated. In total we assessed repeated scanning in 24 subjects (15 scans in eight healthy volunteers and 31 scans in 16 subjects with COPD) and only a single subject (with stage II COPD and BMI 38) reported mild and transient hypoxemia with complete recovery in 5s and without clinical symptoms. This finding, along with previously reported work at other sites and field strengths<sup>19,20,28</sup>, supports the use of  $^3\text{He}$  MRI at 3T in longitudinal studies of older subjects -even those with significant respiratory compromise.

We also noted the difference in mean ADC and VDV between subject subgroups which is a measure of  $^3\text{He}$  MRI sensitivity. Mean ADC differences existed between healthy volunteers and subjects with stage II ( $p<.05$ ) and stage III COPD ( $p<.01$ ), but not between subjects with stage III COPD and those with milder disease. While the mean ADC for stage III COPD subjects was in fact greater, a larger SD for this population likely resulted in the difference being not statistically significant. However, the inherent advantage of quantitative imaging is that each image voxel represents a quantitative measure of disease; the reduction of all voxels to a whole lung mean or center slice mean effectively masks any of the regional differences between subjects and subject subgroups. In other words, although differences were not detected using whole lung and center slice mean values, regional analysis<sup>30</sup> may well show differences between subject subgroups even with small sample sizes. ADC SD, which is a measure of the variability of the ADC measurement over the region of interest assessed (center coronal slice), also significantly differed ( $p<.01$ ) between subjects with stage III COPD and the healthy volunteers and subjects with less severe disease. This suggests that the stage III COPD subgroup has higher ADC heterogeneity within the region of interest assessed which has also been previously reported.<sup>9</sup> For mean VDV, there was no significant difference between healthy volunteers and subjects with stage II COPD at any time point. However, there was a significant difference between subjects with stage III COPD and both healthy volunteers and subjects with stage II COPD ( $p<.01$ ) at all time-points. The finding of reproducible ventilation defects (no difference in VDV between visits according to ANOVA results) in the healthy elderly subgroup was not anticipated and suggests caution

must be used in interpreting results from  $^3\text{He}$  studies of elderly subjects with underlying disease. This finding also underscores the value of including a healthy elderly volunteer control group as in this study and those planned in future that utilize  $^3\text{He}$  MRI in studies of older COPD subjects. Perhaps as part of the normal aging processes in the lung, non-random airway narrowing occurs even in the absence of known or detectable respiratory or cardiovascular disease, which may account for the VDV results shown here in healthy elderly subjects.

The primary limitation of this study is the small sample size of each of the subgroups, which may have limited the power to detect ADC differences between the stage II and stage III COPD subject subgroups and to detect VDV differences between the healthy volunteers and subjects with stage II COPD. Another limitation of this study was the fact that we did not prospectively acquire  $^1\text{H}$  and  $^3\text{He}$  images with the same breath-hold thoracic volumes (using the methods previously described by van Beek and co-workers<sup>18</sup>). Hence for the majority of subjects at each time point,  $^1\text{H}$  and  $^3\text{He}$  thoracic image volumes were not well-matched, so that a reproducibility analysis of percent ventilation volume as previously developed by van Beek<sup>18</sup> was not possible in this study. Nevertheless, in spite of the fact that the  $^3\text{He}$  and  $^1\text{H}$  images were acquired under similar, but not exactly the same breath-hold volume, we were able to calculate percent ventilated volume for 18 subjects who had well-matched  $^1\text{H}$  and  $^3\text{He}$  volumes for same-day rescans (as assessed by a radiologist who visually compared the  $^3\text{He}$  and  $^1\text{H}$  image slices) using manual segmentation of ventilated volumes.<sup>29</sup> Elderly healthy volunteers (n=5) exhibited  $94\pm 20\%$  ventilation volume, whereas subjects with stage II COPD (n=6) showed  $77\pm 19\%$  ventilation volume and subjects with stage III COPD (n=7) had  $68\pm 14\%$  ventilation volume, which is in good agreement with results of a previous study in COPD.<sup>18</sup> Although we could not assess reproducibility of percent ventilation volume in this study, the percent ventilation volume result for a subset of patients at a single time point using manual segmentation suggests that this is a robust measurement that may provide valuable measurement of airway disease in longitudinal studies. In addition, because  $^1\text{H}$  and  $^3\text{He}$  images were not acquired with exactly matching breath-holds and very different slice thickness, we limited the analysis of defect volume reproducibility to the center coronal slice where the edge of the thoracic cavity and ventilation defects were most

easily discerned. Hence in this study, center coronal slice VDV represented the area of ventilation defect for the center slice which was then multiplied by the 30 mm slice thickness reflecting contributions from the entire slice. Because of the rather thick slices used, VDV as measured in this study, though precise, provides only an estimate of the true ventilation defect volume. The use of thinner slices and 3D imaging approaches will allow for an estimate of ventilation defect volume that is likely more accurate. Another shortcoming of the study design was related to the fact that repeated scanning visits were prospectively designed to assess the reproducibility of the  $^3\text{He}$  ADC. For ventilation defect volume quantification we utilized the first of the interleaved diffusion-weighted pair of images (typically acquired for ADC calculation) which has intrinsically lower signal-to-noise ratio than do  $^3\text{He}$  spin density (ventilation) images. Despite this, one of the major advantages of our approach is that a single patient breath-hold can be used to assess both ADC value contributions from the ventilated lung and VDV contributions from those areas of the lung that are not ventilated. The pragmatic use of a single breath-hold imaging session results in an increased subject convenience and tolerability and decreases cost and time for the subject scan, which are important considerations for clinical studies aimed at assessing new treatments as well as longitudinal studies.

During progressive COPD, it is believed that adaptive remodeling of the lung and thoracic gross anatomy such as the diaphragm, muscles and skeleton occurs to accommodate the microscopic remodeling of the airways and airspaces. Clinical research studies of COPD continue to focus on spirometric measurement of  $\text{FEV}_1$ , and in some cases high resolution or multi-detector x-ray CT methods to assess novel interventions and disease progression. The results of the current study suggest that  $^3\text{He}$  MRI at 3T provides another radiological tool for the assessment of both airway and airspace changes in COPD with sufficient precision for clinical research studies. Moreover, the method also provides a relatively rapid and safe method of visualizing and quantifying both spatial and temporal lung structural and functional dynamics related to disease progression or concomitant with novel treatments.

## 2.5 Conclusion

In this study of a relatively small group of elderly healthy volunteers and subjects with stage II and stage III COPD, both  $^3\text{He}$  MRI ADC and VDV measurements were highly reproducible in repeated scans within a few minutes.  $^3\text{He}$  MRI ADC also showed high reproducibility at 7-day rescan and  $^3\text{He}$  MRI VDV was significantly less reproducible in 7-day rescan visits, providing evidence of spatial and temporal changes in ventilation defect size over the seven day rescan period. In healthy age-matched elderly subjects,  $^3\text{He}$  MRI ADC was significantly different as compared to subjects with stage II COPD whereas  $^3\text{He}$  MRI VDV was significantly different between subjects with stage III COPD and those without disease or with stage II COPD.

## 2.6 References

- (1) National Heart Lung and Blood Institute. Chronic Obstructive Pulmonary Disease. Morbidity and Mortality: 2002 Chartbook on Cardiovascular, Lung and Blood Diseases. Bethesda: Department of Health and Human Services, 2002.
- (2) de Lange EE, Mugler JP, III, Brookeman JR et al. Lung air spaces: MR imaging evaluation with hyperpolarized  $^3\text{He}$  gas. *Radiology*. 1999; 210(3):851-857.
- (3) Kauczor HU, Ebert M, Kreitner KF et al. Imaging of the lungs using  $^3\text{He}$  MRI: preliminary clinical experience in 18 patients with and without lung disease. *J Magn Reson Imaging*. 1997; 7(3):538-543.
- (4) Moller HE, Chen XJ, Saam B et al. MRI of the lungs using hyperpolarized noble gases. *Magn Reson Med*. 2002; 47(6):1029-1051.
- (5) Salerno M, Altes TA, Brookeman JR et al. Dynamic spiral MRI of pulmonary gas flow using hyperpolarized ( $^3\text{He}$ ): preliminary studies in healthy and diseased lungs. *Magn Reson Med*. 2001; 46(4):667-677.
- (6) Yablonskiy DA, Sukstanskii AL, Leawoods JC et al. Quantitative in vivo assessment of lung microstructure at the alveolar level with hyperpolarized  $^3\text{He}$  diffusion MRI. *Proc Natl Acad Sci U S A*. 2002; 99(5):3111-3116.
- (7) Saam BT, Yablonskiy DA, Kodibagkar VD et al. MR imaging of diffusion of ( $^3\text{He}$ ) gas in healthy and diseased lungs. *Magn Reson Med*. 2000; 44(2):174-179.
- (8) Woods JC, Choong CK, Yablonskiy DA et al. Hyperpolarized  $^3\text{He}$  diffusion MRI and histology in pulmonary emphysema. *Magn Reson Med*. 2006; 56(6):1293-1300.
- (9) Morbach AE, Gast KK, Schmiedeskamp J et al. Diffusion-weighted MRI of the lung with hyperpolarized helium-3: a study of reproducibility. *J Magn Reson Imaging*. 2005; 21(6):765-774.
- (10) Salerno M, de Lange EE, Altes TA et al. Emphysema: hyperpolarized helium 3 diffusion MR imaging of the lungs compared with spirometric indexes--initial experience. *Radiology*. 2002; 222(1):252-260.
- (11) Woods JC, Yablonskiy DA, Choong CK et al. Long-range diffusion of hyperpolarized  $^3\text{He}$  in explanted normal and emphysematous human lungs via magnetization tagging. *J Appl Physiol*. 2005; 99(5):1992-1997.
- (12) Tanoli TS, Woods JC, Conradi MS et al. In vivo lung morphometry with hyperpolarized  $^3\text{He}$  diffusion MRI in canines with induced emphysema: disease

- progression and comparison with computed tomography. *J Appl Physiol*. 2007; 102(1):477-484.
- (13) Fain SB, Altes TA, Panth SR et al. Detection of age-dependent changes in healthy adult lungs with diffusion-weighted <sup>3</sup>He MRI. *Acad Radiol*. 2005; 12(11):1385-1393.
  - (14) Parraga G, Ouriadov A, Evans A et al. Hyperpolarized <sup>3</sup>He ventilation defects and apparent diffusion coefficients in chronic obstructive pulmonary disease: preliminary results at 3.0 Tesla. *Invest Radiol*. 2007; 42(6):384-391.
  - (15) Swift AJ, Wild JM, Fichele S et al. Emphysematous changes and normal variation in smokers and COPD patients using diffusion <sup>3</sup>He MRI. *Eur J Radiol*. 2005; 54(3):352-358.
  - (16) Fain SB, Panth SR, Evans MD et al. Early emphysematous changes in asymptomatic smokers: detection with <sup>3</sup>He MR imaging. *Radiology*. 2006; 239(3):875-883.
  - (17) Choudhri A, Altes, TA, Stay R, et al. The occurrence of ventilation defects in the lungs of healthy subjects as demonstrated by hyperpolarized helium-3 MR imaging. *RSNA*. 2007; SSA21-05
  - (18) Woodhouse N, Wild JM, Paley MN et al. Combined helium-3/proton magnetic resonance imaging measurement of ventilated lung volumes in smokers compared to never-smokers. *J Magn Reson Imaging*. 2005; 21(4):365-369.
  - (19) de Lange EE, Altes TA, Harding D et al. Hyperpolarized gas MR imaging of the lung: safety assessment of inhaled Helium-3. *RSNA*. 2003; K03-879
  - (20) Woodhouse N, Mills GH, Flemming S et al. Comparison of hyperpolarized 3-He administration methods in healthy and diseased subjects. *Proc ISMRM*. 2006; 1288
  - (21) Global strategy for the diagnosis, management, and prevention of chronic obstructive pulmonary disease. NHLBI/WHO Workshop Report Update. 2701. 2003.
  - (22) de Lange EE, Altes TA, Patrie JT et al. The variability of regional airflow obstruction within the lungs of patients with asthma: assessment with hyperpolarized helium-3 magnetic resonance imaging. *J Allergy Clin Immunol*. 2007; 119(5):1072-1078.
  - (23) Landry A, Spence JD, Fenster A. Measurement of carotid plaque volume by 3-dimensional ultrasound. *Stroke*. 2004; 35(4):864-869.



- (24) Landry A, Fenster A. Theoretical and experimental quantification of carotid plaque volume measurements made by three-dimensional ultrasound using test phantoms. *Med Phys.* 2002; 29(10):2319-2327.
- (25) Landry A, Spence JD, Fenster A. Quantification of carotid plaque volume measurements using 3D ultrasound imaging. *Ultrasound Med Biol.* 2005; 31(6):751-762.
- (26) Lin LI. A concordance correlation coefficient to evaluate reproducibility. *Biometrics.* 1989; 45(1):255-268.
- (27) Howell DC. *Fundamental Statistics for the Behavioural Sciences.* Belmont: Brooks/Cole - Thomas Learning Inc., 2004
- (28) Altes TA, Gersbach JC, Mata JF et al. Evaluation of the safety of hyperpolarized helium-3 gas as an inhaled contrast agent for MRI. *Proc ISMRM.* 2007; 1305
- (29) Mathew L, McCallum JM, McKay S et al. Hyperpolarized 3He magnetic resonance imaging of ventilation defect volume variability in COPD. *Proc ISMRM.* 2007; 1306

## CHAPTER 3: HYPERPOLARIZED $^3\text{He}$ MAGNETIC RESONANCE IMAGING OF VENTILATION DEFECTS IN HEALTHY ELDERLY VOLUNTEERS: INITIAL FINDINGS AT 3.0 TESLA

The work presented in this chapter has been previously published in *Academic Radiology* as indicated below, and is reproduced here with permission (Appendix C).

G. Parraga, L. Mathew, R. Etemad-Rezai, D.G. McCormack, G. Santyr. "Hyperpolarized  $^3\text{He}$  Magnetic Resonance Imaging Ventilation Defects in Healthy Elderly Volunteers: Initial Findings at 3.0 Tesla" *Acad Radiol.* 2008 Jun;15(6):776-85

### 3.1 Introduction

New methods of pulmonary magnetic resonance imaging (MRI) with inhaled hyperpolarized helium-3 ( $^3\text{He}$ ), have been shown to provide regional pulmonary  $^3\text{He}$  ventilation maps and the location and size of ventilation changes within the lung in asthma<sup>1-4</sup>, cystic fibrosis<sup>5-10</sup> and chronic obstructive pulmonary disease (COPD).<sup>11-19</sup> In patients with respiratory disease, areas of decreased ventilation from airflow changes are observed as "ventilation defects" that are visualized as decreased or an absence of  $^3\text{He}$  intensity in  $^3\text{He}$  MRI spin density images.

Previously, both the size and number of these ventilation defects has been shown to correlate with severity in asthma<sup>3,4,20,21</sup> and in addition, exercise and methacholine challenge has been shown to alter the size, location and number of defects that occur in asthma.<sup>3</sup> We have also previously described a preliminary analysis of ventilation defect score and ventilation defect volume (VDV) in 3 subjects – one with mild-moderate COPD, one with severe COPD and a single healthy age-matched control.<sup>17</sup> We noted in this study that significant ventilation defects were observed even in the healthy elderly subject. The finding of ventilation defects in an older healthy individual who was not a smoker, did not have asthma, or cardiovascular disease and who had normal pulmonary function tests<sup>17</sup> was surprising and had not been reported previously in other studies of younger healthy volunteers. This result challenged us to explain the physiological mechanisms related to ventilation defects in healthy lung as well as the prevalence of ventilation defects in older and middle-aged individuals. To try to address some of these issues, the goal of this study was to examine and compare, with the use of  $^3\text{He}$  MRI,

ventilation defects in elderly and middle-aged subjects who had no history of smoking, respiratory or cardiovascular disease.

## **3.2 Methods**

### **3.2.1 Study Population**

Subjects were recruited from the general population by newspaper advertisement and media coverage and they provided written informed consent to study protocols approved by The University of Western Ontario Standing Board of Human Research Ethics and by Health Canada. In order to qualify as a healthy subject, volunteers had no history of chronic respiratory disease or cardiovascular disease and less than 1 pack-year of smoking over their lifetime. In addition, subjects were enrolled based on forced expiratory volume in 1s ( $FEV_1$ )  $\geq$  80% predicted and  $FEV_1$  divided by the forced vital capacity (FVC) ( $FEV_1/FVC$ )  $\geq$  70%, measured using spirometry, according to the GOLD classification for healthy subjects.<sup>22</sup> For the elderly cohort, subjects were recruited between the ages of 50 and 75 years and enrolled between the ages of 58 and 74 years inclusive, whereas for the younger subgroup, subjects were recruited between the ages of 18 and 60 years of age and enrolled between the ages of 23 and 57 years inclusive.

### **3.2.2 Spirometry**

Spirometry was performed at screening and at each MRI visit using an *ndd EasyOne* spirometer (ndd Medizintechnik AG, Zurich, CH) reporting forced  $FEV_1$  (absolute and percent predicted) and FVC.

### **3.2.3 Magnetic Resonance Imaging**

For both subject subgroups, MRI was performed on a whole body 3.0 Tesla Excite 12.0 MRS system (GEHC, Milwaukee, WI USA) with broadband imaging capability as previously described.<sup>17</sup> All helium imaging employed a whole body gradient set with maximum gradient amplitude of 19.4 mT/m and a single channel, elliptical transmit/receive chest coil (RAPID Biomedical GmbH, Wuerzburg Germany). The basis frequency of the coil was 97.3 MHz and excitation power was 3.2 kW using an AMT 3T90 RF power amplifier (GEHC, Milwaukee WI USA).

The elderly subgroup was scanned twice within  $7 \pm 2$  minutes (scan and same-day rescan) and then again once within  $7 \pm 2$  days (7-day rescan). All but two of the younger subjects were scanned on a single occasion only, with two subjects being scanned up to 20 times each within 2 years. Multi-slice  $^3\text{He}$  coronal images were obtained using a fast gradient-echo method (FGRE) with centric k-space sampling (FOV 40x40cm). Two interleaved images (TE = 3.7 ms, TR = 7.6 ms, 128 x 128, flip angle = 7 degrees, 7 slices 30 mm thick), with and without additional diffusion sensitization ( $G = 19.4\text{mT/m}$ , rise and fall time = 0.5 ms, gradient duration = 0.46ms, diffusion time = 1.46ms, b value =  $1.6\text{s/cm}^2$ ), were acquired for each slice with the non-diffusion-weighted image serving as a  $^3\text{He}$  ventilation image for analysis. The total image acquisition time was 14s. Each subject inhaled  $^3\text{He}$  gas as previously described<sup>17</sup> from a 1 L  $^3\text{He}/\text{N}_2$  gas mixture consisting of a dose of 5ml/kg of hyperpolarized  $^3\text{He}$  (i.e. for a 50 kg subject, 250ml would be dispensed and diluted with medical  $\text{N}_2$  to a total volume of 1L). The  $^3\text{He}$  gas dose was administered to subjects after completing a tidal breath exhalation and imaging was performed with the subject in breath-hold, once the subject had completed inhaling the 1L volume of gas. Proton imaging was performed after completion of  $^3\text{He}$  imaging and subjects were rescanned using a 4-channel radiofrequency coil (GEHC, Milwaukee, WI) with the subject holding their breath after completing a tidal breath inhalation. Multi-slice  $^1\text{H}$  coronal images were obtained using a fast spoiled gradient recalled echo sequence (256x256 matrix, FOV 40x40cm, TR= 2.7, TE= 1.3, flip angle = 8 degrees). All scanning was completed within approximately 10 minutes of first lying in the scanner.

Hyperpolarized  $^3\text{He}$  gas was provided by a turn-key, spin-exchange optical pumping system (HeliSpin™, GEHC, Durham, NC) as previously described.<sup>17</sup>

### 3.2.4 Image Analysis

Center slice  $^3\text{He}$  images were analyzed for ventilation defect score (VDS) and ventilation defect volume (VDV) in a dedicated radiological viewing room which provided a constant image visualization environment with consistent (darkened) room lighting. Ventilation defect score and volumetric segmentation were performed for the center coronal slice only, determined by the presence of the carina, with the aid of the  $^1\text{H}$  center-slice images (also determined by the presence of the carina).  $^3\text{He}$  center-slice images

were visually compared alone and registered together with  $^1\text{H}$  center slice images. While all slices were reviewed, only the center coronal slice was quantitatively assessed because in this study,  $^1\text{H}$  image slices were not acquired with the same slice thickness or breath-hold as the  $^3\text{He}$  images (slice thickness of 10mm for  $^1\text{H}$  as compared to 30mm slice thickness for  $^3\text{He}$ ).

Images were examined in the same image visualization environment by four trained observers for analysis of ventilation defects with the observers blinded to subject identity, disease status and scan time-point.  $^3\text{He}$  ventilation defects were identified as areas with an absence of  $^3\text{He}$  signal with a fixed signal-to-noise (SNR) threshold of 22 and fixed contrast level, which were empirically established after reviewing all images. Images were reviewed such that for each subject all time points examined were displayed on a digital workstation monitor system (consisting of identical 19 inch flat panel monitors). Thus, all  $^3\text{He}$  images for each subject were scored together with the observers blinded to the demographic, clinical, and spirometric information of the subjects. A ventilation defect was defined as previously described by Altes and co-workers<sup>23</sup> as any well-defined area of the lung showing no or low signal intensity compared with the remaining ventilated lung. Areas of absent signal associated with the pulmonary vascular structures, heart, hilum and mediastinum were not considered to be ventilation defects. No lower boundary for defect size detection or quantification was used. After scoring ventilation defects, manual segmentation of the defects was performed on 32 bit image slices randomized together (subject and scan time) that were imported into a 3D image visualization platform developed in our laboratory<sup>24,25</sup> for MR and ultrasound applications as previously described.<sup>26</sup> The image visualization software tool used also provided a method for 2-dimensional rigid image overlay or registration (of the center slice  $^1\text{H}$  image and the center slice  $^3\text{He}$  image), facilitating the manual segmentation of center-slice ventilation defect volume even in the case where poor registration occurred due to breath-hold mismatch. As shown in Figure 3-1, 2-dimensional image overlay (of the center slice  $^1\text{H}$  image and the center slice  $^3\text{He}$  image) facilitated the identification and manual segmentation of center slice ventilation defects.  $^3\text{He}$  ventilation defects were manually segmented, recorded and multiplied by the slice thickness (30mm) to approximate VDV, which was recorded in dedicated source documents. Inter-scan and

inter-observer variability was assessed using the coefficient of variation (COV), which was calculated as the standard deviation of the difference (between scans for inter-scan and between observers for inter-observer) divided by mean VDV.

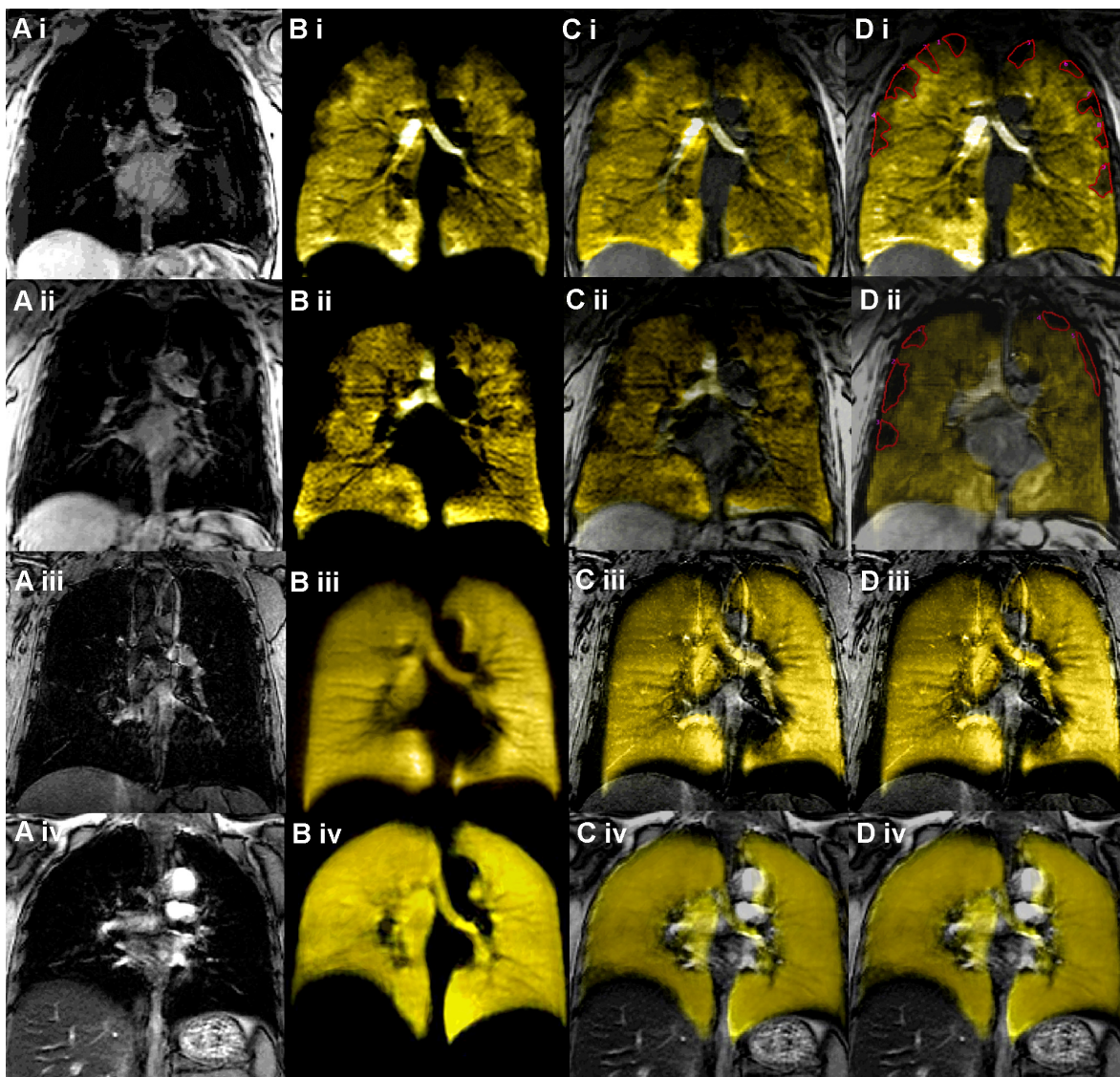


**Figure 3-1: Hyperpolarized  $^3\text{He}$  Magnetic Resonance Imaging Ventilation Defect Volume Segmentation Approach.**

A.  $^1\text{H}$  thoracic cavity (i) Subject 7-1003, (ii) Subject 7-1008, (iii) Subject 6-007, (iv) Subject 6-001

B. Hyperpolarized  $^3\text{He}$  Ventilation Image (i) Subject 7-1003, (ii) Subject 7-1008, (iii) Subject 6-007, (iv) Subject 6-001

C. Overlay of  $^3\text{He}$  ventilation Image (yellow) on  $^1\text{H}$  thoracic cavity (grey) (i) Subject 7-1003, (ii) Subject 7-1008, (iii) Subject 6-007, (iv) Subject 6-001

D. Segmentation of  $^3\text{He}$  ventilation defects (red) (i) Subject 7-1003, (ii) Subject 7-1008, (iii) Subject 6-007, (iv) Subject 6-001

### 3.3 Results

#### 3.3.1 Study Subjects

Eight elderly healthy subjects (five males) were enrolled (mean age  $67 \pm 6$  years, range 58-74 years) as well as 24 (14 males) middle-aged healthy volunteers (mean age  $44 \pm 10$  years, range 23-57 years). Baseline subject demographic data and pulmonary function test results are reported in Table 3-1. Both subgroups had similar baseline mean weight, FEV<sub>1</sub> (% predicted) and FEV<sub>1</sub>/FVC. None of the subjects had a history of cardiovascular or respiratory disorders, obesity, sleep disorders and none of the subjects had smoked within the last 10 years or had a smoking history of > 1 pack-year over their lifetime. Body mass indices ranged from 24-35 for the elderly subjects and 20-24 for the middle-aged subjects. The two subgroups had significantly different mean age ( $p < .001$ ). All subjects except for a single elderly subject who withdrew from the 7-day scanning visit due to claustrophobia were able to complete all scans and visits. The single subject who withdrew after his first scanning visit was scanned twice during his single scanning visit. Two middle-aged healthy subjects were scanned up to 20 times each within two years.

**Table 3-1: Study Subject Demographic Characteristics.**

	Elderly Healthy Volunteers (n=8)	Middle-aged Healthy Volunteers (n=24)
Male (n)	5	14
Age ( $\pm$ SD) [range] Y	67 (6) [58-74]	44 (10) [23-57]
Weight ( $\pm$ SD) kg	76 (17)	76 (13)
Body Mass Index ( $\pm$ SD) [range]	27 (4) [24-35]	25 (3) [20-34]
FEV <sub>1</sub> % Predicted ( $\pm$ SD)	106 (19)	101 (11)
FEV <sub>1</sub> /FVC % ( $\pm$ SD)	77 (5)	80 (8)
Subjects with Ventilation Defects N (male)	6 (3)	0 (0)
Total Ventilation Defects N		
Scan	16	0
Same-day Rescan	15	0
7-day Rescan	18	0
Mean VDV cm <sup>3</sup> ( $\pm$ SD)		
Scan	52 (34)	0
Same-day Rescan	53 (35)	0
7-day Rescan	48 (39)	0

SD is subgroup standard deviation for eight healthy volunteers

### 3.3.2 Ventilation Defects and Ventilation Defect Volume

As shown in Table 3-1, none of the middle-aged healthy volunteers showed evidence of center coronal slice  $^3\text{He}$  ventilation defects, including two of these subjects who were scanned up to 20 times each within a two-year time frame. Although only the center slice was quantitatively assessed, for these younger subjects, ventilation defects were not observed in any slices. However, six of eight elderly healthy volunteers exhibited visibly obvious  $^3\text{He}$  ventilation defects in scans acquired at baseline scan, same-day rescan and

**Table 3-2: Ventilation Defects in Healthy Elderly Volunteers.**

	Scan	Number of Defects in Center Slice	
		Same-day Rescan	7-day Rescan
Subject 1001	0	0	0
Subject 1002	3	3	NA
Subject 1003	3	3	5
Subject 1004	2	2	4
Subject 1005	3	2	3
Subject 1006	0	0	0
Subject 1007	2	2	3
Subject 1008	3	3	3
Total Sum Defects	16	15	18
Mean Defect Score	2.7	2.5	3.6

NA is not assessable

7-day rescan, as results indicate in Table 3-2. Two of the eight healthy elderly subjects had no ventilation defects in any slice during scan, same-day rescan or 7-day rescan and these were both male subjects and the youngest in the subgroup (age 58 BMI 27 and age 60 BMI 35, respectively). For all healthy elderly subjects, the total number of center slice defects summed across all subjects was 16 at scan, with mean VDS of 2.5. For same day rescan, VDS was 2.7 and the sum of total defects was 15 whereas for 7-day rescan, VDS was 3.6 and the sum of total defects was 18. Mean VDV was  $52 \pm 34 \text{ cm}^3$  at scan,  $53 \pm 35 \text{ cm}^3$  at same-day rescan and  $48 \pm 39 \text{ cm}^3$  at 7-day rescan. Figure 3-2 shows  $^3\text{He}$  ventilation images with defects identified with arrows (Figure 3-2(i)) and the overlay of  $^3\text{He}$  ventilation images on the  $^1\text{H}$  thoracic cavity image (Figure 3-2(ii)) for three representative healthy elderly subjects (ages 70, 73 and 74 years respectively). Figure 3-3 provides representative  $^3\text{He}$  ventilation scans for three representative healthy middle-aged subjects (ages 45, 43 and 39 years respectively). The range of signal-to-noise (SNR) for the images in both subgroups was similar.



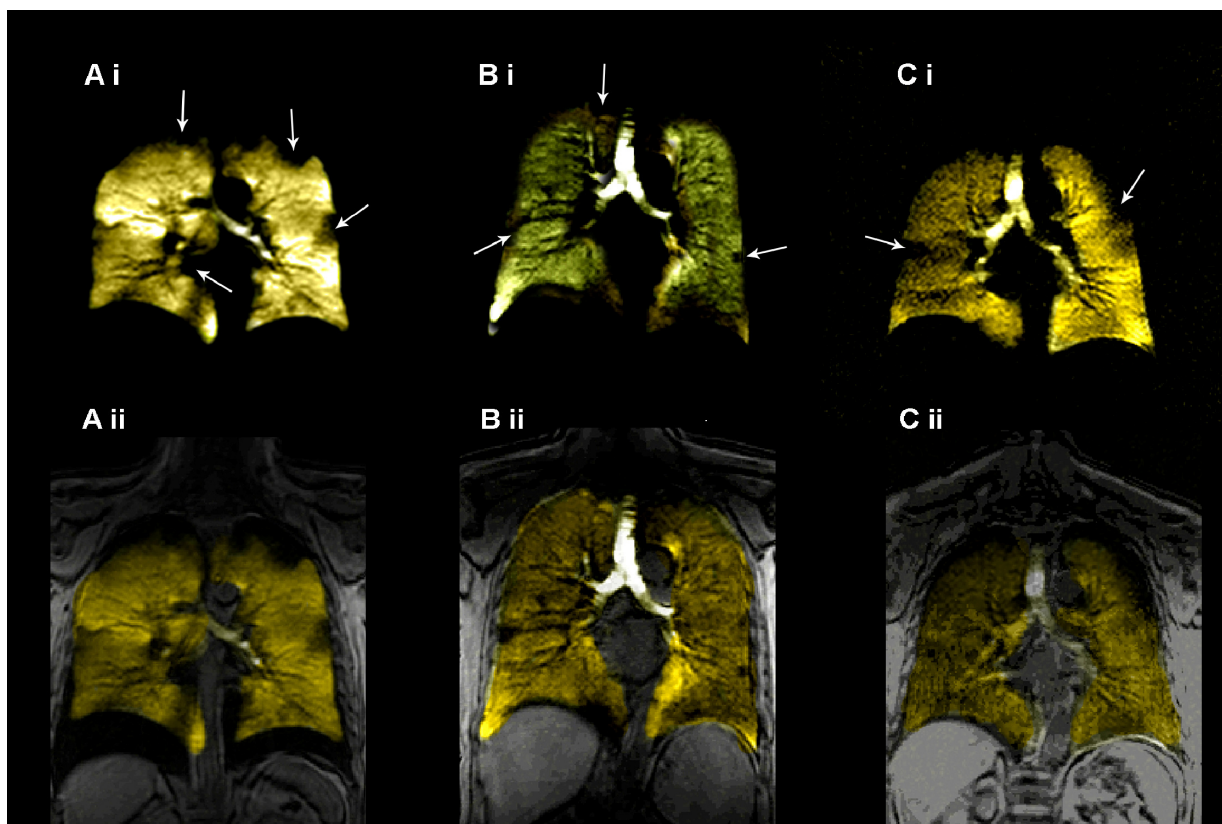


**Figure 3-2: Elderly Healthy Volunteers  $^3\text{He}$  Magnetic Resonance Imaging.**

A. Subject 7-1004 70 yr old female  $\text{FEV}_1 = 149\%$  predicted,  $\text{FEV}_1/\text{FVC}=75\%$  (i)  $^3\text{He}$  image (ii) overlay of  $^3\text{He}$  image with  $^1\text{H}$  thorax image

B. Subject 7-1007 73 yr old male  $\text{FEV}_1= 104\%$  predicted,  $\text{FEV}_1/\text{FVC}=84\%$  (i)  $^3\text{He}$  image (ii) overlay of  $^3\text{He}$  image with  $^1\text{H}$  thorax image

C. Subject 7-1008 74 yr old male  $\text{FEV}_1 = 91\%$  predicted,  $\text{FEV}_1/\text{FVC}=79\%$  (i)  $^3\text{He}$  image (ii) overlay of  $^3\text{He}$  image with  $^1\text{H}$  thorax image

### 3.3.3 Ventilation Defect Volume Interscan and Inter-observer Reproducibility

For all eight elderly subjects who underwent scanning, inter-scan COV for mean VDV was 1.8% for same-day scanning and 5.3% for 7-day scanning (as compared to baseline scan). Figure 3-4 shows  $^3\text{He}$  ventilation images providing visual evidence of the reproducibility of VDV for two representative elderly subjects with ventilation defects that completed both same-day and 7-day scanning visits. For both subjects, the magnitude and location of many of the defects are very similar during same-day scanning; there are a few differences in the number of defects, the location of the defects and the size of the defects observed in the 7-day rescan. For comparison, repeated scans of two middle-aged subjects are also provided in Figure 3-4 with rescan performed within

8 months of baseline and the second rescan performed within 2 years of baseline. No defects or visual differences were observed in the scans for the middle-aged subjects. While a single observer's results are provided for mean VDV in Table 3-1, the results for three additional observers are provided in Table 3-3 as well as inter-observer COV, which ranged from 10% to 12%.

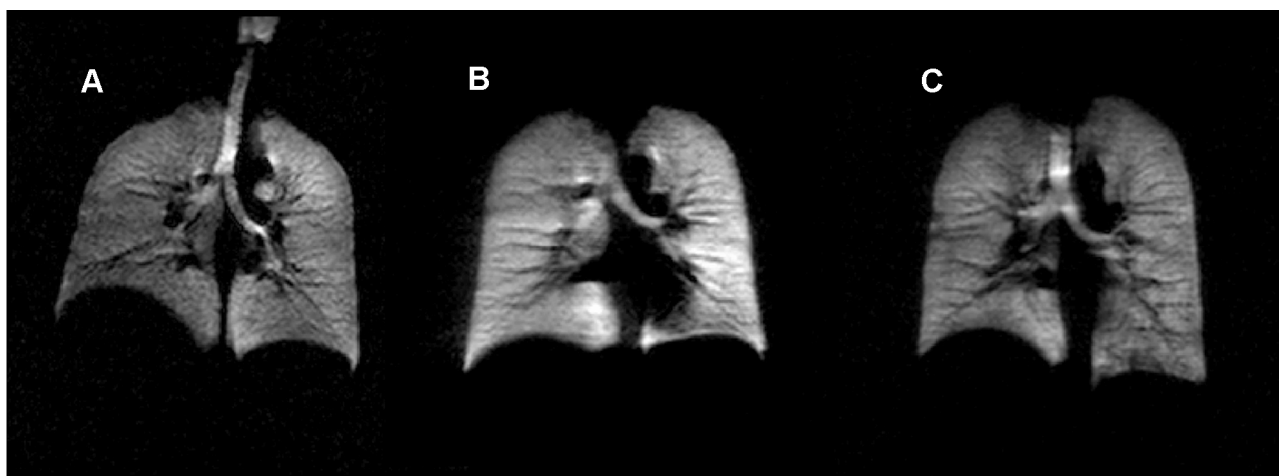


**Figure 3-3: Middle-aged Healthy Volunteers  $^3\text{He}$  Magnetic Resonance Imaging.**

- A. Subject 6-1001 45 yr old female
- B. Subject 6-1003 42 yr old male
- C. Subject 6-1010 39 yr old male

**Table 3-3: Elderly Volunteer Ventilation Defect Volume Inter-observer Reproducibility.**

	Scan	Mean VDV cm <sup>3</sup> ( $\pm$ SD)	
		Same-day Rescan	7-day Rescan
Observer 1	52 (34)	53 (35)	48 (39)
Observer 2	72 (55)	67 (47)	60 (48)
Observer 3	67 (43)	64 (42)	53 (40)
Observer 4	70 (63)	65 (61)	46 (44)
Mean Ob1-4	66 (8)*	62 (6)*	52 (6)*
COV (%)	12	10	12

SD is subgroup standard deviation for eight healthy volunteers except for \*SD is observer standard deviation

COV is SD/ mean VDV for observers

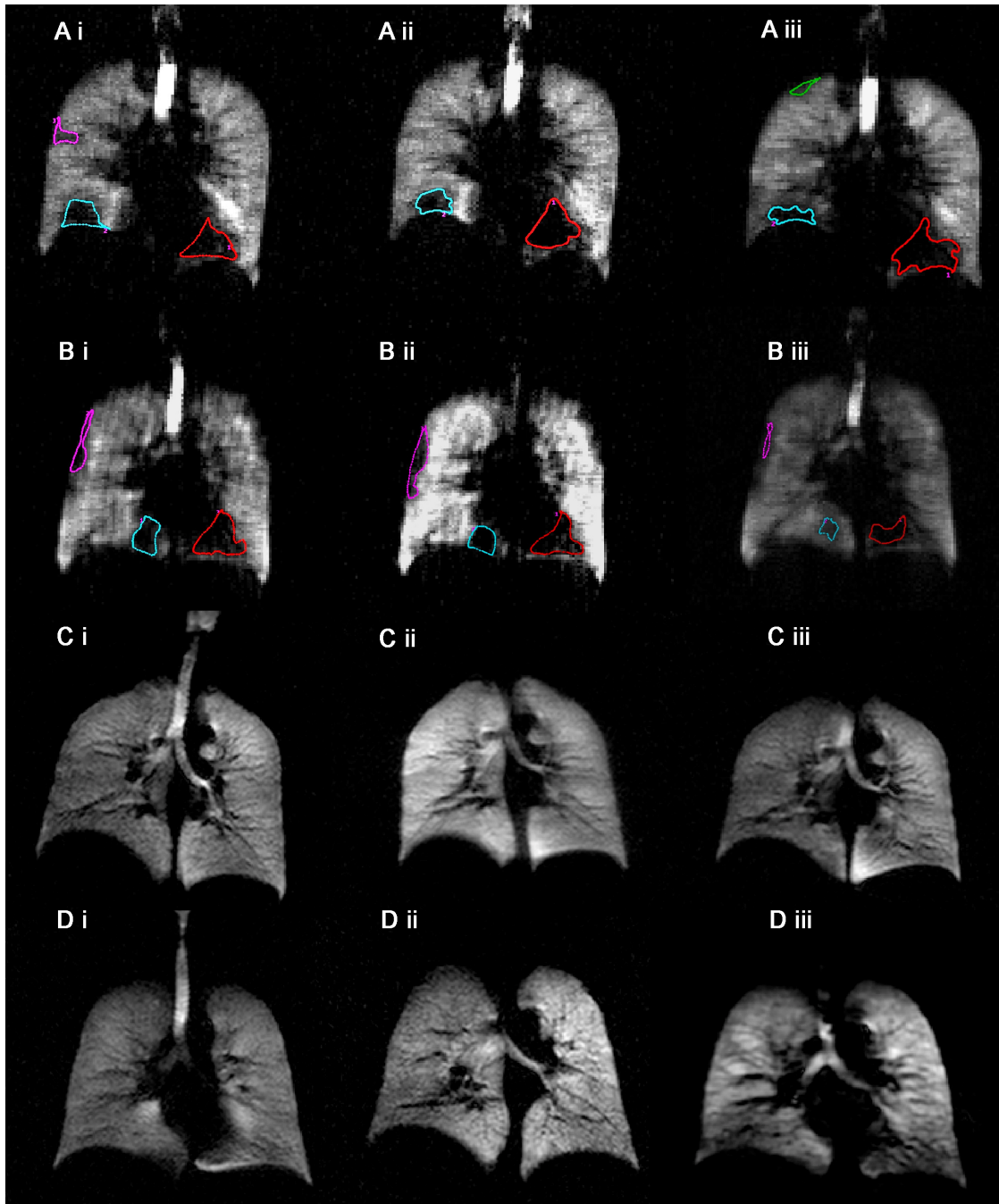


**Figure 3-4: Reproducibility of  $^3\text{He}$  Ventilation in Healthy and Middle-aged Healthy Volunteers**

A. Subject 7-1005 Elderly Volunteer (i) Scan, (ii) Same-day Rescan, (iii) 7-day Rescan  
 B. Subject 7-1008 Elderly Volunteer (i) Scan, (ii) Same-day Rescan, (iii) 7-day Rescan  
 C. Subject 6-1001 Middle-aged Volunteer (i) Scan, (ii) Rescan 1, (iii) Rescan 2  
 D. Subject 6-1002 Middle-aged Volunteer (i) Scan, (ii) Rescan 1, (iii) Rescan 2

### 3.4 Discussion

A number of important observations were made in this study. First, all subjects in this study who were age 63 years and older displayed ventilation defects in the center coronal slice and the number, location and size of these defects were highly reproducible for same day scanning sessions with mean inter-scan VDV COV 1.8% and the total number of defects at 16 and 15 for same-day scan and rescan respectively. Somewhat lower reproducibility was observed for the 7-day scanning visit as compared to baseline with a mean inter-scan VDV COV of 5.3% and the total number of defects scored at 18, with a mean VDS of 3.6 defects. However, all of the six elderly subjects who displayed ventilation defects at baseline displayed very similar number and size of ventilation defects at the 7-day scanning session. In addition, none of the 24 healthy volunteers in the middle-aged subgroup displayed ventilation defects during any scanning session and neither did the two youngest subjects in the elderly subgroup. As shown in Table 3, four observers measured VDV over a 1.5 year period with inter-observer COV ranging from 10% to 12%. In recent work, Altes and co-workers<sup>27</sup>, have shown the association of age and ventilatory defects which supports the finding reported here of significantly different size and number of defects in the centre coronal slice of healthy younger and elderly volunteers. Their previous work also reported small mean numbers (<2) of ventilation defects in younger healthy volunteers<sup>6</sup> when the entire lung was assessed. In current studies of healthy volunteers at 3.0 Tesla at our site, there is little evidence of posterior or other slice defects in healthy volunteers who have less than 1-pack-year smoking and no evidence of cardiovascular or respiratory disease. This may be the case because 3.0 Tesla <sup>3</sup>He MRI at our site has been limited to <50 healthy volunteers; it is possible that with more subjects scanned over time small mean numbers of ventilation defects will be detected in some young healthy subjects.

A second finding from this preliminary study was that for the six elderly subjects for whom defects were observed at baseline, there was a tendency for these to appear in the same locations 7 days later. In some cases, the original defects were accompanied by new defects and/or slightly altered sizes. Regional persistence or recurrence of ventilation defects has also been recently described in asthma by Altes, de Lange and co-

workers<sup>28</sup> with specific regions of the lung appearing to be more likely to display altered ventilation patterns. The observation in this study that regional persistence is also a feature of ventilatory defects in healthy elderly subjects suggests that specific airways appear to be preferentially closed in the aging lung and that these airways are more likely to be closed on sequential days. It is important to point out that all subject scanning sessions were scheduled for the same time of day on the second scanning visit as the first scanning visit ( $\pm 1$  hour from baseline scan for each subject) and always during mid-morning. Spirometry measurements were also recorded before and after each scanning session and there was no change in spirometry measures observed for any subjects between scanning dates or after MR scanning. Finally, obesity is a critical issue to consider when imaging subjects in the supine position, as extra weight directly influences respiratory mechanics in the supine and upright position. None of the subjects who displayed ventilation defects were obese, and hence it is unlikely that any of the ventilatory defects observed were related to BMI.

Thirdly, we observed that for the elderly healthy volunteers, all defects in the center coronal slice appeared on the periphery of the coronal slice, which is similar to previously published work in asthma.<sup>3,29-31</sup> This finding of peripheral lung ventilation defects in the elderly healthy lung and in asthma is in contrast to previously published <sup>3</sup>He results for subjects with COPD in our lab<sup>17</sup> and others<sup>11-16,18,19</sup> and in cystic fibrosis<sup>7-10</sup>, where numerous and large defects are observed throughout the coronal and axial plane and not on the periphery alone.

The primary limitation of this preliminary study is the small sample size of the elderly subject group and the fact that for the majority of the middle-aged subjects group there was no protocol specification for prospective repeated scanning because no ventilation defects were observed at baseline. For two middle-aged subjects, repeated scanning was undertaken, only because these subjects were enrolled in a hardware and software development protocol requiring multiple scanning visits to enable pulse programming alteration assessments. Both of these subjects were scanned up to 20 times over two years and these subjects (both with ages very close to the mean of the middle-aged group) never displayed ventilation defects during any scanning visit.

Another shortcoming of the study is related to the fact that subjects were scanned in a study designed to assess the reproducibility of the  $^3\text{He}$  ADC and hence the images had lower SNR and thicker slices than do spin density images. Nevertheless, the finding of ventilation defects is still very evident and the difference in younger and older subjects is significant. This suggests that the current result is robust and provides a conservative estimate of the defects that may be observed in older subjects. Elderly subjects were enrolled in the current study with ADC reproducibility as the primary end-point and as such protocol utilized an optimized ADC sequence. The primary focus on ADC required necessary trade-offs be made in the use of the non-diffusion-weighted images as a indication of ventilation (i.e. increased TE, diffusion time). We acknowledge that the longer TE will introduce undesirable  $T2^*$  weighting into the ventilation, but expect that this effect would lead to less than 50% signal reduction even with the largest ADC (larger airways). Indeed, the signal in the airways is well appreciated in our images. Therefore, we are confident that the regions of signal void in the lung parenchyma attributed to ventilation defect in this study represent the absence of helium gas and not signal decay. This is confirmed by the measurement of the same signal voids in T1-weighted image (obtained on Visit 2, data not shown) which was obtained with TE of about half that of the non-diffusion-weighted images. It may be possible that with  $^3\text{He}$  ventilation imaging, the improvement in SNR might result in better measured reproducibility for the same-day and 7-day scanning visits.

Another limitation of this study is the fact that  $^3\text{He}$  and  $^1\text{H}$  images were acquired at somewhat different lung volumes and that this may have influenced the segmentation of ventilation defects that appeared on the lung-pleura boundaries. For example, the  $^1\text{H}$  images were acquired in breath-hold fashion after blowing out to the bottom of tidal volume and holding their breath at the top of tidal volume. The  $^3\text{He}$  images were acquired after blowing out to the bottom of tidal volume and in breath-hold after inhaling 1L of the  $^3\text{He}/\text{N}_2$  gas mixture. Therefore the volumes were not exactly matched and overlay of  $^3\text{He}$  and  $^1\text{H}$  images were not perfectly registered. However, although the images were acquired at slightly different volumes, the lung boundaries were readily discerned when the  $^1\text{H}$  and  $^3\text{He}$  images are provided in overlay and identification of these are facilitated in all six cases where there were clear ventilation defects at the outer

boundary of the lungs. In addition, because  $^1\text{H}$  and  $^3\text{He}$  images were not acquired with exactly matching breath-holds and very different slice thickness, we limited the analysis of defect volume reproducibility to the center coronal slice where the edge of the thoracic cavity and ventilation defects were most easily discerned. Hence, in this study center coronal slice VDV represented the area of ventilation defect for the center slice, which was then multiplied by the 30 mm slice thickness to reflect contributions from the entire slice. We also point out that for some subject images, the apices of the lung have complex ventilation patterns that might be interpreted as ventilation defects. In most cases, the overlay of proton and helium images allows for interpretation of the irregular shape of the ventilation image as dependent upon tissue and bone anatomy at the top of the lung. We investigated coil coverage and found that there is excellent signal intensity in the trachea up to and including the cricoid/larynx. We have also directly assessed coil inhomogeneity quantitatively (ISMRM abstract 2008 #5175) and observed less than 20% in the superior-inferior direction over a 44 cm FOV, which is likely adequate for the imaging results we have presented here.

Why do elderly healthy volunteers display  $^3\text{He}$  MRI ventilation defects along the periphery of the coronal plane of the lung? How is this finding related to the increased ADC values shown previously for older subjects<sup>17,32,33</sup> and in the six elderly subjects in this study with ventilation defects (with mean ADC = 0.27 cm<sup>2</sup>/s)? How might this finding be related to other measurements of pulmonary physiology that are also known to change with aging such as FEV<sub>1</sub> and closing volume? It is possible that along with changes in the lung airspaces such as alveoli and acinar ducts, (as evidenced by increased ADC) changes in airways may also occur over time, and perhaps correlated to increased closing volumes with advancing age. In this study, the majority of defects were observed along the periphery of the coronal slice which suggests that terminal airway closure or narrowing may be an age-dependent pathology of the lung. Altes and co-workers have also observed ventilation defects in healthy volunteers are positively correlated with age<sup>27</sup>, suggesting that the finding here in a few elderly subjects should be assessed in more volunteers in multi-center studies. While the etiology of ventilation defects is yet unknown, we are currently assessing the presence and reproducibility of ventilation defects in a greater number of elderly COPD subjects and elderly (age-matched) healthy

volunteers over a five-year period in order to better understand this radiological finding. The observation of reproducible pulmonary ventilation defects in otherwise healthy elderly volunteers suggests caution must be used in interpreting results from  $^3\text{He}$  studies of elderly subjects with underlying disease. This finding further suggests that inclusion of a healthy elderly volunteer control group may be required when using  $^3\text{He}$  MRI in treatment studies of elderly COPD, subjects in order to appropriately relate potential treatment effects to underlying disease and not other processes related to aging. If the results of this preliminary study are observed in the majority of elderly volunteers scanned in our laboratory and elsewhere, this may potentially result in increased subject sample sizes required in cohort and treatment studies of elderly subjects with respiratory disease where  $^3\text{He}$  MRI phenotypes are used as measurements or biomarkers of disease.

### **3.5 Conclusion**

In conclusion, the observations made in this study of a relatively small group of elderly and middle-aged healthy volunteers indicated that regional ventilation defects within the lung as demonstrated using  $^3\text{He}$  MRI were present in six elderly subjects aged 63-74 years. These ventilation defects were highly reproducible in size and location in repeated scans within a few minutes and again 7 days later. These results suggest that as part of the aging processes in the lung, non-random airway closure or narrowing occurs that is restricted to the lung periphery and is regionally recurrent or persistent. The results further suggest that these airway changes are occurring in the absence of known or detectable respiratory or cardiovascular disease, perhaps as part of normal aging processes. Further work is required to unravel the etiology of these defects in healthy elderly volunteers.



### 3.6 References

- (1) Altes TA, Powers PL, Knight-Scott J et al. Hyperpolarized  $^3\text{He}$  MR lung ventilation imaging in asthmatics: preliminary findings. *J Magn Reson Imaging*. 2001; 13(3):378-384.
- (2) de Lange EE, Altes TA, Patrie JT et al. The variability of regional airflow obstruction within the lungs of patients with asthma: assessment with hyperpolarized helium-3 magnetic resonance imaging. *J Allergy Clin Immunol*. 2007; 119(5):1072-1078.
- (3) Samee S, Altes T, Powers P et al. Imaging the lungs in asthmatic patients by using hyperpolarized helium-3 magnetic resonance: assessment of response to methacholine and exercise challenge. *J Allergy Clin Immunol*. 2003; 111(6):1205-1211.
- (4) de Lange EE, Altes TA, Patrie et al. Evaluation of Asthma with Hyperpolarized Helium-3 MRI: Correlation with Clinical Severity and Spirometry. *Chest*. 2006; 130(4): 1055-1062.
- (5) Altes TA, de Lange EE. Applications of hyperpolarized helium-3 gas magnetic resonance imaging in pediatric lung disease. *Top Magn Reson Imaging*. 2003; 14(3):231-236.
- (6) Altes TA, Eichinger M, Puderbach M. Magnetic resonance imaging of the lung in cystic fibrosis. *Proc Am Thorac Soc*. 2007; 4(4):321-327.
- (7) Donnelly LF, MacFall JR, McAdams HP et al. Cystic fibrosis: combined hyperpolarized  $^3\text{He}$ -enhanced and conventional proton MR imaging in the lung--preliminary observations. *Radiology*. 1999; 212(3):885-889.
- (8) Koumellis P, Van Beek EJ, Woodhouse N et al. Quantitative analysis of regional airways obstruction using dynamic hyperpolarized  $^3\text{He}$  MRI-preliminary results in children with cystic fibrosis. *J Magn Reson Imaging*. 2005; 22(3):420-426.
- (9) Mentore K, Froh DK, de Lange EE et al. Hyperpolarized  $^3\text{He}$  MRI of the lung in cystic fibrosis: assessment at baseline and after bronchodilator and airway clearance treatment. *Acad Radiol*. 2005; 12(11):1423-1429.
- (10) Salerno M, Altes TA, Brookeman JR et al. Dynamic spiral MRI of pulmonary gas flow using hyperpolarized ( $^3\text{He}$ ): preliminary studies in healthy and diseased lungs. *Magn Reson Med*. 2001; 46(4):667-677.
- (11) Ebert M, Grossmann T, Heil W et al. Nuclear magnetic resonance imaging with hyperpolarised helium-3. *Lancet*. 1996; 347(9011):1297-1299.

- (12) Fain SB, Panth SR, Evans MD et al. Early emphysematous changes in asymptomatic smokers: detection with  $^3\text{He}$  MR imaging. *Radiology*. 2006; 239(3):875-883.
- (13) Kauczor HU, Hofmann D, Kreitner KF et al. Normal and abnormal pulmonary ventilation: visualization at hyperpolarized  $\text{He-3}$  MR imaging. *Radiology*. 1996; 201(2):564-568.
- (14) Ley S, Zaporozhan J, Morbach A et al. Functional evaluation of emphysema using diffusion-weighted  $^3\text{He}$ -magnetic resonance imaging, high-resolution computed tomography, and lung function tests. *Invest Radiol*. 2004; 39(7):427-434.
- (15) MacFall JR, Charles HC, Black RD et al. Human lung air spaces: potential for MR imaging with hyperpolarized  $\text{He-3}$ . *Radiology*. 1996; 200(2):553-558.
- (16) Morbach AE, Gast KK, Schmiedeskamp J et al. Diffusion-weighted MRI of the lung with hyperpolarized helium-3: a study of reproducibility. *J Magn Reson Imaging*. 2005; 21(6):765-774.
- (17) Parraga G, Ouriadov A, Evans A et al. Hyperpolarized  $^3\text{He}$  ventilation defects and apparent diffusion coefficients in chronic obstructive pulmonary disease: preliminary results at 3.0 Tesla. *Invest Radiol*. 2007; 42(6):384-391.
- (18) Swift AJ, Wild JM, Fichelle S et al. Emphysematous changes and normal variation in smokers and COPD patients using diffusion  $^3\text{He}$  MRI. *Eur J Radiol*. 2005; 54(3):352-358.
- (19) Woodhouse N, Wild JM, Paley MN et al. Combined helium-3/proton magnetic resonance imaging measurement of ventilated lung volumes in smokers compared to never-smokers. *J Magn Reson Imaging*. 2005; 21(4):365-369.
- (20) Altes TA, Powers PL, Knight-Scott J et al. Hyperpolarized  $^3\text{He}$  MR lung ventilation imaging in asthmatics: preliminary findings. *J Magn Reson Imaging*. 2001; 13(3):378-384.
- (21) de Lange EE, Altes TA, Patrie JT et al. The variability of regional airflow obstruction within the lungs of patients with asthma: assessment with hyperpolarized helium-3 magnetic resonance imaging. *J Allergy Clin Immunol*. 2007; 119(5):1072-1078.
- (22) Pauwels RA, Buist AS, Calverley PM et al. Global strategy for the diagnosis, management, and prevention of chronic obstructive pulmonary disease. NHLBI/WHO Global Initiative for Chronic Obstructive Lung Disease (GOLD) Workshop summary. *Am J Respir Crit Care Med*. 2001; 163(5):1256-1276.
- (23) de Lange EE, Altes TA, Patrie JT et al. The variability of regional airflow obstruction within the lungs of patients with asthma: assessment with

- hyperpolarized helium-3 magnetic resonance imaging. *J Allergy Clin Immunol.* 2007; 119(5):1072-1078.
- (24) Landry A, Spence JD, Fenster A. Measurement of carotid plaque volume by 3-dimensional ultrasound. *Stroke.* 2004; 35(4):864-869.
- (25) Landry A, Fenster A. Theoretical and experimental quantification of carotid plaque volume measurements made by three-dimensional ultrasound using test phantoms. *Med Phys.* 2002; 29(10):2319-2327.
- (26) Landry A, Spence JD, Fenster A. Quantification of carotid plaque volume measurements using 3D ultrasound imaging. *Ultrasound Med Biol.* 2005; 31(6):751-762.
- (27) Choudhri A, Altes TA, Stay R et al. The Occurrence of Ventilation Defects in the Lungs of Healthy Subjects as Demonstrated by Hyperpolarized Helium-3 MR Imaging. *RSNA. SSA21-05.* 2007.
- (28) de Lange EE, Altes TA, Patrie JT et al. The variability of regional airflow obstruction within the lungs of patients with asthma: assessment with hyperpolarized helium-3 magnetic resonance imaging. *J Allergy Clin Immunol.* 2007; 119(5):1072-1078.
- (29) Altes TA, Powers PL, Knight-Scott J et al. Hyperpolarized 3He MR lung ventilation imaging in asthmatics: preliminary findings. *J Magn Reson Imaging.* 2001; 13(3):378-384.
- (30) de Lange EE, Altes TA, Patrie JT et al. Evaluation of asthma with hyperpolarized helium-3 MRI: correlation with clinical severity and spirometry. *Chest.* 2006; 130(4):1055-1062.
- (31) de Lange EE, Altes TA, Patrie JT et al. The variability of regional airflow obstruction within the lungs of patients with asthma: assessment with hyperpolarized helium-3 magnetic resonance imaging. *J Allergy Clin Immunol.* 2007; 119(5):1072-1078.
- (32) de Lange EE, Altes TA, Patrie JT et al. Evaluation of asthma with hyperpolarized helium-3 MRI: correlation with clinical severity and spirometry. *Chest.* 2006; 130(4):1055-1062.
- (33) Fain SB, Altes TA, Panth SR et al. Detection of age-dependent changes in healthy adult lungs with diffusion-weighted 3He MRI. *Acad Radiol.* 2005; 12(11):1385-1393.

## CHAPTER 4: HYPERPOLARIZED $^3\text{He}$ MAGNETIC RESONANCE IMAGING: PRELIMINARY EVALUATION OF PHENOTYPING POTENTIAL IN CHRONIC OBSTRUCTIVE PULMONARY DISEASE

The work presented in this chapter has been previously published in the *European Journal of Radiology* as follows, and is reproduced here with permission (Appendix C).  
*L. Mathew, M Kirby, A. Wheatley, DG McCormack, G. Parraga. "Hyperpolarized  $^3\text{He}$  Magnetic Resonance Imaging: Preliminary Evaluation of Phenotyping Potential in Chronic Obstructive Pulmonary Disease" Eur J Radiol. 2009 Nov 20. [Epub ahead of print]*

### 4.1 Introduction

Chronic obstructive pulmonary disease (COPD) is the most common chronic, terminal respiratory disease worldwide and it continues to grow in prevalence<sup>1</sup> and yet has a very poor prognosis, despite aggressive therapy.<sup>1-3</sup> Although widespread pulmonary inflammation<sup>4,5</sup> and diffuse lung tissue alterations are often observed<sup>5</sup>, obstruction of the small airways (airways disease) and tissue destruction in the pulmonary parenchyma (emphysema) are the hallmark pathologies.<sup>6</sup> Accordingly, both airways disease and emphysema contribute to the clinical course of COPD, although the underlying mechanisms of both pathologies and the proportional contributions of these and their relationship to outcomes are not completely understood.

The current functional definition of COPD<sup>7</sup> relies on the spirometric measurement of airflow obstruction. A fundamental limitation exists however, because the anatomy and physiology of the lung is complex and spirometry measurements reflect the global sum of all the different possible COPD pathologies including small airways disease, emphysema (i.e. parenchymal destruction), chronic bronchitis (i.e. large airway remodeling), and bronchiectasis (i.e. abnormal dilation of bronchi and bronchioles).<sup>8</sup>

The limitation of spirometry for differentiating between these pathologies or phenotypes has severely limited the scope of basic research and clinical studies that evaluate the relationship between these morphological phenotypes, disease pathogenesis and progression, and patient outcomes. Accordingly, one major goal of COPD research is to

find a way to identify patients with these different underlying pathological “phenotypes”, which has the potential to have a profound effect on patient care and treatment options. In this regard, non-invasive high resolution multi-detector x-ray computed tomography (CT)<sup>9-12</sup> has been shown to detect unique and quantitative phenotypes of both emphysema and airway disease<sup>13-15</sup> with the potential to determine the contributions of both airway and airspace changes in COPD. Previously published results suggest that CT-derived phenotypes provide evidence of underlying phenotype dominance in approximately 40% of subjects.<sup>13</sup>

Hyperpolarized <sup>3</sup>He magnetic resonance imaging (MRI) has emerged as research method that is complementary to CT because it allows for simultaneous visualization of tissue structure and regional airway function at high spatial and temporal resolution, without the use of ionizing radiation. In particular, the measurement of the <sup>3</sup>He apparent diffusion coefficient (ADC)<sup>16</sup>, which is a surrogate measurement of airspace size<sup>17-20</sup>, has been previously histologically-validated<sup>21</sup> and correlated with CT measurements of emphysema.<sup>22</sup> Ventilation defects or signal voids in <sup>3</sup>He spin density images are hypothesized to reflect airflow limitation related to airway narrowing or closure<sup>23</sup>, but the exact pathology underlying <sup>3</sup>He ventilation defects has yet to be determined. Importantly, both <sup>3</sup>He MRI ADC and ventilation measurements have been shown to be highly reproducible<sup>24-26</sup>, sensitive to age<sup>27-29</sup> and to disease-related changes.<sup>26,30-33</sup>

Here we describe the results of a proof-of-principle and hypothesis-generating preliminary study where we explore the potential of hyperpolarized <sup>3</sup>He MRI to classify (or phenotype) individual COPD ex-smokers based on the relative contributions of ventilation defect and ADC measurements. To our knowledge, this is the first study aimed at evaluating the potential for <sup>3</sup>He MRI to detect phenotypes based on the proportional contributions of COPD structural and functional measurements.

## **4.2 Methods**

### **4.2.1 Subjects**

Twenty subjects were enrolled from the general population of the local tertiary health care center as well as directly from the COPD clinics at three local teaching hospitals. All subjects provided written informed consent to the study protocol approved by the local research ethics board and Health Canada and the study was compliant with both the Health Insurance Portability and Accountability Act (HIPAA, USA) and the Personal Information Protection and Electronic Documents Act (PIPEDA, Canada). Subjects were categorized according to Global initiative for Obststructive Lung Disease (GOLD) criteria<sup>34</sup> and required a COPD diagnosis of at least one year, with a smoking history of at least 10-pack-years and additional inclusion and exclusion criteria as previously reported.<sup>26</sup>

### **4.2.2 Pulmonary Function Tests**

Subjects were screened for MRI and coil compatibility (inner diameter of elliptical coil = 50cm) and underwent a physical exam, plethysmography and spirometry both of which were performed according to American Thoracic Society guidelines.<sup>35</sup> Briefly, spirometry was performed pre- and post-bronchodilator using an *ndd EasyOne* spirometer (ndd Medizintechnik AG, Zurich, CH) reporting forced expiratory volume in 1 s (FEV<sub>1</sub>) and forced vital capacity (FVC) and a minimum of three acceptable spirometry maneuvers were carried out with the best FEV<sub>1</sub> and FVC selected for analysis. Whole body plethysmography (MedGraphics Corporation, 350 Oak Grove Parkway St. Paul MN USA) was also performed within meters of the MR scanner for the measurement of total lung capacity (TLC), inspiratory capacity (IC), residual volume (RV), and functional residual capacity (FRC).

### **4.2.3 Safety Monitoring and Hyperpolarized <sup>3</sup>He Administration**

Prior to MRI, supine vital signs and arterial O<sub>2</sub> levels measured by pulse oximetry were recorded, and subjects were administered a practice dose of mixed <sup>4</sup>He-N<sub>2</sub> gas while seated outside the scanner. Digital pulse oximetry was used to monitor arterial blood

oxygen levels during MR scanning and all breath-hold maneuvers. Hyperpolarized  $^3\text{He}$  gas was provided by a turn-key, spin-exchange polarizer system (HeliSpin™, GEHC, Durham, NC) as previously described.<sup>36</sup> In a typical study this system provided 30% polarization in 12 hours. Doses (5 mL/kg) were delivered in 1 L plastic bags (Tedlar®, Jensen Inert Products, Coral Springs, FL) diluted with ultrahigh purity, medical grade nitrogen (Spectra Gases, Alpha, NJ). The  $^3\text{He}$  gas dose was administered to subjects after completing a tidal breath exhalation (ie. FRC) and imaging was performed with the subject in breath-hold from FRC.

#### 4.2.4 Imaging

Magnetic resonance imaging was performed on a whole body 3.0 Tesla Excite 12.0 MRI system (GEHC, Milwaukee, WI USA) with broadband imaging capability as previously described.<sup>36</sup> All helium imaging employed a whole body gradient set with maximum gradient amplitude of 19.4 mT/m and a single channel, rigid elliptical transmit/receive chest coil (RAPID Biomedical GmbH, Wuerzburg Germany). The basis frequency of the coil was 97.3 MHz and maximum excitation power was 3.2 kW using an AMT 3T90 RF power amplifier (GEHC, Milwaukee WI USA).

Two-dimensional multi-slice coronal  $^1\text{H}$  scans were acquired prior to  $^3\text{He}$  imaging with subjects scanned during 1-L breath-hold of  $^4\text{He}/\text{N}_2$  from FRC using the whole body radiofrequency (RF) coil and proton fast spoiled gradient-echo (16s total data acquisition, repetition time (TR)=4.7ms, echo time (TE)=1.2 ms, flip angle=30°, bandwidth (BW)=31.25, field-of-view (FOV)=40cm x 40cm, matrix 128 x 128, 14 slices, 15mm slice thickness, 0mm gap). For diffusion-weighted  $^3\text{He}$  imaging, multi-slice coronal images were obtained using a fast gradient-echo method (FGRE) with centric k-space sampling. Two interleaved images (14s total data acquisition, TR=7.6 ms, TE=3.7 ms, flip angle=8°, BW=31.25, FOV=40cm x 40cm, matrix=128 x 128, 7 slices, 30 mm slice thickness), with and without additional diffusion sensitization ( $G=19.4\text{mT/m}$ , rise and fall time=0.5 ms, gradient duration=0.46ms, diffusion time=1.46ms, b value=1.6s/cm<sup>2</sup>), were acquired for each slice. For ventilation images, multi-slice coronal images were also obtained using the same chest coil (14s total data acquisition, TR=4.3ms, TE=1.4ms, flip

angle=7°, BW=31.25, FOV=40cm x 40cm, matrix 128 x 128, 15 slices, 10mm slice thickness, 0mm gap).

#### 4.2.5 Image Analysis

<sup>3</sup>He ventilation image measurements and <sup>3</sup>He diffusion-weighted image analyses were performed in an image visualization environment with room lighting levels equivalently established for all image analysis sessions as previously described.<sup>26,37</sup> Mean apparent diffusion coefficient (ADC) and ADC maps were processed for all slices using in-house software programmed in the IDL Virtual Machine platform (Research Systems Inc., Denver, CO) as previously described<sup>36</sup>, with the trachea and main bronchi removed prior to analysis and  $b = 1.6 \text{ s/cm}^2$ . <sup>3</sup>He ventilation images were examined by a single trained observer for analysis of ventilation defects in all coronal slices. A ventilation defect was defined as previously described<sup>38</sup>, and manual segmentation of the ventilation defects was performed with the observer blinded to subject identity, clinical characteristics and disease stage. Segmentation was performed using custom-designed image visualization software which provides for two-dimensional rigid image registration (of the <sup>1</sup>H and <sup>3</sup>He slices), facilitating the manual segmentation of ventilation defects in all slices. It is important to note that using this method and images from this dataset, intra- and inter-observer coefficients of variation of <10% were previously determined (unpublished data); inter-scan ventilation defect volume (VDV) coefficients of variation were previously reported and were very similar.<sup>26</sup> To generate ventilation volumes, for each slice, the average contour area was multiplied by the slice thickness and all slices were summed to obtain a total volume.<sup>39</sup> As shown in Figure 4-1, manual segmentation of the <sup>3</sup>He signal provided a VDV while thoracic cavity volume (TV) was recorded following segmentation of <sup>1</sup>H images, and both were used to calculate ventilation defect percent (VDP), or the percentage of the thoracic cavity occupied by ventilation defects.

To determine the proportional contribution of ADC to total <sup>3</sup>He MRI measured disease, we normalized ADC values using a linear scale. The scale ranged from 0% representing the mean ADC for healthy age-matched (elderly) never-smoking volunteers (ADC=0.27cm<sup>2</sup>/s)<sup>29</sup> to 100% (ADC=0.88cm<sup>2</sup>/s) for helium in an infinitely large container. Normalized parameters representing airway functional (VDP) and airspace





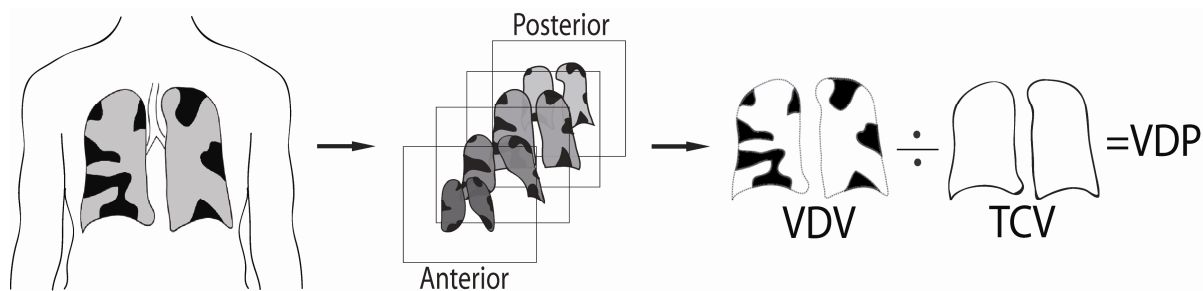


**Figure 4-1: Schematic for  $^3\text{He}$  MRI Ventilation Analysis.**

$^3\text{He}$  MRI ventilation images manually segmented to provide  $^3\text{He}$  derived ventilation defect volume (VDV) by manual segmentation of  $^3\text{He}$  focal signal voids.  $^1\text{H}$  MRI thoracic cavity images manually segmented on a slice-by-slice basis to provide a  $^1\text{H}$  MRI derived thoracic cavity volume (TCV). Ventilation defect percent (VDP) is generated as VDV normalized or divided by TCV.

structural (ADC%) measurements for the center slice (with the highest SNR) were summed to provide a total MRI disease measurement based on the assumption of a linear relationship between these variables. From this total disease measurement, the proportional contribution of ventilation defects (VDP) and emphysema (ADC%) was evaluated for each subject.

#### 4.2.6 Statistical Methods

Mean ADC and VDV were calculated by summing the data and dividing by the number of subjects (n) and standard deviations were calculated as the square root of the sum of the differences between the squared data and the squared mean, divided by n. Comparison of ADC and VDV means was performed using the one-way analysis of variance (ANOVA) in SPSS 16.00 (SPSS Inc., USA LEAD Technologies, Inc., Chicago, IL). The relationship between  $^3\text{He}$  MRI ADC and ventilation measurements was determined using linear regression and Pearson correlation coefficients (GraphPad Prism version 4.00, GraphPad Software Inc, San Diego California, USA). A Holm-Bonferroni correction was applied to account for multiple comparisons.<sup>40</sup> Classification of subjects into three categories based on ADC% and VDP was based on the proportional contribution of ADC% or VDP to total measurement of underlying disease pathology using an arbitrary 2/3 threshold – indicating either ADC% or VDP was the major

contributor to  $^3\text{He}$  MRI measured disease. A multivariate ANOVA was performed to determine significant differences between the three groups.

## 4.3 Results

### 4.3.1 Study Subjects

Baseline demographic characteristics are provided in Table 4-1 for the 20 subjects enrolled (13 male) by GOLD criteria.<sup>34</sup> A single subject presented with normal FEV<sub>1</sub> and low FEV<sub>1</sub>/FVC (stage I) with a prior diagnosis of emphysema from thoracic CT. All other subjects were either categorized as GOLD stage II or stage III COPD according to post-bronchodilator spirometry performed on the same day as MRI. Mean body mass index (BMI) and BMI range for each subject subgroup was similar. As the COPD subjects were enrolled according to GOLD criteria<sup>34</sup>, the mean values for FEV<sub>1</sub> and FEV<sub>1</sub>/FVC for each subgroup reflected the GOLD categorization. In addition to the expected and significantly decreased FEV<sub>1</sub> percent predicted (%<sub>pred</sub>) and FEV<sub>1</sub>/FVC for the stage III COPD subgroup, baseline FRC and RV were significantly increased and IC significantly decreased for stage III COPD subjects consistent with lung hyperinflation.

**Table 4-1: Subject Demographics.**

	Stage I COPD n=1	Stage II COPD n=9	Stage III COPD n=10	Significance Difference SII -SIII  p
Age yrs ( $\pm$ SD) [range]	67 -	68(6) [59-74]	68(7) [52-75]	NS
Male Sex	1	4	8	
Body Mass Index ( $\pm$ SD) [range]	33 -	29 (4) [22-38]	25 (4) [18-34]	NS
FEV <sub>1</sub> %*( $\pm$ SD)	90	61 (6)	39 (7)	<.001
FEV <sub>1</sub> /FVC % ( $\pm$ SD)	61	54 (11)	36 (9)	.003
IC %* ( $\pm$ SD)	128	95 (18)	59 (34)	.006
RV %* ( $\pm$ SD)	161	141 (21)	191 (47)	.009
FRC %* ( $\pm$ SD)	139	118 (16)	164 (39)	.01
TLC %* ( $\pm$ SD)	135	108 (9)	119 (23)	NS

\*Percent predicted, FEV<sub>1</sub> = Forced Expiratory Volume in 1s, FVC= Forced Vital Capacity FRC= Functional Residual Capacity, TLC= Total Lung Capacity NS= Not significant, SII = stage II COPD, SIII= stage III COPD.

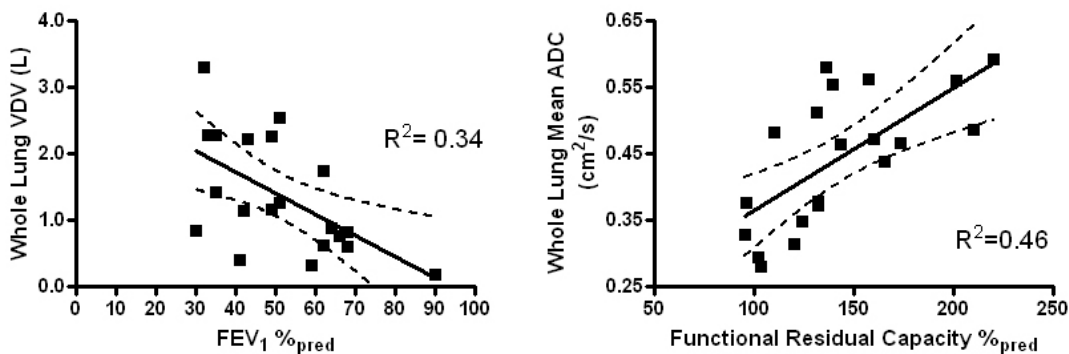


**Figure 4-2: Linear Regression.**

A) shows the relationship between FEV<sub>1</sub> %<sub>pred</sub> and whole lung VDV ( $y = -0.03x + 3.01$ ,  $p = 0.007$ ). B) shows the relationship between FRC %<sub>pred</sub> and whole lung ADC ( $y = -0.002x + 0.18$ ,  $p = 0.001$ ). Dashed line shows the 95% confidence interval.

### 4.3.2 <sup>3</sup>He MRI Measurements

Table 4-2 shows mean <sup>3</sup>He ADC as well as <sup>3</sup>He ventilation measurements (VDV and VDP) for the single patient with normal FEV<sub>1</sub>, and all patients with stage II and stage III disease. No significant difference was observed for any of the <sup>3</sup>He MR measurements between stage II and stage III subgroups. Pearson correlation coefficients for <sup>3</sup>He ADC and VDV are provided in Table 4-3 which shows significant and modest correlations for ADC and VDV with FRC %<sub>pred</sub> and significant association between TLC and ADC. Figure 4-2 shows the relationship between FEV<sub>1</sub> %<sub>pred</sub> and VDP (Figure 4-2A), and the relationship between ADC and FRC %<sub>pred</sub> (Figure 4-2B). Table 4-4 shows center slice <sup>3</sup>He MRI measurements and the relative contributions of these measurements for each subject. The sum of ADC% + VDP is provided for each patient in Figure 4-3, where centre slice VDP and ADC% values are summed together and expressed as a percentage of total <sup>3</sup>He MRI measured disease (total sum divided by 2). The sum of ADC% + VDP, was statistically significantly lower ( $p = 0.006$ ) for subjects classified as ADC (AD) or VDP dominant (VD) compared to the mixed group. There was also a significant difference for FEV<sub>1</sub> %<sub>pred</sub> between subjects with a single predominant <sup>3</sup>He MR measurement (either ADC or VDP) and subjects in the mixed group ( $p = 0.008$ ). Subject classification results based on an arbitrary 10% threshold are shown in Figure 4-4 with the threshold denoted as a dotted line and subjects with ADC% and VDP values close to the threshold denoted

with asterisks. Both the 10% threshold and 2/3 contribution to total MRI-measured disease classified the same three subjects as VD and the same four

**Table 4-2: Whole Lung  $^3\text{He}$  MRI ADC and Ventilation Measurements.**

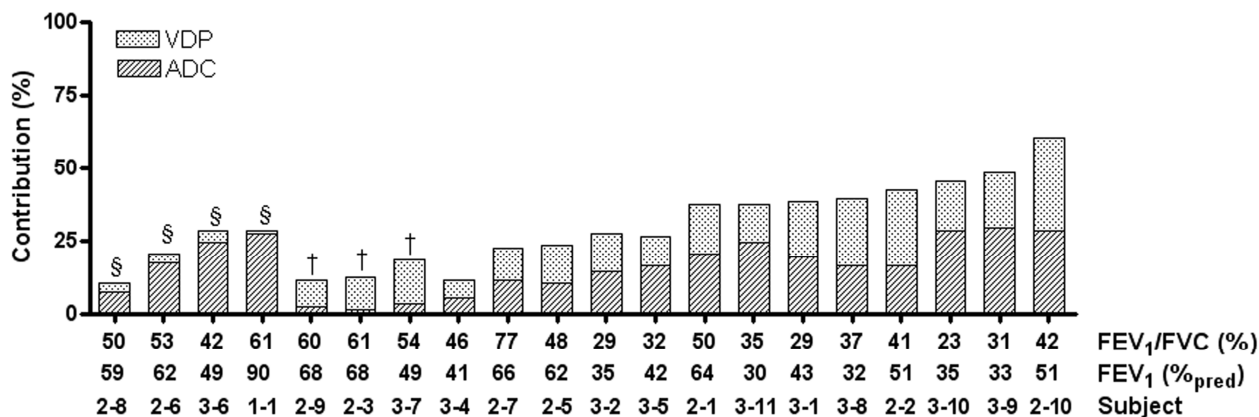
	Stage I n=1	Stage II COPD n=9	Stage III COPD n=10
ADC ( $\pm$ SD) $\text{cm}^2/\text{s}$	0.58	0.42 (0.10)	0.48 (0.09)
ADC <sub>SD</sub> ( $\pm$ SD) $\text{cm}^2/\text{s}$	0.27	0.23 (0.04)	0.26 (0.05)
VDV ( $\pm$ SD) L	0.19	1.07 (0.69)	1.74 (0.88)
VDP ( $\pm$ SD) (%)	6	22 (16)	28 (12)

ADC is  $^3\text{He}$  apparent diffusion coefficient, SD is standard deviation, VDV is ventilation defect volume, VDP is ventilation defect percent

subjects as AD. The results of the multivariate ANOVA showed the VD subgroup had significantly different, and lower ADC% values than the AD subgroup ( $p=0.02$ ) and mixed groups ( $p=0.008$ ). The AD subgroup showed statistically significantly different, lower VDP values than the mixed group ( $p=0.003$ ). In Figure 4-5  $^3\text{He}$  MR ventilation images (i), ADC maps (ii) and ADC histograms (iii) are provided for the subjects identified by both classification methods as in the AD subgroup with high ADC pixel values, increased mean ADC and broader ADC histograms (Subjects 2-8 (A), 2-6 (B), 3-6 (C) and 1-1 (D)). Figure 4-5 also shows the subjects in the VD subgroup (and one subject on the 10% threshold) with increased ventilation defects and low ADC pixel values, decreased mean ADC and narrow peak ADC histograms (Subjects 3-4 (E), 2-9 (F), 2-3 (G), 3-7 (H)).

**Table 4-3: Whole lung <sup>3</sup>He MRI Correlations with Pulmonary Function.**

	ADC	Holm-Bonferroni p value	VDV	Holm-Bonferroni p value
FEV <sub>1</sub> % <sub>pred</sub> (p)	-0.26 (0.27)	0.27	-0.58 (0.007)	0.07
FEV <sub>1</sub> /FVC (p)	-0.53 (0.02)	0.12	-0.54 (0.01)	0.08
FRC % <sub>pred</sub> (p)	0.68 (0.001)	0.012	0.62 (0.003)	0.033
IC % <sub>pred</sub> (p)	-0.39 (0.09)	0.27	-0.55 (0.01)	0.09
TLC % <sub>pred</sub> (p)	-0.53 (0.02)	0.014	0.34 (0.14)	0.28
RV % <sub>pred</sub> (p)	0.43 (0.06)	0.24	0.48 (0.03)	0.15

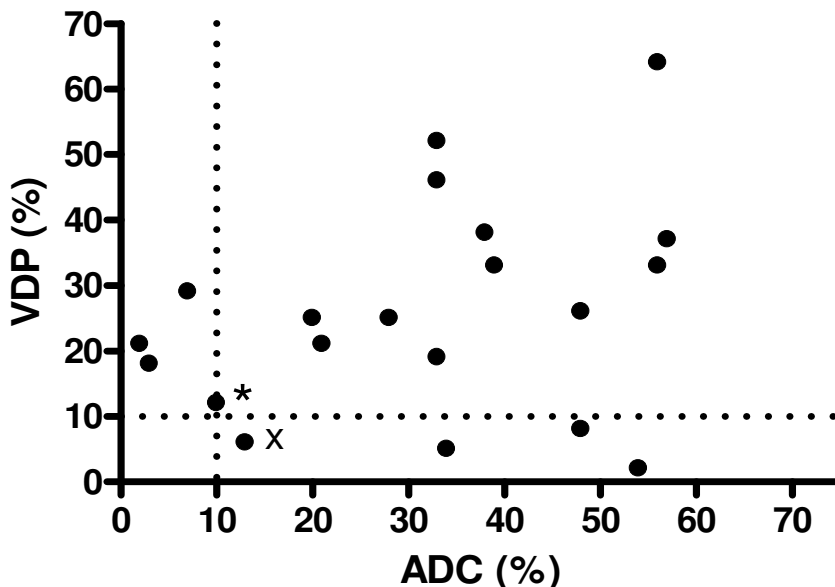
**Figure 4-3: <sup>3</sup>He MRI VDP and ADC % Contributions in COPD.**

Center slice VDP and ADC% values are summed together and expressed as a percentage of total <sup>3</sup>He MRI measured disease (total sum divided by 2), where 100% disease would be 100% VDP and ADC = 0.88 cm<sup>2</sup>/s. Subjects § are classified as primarily ADC by both classification methods, whereas subjects † are classified as primarily VDP by the classification methods.

**Table 4-4: Center slice  $^3\text{He}$  Measurement Contributions by Subject.**

Subject	FEV <sub>1</sub>	FEV <sub>1</sub> /FVC	VDP (%)	ADC %	ADC%+VDP	Contribution ADC	Contribution VDP
<b>1-1</b>	<b>90%</b>	<b>61%</b>	<b>2</b>	<b>54</b>	<b>56</b>	<b>96%</b>	<b>4%</b>
2-1	64%	50%	33	39	72	54%	46%
2-2	51%	41%	52	33	85	39%	61%
<b>2-3</b>	<b>68%</b>	<b>61%</b>	<b>21</b>	<b>2</b>	<b>23</b>	<b>7%</b>	<b>93%</b>
2-5	62%	48%	25	20	45	44%	56%
<b>2-6</b>	<b>62%</b>	<b>53%</b>	<b>5</b>	<b>34</b>	<b>39</b>	<b>87%</b>	<b>13%</b>
2-7	66%	77%	21	21	42	50%	50%
<b>2-8</b>	<b>59%</b>	<b>50%</b>	<b>6</b>	<b>13</b>	<b>19</b>	<b>69%</b>	<b>31%</b>
<b>2-9</b>	<b>68%</b>	<b>60%</b>	<b>18</b>	<b>3</b>	<b>21</b>	<b>15%</b>	<b>85%</b>
2-10	51%	42%	64	56	120	47%	53%
3-1	43%	29%	38	38	76	50%	50%
3-2	35%	29%	25	28	53	53%	47%
3-4	41%	46%	12	10	22	45%	55%
3-5	42%	32%	19	33	52	63%	37%
<b>3-6</b>	<b>49%</b>	<b>42%</b>	<b>8</b>	<b>48</b>	<b>56</b>	<b>86%</b>	<b>14%</b>
<b>3-7</b>	<b>49%</b>	<b>54%</b>	<b>29</b>	<b>7</b>	<b>36</b>	<b>18%</b>	<b>82%</b>
3-8	32%	37%	46	33	79	42%	58%
3-9	33%	31%	37	57	94	61%	39%
3-10	35%	23%	33	56	89	63%	42%
3-11	30%	35%	26	48	74	65%	45%

**Bolded** subjects were classified as having a single predominant measurement by the 2/3 approach.

**Figure 4-4:  $^3\text{He}$  MRI Classification by Thresholding.**

VDP and ADC% scatter plot for all subjects with dashed line denoting 10% threshold cutoff. The asterisks represent two subjects close to the threshold line, <sup>x</sup> represents subject 2-8, and the \* represents subject 3-4.

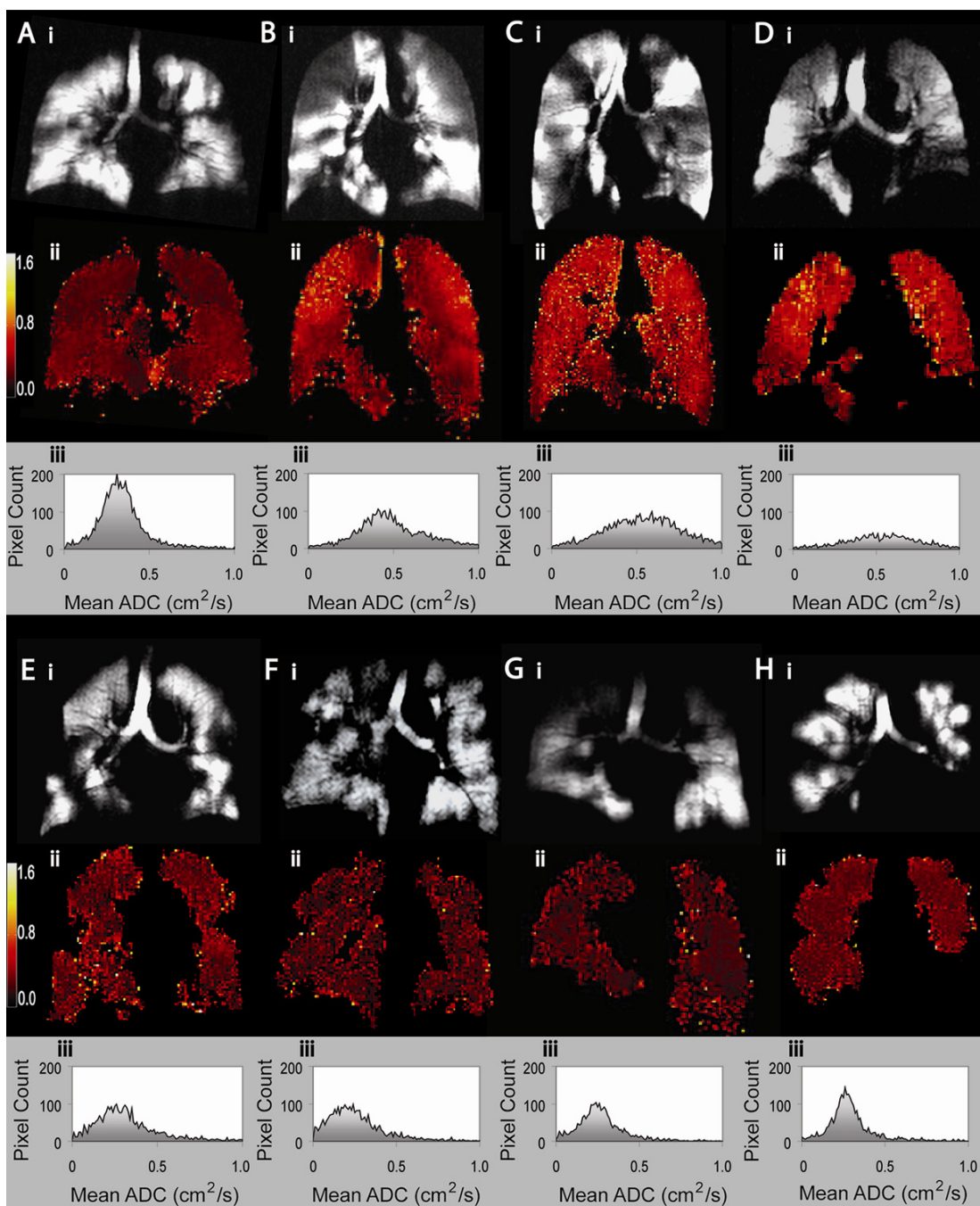


**Figure 4-5:  $^3\text{He}$  VDP and ADC Dominance.**

A-D) ADC dominant subjects identified in both classification methods A) subject 2-8 B) subject 2-6 C) subject 3-6 D) subject 1-1

E) Subject 3-4, on the 10% threshold of mainly VDP classification

F-H) predominantly elevated VDP subjects identified in both classification methods F) subject 2-9 G) subject 2-3 H) subject 3-7

Predominantly ADC subject images have fewer ventilation defects (i) with brighter red/yellow ADC maps (ii) and broader histograms (iii), whereas predominantly VDP subjects show increased ventilation defects and darker red/black ADC maps.



## 4.4 Discussion

In this pilot study of COPD ex-smokers, we made a number of important observations that are relevant to the potential use of  $^3\text{He}$  MRI. First, although this was a relatively small pilot study, preliminary analysis showed that there was evidence of a single  $^3\text{He}$  measurement – either VDP or ADC providing the main contribution to  $^3\text{He}$  MRI measured disease in a subset of subjects (35%) evaluated. In particular, some patients reported high ADC and nearly normal  $^3\text{He}$  ventilation images with normal ADC based on age-matched healthy non-smoker volunteers.<sup>37</sup> Another small group of patients reported nearly normal (age-adjusted) ADC but significantly elevated VDP (where normal VDP is defined as equivalent to no defects, a finding in the healthy young, and some healthy elderly subjects<sup>26</sup>). We acknowledge that these results are descriptive, the threshold approach is simplistic, appears arbitrary, and can only be viewed as a first step towards a more quantitative and mathematical-based understanding of phenomenological observations that can be achieved when more patients are evaluated. Furthermore, we acknowledge that this is a preliminary analysis, and that our findings are based on the assumption that there is a linear relationship between ADC%, VDP and overall disease. It is important to note that currently the exact relationship between emphysema, airways disease and a “total disease index or measurement” has not been evaluated or at least published. Therefore, our approach should be considered a first order approximation with regard to the extent that emphysema and airways disease contribute to COPD. Clearly, these concepts require further testing or modelling to determine the extent to which tissue destruction and airway inflammation or obstruction contribute to overall disease. Despite the preliminary and somewhat straightforward approach presented here, our results support further testing of the hypothesis that non-invasive  $^3\text{He}$  MRI can provide unique information that can be used to phenotype COPD subjects.

Second, we observed that the seven subjects with evidence of a single dominant  $^3\text{He}$  MRI measurement had significantly higher FEV<sub>1</sub>, compared to the mixed subgroup (n=13). This suggests that subjects with mainly elevated VDP or ADC showed decreased disease severity measured using spirometry. Additionally, for these seven patients, the

sum of VDP + ADC% was significantly lower than for the 13 mixed subgroup patients, also suggesting the presence of less severe underlying disease. In a follow-up to the analysis presented here, we will evaluate these same 20 patients over time to evaluate VDP and ADC to help to clarify the role of disease progression and severity on subject classification. Nevertheless this study suggests that in COPD subjects with higher FEV<sub>1</sub> and lower <sup>3</sup>He MRI measurements of disease there is the potential for either tissue destruction or ventilation defects to dominate.

Third, we observed significant but modest associations between some imaging measurements with spirometry and plethysmography, consistent with previous <sup>3</sup>He MRI studies of COPD.<sup>22,30-32</sup> We note however that these associations were not strong which is perhaps consistent with the small patient group studied, the limitations of spirometry and plethysmography as determinants of disease classification or severity and the fact that COPD itself is very heterogeneous.

We acknowledge that this pilot study is limited by the small number of subjects studied and the fact that the analysis was restricted mainly to subjects with stage II and III COPD. Therefore, caution should be exercised in extrapolating these results to the general COPD population and more specifically to patients with stage I or IV disease. Another shortcoming of this study is the lack of high resolution CT data with which to directly compare the <sup>3</sup>He MRI findings. Nakano and colleagues have already reported CT phenotype dominance<sup>14</sup> in COPD and it will be critical to evaluate and compare both tools in the same patients. A further limitation of this study is that without histology, we cannot definitively ascribe ventilation defects to specific airway pathologies such as airway occlusion via mucous plugs, airway narrowing, airway wall thickening or bullae. Nevertheless, regardless of the specific underlying pathology, airway changes are a likely prerequisite for the ventilation defects that can be visualized within the time-frame of the <sup>3</sup>He MR breath-hold scan.

## 4.5 Conclusion

In conclusion, the results of this pilot study of a small group of COPD ex-smokers show differences in the proportional contributions of  $^3\text{He}$  ventilation defects and ADC, suggesting a potential new role for  $^3\text{He}$  MRI in COPD studies. These findings indicate that  $^3\text{He}$  MRI should be more extensively evaluated in a larger and more diverse group of COPD patients, allowing for confirmation of these results with more complex statistical analyses. Future studies should aim to address the research questions generated in this pilot study: can  $^3\text{He}$  MRI be used to phenotype subjects in a larger COPD population encompassing subjects across GOLD categories; does COPD, as these preliminary data would suggest, develop as mainly ventilation defects or tissue alterations in the early stages of disease; what is the relationship between the phenotypes detected by  $^3\text{He}$  MRI and those determined by CT? Future evaluation of  $^3\text{He}$  MRI phenotypes of COPD will shed light on this very important potential application for this technology.

## 4.6 References

- (1) Pauwels RA, Buist AS, Calverley PM et al. Global strategy for the diagnosis, management, and prevention of chronic obstructive pulmonary disease. NHLBI/WHO Global Initiative for Chronic Obstructive Lung Disease (GOLD) Workshop summary. *Am J Respir Crit Care Med.* 2001; 163(5):1256-1276.
- (2) Continuous or nocturnal oxygen therapy in hypoxemic chronic obstructive lung disease: a clinical trial. Nocturnal Oxygen Therapy Trial Group. *Ann Intern Med.* 1980; 93(3):391-398.
- (3) Standards for the diagnosis and care of patients with chronic obstructive pulmonary disease. American Thoracic Society. *Am J Respir Crit Care Med.* 1995; 152(5 Pt 2):S77-121.
- (4) Hogg JC, Macklem PT, Thurlbeck WM. Site and nature of airway obstruction in chronic obstructive lung disease. *N Engl J Med.* 1968; 278(25):1355-1360.
- (5) Hogg JC, Chu F, Utokaparch S et al. The nature of small-airway obstruction in chronic obstructive pulmonary disease. *N Engl J Med.* 2004; 350(26):2645-2653.
- (6) Rabe KF, Hurd S, Anzueto A et al. Global strategy for the diagnosis, management, and prevention of chronic obstructive pulmonary disease: GOLD executive summary. *Am J Respir Crit Care Med.* 2007; 176(6):532-555.
- (7) Mead J, Turner JM, Macklem PT et al. Significance of the relationship between lung recoil and maximum expiratory flow. *J Appl Physiol.* 1967; 22(1):95-108.
- (8) Rabe KF, Hurd S, Anzueto A et al. Global strategy for the diagnosis, management, and prevention of chronic obstructive pulmonary disease: GOLD executive summary. *Am J Respir Crit Care Med.* 2007; 176(6):532-555.
- (9) Hayhurst MD, MacNee W, Flenley DC et al. Diagnosis of pulmonary emphysema by computerised tomography. *Lancet.* 1984; 2(8398):320-322.
- (10) Muller NL, Staples CA, Miller RR et al. "Density mask". An objective method to quantitate emphysema using computed tomography. *Chest.* 1988; 94(4):782-787.
- (11) Gevenois PA, de M, V, De Vuyst P et al. Comparison of computed density and macroscopic morphometry in pulmonary emphysema. *Am J Respir Crit Care Med.* 1995; 152(2):653-657.
- (12) Coxson HO, Rogers RM, Whittall KP et al. A quantification of the lung surface area in emphysema using computed tomography. *Am J Respir Crit Care Med.* 1999; 159(3):851-856.

- (13) Nakano Y, Muro S, Sakai H et al. Computed tomographic measurements of airway dimensions and emphysema in smokers. Correlation with lung function. *Am J Respir Crit Care Med.* 2000; 162(3 Pt 1):1102-1108.
- (14) Nakano Y, Muller NL, King GG et al. Quantitative assessment of airway remodeling using high-resolution CT. *Chest.* 2002; 122(6 Suppl):271S-275S.
- (15) Nakano Y, Wong JC, de Jong PA et al. The prediction of small airway dimensions using computed tomography. *Am J Respir Crit Care Med.* 2005; 171(2):142-146.
- (16) Yablonskiy DA, Sukstanskii AL, Leawoods JC et al. Quantitative in vivo assessment of lung microstructure at the alveolar level with hyperpolarized  $^3\text{He}$  diffusion MRI. *Proc Natl Acad Sci U S A.* 2002; 99(5):3111-3116.
- (17) de Lange EE, Mugler JP, III, Brookeman JR et al. Lung air spaces: MR imaging evaluation with hyperpolarized  $^3\text{He}$  gas. *Radiology.* 1999; 210(3):851-857.
- (18) Kauczor HU, Hofmann D, Kreitner KF et al. Normal and abnormal pulmonary ventilation: visualization at hyperpolarized He-3 MR imaging. *Radiology.* 1996; 201(2):564-568.
- (19) Kauczor HU, Ebert M, Kreitner KF et al. Imaging of the lungs using  $^3\text{He}$  MRI: preliminary clinical experience in 18 patients with and without lung disease. *J Magn Reson Imaging.* 1997; 7(3):538-543.
- (20) MacFall JR, Charles HC, Black RD et al. Human lung air spaces: potential for MR imaging with hyperpolarized He-3. *Radiology.* 1996; 200(2):553-558.
- (21) Woods JC, Choong CK, Yablonskiy DA et al. Hyperpolarized  $^3\text{He}$  diffusion MRI and histology in pulmonary emphysema. *Magn Reson Med.* 2006; 56(6):1293-1300.
- (22) Diaz S, Casselbrant I, Piitulainen E et al. Validity of apparent diffusion coefficient hyperpolarized ( $^3\text{He}$ )-MRI using MSCT and pulmonary function tests as references. *Eur J Radiol.* 2008.
- (23) Coxson HO, Mayo J, Lam S et al. New and Current Clinical Imaging Techniques To Study Chronic Obstructive Pulmonary Disease. *Am J Respir Crit Care Med.* 2009.
- (24) Diaz S, Casselbrant I, Piitulainen E et al. Hyperpolarized  $^3\text{He}$  apparent diffusion coefficient MRI of the lung: reproducibility and volume dependency in healthy volunteers and patients with emphysema. *J Magn Reson Imaging.* 2008; 27(4):763-770.
- (25) Morbach AE, Gast KK, Schmiedeskamp J et al. Diffusion-weighted MRI of the lung with hyperpolarized helium-3: a study of reproducibility. *J Magn Reson Imaging.* 2005; 21(6):765-774.

- (26) Mathew L, Evans A, Ouriadov A et al. Hyperpolarized (3)He magnetic resonance imaging of chronic obstructive pulmonary disease reproducibility at 3.0 tesla. *Acad Radiol.* 2008; 15(10):1298-1311.
- (27) Altes TA, Mata J, de Lange EE et al. Assessment of lung development using hyperpolarized helium-3 diffusion MR imaging. *J Magn Reson Imaging.* 2006; 24(6):1277-1283.
- (28) Fain SB, Altes TA, Panth SR et al. Detection of age-dependent changes in healthy adult lungs with diffusion-weighted 3He MRI. *Acad Radiol.* 2005; 12(11):1385-1393.
- (29) Parraga G, Mathew L, Etemad-Rezai R et al. Hyperpolarized 3He magnetic resonance imaging of ventilation defects in healthy elderly volunteers: initial findings at 3.0 Tesla. *Acad Radiol.* 2008; 15(6):776-785.
- (30) Salerno M, de Lange EE, Altes TA et al. Emphysema: hyperpolarized helium 3 diffusion MR imaging of the lungs compared with spirometric indexes--initial experience. *Radiology.* 2002; 222(1):252-260.
- (31) Swift AJ, Wild JM, Fischele S et al. Emphysematous changes and normal variation in smokers and COPD patients using diffusion 3He MRI. *Eur J Radiol.* 2005; 54(3):352-358.
- (32) Woodhouse N, Wild JM, Paley MN et al. Combined helium-3/proton magnetic resonance imaging measurement of ventilated lung volumes in smokers compared to never-smokers. *J Magn Reson Imaging.* 2005; 21(4):365-369.
- (33) van Beek EJ, Dahmen AM, Stavngaard T et al. Hyperpolarised 3-He MRI vs HRCT in COPD and normal volunteers - PHIL trial. *Eur Respir J.* 2009.
- (34) Global strategy for the diagnosis, management, and prevention of chronic obstructive pulmonary disease. *NHLBI/WHO Workshop Report Update.* 2003.
- (35) Standardization of Spirometry, 1994 Update. American Thoracic Society. *Am J Respir Crit Care Med.* 1995; 152(3):1107-1136.
- (36) Parraga G, Ouriadov A, Evans A et al. Hyperpolarized 3He ventilation defects and apparent diffusion coefficients in chronic obstructive pulmonary disease: preliminary results at 3.0 Tesla. *Invest Radiol.* 2007; 42(6):384-391.
- (37) Evans A, McCormack D, Ouriadov A et al. Anatomical distribution of 3He apparent diffusion coefficients in severe chronic obstructive pulmonary disease. *J Magn Reson Imaging.* 2007; 26(6):1537-1547.
- (38) de Lange EE, Altes TA, Patrie JT et al. The variability of regional airflow obstruction within the lungs of patients with asthma: assessment with

hyperpolarized helium-3 magnetic resonance imaging. *J Allergy Clin Immunol.* 2007; 119(5):1072-1078.

- (39) Landry A, Spence JD, Fenster A. Quantification of carotid plaque volume measurements using 3D ultrasound imaging. *Ultrasound Med Biol.* 2005; 31(6):751-762.
- (40) VanBell G, Fisher L, Heagerty P et al. Multiple Comparisons. *Biostatistics: A Methodology for the Health Sciences.* Seattle, Washington: Wiley-Interscience, 2004.

## CHAPTER 5: DETECTION OF LONGITUDINAL STRUCTURAL AND FUNCTIONAL CHANGES AFTER DIAGNOSIS OF RADIATION-INDUCED LUNG INJURY USING HYPERPOLARIZED $^3\text{He}$ MAGNETIC RESONANCE IMAGING

The work presented in this chapter has been previously published in *Medical Physics* as follows, and is reproduced here with permission (Appendix C).

*L. Mathew, S. Gaede, A. Wheatley, R. Etemad-Rezai, G.B. Rodrigues G. Parraga "Detection of Longitudinal Lung Structural and Functional Changes after Diagnosis of Radiation-induced lung injury using Hyperpolarized  $^3\text{He}$  Magnetic Resonance Imaging" Med Phys.2010 Jan;37(1):22-31*

### 5.1 Introduction

The lung is extremely radiosensitive and therefore highly susceptible to radiation-induced injury.<sup>1</sup> Although radiation treatment doses for thoracic tumours are modified in order to decrease the risk of tissue damage, radiation-induced lung injury (RILI) still occurs in as many as 37% of thoracic cancer cases involving radiation treatment.<sup>2-5</sup> Moderate to severe injury occurs in about 20% of RILI cases<sup>6</sup> and is manifested as: 1) symptoms that significantly interfere with activities of daily life including shortness of breath, cough, and fever, 2) the requirement for oxygen therapy or ventilatory support, and, 3) premature death. These symptoms and adverse effects are a result of structural changes in the lung including capillary obstruction and septal thickening<sup>7,8</sup> resulting in smaller alveolar spaces in the pneumonitis phase of the injury, and further septal thickening with obliteration of the alveolar space in the fibrotic phase,<sup>8-10</sup> all of which result in the functional impairment of the lung. Significant declines in pulmonary function are typically observed in the months immediately following radiation therapy, and global lung function measurements such as the forced expiratory volume in one second ( $\text{FEV}_1$ ), and forced vital capacity (FVC) as well as the diffusing capacity of carbon monoxide ( $\text{DL}_{\text{CO}}$ ) continue to decline even two years post-radiation treatment.<sup>11</sup> Although these pulmonary function measurements are often used as indicators of overall lung function, the regional functional impact of inflammation and fibrosis in the lung over time are still not well understood. Novel non-invasive imaging methods which provide high spatial and temporal resolution such as hyperpolarized helium-3 magnetic resonance imaging (MRI) may provide some clues as to where and how structural and functional changes



occur in RILI over time. Hyperpolarized  $^3\text{He}$  MRI is being developed in a handful of respiratory and MR imaging research centers to provide a quantitative method for the measurement of lung function and tissue microstructure by exploiting the diffusion properties of  $^3\text{He}$ .<sup>12</sup> Over the past decade, this method has been pioneered to probe lung structure and function in healthy volunteers,<sup>13-16</sup> chronic obstructive pulmonary disease,<sup>17-21</sup> cystic fibrosis,<sup>22-24</sup> asthma.<sup>25-28</sup> and for applications in radiation treatment planning.<sup>29,30</sup>

Although  $^3\text{He}$  MRI has been explored as a potential radiation treatment planning tool,<sup>29</sup> it has not yet been used in clinical research to monitor RILI changes post-diagnosis, which we believe is important to further our understanding of both the regional distribution and functional and structural nature of changes that accompany the global decline in pulmonary function. Accordingly, here we present the first longitudinal  $^3\text{He}$  MRI results in a small group of patients after diagnosis of RILI.

## 5.2 Methods

### 5.2.1 Study Subjects

Study subjects were recruited and enrolled from the London Regional Cancer Program (London, Canada) with a clinical diagnosis of RILI (symptomatic, with or without radiological evidence) based on respiratory symptoms following radiation therapy for lung or breast cancer. Informed consent was obtained prior to participation in this study, which was approved by the local research ethics board and Health Canada.

### 5.2.2 Study Evaluations

All subjects consented to a baseline and follow-up visit prospectively planned for 20 to 24 weeks post-baseline visit to capture short-term differences in  $^3\text{He}$  imaging measurements of RILI diagnosed based on symptomatic evidence. At both visits, vital signs and a short clinical history were recorded, followed by spirometry and plethysmography performed according to ATS guidelines<sup>31</sup>. Spirometry was performed using an *ndd EasyOne* spirometer (ndd Medizintechnik AG, Zurich, Switzerland) for FEV<sub>1</sub> and FEV<sub>1</sub>/FVC. Whole-body plethysmography was performed (MedGraphics Elite

Series, MedGraphics Corporation. St. Paul, USA) and total lung capacity (TLC), functional residual capacity (FRC), residual volume (RV), expiratory reserve volume (ERV) and inspiratory capacity (IC) were recorded. The  $DL_{CO}$  was also tested and recorded. All pulmonary function values were recorded as absolute and normalized percent predicted values based on sex, age and body mass index.

### 5.2.3 Imaging

Helium-3 was polarized as previously described<sup>19,32,33</sup> using a turn-key, spin-exchange polarizer (HeliSpin, GEHC, Durham, NC) and dispensed in a room adjacent to the MR suite with a dose of 5ml/kg body weight.  $^3\text{He}$  was mixed with medical grade  $\text{N}_2$  (Spectra Gases, Alpha, NJ) to a total volume of 1.0L.

Imaging was performed on a whole-body 3.0T MR system (Excite 12.0, GEHC, Milwaukee, WI) as previously reported.<sup>15,32-35</sup> Subjects were positioned supine in the MRI scanner with arms at sides, and pulse oximetry was used to monitor blood oxygenation throughout the course of image acquisition. All imaging was performed in a breath-hold fashion, with subjects instructed to inhale a gas mixture from a 1.0 L Tedlar<sup>®</sup> bag (Jensen Inert Products, Coral Springs, FL) from the bottom of tidal volume, and to hold their breath for 15 seconds.

Proton MR images were acquired in the coronal plane with patients in breath-hold (1.0L of a  $^4\text{He}/\text{N}_2$  mixture), to mimic the  $^3\text{He}$  MRI breathhold maneuver. For proton imaging, a fast spoiled gradient recalled echo sequence was applied with a matrix size of 256x256, field of view (FOV) = 40 cm x 40 cm or 44 cm x 44 cm (depending on subject size), 15 slices each 10mm thick, repetition time (TR) of 2.7 seconds, echo time (TE) of 1.3 seconds and a flip angle of 8°.

A single-channel rigid elliptic transmit/receive chest coil (RAPID Biomedical GmbH, Wuerzburg, Germany) with a basis frequency of 97.3 MHz and an excitation power of 3.2kW was used for all  $^3\text{He}$  imaging with a maximum gradient amplitude of 19.4mT/m. Multi-slice 2-D  $^3\text{He}$  MR static ventilation images were acquired using the unweighted image (no T1 sensitization) of a T1-weighted sequence applied following inspiration of

hyperpolarized  $^3\text{He}$  with the following parameters: TR = 4.3s, TE = 1.4s, flip angle =  $7^\circ$ , matrix = 128x128, a FOV = 40 cm x 40 cm, slice thickness = 10mm, number of slices = 15, 0 mm gap. Following ventilation imaging, diffusion-weighted imaging was performed as previously described<sup>19,35</sup> with the same  $^3\text{He}/\text{N}_2$  dose and breath-hold maneuver.  $^3\text{He}$  multislice images were obtained in the coronal plane using a fast gradient-recalled echo (FGRE) method with centric k-space sampling. Two interleaved images (TE = 3.7 ms, TR = 7.6 ms, 128 x 128, 7 slices, 30 mm slice thickness, FOV = 40cm x 40cm) without and with additional diffusion sensitization (G = 19.4 mT/m, rise and fall time = 0.5 ms, duration = 0.46 ms, b value = 1.6 s/cm<sup>2</sup>) were acquired for each slice. All scanning was completed within approximately 10 minutes of the subject first lying in the scanner.

#### 5.2.4 Image Analysis

All image analysis was performed in a room with controlled lighting by a single expert observer (LM). Image analysis was performed blinded to subject identity, clinical status and timepoint. Ventilation image analysis was performed using manual segmentation of hyper-intense  $^3\text{He}$  regions on a slice by slice basis independently for each lung as previously described to obtain a ventilated volume (VV).<sup>32,36</sup> In addition, proton images were reviewed and the thoracic cavity was segmented to obtain a thoracic cavity volume (TCV) for both the ipsilateral and contralateral lungs. All image segmentation was performed using an in-house image processing software platform as previously described.<sup>37</sup> Helium and proton image segmentation were both repeated three times and the mean values were recorded. For the  $^3\text{He}$  VV and  $^1\text{H}$  TCV, ipsilateral and contralateral lung volumes were summed to obtain the totals. Percent ventilated volume (PVV)<sup>36</sup> was generated as the VV divided by the TCV, and was computed for each lung independently as well as combined.

Diffusion-weighted images were analyzed by the same single trained observer in a controlled image visualization environment (digital copy) with room lighting levels equivalently established for all image analysis sessions. The mean apparent diffusion coefficient (ADC) and ADC maps were generated as previously reported<sup>33,35</sup> for the ipsilateral and contralateral lungs independently and for the whole lung (5 center slices)

using in-house software programmed in the IDL Virtual Machine platform (Research Systems Inc., Denver, CO as previously described<sup>19</sup> with  $b = 1.6 \text{ s/cm}^2$ . The anterior and posterior slices were not used for analysis due to insufficient signal-to-noise ratio (SNR).

### 5.2.5 $^3\text{He} - ^1\text{H}$ Image Registration

$^3\text{He} - ^1\text{H}$  MR image registration was performed to facilitate the segmentation of ventilated areas to compute a ventilated volume. Hyperpolarized  $^3\text{He}$  and  $^1\text{H}$  MR images were imported into an in-house image processing software application as previously described.<sup>37</sup> Prior to importing images and image registration  $^3\text{He}$  MR images were first viewed in ImageJ 1.33u (National Institutes of Health, USA) where the green and blue channels in the RGB scale were set to zero to achieve a red scale image. The center slice  $^3\text{He}$  and  $^1\text{H}$  images were viewed simultaneously and a single point rigid registration of coronal images was performed. The carina was used for single point rigid registration for all  $^3\text{He}$  and  $^1\text{H}$  images, and was selected as this point was consistently evident for image registration purposes in both functional and structural MR images across all study subjects.  $^3\text{He} - ^1\text{H}$  MRI registration accuracy was determined using the overlap coefficient, as previously described by Ireland and co-workers,<sup>30</sup> and modified for  $^1\text{H} - ^3\text{He}$  images. This method was adapted for image registration of the center slice only excluding the trachea and main bronchi, and was calculated using Equation 1 where  $A_{^3\text{He MRI}}$  is the area of  $^3\text{He}$  MR ventilation and  $A_{^1\text{H MRI}}$  is the area of  $^1\text{H}$  MR thoracic cavity.

$$\Omega = 100 \times \frac{A_{^3\text{He MRI}} \cap A_{^1\text{H MRI}}}{A_{^3\text{He MRI}}} \quad (1)$$

### 5.2.6 Statistical Analysis

Mean ADC and ADC standard deviation were calculated for the 5 center slices as previously described.<sup>35</sup> Mean VV, TCV and PVV and standard deviations were calculated from repeated measures for the ipsilateral, contralateral and combined lung volume. The difference between baseline and follow-up pulmonary function test results and MRI measurements were calculated for the four subjects returning for a second visit, and a mean difference was reported. Differences between ipsilateral and contralateral lung measurements were evaluated using a paired t-test. The paired t-test was also used

to evaluate differences between parameters measured at both baseline and follow-up. Correlations between imaging, radiation treatment and pulmonary function parameters were assessed using Pearson's product moment correlation coefficient. All statistical analysis was performed using SPSS 17.0 (SPSS Inc, Chicago, IL) and results were considered significant when the probability of making a Type I error was less than 5% ( $p < 0.05$ ).

## 5.3 Results

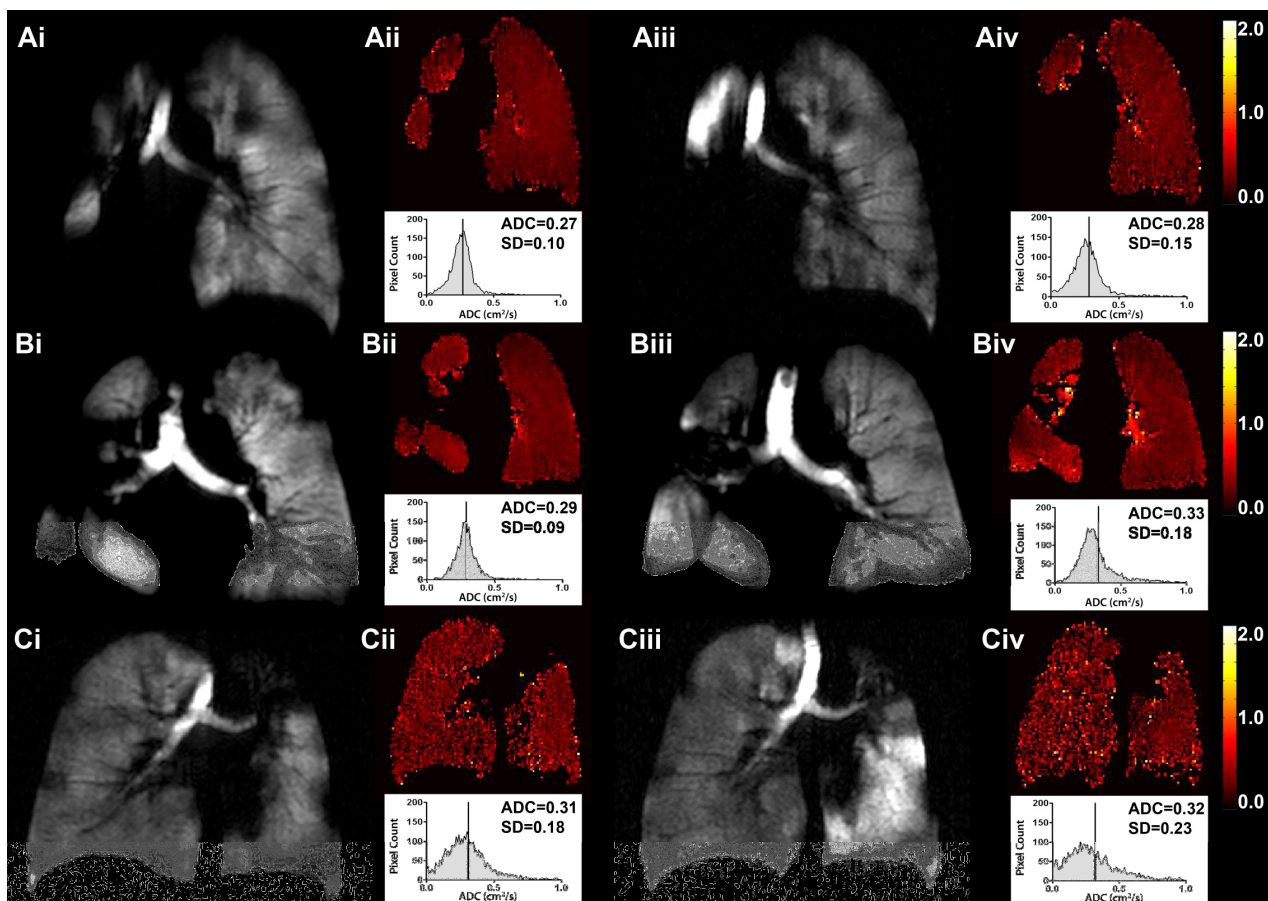
### 5.3.1 Study Subjects

Study subject demographics at baseline and follow-up are provided in Table 5-1. Seven subjects were enrolled following a clinical diagnosis of RILI based on symptomatic presentation, six after radiation treatment for lung cancer and one after breast cancer treatment. The mean period of time between the start of radiation and the first scanning visit was  $35.1 \pm 12.2$  weeks, with the first scanning visit  $9.1 \pm 5.1$  weeks following the initial report of RILI symptoms. Four subjects returned for a follow-up visit  $22.0 \pm 0.8$  weeks after the first visit. The three subjects who did not return for repeat scanning were deceased ( $n=2$ ) or too ill ( $n=1$ ) to return for follow-up. Five of the seven subjects had a smoking history of  $>10$ -pack-years. Two subjects reported an  $FEV_1 \%_{\text{predicted}} < 50\%$  at baseline and the single breast cancer subject reported an  $FEV_1 \%_{\text{predicted}} > 80\%$ . At follow-up, three subjects reported a change in  $FEV_1 \%_{\text{predicted}} < 10\%$ , while one subject reported an increase of 17%. Radiation parameters for all seven subjects are provided in Table 5-2. Subjects were treated with a mean dose to the target of  $58 \pm 7$  Gy, and for those subjects treated for lung cancer the mean lung dose (MLD) was  $17 \pm 2$  Gy and  $V_{20\text{Gy}}$  was  $32\% \pm 3\%$ , where  $V_{20\text{Gy}}$  is the percentage of lung volume receiving at least 20 Gy. The mean  $V_{20\text{Gy}}$  was calculated for five subjects, as one subject was imaged again using CT for a radiation boost and calculation of an accurate  $V_{20\text{Gy}}$  would have required dose warping, currently not available in our centre.

**Table 5-1: Subject Demographics.**

	Baseline n=7	5 month Follow-up n=4
Age yrs (SD) [range]	63 (11) [50-76]	60 (12) [51-77]
Sex- Male	2	2
Body Mass Index (SD)	28 (4)	28 (3)
FEV <sub>1</sub> % <sub>pred</sub> (SD)	62 (18)	68 (17)
FEV <sub>1</sub> /FVC % (SD)	70 (7)	74 (12)
IC (L) (SD)	1.4 (0.4) *	1.8 (0.7)
RV (L) (SD)	1.2 (0.6) *	1.7 (0.7)
FRC (L) (SD)	2.7 (0.4) *	2.9 (0.5)
TLC (L) (SD)	4.2 (0.7) *	4.7 (0.7)
DL <sub>CO</sub> % <sub>pred</sub> (SD)	62 (24) *	64 (26)

\*n=4

**Figure 5-1: Representative Baseline and Follow-up Hyperpolarized <sup>3</sup>He Ventilation Images, ADC Maps and ADC Histograms.**

A, B and C representative subjects at Baseline (i and ii) and Follow-up (iii and iv)  
 (i and iii) <sup>3</sup>He MR ventilation images at Baseline and Follow-up respectively  
 (ii and iv) <sup>3</sup>He MR ADC Map and Histogram Baseline and Follow-up respectively

**Table 5-2: Radiation Parameters.**

$V_{xGy}(\%)$  is the volume of normal lung receiving xGy radiation.

	All Subjects N=7		
	Ipsilateral Lung Mean (SD)	Contralateral Lung Mean (SD)	Total Lung Mean (SD)
Total Dose (Gy)			58.1 (7.0)
Dose Fraction (Gy)			2.01 (0.2)
Mean Lung Dose (Gy)	26.1 (9.9)	7.7 (5.6)	15.1 (5.6)
$V_{5Gy}(\%)*$	70.3 (22.8)	37.7 (30.6)	52.1 (22.7)
$V_{10Gy}(\%)*$	60.3 (23.3)	25.0 (21.9)	40.0 (17.1)
$V_{13Gy}(\%)*$	56.7 (23.1)	19.3 (17.0)	34.7 (14.4)
$V_{20Gy}(\%)*$	50.6 (21.5)	11.8 (10.7)	27.3 (10.8)

\*Calculated for 6 subjects (five lung cancer, single breast cancer) only because a single lung cancer subject underwent two separate phases of radiation with different planning CTs, and therefore these parameters could not be obtained. Dose fraction is the dose delivered in each treatment fraction (i.e. A dose fraction of 2Gy in 30 fractions results in a total dose of 60Gy).

### 5.3.2 $^3\text{He}$ MRI

Representative baseline and follow-up center slice ventilation images as well as the corresponding ADC maps and ADC histograms are provided in Figure 5-1 for three representative subjects with RILI following radiation treatment for a right hilar mass (Figure 5-1a), a right upper lobe mass (Figure 5-1b), and a left hilar mass (Figure 5-1c). All mean  $^3\text{He}$  MRI ADC and ventilation measurements are reported in Table 5-3 for the ipsilateral, contralateral and total lung for both baseline and follow-up visits. For the baseline scan, a difference in the mean ADC of  $0.03 \text{ cm}^2/\text{s}$  between lungs was observed, that was not significant ( $p=0.053$ ) (Figure 5-2a). As shown in Figure 5-2b, ventilation images showed a significant difference in VV ( $p=0.014$ ) and TCV ( $p=0.027$ ) between ipsilateral and contralateral lungs. PVV was significantly different ( $p=0.025$ ), and 33% lower in the ipsilateral lung as compared to the contralateral lung (Figure 5-2c). Longitudinal differences between baseline and follow-up for all parameters are provided in Table 5-4 and Figure 5-3 for each of the four subjects returning for the second visit. At follow-up, total mean ADC was significantly higher than at baseline ( $p=0.016$ ). When measured independently, ipsilateral mean ADC was not significantly different between baseline and follow-up ( $p=0.053$ ), while the contralateral mean ADC at follow-up was significantly increased compared to baseline ( $p=0.003$ , Figure 5-3b). As shown in Figure

5-3d, the contralateral lung also showed a significant increase in PVV at follow-up ( $p=0.012$ ), while no other  $^3\text{He}$  MRI measurements showed a statistically significant change.

### 5.3.3 Correlations

Figure 5-4 shows a graphical presentation of the longitudinal changes in ADC and PVV for ipsilateral, contralateral and whole lung with the  $V_{5\text{Gy}}$ ,  $V_{10\text{Gy}}$ ,  $V_{13\text{Gy}}$  and  $V_{20\text{Gy}}$  identified for each of the four patients who returned for follow-up imaging. For patients returning at follow-up Figure 5-4 Ai shows a trend towards improved PVV over time with lower doses to the ipsilateral lung in subjects treated for lung cancer, while Figure 5-4 Cii indicates that with lower total  $V_{x\text{Gy}}$  there is a greater increase in total ADC with time.

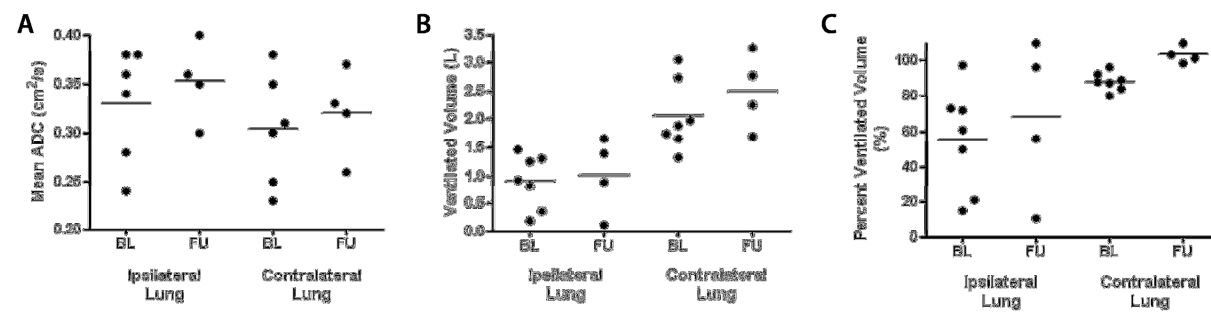


**Figure 5-2: Baseline and Follow-up Hyperpolarized  $^3\text{He}$  MRI Measurements.**

Baseline and Follow-up for the ipsilateral and contralateral lungs for all subjects.

A) mean  $^3\text{He}$  MRI ADC, B)  $^3\text{He}$  MRI VV, and C)  $^3\text{He}$  MRI PVV.



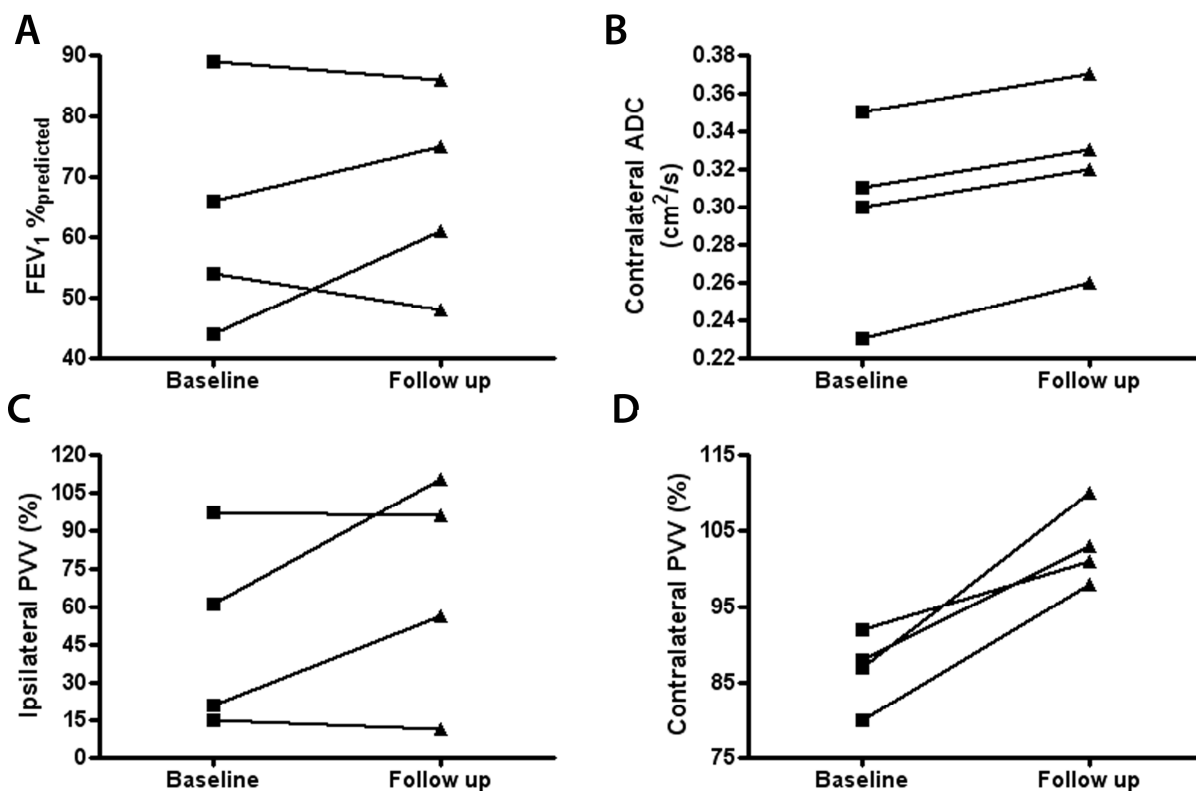


**Figure 5-3: Mean Longitudinal Differences in  $^3\text{He}$  MRI and spirometry measurements.**

Differences between Baseline and Follow-up for subjects returning for a second visit (n=4)  
 A) FEV<sub>1</sub> %<sub>pred</sub>, B) mean contralateral ADC, C) mean ipsilateral PVV and D) contralateral PVV.

At baseline there was a statistically significant correlation observed for ipsilateral VV and PVV with inspiratory capacity ( $R=0.97$ ,  $p=0.007$ ,  $R=0.89$ ,  $p=0.045$  respectively). DL<sub>CO</sub> also correlated with ipsilateral VV ( $R=0.83$ ,  $p=0.041$ ) at baseline, while ERV correlated with ipsilateral PVV ( $R= -0.89$ ,  $p=0.041$ ). Radiation parameters related to the ipsilateral lung including MLD, V<sub>5Gy</sub>, V<sub>10Gy</sub>, V<sub>13Gy</sub>, and V<sub>20Gy</sub> correlated with ipsilateral PVV ( $R= -0.79$ ,  $p=0.035$ ;  $R= -0.83$ ,  $p=0.040$ ;  $R= -0.89$ ,  $p=0.018$ ;  $R= -0.89$ ,  $p=0.018$ ;  $R= -0.85$ ,  $p=0.031$ , respectively). No other correlations between radiation parameters and  $^3\text{He}$  MRI measurements were observed.

**Table 5-3:  $^3\text{He}$  MRI ADC and Ventilation Measurements.**

	Baseline N=7			5 month Follow-up N=4		
	Ipsilateral	Contralateral	Total	Ipsilateral	Contralateral	Total
WL ADC (SD) $\text{cm}^2/\text{s}^*$	0.33 (0.06)	0.30 (0.06)	0.31 (0.05)	0.35 (0.04)	0.32 (0.04)	0.32 (0.04)
WL ADC SD (SD) $\text{cm}^2/\text{s}^*$	0.12 (0.07)	0.11 (0.07)	0.11 (0.08)	0.24 (0.02)	0.19 (0.05)	0.20 (0.04)
WL VV (SD) L	0.9 (0.5)	2.1 (0.6)	3.0 (0.7)	1.0 (0.7)	2.5 (0.7)	3.5 (0.6)
WL TCV (SD) L	1.6 (0.3)	2.3 (0.7)	3.9 (0.8)	1.4 (0.2)	2.4 (0.7)	3.8 (0.5)
WL PVV (SD) %	55 (29)	88 (5)	76 (12)	68 (45)	103 (5)	92 (15)

\*ADC data for n=6 at baseline

At follow-up whole lung PVV correlated with IC ( $R=0.97$ ,  $p=0.033$ ), FVC  $\%_{\text{predicted}}$  ( $R=0.99$ ,  $p=0.005$ ) and total dose ( $R= -0.98$ ,  $p=0.021$ ). Total dose also correlated with the follow-up ipsilateral VV and PVV ( $R= -0.98$ ,  $p=0.024$  and  $R= -0.98$ ,  $p=0.015$  respectively). The change in ipsilateral VV between baseline and follow-up correlated with the change in FEV<sub>1</sub> absolute and percent predicted ( $R=0.98$ ,  $p=0.023$  and  $R=0.99$ ,  $p=0.009$  respectively). There was no correlation between changes in spirometry values and changes in contralateral or total lung VV or PVV.

**Table 5-4: Longitudinal Differences.**

	002	003	004	005	Mean (SD)	BL -FU P
FEV <sub>1</sub> $\%_{\text{pred}}$	-6	-3	17	9	4.3 (10.7)	0.485
FVC $\%_{\text{pred}}$	-2	1	16	14	7.3 (9.1)	0.208
FEV <sub>1</sub> /FVC	14	-3	2	-2	2.8 (7.8)	0.532
TLC (L)	ND	0.54	1.16	0.47	0.7 (0.4)	0.081
DL <sub>CO</sub> $\%_{\text{pred}}$	1	0	ND	7	2.7 (3.8)	0.500
Ipsilateral WL ADC ( $\text{cm}^2/\text{s}$ )	0.02	0.05	0.02	-0.01	0.02(0.02)	0.215
Contralateral WL ADC ( $\text{cm}^2/\text{s}$ )	0.02	0.04	0.02	0.02	0.02(0.01)	0.003
Total WL ADC ( $\text{cm}^2/\text{s}$ )	0.02	0.03	0.02	0.01	0.02 (0.01)	0.016
Ipsilateral PVV	-4	0	35	49	20 (26)	0.231
Contralateral PVV	9	15	18	23	16 (6)	0.012
Total PVV	7	8	26	33	19 (13)	0.068

ND = No data for one of the two visits, BL = Baseline, FU = Follow-up

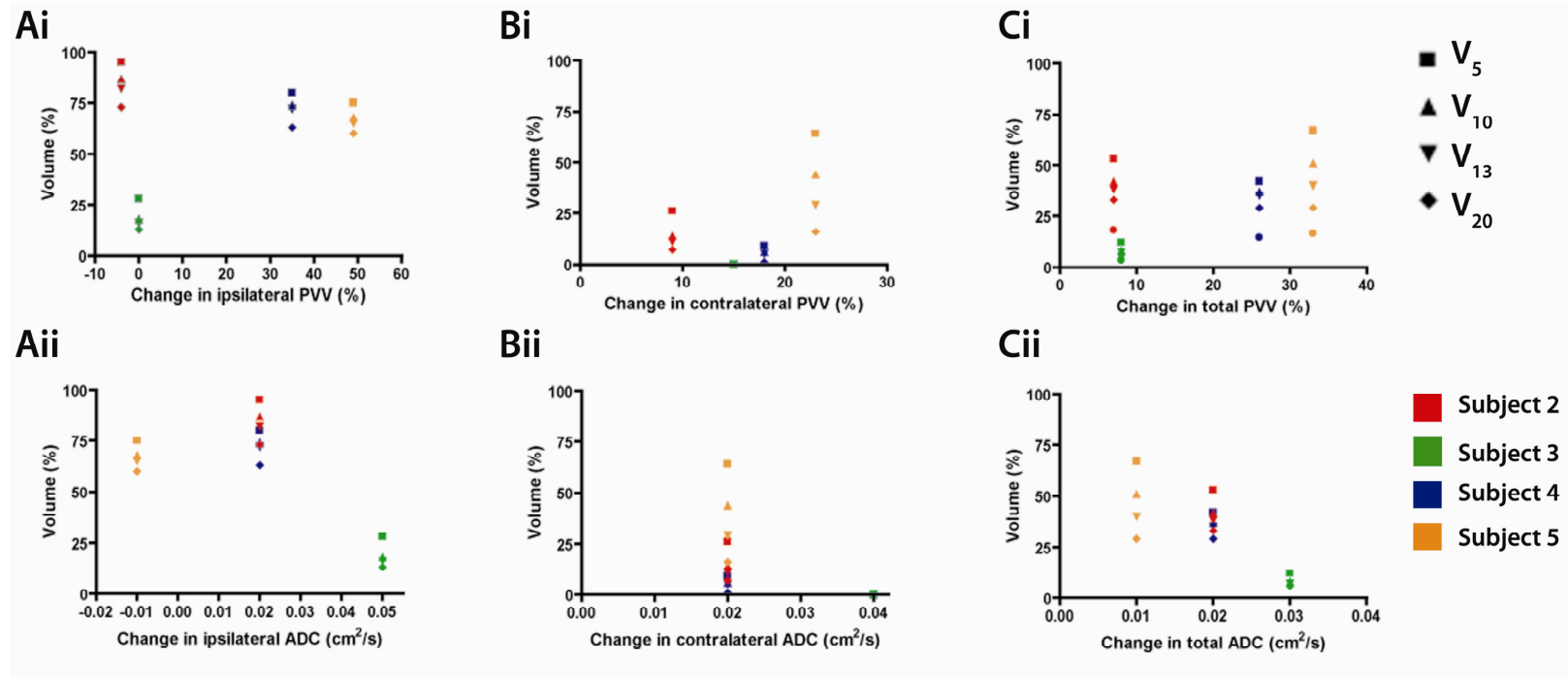


**Figure 5-4:  $^3\text{He}$  MRI longitudinal changes compared to Radiation Parameters**

A) MRI measurements ipsilateral lung of four subjects returning at follow-up compared to  $V_{x\text{Gy}}\%$  (the volume of normal lung receiving  $x$  Gy of radiation).

B) MRI measurements contralateral lung compared to  $V_{x\text{Gy}}(\%)$

C) MRI measurements both lungs compared to  $V_{x\text{Gy}}(\%)$  (i) PVV, (ii) ADC.

### 5.3.4 Image Registration

Image registration results are provided in Figure 5-5 showing  $^3\text{He} - ^1\text{H}$  registration for subjects 002, 004, 005 and 008, with the  $^3\text{He}$  signal in red and the  $^1\text{H}$  signal in gray scale.  $^3\text{He} - ^1\text{H}$  registration accuracy was evaluated at baseline for all seven subjects with a mean overlap coefficient of  $93.6 \pm 4.6\%$ .

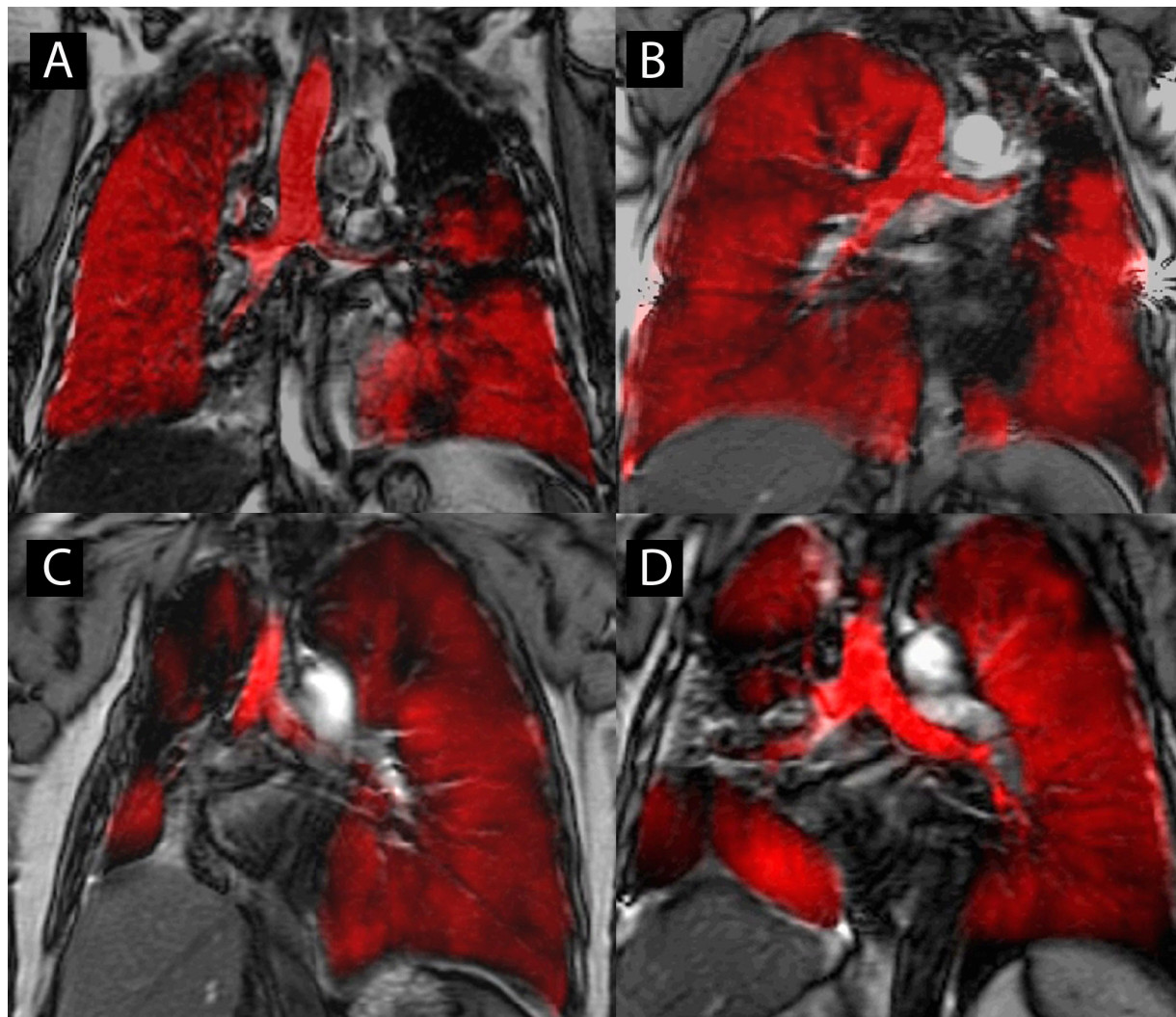


**Figure 5-5: Representative subjects showing  $^3\text{He} - ^1\text{H}$  MR Image Registration.**

Centre slice  $^3\text{He} - ^1\text{H}$  image registration is shown with the  $^3\text{He}$  signal intensity in red, and the  $^1\text{H}$  signal intensity in grey scale for a) subject 008, b) subject 005, c) subject 002 and d) subject 004.

## 5.4 Discussion

*In vivo* imaging provides a way to quantitatively evaluate spatial and temporal changes in the lung, post-radiation, such as consolidation within the lung visualized using CT for which various patterns have been described<sup>38</sup> ranging from slightly increased density to solid consolidation and irregular bronchi. As another example, functional imaging of RILI using SPECT provides images which can be evaluated for ventilation and perfusion defects,<sup>39-41</sup> and while the incidence of the latter is more common, both measurements appear to be more sensitive than CT measurements for the detection of functional lung changes.<sup>42</sup> Despite the development of these important imaging approaches, and the elegant work of a number of teams using CT,<sup>38,43-45</sup> the temporal and spatial aspects of RILI initiation and progression are still not well understood, partially because of the widely varying imaging protocols and a lack of intensive serial studies reported in the literature. Emerging hyperpolarized noble gas MRI methods may provide a way to measure specific RILI effects that are often very complex given the myriad of other malignancy-related changes occurring prior to and after radiation. The advantage of <sup>3</sup>He MRI approaches for RILI may derive from the fact that the method is rapid, well-tolerated,<sup>46</sup> provides regional functional information with relatively high spatial resolution, and enables intensive serial studies that could potentially identify early and late mechanisms of disease initiation and progression, respectively. Once specific measurements and potential mechanisms are identified, it is theoretically possible to improve the spatial resolution of therapy (guidance) and perhaps increase doses to improve tumour response with decreased normal tissue (or at least normal functioning tissue) damage. This is critical in the lung in particular where improvements in radiation therapy methods have not resulted in significantly improved patient survival.<sup>47</sup>

Here in a small pilot study of RILI patients, we provide quantitative structural and functional <sup>3</sup>He MRI measurements in subjects after symptomatic RILI onset. Accordingly we report: 1) <sup>3</sup>He MRI ADC, VV, PVV and <sup>1</sup>H MRI TCV for seven subjects approximately 8 months after radiation therapy and again 6 months later for four of these subjects, 2) correlations between <sup>3</sup>He MRI measurements, well-established pulmonary function and lung volume measurements and radiation parameters, and, 3) feasibility and implementation of functional <sup>3</sup>He MR image

registration with structural  $^1\text{H}$  MR images. To our knowledge, this is the first longitudinal application of hyperpolarized  $^3\text{He}$  MRI in subjects after clinical diagnosis of RILI.

First, and as might be expected, at baseline we observed a significant difference in TCV of the ipsilateral and contralateral lungs, suggestive of gross thoracic cavity remodelling following radiation injury. Additionally  $^3\text{He}$  VV in the ipsilateral and contralateral lung was significantly different, likely reflecting the decreased lung volume available for ventilation in the target lung. Importantly, we noted a significant difference in PVV, which was higher in the contralateral lung, suggesting that the functional capacity of the contralateral lung remained high following radiation treatment. The lower PVV reported in the ipsilateral lung may be due to inflammation or scarring related to the radiation dose and for some patients, due to residual tumour burden; however, the direct cause cannot be directly ascertained due lack of histological confirmation. At baseline, the contralateral lung reported a lower mean ADC and the difference was below the threshold for statistical significance ( $p=0.053$ ). If this result is indeed found to be significant in a larger group of patients, this would contradict previous studies in animals<sup>48</sup> where the ipsilateral lung showed lower ADC (suggestive of fibrosis) than the contralateral lung. One possible explanation for the result obtained here is that the severely fibrosed regions of the ipsilateral lung could not be ventilated and therefore could not contribute to the ADC measurement, resulting in an increased ADC. Additionally, the increased contralateral lung ADC values might alternatively reflect increased inflammation at the baseline scan, or increased alveolar dimensions due to increased ventilation in the contralateral lung.

Second, for the small number of patients who were scanned at follow-up, there was a significant change in the contralateral PVV and both the contralateral and whole lung  $^3\text{He}$  ADC. Both results show that in small numbers of subjects  $^3\text{He}$  MRI can sensitively detect lung structural and functional changes as RILI progresses. We were surprised to observe the unexpected increase in contralateral PVV that occurred between weeks 35 and 57 post-radiation. This indicated that although the TCV did not change over the 22 week period, the functional capacity of that volume showed a significant increase, suggesting that functional, but not gross structural remodelling occurred in response to the apparent loss of function in the ipsilateral lung (as evidenced by low

ipsilateral PVV in the majority of subjects). To our knowledge this increase in functional capacity of the contralateral lung, long after radiation treatment, and in isolation of structural lung volume change, is a novel finding, not previously reported in the literature. The statistically significant increase in ADC we observed (which in COPD has been validated using histology<sup>49</sup> and CT<sup>50</sup> as an increase of alveolar dimensions reflecting emphysema) over a relatively short period of 22 weeks was greater than the rate previously established for healthy aging non-smokers,<sup>14</sup> and therefore is unlikely related to age-related emphysema. In a previous animal model study of radiation fibrosis, alveolar septal thickening was suggested as the explanation for decreased <sup>3</sup>He MRI ADC post-radiation.<sup>48</sup> For the patients studied here, imaging was approximately 8 months post-radiation therapy which is most likely within the radiation fibrosis timeframe.<sup>51</sup> Therefore, the increase in ADC observed in the contralateral lung may reflect decreased or perhaps resolution/improvement of radiation-induced inflammation or fibrosis over time; no change in the ipsilateral ADC was reported perhaps because of irreversible fibrosis in that lung.

Third, correlations were observed between <sup>3</sup>He MRI measurements, pulmonary function measurements and radiation parameters. The significant negative correlation between radiation parameters (MLD, V<sub>5Gy</sub>, V<sub>10Gy</sub>, V<sub>13Gy</sub>, and V<sub>20Gy</sub>) and PVV for the ipsilateral lung is in agreement with our understanding of the direct negative relationship between lung function and radiation treatment. Additionally, DL<sub>CO</sub> which is commonly impaired in subjects with RILI,<sup>6,11,52,53</sup> was significantly correlated with ipsilateral VV, which is in agreement with our understanding that the lungs diminished capacity to ventilate can result in significant decreases in gas transfer.

Finally, we showed that MR image registration was feasible in this patient group and over these time periods. <sup>3</sup>He-<sup>1</sup>H registration resulted in an overlap coefficient of 93.6%, likely due to the fact that the elapsed time between scans was on the order of minutes, and subjects were not moved between scans. This registration may be used in future to aid lung volume segmentation and for the development of semi- and fully-automated segmentation of <sup>3</sup>He MRI lung volumes. Furthermore, future studies should involve registration of <sup>3</sup>He MR ventilation images to CT

images both pre- and post-radiation, to aid in ascertaining a direct relationship between scarring and functional impairment in the lungs of subjects with RILI.

We acknowledge a number of specific limitations of this study, the first of which is the small sample size at baseline (n=7) and follow-up (n=4). This may have restricted our ability to detect other significant differences between lungs at baseline and longitudinally. In future studies with larger sample sizes it will be important to closely monitor additional clinical factors such as specific treatment regimes (specific chemotherapies administered concurrently), specific post-radiation respiratory difficulties experienced, smoking status and O<sub>2</sub> usage to determine whether any of these variables directly affect the functional or structural changes reported in subjects with RILI that could not be evaluated here due to limited sample size. We also recognize that a multi-modality comparison using CT would have provided an opportunity to directly compare and contrast the sensitivity of <sup>3</sup>He MRI and quantitative high resolution CT which would provide critical context for the functional and structural findings we report here. Finally, another potential shortcoming of this pilot study relates to the fact that we only implemented rudimentary registration methods in this study and that in future whole lung registration should be evaluated as well as image registration with a greater number of fiducial markers.

A previous study using <sup>3</sup>He MRI by Ireland and co-workers<sup>29</sup> showed that functional information obtained prior to radiation could be used in conjunction with CT for radiation planning. Here in this small pilot study of seven patients, we add to this significant body of work and show that <sup>3</sup>He MRI provides quantitative and regional measurements of RILI post-diagnosis and longitudinally for the target and non-target lung.

## 5.5 Conclusion

In conclusion, hyperpolarized <sup>3</sup>He MRI provides a way to acquire quantitative lung functional information as well as a method to measure <sup>3</sup>He diffusion to probe airway and airspace sizes. Furthermore, for the first time we showed that lung function in the contralateral lung significantly increased over time following the onset of symptomatic RILI, likely to compensate



for the radiation-induced functional damage that was largely restricted to the ipsilateral lung and constant over the time course of this study.

## 5.6 References

- (1) Bentzen SM, Skoczylas JZ, Bernier J. Quantitative clinical radiobiology of early and late lung reactions. *Int J Radiat Biol.* 2000; 76(4):453-462.
- (2) Movsas B, Raffin TA, Epstein AH et al. Pulmonary radiation injury. *Chest.* 1997; 111(4):1061-1076.
- (3) Kocak Z, Evans ES, Zhou SM et al. Challenges in defining radiation pneumonitis in patients with lung cancer. *Int J Radiat Oncol Biol Phys.* 2005; 62(3):635-638.
- (4) McDonald S, Rubin P, Phillips TL et al. Injury to the lung from cancer therapy: clinical syndromes, measurable endpoints, and potential scoring systems. *Int J Radiat Oncol Biol Phys.* 1995; 31(5):1187-1203.
- (5) Rodrigues G, Lock M, D'Souza D et al. Prediction of radiation pneumonitis by dose-volume histogram parameters in lung cancer--a systematic review. *Radiotherapy and Oncology.* 2004; 71(2):127-138.
- (6) Mehta V. Radiation pneumonitis and pulmonary fibrosis in non-small-cell lung cancer: Pulmonary function, prediction, and prevention. *Int J Radiat Oncol Biol Phys.* 2005; 63(1):5-24.
- (7) Gross NJ. Pulmonary effects of radiation therapy. *Ann Intern Med.* 1977; 86(1):81-92.
- (8) Rubin P, Casarett G. Respiratory system in clinical radiation pathology. *Clinical Radiation Pathology.* Philadelphia, PA: W.B. Saunders, 1968: 423-470.
- (9) Abratt RP, Morgan GW. Lung toxicity following chest irradiation in patients with lung cancer. *Lung Cancer.* 2002; 35(2):103-109.
- (10) Roswit B, White DC. Severe radiation injuries of the lung. *AJR Am J Roentgenol.* 1977; 129(1):127-136.
- (11) Miller KL, Zhou SM, Barrier RC, Jr. et al. Long-term changes in pulmonary function tests after definitive radiotherapy for lung cancer. *Int J Radiat Oncol Biol Phys.* 2003; 56(3):611-615.
- (12) Yablonskiy DA, Sukstanskii AL, Leawoods JC et al. Quantitative in vivo assessment of lung microstructure at the alveolar level with hyperpolarized <sup>3</sup>He diffusion MRI. *Proc Natl Acad Sci U S A.* 2002; 99(5):3111-3116.

- (13) Kauczor HU, Ebert M, Kreitner KF et al. Imaging of the lungs using  $^3\text{He}$  MRI: preliminary clinical experience in 18 patients with and without lung disease. *J Magn Reson Imaging*. 1997; 7(3):538-543.
- (14) Fain SB, Altes TA, Panth SR et al. Detection of age-dependent changes in healthy adult lungs with diffusion-weighted  $^3\text{He}$  MRI. *Acad Radiol*. 2005; 12(11):1385-1393.
- (15) Parraga G, Mathew L, Etemad-Rezai R et al. Hyperpolarized  $^3\text{He}$  magnetic resonance imaging of ventilation defects in healthy elderly volunteers: initial findings at 3.0 Tesla. *Acad Radiol*. 2008; 15(6):776-785.
- (16) de Lange EE, Mugler JP, III, Brookeman JR et al. Lung air spaces: MR imaging evaluation with hyperpolarized  $^3\text{He}$  gas. *Radiology*. 1999; 210(3):851-857.
- (17) Salerno M, Altes TA, Mugler JP, III et al. Hyperpolarized noble gas MR imaging of the lung: potential clinical applications. *Eur J Radiol*. 2001; 40(1):33-44.
- (18) Salerno M, de Lange EE, Altes TA et al. Emphysema: hyperpolarized helium 3 diffusion MR imaging of the lungs compared with spirometric indexes--initial experience. *Radiology*. 2002; 222(1):252-260.
- (19) Parraga G, Ouriadov A, Evans A et al. Hyperpolarized  $^3\text{He}$  ventilation defects and apparent diffusion coefficients in chronic obstructive pulmonary disease: preliminary results at 3.0 Tesla. *Invest Radiol*. 2007; 42(6):384-391.
- (20) Saam BT, Yablonskiy DA, Kodibagkar VD et al. MR imaging of diffusion of ( $^3\text{He}$ ) gas in healthy and diseased lungs. *Magn Reson Med*. 2000; 44(2):174-179.
- (21) Swift AJ, Wild JM, Fichele S et al. Emphysematous changes and normal variation in smokers and COPD patients using diffusion  $^3\text{He}$  MRI. *Eur J Radiol*. 2005; 54(3):352-358.
- (22) McMahon CJ, Dodd JD, Hill C et al. Hyperpolarized  $^3\text{He}$  magnetic resonance ventilation imaging of the lung in cystic fibrosis: comparison with high resolution CT and spirometry. *Eur Radiol*. 2006; 16(11):2483-2490.
- (23) van Beek EJ, Hill C, Woodhouse N et al. Assessment of lung disease in children with cystic fibrosis using hyperpolarized  $^3\text{He}$ -MRI: comparison with Shwachman score, Crispin-Norman score and spirometry. *Eur Radiol*. 2007; 17(4):1018-1024.
- (24) Mentore K, Froh DK, de Lange EE et al. Hyperpolarized  $^3\text{He}$  MRI of the lung in cystic fibrosis: assessment at baseline and after bronchodilator and airway clearance treatment. *Acad Radiol*. 2005; 12(11):1423-1429.

- (25) Altes TA, Powers PL, Knight-Scott J et al. Hyperpolarized  $^3\text{He}$  MR lung ventilation imaging in asthmatics: preliminary findings. *J Magn Reson Imaging*. 2001; 13(3):378-384.
- (26) de Lange EE, Altes TA, Patrie JT et al. The variability of regional airflow obstruction within the lungs of patients with asthma: assessment with hyperpolarized helium-3 magnetic resonance imaging. *J Allergy Clin Immunol*. 2007; 119(5):1072-1078.
- (27) Samee S, Altes T, Powers P et al. Imaging the lungs in asthmatic patients by using hyperpolarized helium-3 magnetic resonance: assessment of response to methacholine and exercise challenge. *J Allergy Clin Immunol*. 2003; 111(6):1205-1211.
- (28) Fain SB, Gonzalez-Fernandez G, Peterson ET et al. Evaluation of structure-function relationships in asthma using multidetector CT and hyperpolarized He-3 MRI. *Acad Radiol*. 2008; 15(6):753-762.
- (29) Ireland RH, Bragg CM, McJury M et al. Feasibility of image registration and intensity-modulated radiotherapy planning with hyperpolarized helium-3 magnetic resonance imaging for non-small-cell lung cancer. *Int J Radiat Oncol Biol Phys*. 2007; 68(1):273-281.
- (30) Ireland RH, Woodhouse N, Hoggard N et al. An image acquisition and registration strategy for the fusion of hyperpolarized helium-3 MRI and x-ray CT images of the lung. *Phys Med Biol*. 2008; 53(21):6055-6063.
- (31) Standardization of Spirometry, 1994 Update. American Thoracic Society. *Am J Respir Crit Care Med*. 1995; 152(3):1107-1136.
- (32) Mathew L, Evans A, Ouriadov A et al. Hyperpolarized ( $^3\text{He}$ ) magnetic resonance imaging of chronic obstructive pulmonary disease reproducibility at 3.0 tesla. *Acad Radiol*. 2008; 15(10):1298-1311.
- (33) Evans A, McCormack DG, Santyr G et al. Mapping and quantifying hyperpolarized  $^3\text{He}$  magnetic resonance imaging apparent diffusion coefficient gradients. *J Appl Physiol*. 2008; 105(2):693-699.
- (34) Parraga G, Ouriadov A, Evans A et al. Hyperpolarized  $^3\text{He}$  ventilation defects and apparent diffusion coefficients in chronic obstructive pulmonary disease: preliminary results at 3.0 Tesla. *Invest Radiol*. 2007; 42(6):384-391.
- (35) Evans A, McCormack D, Ouriadov A et al. Anatomical distribution of  $^3\text{He}$  apparent diffusion coefficients in severe chronic obstructive pulmonary disease. *J Magn Reson Imaging*. 2007; 26(6):1537-1547.

- (36) Woodhouse N, Wild JM, Paley MN et al. Combined helium-3/proton magnetic resonance imaging measurement of ventilated lung volumes in smokers compared to never-smokers. *J Magn Reson Imaging*. 2005; 21(4):365-369.
- (37) Landry A, Spence JD, Fenster A. Quantification of carotid plaque volume measurements using 3D ultrasound imaging. *Ultrasound Med Biol*. 2005; 31(6):751-762.
- (38) Libshitz HI, Shuman LS. Radiation-induced pulmonary change: CT findings. *J Comput Assist Tomogr*. 1984; 8(1):15-19.
- (39) Seppenwoolde Y, Muller SH, Theuws JC et al. Radiation dose-effect relations and local recovery in perfusion for patients with non-small-cell lung cancer. *Int J Radiat Oncol Biol Phys*. 2000; 47(3):681-690.
- (40) Marks LB, Munley MT, Spencer DP et al. Quantification of radiation-induced regional lung injury with perfusion imaging. *Int J Radiat Oncol Biol Phys*. 1997; 38(2):399-409.
- (41) Boersma LJ, Damen EM, de Boer RW et al. Estimation of overall pulmonary function after irradiation using dose-effect relations for local functional injury. *Radiother Oncol*. 1995; 36(1):15-23.
- (42) Evans ES, Hahn CA, Kocak Z et al. The Role of Functional Imaging in the Diagnosis and Management of Late Normal Tissue Injury. *Seminars in Radiation Oncology*. 2007; 17(2):72-80.
- (43) Mah K, Poon PY, Van Dyk J et al. Assessment of acute radiation-induced pulmonary changes using computed tomography. *J Comput Assist Tomogr*. 1986; 10(5):736-743.
- (44) Mah K, Van Dyk J, Keane T et al. Acute radiation-induced pulmonary damage: a clinical study on the response to fractionated radiation therapy. *Int J Radiat Oncol Biol Phys*. 1987; 13(2):179-188.
- (45) Pagani JJ, Libshitz HI. CT manifestations of radiation-induced change in chest tissue. *J Comput Assist Tomogr*. 1982; 6(2):243-248.
- (46) Lutey BA, Lefrak SS, Woods JC et al. Hyperpolarized  $^3\text{He}$  MR imaging: physiologic monitoring observations and safety considerations in 100 consecutive subjects. *Radiology*. 2008; 248(2):655-661.
- (47) Spiro SG, Silvestri GA. One hundred years of lung cancer. *Am J Respir Crit Care Med*. 2005; 172(5):523-529.
- (48) Ward ER, Hedlund LW, Kurylo WC et al. Proton and hyperpolarized helium magnetic resonance imaging of radiation-induced lung injury in rats. *Int J Radiat Oncol Biol Phys*. 2004; 58(5):1562-1569.

- (49) Woods JC, Choong CK, Yablonskiy DA et al. Hyperpolarized  $^3\text{He}$  diffusion MRI and histology in pulmonary emphysema. *Magn Reson Med.* 2006; 56(6):1293-1300.
- (50) Diaz S, Casselbrant I, Piitulainen E et al. Validity of apparent diffusion coefficient hyperpolarized ( $^3\text{He}$ )-MRI using MSCT and pulmonary function tests as references. *Eur J Radiol.* 2008.
- (51) Rubin P, Johnston CJ, Williams JP et al. A perpetual cascade of cytokines postirradiation leads to pulmonary fibrosis. *Int J Radiat Oncol Biol Phys.* 1995; 33(1):99-109.
- (52) De Jaeger K, Seppenwoolde Y, Boersma LJ et al. Pulmonary function following high-dose radiotherapy of non-small-cell lung cancer. *Int J Radiat Oncol Biol Phys.* 2003; 55(5):1331-1340.
- (53) Gopal R, Tucker SL, Komaki R et al. The relationship between local dose and loss of function for irradiated lung. *Int J Radiat Oncol Biol Phys.* 2003; 56(1):106-113.

## CHAPTER 6: CONCLUSIONS AND FUTURE DIRECTIONS

### 6.1 Overview and Summary

The development of new, sensitive and precise measurements of lung function are critical for a better understanding of the structure-function paradigm that exists in the lung in both the normal and disease states.<sup>1,2</sup> Currently, the gold standard method for evaluating lung function is spirometry. Specifically FEV<sub>1</sub>, measuring airflow limitation, is influenced by both regions of functional impairment and anatomical changes in the lung tissue microstructure and airway calibre. Thus, FEV<sub>1</sub> is a good indicator of disease presence, but cannot provide any information on the contribution of underlying structural impairments or ventilation abnormalities that contribute to airflow obstruction. Furthermore, it does not give any indicator of the regional burden of disease, which is important for disease classification and guiding interventions and treatments. Therefore, when airflow limitation is detected further examination is often required. Chest x-rays are most commonly used for subsequent evaluation, but provide extremely limited quantitative information. CT is often the imaging modality of choice for high resolution pulmonary imaging.<sup>3</sup> Using CT, it is possible to evaluate the lung microstructure by way of lung attenuation measurements<sup>3-6</sup> and to evaluate the airways through measurements of the airway wall<sup>7-10</sup>, but the relationship these structural measurements have with lung function is often not clear. Moreover, CT is associated with significant increase in radiation exposure compared to chest x-ray, and because of the high radiation dose, serial CT exams over short time frames and longitudinal studies are not practical or safe even in elderly subjects. Thus, using clinically available imaging tools, lung structure can be probed without any information on the functional impact of structural abnormalities observed. Nuclear medicine techniques could fill this functional imaging gap, but they too are associated with radiation dose, suffer from poor resolution, and deposition of tracer particles in the central airways.<sup>11,12</sup> Given that loss of lung function often occurs regionally within the lung, and may be associated with changes in lung microstructure, airway remodelling, or both, an ideal imaging tool would allow for quantitative

measurements of functional impairments in both cross-sectional and longitudinal studies, in conjunction with measurements of underlying lung structure.<sup>2</sup>

It is in this context that we embarked on developing quantitative measurements of lung function derived from hyperpolarized <sup>3</sup>He MR images. In this thesis we evaluated <sup>3</sup>He MRI measurements of lung function in cross-sectional and longitudinal studies of healthy volunteers and subjects with smoking-related lung disease. In regard to these measurements, we tested the following hypotheses: 1) metrics for quantifying <sup>3</sup>He MR ventilation images have high short-term reproducibility 2) changes in lung function occurring with normal healthy aging can be detected using measurements of functional <sup>3</sup>He MR images, 3) functional and structural <sup>3</sup>He MRI measurements of COPD subjects, taken together, can be used to stratify disease, and, 4) radiation-induced lung injury results in long-term changes in lung function that can be measured using <sup>3</sup>He MRI.

In Chapter 2, the same-day and seven-day reproducibility of VDV was evaluated from <sup>3</sup>He MR images acquired at 3.0T. Twenty-four age-matched subjects were imaged with <sup>3</sup>He MRI twice within  $7 \pm 2$  minutes and again  $7 \pm 2$  days later. Same-day and seven-day reproducibility were evaluated using ICC, CCC and linear regression. Same-day VDV was highly reproducible for all subjects (ICC = 0.97, CCC = 0.98,  $r^2 = 0.94$ ), while seven-day VDV was significantly lower ( $p < 0.01$ , ICC = 0.74, CCC = 0.75,  $r^2 = 0.58$ ). Over the seven day time period there were no significant differences in FEV<sub>1</sub> and FEV<sub>1</sub>/FVC. ADC, derived from diffusion-weighted <sup>3</sup>He MRI, was also evaluated for reproducibility over the same time period. ADC was not significantly different at the seven minute or seven day time mark, and was found to be highly reproducible at both time points (same-day  $r^2 = 0.93$ , seven-day  $r^2 = 0.96$ ). This is the first study to report the reproducibility of VDV, and more importantly, the first to report on the reproducibility of any method for quantifying ventilation defects with <sup>3</sup>He MRI. Additionally, this is the first study to report on the reproducibility of <sup>3</sup>He MRI evaluated at 3.0T. Overall, in Chapter 2 we demonstrate that <sup>3</sup>He MRI VDV has high short-term reproducibility, and therefore has potential as a non-invasive quantitative marker of lung function for use in clinical trials



evaluating new treatments, as well as in longitudinal and cross-sectional research studies of smoking-related lung disease.

In Chapter 3,  $^3\text{He}$  MRI VDV was measured in a group of young healthy volunteers (mean age = 44), and another group of elderly healthy volunteers (mean age = 67). Images were acquired twice in one day, and again one week later to evaluate the inter-scan VDV variability. Images were scored and analyzed by four trained observers to assess the inter-observer variability of VDV. No ventilation defects were observed in the younger subjects, while in the older subject group, six of eight subjects had ventilation defects, with a mean VDV =  $52 \pm 34 \text{ cm}^3$ . Same-day and seven-day COVs were 1.8% and 5.3% respectively, while the inter-observer COV ranged from 10-12%. Overall, this study demonstrates that there are ventilation defects present in healthy elderly adults that are quantifiable using VDV, and that these age-related changes in lung function are highly reproducible over short time periods. Smoking-related lung disease, specifically COPD, tends to occur in elderly individuals, and thus it will be important in future studies quantifying lung function using  $^3\text{He}$  MRI to differentiate between  $^3\text{He}$  MRI VDV likely related to age alone, and volumes likely related to both age and COPD in this elderly diseased population.

In Chapter 4, functional and structural  $^3\text{He}$  MRI measurements were captured and used to stratify subjects with COPD according to the proportional contribution of these measurements to the overall sum of disease. Twenty former smokers with mainly stage II and stage III COPD were imaged using  $^3\text{He}$  MRI at a single time-point. Based on the relative contribution of normalized ADC and VDP, there was evidence of a predominant measurement in seven of the twenty subjects, three having mainly ventilation defects and four having mainly emphysema. Additionally, those with a predominant measurement had less overall disease, suggesting that mainly ventilation defects or tissue destruction develop early in the disease, with both being present at later stages. This was the first study to explore the potential of  $^3\text{He}$  MRI derived measurements to stratify subjects with COPD, and results suggest that 35% of subjects had a single predominant measurement – which is in agreement with previously published CT data.<sup>9</sup> Further studies with increased sample size should be performed to evaluate  $^3\text{He}$  MRI based

measurements as a tool for phenotyping COPD. With further validation,  $^3\text{He}$  MRI VDP and ADC phenotypes may allow for identification and selection of COPD subjects based on their baseline  $^3\text{He}$  MRI-derived phenotype for clinical studies. Potential new treatments could then be evaluated in a specific  $^3\text{He}$  MRI phenotype, and specific underlying changes in lung function and structure evaluated.

In Chapter 5,  $^3\text{He}$  MRI derived measurements of lung function were used for the longitudinal evaluation of subjects with a clinical diagnosis of radiation-induced lung injury. Static ventilation and diffusion-weighted MR images were acquired  $35 \pm 12$  weeks after radiation therapy began and again  $22.0 \pm 0.8$  weeks later. At baseline, PVV was significantly lower ( $p < 0.05$ ) in the ipsilateral diseased lung. In four subjects returning for follow-up evaluation significant differences in both PVV and ADC were reported.  $^3\text{He}$  MRI PVV increased by  $16\% \pm 6\%$  ( $p < 0.05$ ), and  $^3\text{He}$  ADC increased by  $0.02 \pm 0.01 \text{ cm}^2/\text{s}$  ( $p < 0.01$ ). Hyperpolarized  $^3\text{He}$  MRI was well tolerated in all subjects with moderate to severe RILI. Functional improvements and microstructural changes were observed in the contralateral lung, while the ipsilateral lung remained stable, suggesting that functional compensatory changes may have occurred in the contralateral lung due to ipsilateral radiation-induced lung injury. These findings highlight the sensitivity of  $^3\text{He}$  MRI VDV to changes in lung function, and for the first time provide evidence of functional changes in the fibrotic stage of RILI. Specifically, this is the first report to suggest that the lung has the ability to compensate for a severe, local functional injury by increasing its functional capacity in other regions.

In Appendix A current methods for analyzing static ventilation images found in the  $^3\text{He}$  MRI literature were described along with their limitations. Specific needs for  $^3\text{He}$  MRI ventilation analysis were addressed, and most importantly methods needed for quantitative comparative analysis of  $^3\text{He}$  MR ventilation images acquired from the same subject at multiple time-points were described. Requirements for image analysis include registration, signal normalization, and image subtraction for regional difference analysis. Development of these quantitative tools will further establish the potential of  $^3\text{He}$  ventilation image-derived measurements as sensitive markers of regional lung function that can be used as an analysis tool in clinical trials.

Appendix B described a case study of a single subject imaged pre- and post-Airway Bypass (AB). The subject was imaged over a four year time-period; at baseline, two years later, and again six and twelve months following AB. In the two years between baseline and first follow-up visit, there was a decrease in VDP that corresponded to a visually apparent worsening on the  $^3\text{He}$  MR images. Following the AB procedure VDV and VDP improved, which corresponded to a self-reported improvement according to the mMRC scale, along with an improvement in cycle ergometry test time. Although the subject reported feeling better and visually apparent changes in ventilation were observed and quantified, there were minimal change in PFTs. While this is the only subject in the Broncus AB study to have  $^3\text{He}$  MRI data, quantitative  $^3\text{He}$  ventilation results following therapeutic intervention showed an improvement, were reflective of the improvement in dyspnea scores (while PFTs did not show any change), and therefore highlight the potential of this technique as a sensitive measure of lung function in clinical trials.

Here in Chapter 6 the conclusions that can be drawn from the studies presented in this thesis are addressed, as well as the limitations of these studies and possible future work that will expand on the work presented in Chapters 2-5. The conclusions of this thesis are addressed in section 6.2, the limitations of the current studies and solutions are presented in section 6.3, and possible future studies are detailed in section 6.4.

## 6.2 Summary of Conclusions

Overall, we have presented a new method for quantifying  $^3\text{He}$  ventilation defects present in static ventilation MR images. Measurements of ventilation defect volume are shown to have high same-day and moderate seven-day reproducibility in healthy volunteers and subjects with COPD. Furthermore, they are sensitive to changes in ventilation that occur with aging in healthy individuals. The quantification of ventilation changes that occur with age is important, as lung diseases typically occur in elderly individuals, and it is important to differentiate between functional changes occurring due to age, and those occurring due to lung disease. COPD, the most common smoking-related lung disease, is known to be a heterogenous disease and we have shown here that the quantification of ventilation defects in conjunction with the quantification of underlying microstructural abnormalities measured using  $^3\text{He}$  MRI can be used to stratify

subjects according to the proportion of these functional and structural measurements to the overall sum of  $^3\text{He}$  MRI measured disease. This initial report suggests that  $^3\text{He}$  MRI may have a role to play in phenotyping COPD for treatment, and additional larger-scale studies will be needed to confirm this result. Additionally, in a small group of subjects diagnosed with RILI post-radiation therapy, functional and structural changes were observed and quantified in the contralateral lung. The improvement in contralateral lung function observed suggests that there is a compensatory effect following severe radiation injury to the ipsilateral lung. Furthermore, the changes in contralateral lung microstructure observed over 22 weeks in this very small group of RILI subjects speaks to the sensitivity of  $^3\text{He}$  MRI ADC for detecting differences in lung microstructure longitudinally.

In summary, we have provided: 1) evidence that VDV derived from  $^3\text{He}$  MRI images has high short-term reproducibility, 2) evidence of reproducible ventilation defects in healthy elderly subjects, not present in their younger healthy peers, 3) a new method for stratification of subjects with COPD based on  $^3\text{He}$  MRI derived VDP and normalized ADC, and, 4) evidence of longitudinal changes in function and structure of the contralateral lung in subjects clinically diagnosed with RILI.

## **6.3 Limitations of Current Tools and Solutions**

The limitations of the studies presented in this thesis are discussed in this section, along with recommended solutions to address these limitations in future studies. A number of limitations addressed in this section are common to multiple studies described in this thesis, while others are study specific. This section begins by addressing the study-specific limitations in sub-section 6.3.1, while general limitations are discussed in section 6.3.2.

### **6.3.1 Study Specific Limitations**

In Chapter 2 and 3, VDV was measured from hyperpolarized  $^3\text{He}$  MRI. One of the primary goals of the initial  $^3\text{He}$  MRI study of healthy elderly subjects and subjects with COPD was to assess the reproducibility of  $^3\text{He}$  MRI measurements of the ADC; measurements of ventilation derived from these images was a secondary marker and therefore did not drive the data collection

scheme/MR pulse sequence design. The ADC is calculated from DWI, which have inherently thicker slices than  $^3\text{He}$  MR spin density images for the same breath-hold/imaging time, given that a diffusion and non-diffusion weighted image are captured for each slice of the DWI series. For the calculation of VDV the first of the interleaved diffusion-weighted pair of images was used. The thickness of the slices was 30mm, and therefore the ventilation defect area segmented was multiplied by 30mm, representing signal contribution from the entire slice. Given the slice thickness of the images used for image analysis, it is possible that the VDV values presented over-estimate the true ventilation defect volume, and thus should be taken as an estimate of the true VDV of the lung. Additionally, the use of DWI results in images with a lower signal-to-noise ratio than would be obtained had spin-density images been acquired for VDV measurements. Thus, acquiring a spin-density image set or perhaps a three-dimensional volumetric image set would allow for thinner slices and an improved signal-to-noise ratio. It will be important to evaluate thinner slices using spin density images, especially in a young healthy volunteer cohort to determine whether this group truly did not have any ventilation defects, as reported, or whether the thick slices and increased SNR perhaps mask the very small ventilation defects that have been reported in the literature in groups of similar age and health status.<sup>13,14</sup>

A second limitation present in Chapters 2 and 3 is that proton images acquired just prior to  $^3\text{He}$  MRI were not bag-matched to the  $^3\text{He}$  MRI breath-hold scans. In follow-up studies  $^1\text{H}$  scans were acquired following inhalation of 1.0 L of  $^4\text{He}/\text{N}_2$  at the same dosage used for  $^3\text{He}/\text{N}_2$  ventilation imaging. This approach allowed for rigid registration of proton and helium scans, allowing for clear delineation of the thoracic cavity border, and aided in ventilation defect segmentation. However, this was not the approach used in Chapter 2 and 3, when proton images were acquired during a breath-hold at peak-tidal volume. Therefore, the VDP measurement used in Chapter 4, and PVV measurement used in Chapter 5 and pioneered by Woodhouse and co-workers<sup>15</sup>, could not directly be assessed. In subjects with COPD, proton and helium images were registered, and despite these differences in image acquisition techniques,  $^3\text{He}$  MR images visually appeared to have good registration in most COPD subjects, while healthy elderly subjects had poorer registration on visual inspection making ventilation defect delineation difficult. Without a normalized measurement such as VDP or PVV, a true inter-subject

comparison of the extent of ventilation defects in the lung was not possible. In all future studies, this limitation was addressed by acquiring bag-matched  $^1\text{H}$  MRI.

One of the major limitations of the work presented in Chapters 2-5 is the small sample size, each with a study specific impact. In Chapter 2, the group of healthy volunteers had eight subjects, while the Stage II and III groups had nine and seven subjects respectively. The small sample size was selected to detect between group differences in ADC, and was calculated based on ADC and ADC standard deviation (SD) results published by Salerno and co-workers<sup>16</sup>. This sample size may have limited the power necessary to detect differences between VDV in the elderly healthy volunteer and stage II COPD subgroups, which in this study were not statistically significant. However, it is also possible that the reported VDV in subjects with stage II COPD is not due to COPD, but rather predominantly due to aging. Another possibility that would explain the large VDV SD is related to underlying  $^3\text{He}$  MRI phenotypes in the stage II COPD population; a subset of the stage II subjects were likely ADC dominant, having a VDV was due to age alone while another subset had elevated VDV due to both age and COPD (VDP or mixed phenotypes). In Chapter 3, the small sample size of the elderly subgroup may have resulted in an over- or under-estimation of true population ventilation defect volume; however, it is clear that ventilation defects do occur in the elderly, and these defects should not be confused with functional abnormalities related to COPD or other lung diseases. The small sample size in Chapter 4 of twenty subjects resulted in stage II and stage III COPD subjects forming the basis of the COPD group evaluated (one subject with stage I disease was included). The limited sample size evaluated, made up of a small group of mainly stage II and III COPD, indicates caution should be exercised in extrapolating the results presented in this chapter to the general COPD population, and more specifically, more advanced or less severe COPD groups (stage I/IV). In Chapter 5, the small sample size at baseline (n=7) and follow-up (n=4) may have restricted the detection of differences in functional measurements acquired longitudinally in the ipsilateral lung. Additionally, an increase in sample size in this study may have allowed for the detection of a significant difference in ADC between lungs at baseline (p=0.053 in seven subjects), and longitudinal change in ADC in the ipsilateral lung. Thus, increasing sample size

in future studies using  $^3\text{He}$  MRI will increase the power and likely lead to an increase in the number of differences detected between subject groups.

A further limitation in Chapter 3 is the lack of follow-up data for the younger subgroup. Because no defects were present at baseline in any subjects in this young healthy subgroup no follow-up data was acquired. Therefore, it is not known what the short-term reproducibility of this finding is. However, in two young healthy subjects imaged at multiple time points as part of a hardware and software development protocol no ventilation defects were observed in any of the scans collected. Despite this observation, it would be valuable to continue scanning younger healthy volunteers, and to evaluate the short-term reproducibility of ventilation images in these subjects given that previous reports of young healthy volunteers do report the presence of ventilation defects.<sup>13,14</sup>

One specific limitation present in Chapter 5 is the lack of other clinical parameters collected for study purposes. Subjective information regarding post-radiation respiratory difficulties was not obtained, and would have been useful in evaluating the impact of functional changes measured with  $^3\text{He}$  MRI on quality of life scores. Additionally, information related to treatment regime, specifically course of chemotherapy, smoking history and use of oxygen post-treatment, if collected, could give further information in relation to the functional changes reported in this study.

### **6.3.2 General Limitations**

One major limitation of the studies presented in this thesis is the lack of data collected from other imaging modalities in conjunction with  $^3\text{He}$  MRI, specifically CT data that could have been used for validation purposes. CT has largely been used both clinically and as a research tool for quantifying attenuation, related to the lung parenchyma<sup>3-6</sup>, and airway wall dimensions.<sup>7-10</sup> Although a limited number of studies have compared ADC measured from diffusion-weighted  $^3\text{He}$  MRI to attenuation on CT<sup>17</sup>, to date there has not been a direct comparison of  $^3\text{He}$  ventilation defect measurements to airway wall dimensions. It is hypothesized that  $^3\text{He}$  MRI VDV in subjects with COPD is the result of underlying airways disease, and therefore measurements of

airway dimension on CT would provide important complimentary information on airway structure leading to the ventilation defects that could be used to test this hypothesis. In relation to the work presented in Chapter 4 regarding the classification of COPD based on  $^3\text{He}$  MRI measurements, similar work has been done by Nakano and co-workers using CT<sup>9</sup>, and a direct comparison of these two techniques in the same COPD subject group would provide further insight into the surrogate measures of underlying emphysema and airways disease captured by these respective imaging modalities. Additionally, the registration of  $^3\text{He}$  MRI to CT data in Chapter 5 could have potentially been used to correlate regions of ventilation defect with areas of fibrosis on CT, providing a direct link to the etiology of these regions of signal void on  $^3\text{He}$  MRI. Furthermore, in all studies presented here, registration of  $^3\text{He}$  MRI with CT images would allow for a breakdown of ventilation defect analysis by lobe. In Chapter 2, the measurement of lobar VDV could be evaluated for reproducibility, which would have the potential to further solidify  $^3\text{He}$  MRI as a highly reproducible technique for evaluating regional pulmonary ventilation. Overall, CT data collected in conjunction with  $^3\text{He}$  MRI would aid in validating  $^3\text{He}$  MRI measurements against more established CT images, and potentially provide some explanation as to the underlying structural abnormalities that result in diminished ventilation. Finally, nuclear medicine techniques would have been valuable for cross-comparison purposes, especially in Chapter 5, where blood flow measurements would have provided important complimentary information to the ventilation results. We hypothesize in Chapter 5 that the increase in PVV in the contralateral lung may be due to a compensatory increase in ventilation due to the diminished ventilation in the ipsilateral lung. Measurements of blood flow from PET would show whether this ventilation improvement translates to a true improvement in contralateral lung function due to a corresponding improvement in blood flow, or whether the increase in ventilation is not mirrored by an increase in blood flow, simply resulting in a ventilation-perfusion mismatch in the contralateral lung.

The second overall limitation is that the etiology of ventilation defects is currently unknown. While we hypothesize that VDV is reflective of underlying airways disease in subjects with COPD, closing volumes in healthy elderly subjects and radiation fibrosis in subjects with RILI, to date there is no direct evidence to affirm these hypotheses. There is also the possibility that



ventilation defects occur in COPD due to bullous disease, representing structural changes in lung parenchyma rather than the hypothesized changes in lung airway structure, or a combination of the two. Without knowing the underlying cause of the ventilation defect, it is difficult to determine whether  $^3\text{He}$  MRI is truly sensitive to underlying changes in airway structure that may be associated with aging, COPD or fibrosis. Therefore, histological data is necessary to ascertain the direct cause of ventilation defects observed and measured using  $^3\text{He}$  MRI. Given that this is a potentially difficult task to accomplish in humans, a secondary method of validation would be through multi-modality imaging studies. High resolution CT can provide structural information regarding both airway dimensions and lung parenchyma, and thus could be used in conjunction with  $^3\text{He}$  MRI to correlate ventilation defects to regions of inflamed, thickened airways, bullae, or fibrosis.

Finally, one major limitation of all studies presented here is the limited translation of this technique for more widespread research investigating lung diseases in both the research setting and for use in guiding therapy or as an endpoint in clinical trials. There is an extremely limited supply of helium-3<sup>18,19</sup>, and therefore further follow-up studies stemming from the studies presented here may not be possible. It has been pointed out in previous paragraphs that increased sample sizes are needed in future studies to expand on the promising results of these small studies, which will likely not be possible given the current gas supply. Therefore, validation of this technique may not be necessary, but rather these studies should be reproduced, perhaps on a larger scale, with  $^{129}\text{Xe}$ , which is set to replace  $^3\text{He}$  as the noble gas contrast agent for hyperpolarized gas MRI.<sup>20-22</sup> Thus, previous solutions for limitations addressed in the previous paragraphs would be better suited using  $^{129}\text{Xe}$ , which is likely to have increased translational value in the clinical research setting.

## 6.4 Roadmap for Future Studies

### 6.4.1 Quantification of Lung Disease in Patients Diagnosed with Non-Resectable Lung Cancer using Hyperpolarized $^3\text{He}$ MRI

Combining the work presented in Chapters 4 and 5, we are currently evaluating potential functional and structural measurements derived from  $^3\text{He}$  MRI to be used as predictors of radiation-induced lung injury. Lung cancer and COPD are both diseases of tobacco smokers, thus many patients diagnosed with lung cancer will also have underlying, and potentially undiagnosed COPD. Inflammation is the hallmark of both COPD and RILI and we hypothesize that imaging measurements of airway function (airway disease or inflammation) and airspace structure (emphysema) provide a way to predict the enhanced and prolonged inflammatory response to radiation. Previous studies however have failed to establish that spirometric ( $\text{FEV}_1$ ) and other standard measurements of COPD severity are predictive of RILI<sup>23</sup>, likely because spirometry provides a global measurement of disease, and thus tumour burden and underlying COPD have a confounding effect on results. Therefore, in a study currently underway, we aim to evaluate measurements of airway function and tissue destruction typical of COPD in the contralateral lung only using  $^3\text{He}$  MRI, to determine whether they may be useful for predicting RILI onset. The findings presented in Chapter 4, demonstrating the potential of  $^3\text{He}$  MRI to categorize subjects into subgroups according to predominant measures of underlying disease, have led to the current study using hyperpolarized  $^3\text{He}$  MRI to measure the contribution of ADC and VDP to total disease measured in the contralateral lung of patients prior to radiation and evaluate these phenotypes as predictors of RILI. In this study, we hypothesize that quantification of ventilation using  $^3\text{He}$  MRI in patients with advanced lung cancer scheduled for radiation therapy can be used to quantify underlying lung disease, and will be predictive of treatment outcomes.

To date, 17 subjects recruited from the London Regional Cancer Program scheduled for radical radiation therapy (>60Gy) have enrolled in the study, and provided informed consent. Pulmonary function tests including spirometry, plethysmography and  $\text{DL}_{\text{CO}}$  were performed, followed by MRI in a single study visit as described in Chapters 2-5, prior to the first scheduled

radiation treatment. MRI images were analyzed, and VDP and ADC% were measured in the contralateral lung independently (to avoid confounding results due to tumour burden) according to the methods outlined in Chapter 4. Briefly, ADC measurements taken from the contralateral lung were scaled from 0-100% using an ADC range of  $0.24\text{cm}^2/\text{s}$  to  $0.88\text{cm}^2/\text{s}$ , based on the expected healthy ADC value of the youngest subject (47 years old) based on results published by Fain and co-workers<sup>24</sup>, and the maximum ADC value for helium in an infinitely large container.<sup>25</sup> The scaled ADC% values and VDP values were summed to obtain an overall  $^3\text{He}$  MRI total disease measurement. CT data collected for diagnosis, treatment planning and follow-up as part of standard care were acquired for interpretation of radiological changes following radiation therapy. CT images will be evaluated for radiological evidence of RILI by a radiologist specializing in thoracic imaging, and a radiation oncologist with an expertise in lung cancer, according to criteria previously published by Palma and co-workers.<sup>26</sup>

Results to date indicate that 9 of 17 subjects (53%) were VDP dominant, while the remainder had mixed disease according to  $^3\text{He}$  MRI VDP and ADC% measurements. Interestingly, no subjects had ADC dominant disease according to  $^3\text{He}$  MRI measurements of the contralateral lung. Representative VDP dominant subjects are shown in Figure 6-1, representative mixed subjects are shown in Figure 6-2 and all subjects ranked by total disease are shown in Figure 6-3. Total disease (sum of ADC% and VDP) was significantly different ( $p<0.001$ ), and greater in the subjects with mixed disease. Additionally, linear regression showed relationships between VDP in the contralateral lung and  $\text{FEV}_1\%_{\text{pred}}$  ( $r^2=0.57$ ,  $p<0.001$ ),  $\text{FEV}_1/\text{FVC}$  ( $r^2=0.36$ ,  $p<0.05$ ), and  $\text{DL}_{\text{CO}}$  ( $r^2=0.50$ ,  $p<0.01$ ), while contralateral ADC showed a linear relationship with the same pulmonary function test measurement ( $\text{FEV}_1\%_{\text{pred}}$   $r^2=0.45$ ,  $p<0.05$ ;  $\text{FEV}_1/\text{FVC}$   $r^2=0.63$ ,  $p<0.001$ ;  $\text{DL}_{\text{CO}}$   $r^2=0.69$ ,  $p<0.001$ ). Future analysis will determine if these underlying phenotypes play a role in RILI development.

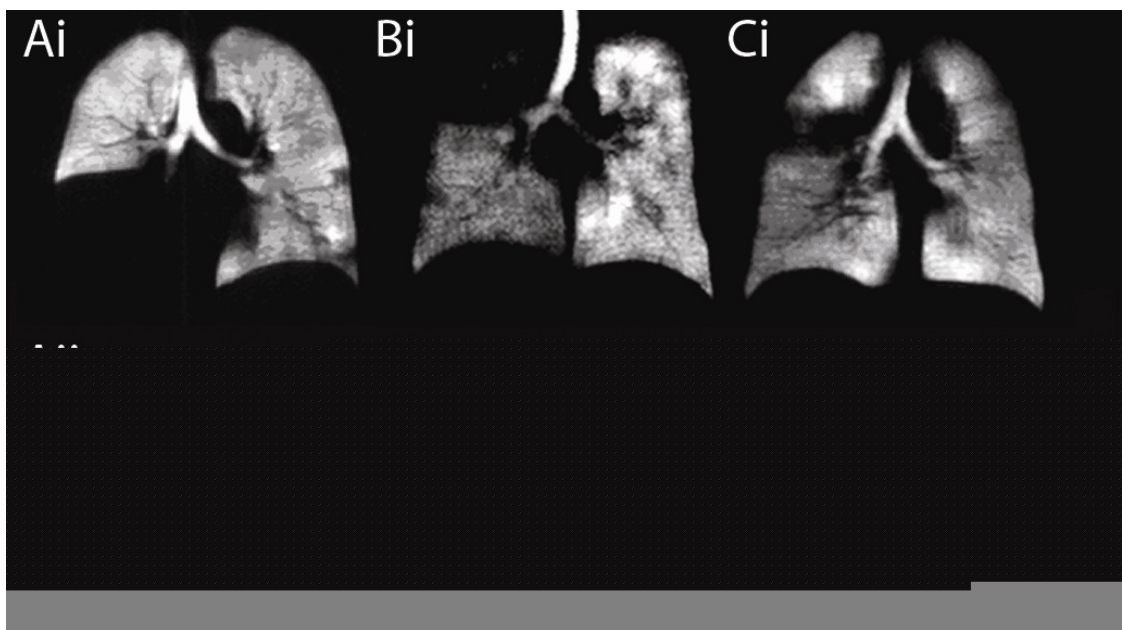


**Figure 6-1: Representative  $^3\text{He}$  VDP dominant subjects**

Static ventilation images are shown in (i), and ADC maps are shown in (ii) for subjects 016 (A), 018 (B) and 015 (C) for lung cancer subjects classified as VDP dominant according to  $^3\text{He}$  MRI measurements of the contralateral lung (left lung in all cases shown).

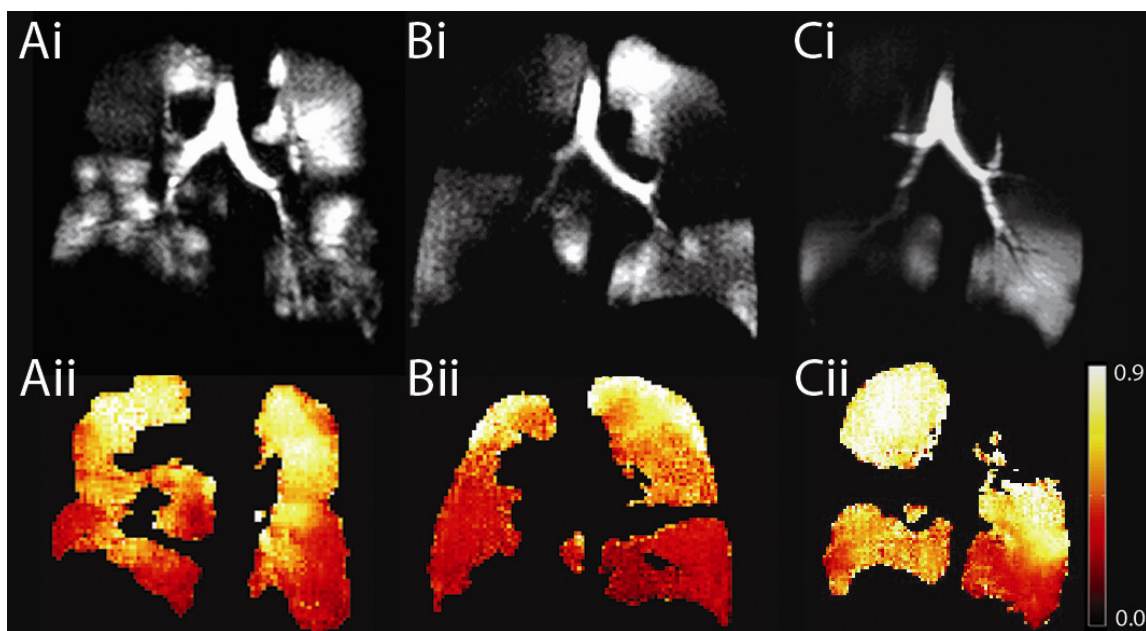


**Figure 6-2: Representative  $^3\text{He}$  mixed subjects**

Static ventilation images are shown in (i), and ADC maps are shown in (ii) for subjects 013 (A), 005 (B) and 017 (C) for lung cancer subjects classified as having mixed disease according to  $^3\text{He}$  MRI measurements of the contralateral lung (left lung in A and B, right lung in C).

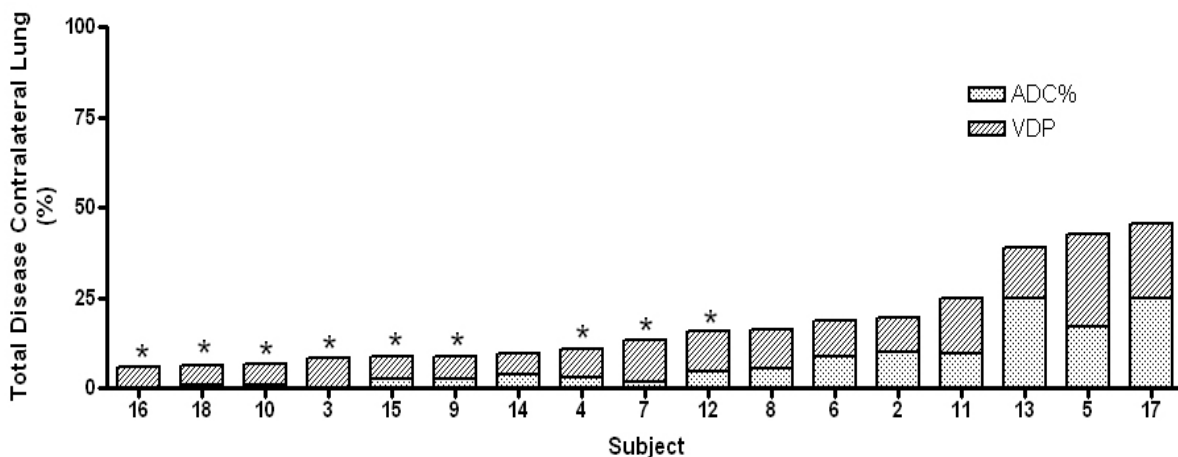


**Figure 6-3.**  $^3\text{He}$  MRI VDP and ADC% contribution in the contralateral lung of Lung Cancer Subjects. VDP and ADC% values are expressed as a percentage of the total  $^3\text{He}$  MRI disease. \* are VDP dominant.

Overall, VDP and ADC% measurements may provide sensitive and specific markers for predicting the development, severity and progression of RILI, with the potential to effect patient care by allowing for radiation treatment planning evaluation in identified high risk patients.

## 6.4.2 Ventilation Defect Etiology

In this thesis we demonstrated that VDV and VDP measured from hyperpolarized  $^3\text{He}$  MRI are sensitive and highly reproducible markers of lung ventilation.  $^3\text{He}$  derived measurements of VDV and VDP have potential as a novel marker of regional pulmonary ventilation abnormalities in longitudinal and cross-sectional studies of lung disease in clinical trials aimed at evaluating new therapeutics. Before this goal can be reached, the etiology of ventilation defects needs to be determined.

To determine the etiology of ventilation defects, there are a number of potential studies that could be performed. Histological validation would of course provide concrete evidence as to the underlying pathology leading to regions of signal void on  $^3\text{He}$  MRI in the lung.  $^3\text{He}$  ADC has been validated in histological studies in canines and humans<sup>27,28</sup>, and should be extended in future studies for evaluating ventilation defect etiology. Woods and co-workers performed the first and only human study assessing  $^3\text{He}$  gas diffusion in patients prior to lung transplantation, with subsequent morphological analysis in the explanted human lung.<sup>28</sup> To evaluate the cause of

ventilation defects, a study following the same protocol should be performed, with  $^3\text{He}$  spin density images replacing the DWI, and used to guide the histological sampling of areas surrounding the defect and within the area of the ventilation defects. Sampling areas within the ventilation defects would allow for the evaluation of the parenchyma in the region of the defect, to determine whether or not bullae were present and might have contributed to the region of  $^3\text{He}$  signal void. Areas of the lung preceding the ventilation defect should also be sampled and evaluated with specific attention on the small airways leading to the ventilation defect. Hogg and co-workers have carefully characterized small airways disease in COPD using histology, and this seminal work should be used to help guide the airways analysis.<sup>1,29</sup> Histological analysis using the techniques described here should be performed in a subject cohort with well described ventilation defects prior to lung transplantation.

Additionally, multi-modality studies should be performed using CT and  $^3\text{He}$  MRI. These studies should evaluate associations between airway dimensions preceding ventilation defects in the airway tree, and quantification of areas of low attenuation within the ventilation defect. Coxson and co-workers as well as Nakano and co-workers have probed airway dimensions using CT in previous studies of COPD.<sup>5,7,9,30</sup> The measurements they have previously employed could be applied in a multi-modality study incorporating  $^3\text{He}$  MRI. Such a study would require registration of  $^3\text{He}$  MRI to CT images, and would also require that CT images be collected in a similar breath-hold fashion to mimic the  $^3\text{He}$  MRI scan, thus emulating the conditions of the airways and parenchyma during the  $^3\text{He}$  MRI scan. Association between airway dimensions,  $^3\text{He}$  VDV and a regional overlap analysis of bullae and ventilation defects should provide further insight into the etiology of the signal void on  $^3\text{He}$  MRI.

### **6.4.3 Hyperpolarized Noble Gas MRI Phenotypes of COPD**

Another key future study that should be performed is a follow-up to the study presented in Chapter 4, using measurements derived from  $^3\text{He}$  MRI to classify patients with COPD according to the proportion of  $^3\text{He}$  MRI measured disease. The follow-up study should begin with a large cross-sectional sample of subjects with COPD, with cohorts of subjects from all four stages of disease. This diverse population will aid in understanding potential underlying phenotypes that

exist across all stages of COPD, detectable through measurements derived from  $^3\text{He}$  MRI. A larger sample size than previously studied will allow for more sophisticated statistical analysis, such as principal component analysis, probing underlying COPD phenotypes detected using  $^3\text{He}$  MRI. Furthermore, this will enhance our understanding of the proportion of subjects with ventilation defect dominant, ADC dominant and mixed disease based on  $^3\text{He}$  MRI in early stages of COPD as compared to the proportion of each subgroup in the later stages of disease. Additionally, these subject cohorts should be followed longitudinally to determine how individuals progress from one classification to another, and how changes in disease severity affect  $^3\text{He}$  MRI disease classification.

#### **6.4.4 Hyperpolarized $^{129}\text{Xe}$ MRI: Ventilation Defects in Health and Disease**

Finally, and as previously eluded to, there is a shortage of  $^3\text{He}$  that limits the future translation of this technique. Currently, studies are underway to evaluate  $^{129}\text{Xe}$  as a  $^3\text{He}$  replacement for hyperpolarized noble gas MRI in human studies.<sup>20-22,31-33</sup> Initial studies using  $^{129}\text{Xe}$  MRI in humans have been completed, and the results from these studies are promising.<sup>20,31-33</sup> Studies presented in this thesis should be repeated using  $^{129}\text{Xe}$ , to evaluate the short-term reproducibility of VDV and VDP measured from  $^{129}\text{Xe}$  MR images, as well as the sensitivity of VDP derived from  $^{129}\text{Xe}$  MR images to age- and disease-related changes.  $^{129}\text{Xe}$  will not only be able to probe alveolar diffusion and ventilation, but it also has the advantage of being a probe for transmembrane diffusion.<sup>21,31-33</sup>  $^{129}\text{Xe}$  is soluble in blood and tissue, and during MR imaging, exhibits a readily discernible frequency shift and retains longitudinal relaxation times of several seconds.<sup>31-33</sup> Thus, using hyperpolarized  $^{129}\text{Xe}$  as an inhaled contrast agent for MR imaging, the intraalveolar diffusion, ventilation and transmembrane diffusion can all be evaluated. Future studies using  $^{129}\text{Xe}$  will be particularly useful in the evaluation of RILI. Probing the transfer of  $^{129}\text{Xe}$  from the alveolar spaces into the capillaries provides information on the thickness of the tissue barrier separating the air spaces and capillaries. Differences detected in thickness of the alveolar tissue, especially thickening in regions will likely be associated with regions of inflamed and fibrosed tissue following radiation therapy. Overall, the addition of xenon transfer constant measurements that accompany  $^{129}\text{Xe}$  MRI may have a potential role in RILI as an early marker

of injury onset. This will largely depend on the sensitivity of  $^{129}\text{Xe}$  MRI xenon transfer constant, which will require evaluation in preliminary studies of this technique.

Overall, studies of lung function using surrogate measurements of ventilation derived from hyperpolarized gas MRI should be further developed. VDV and VDP hold promise as non-invasive, sensitive markers of lung function that will be useful in longitudinal and cross-sectional studies of lung disease, specifically in research studies evaluating the functional burden of structural disease changes and clinical trials evaluating new therapeutics.

## 6.5 Impact and Significance

Overall, in this thesis we have introduced a novel method for quantifying regional and total lung ventilation from  $^3\text{He}$  MR static ventilation images. VDV and VDP, with high short-term reproducibility, are sensitive to age-related differences in lung ventilation, and changes in lung function following treatment in subjects with lung cancer. Furthermore, they can be used to phenotype subjects with lung disease according to the magnitude of functional impairment and the magnitude of structural impairments. The results of studies presented in this thesis provide a foundation for future studies using  $^3\text{He}$  MRI aimed at evaluating longitudinal or treatment related changes in lung function in subjects with smoking related lung disease. Additionally, VDV and VDP measurements are translatable, and can be used to quantify lung function from  $^{129}\text{Xe}$  MR images.  $^3\text{He}$  MRI derived VDV and VDP are sensitive metrics of lung function and can be used both independently and in conjunction with structural  $^3\text{He}$  MR imaging measurements to gain a more complete understanding of the lung in health and disease.



## 6.6 References

- (1) Hogg JC. Pathophysiology of airflow limitation in chronic obstructive pulmonary disease. *Lancet*. 2004; 364(9435):709-721.
- (2) Calverley PM, Rennard SI. What have we learned from large drug treatment trials in COPD? *Lancet*. 2007; 370(9589):774-785.
- (3) Coxson HO, Mayo J, Lam S et al. New and Current Clinical Imaging Techniques To Study Chronic Obstructive Pulmonary Disease. *Am J Respir Crit Care Med*. 2009; 180(7):588-597
- (4) Coxson HO, Rogers RM, Whittall KP et al. A quantification of the lung surface area in emphysema using computed tomography. *Am J Respir Crit Care Med*. 1999; 159(3):851-856.
- (5) Coxson HO, Rogers RM. Quantitative computed tomography of chronic obstructive pulmonary disease. *Acad Radiol*. 2005; 12(11):1457-1463.
- (6) Bankier AA, Madani A, Gevenois PA. CT quantification of pulmonary emphysema: assessment of lung structure and function. *Crit Rev Comput Tomogr*. 2002; 43(6):399-417.
- (7) Kim WJ, Silverman EK, Hoffman E et al. CT metrics of airway disease and emphysema in severe COPD. *Chest*. 2009; 136(2):396-404.
- (8) Nakano Y, Wong JC, de Jong PA et al. The prediction of small airway dimensions using computed tomography. *Am J Respir Crit Care Med*. 2005; 171(2):142-146.
- (9) Nakano Y, Muller NL, King GG et al. Quantitative assessment of airway remodeling using high-resolution CT. *Chest*. 2002; 122(6 Suppl):271S-275S.
- (10) Orlandi I, Moroni C, Camiciottoli G et al. Chronic obstructive pulmonary disease: thin-section CT measurement of airway wall thickness and lung attenuation. *Radiology*. 2005; 234(2):604-610.
- (11) Petersson J, Sanchez-Crespo A, Larsson SA et al. Physiological imaging of the lung: single-photon-emission computed tomography (SPECT). *J Appl Physiol*. 2007; 102(1):468-476.
- (12) Jogi J, Jonson B, Ekberg M et al. Ventilation-Perfusion SPECT with 99mTc-DTPA Versus Technegas: A Head-to-Head Study in Obstructive and Nonobstructive Disease. *J Nucl Med*. 2010; 51(5):735-741.

- (13) Lee EY, Sun Y, Zurakowski D et al. Hyperpolarized  $^3\text{He}$  MR imaging of the lung: normal range of ventilation defects and PFT correlation in young adults. *J Thorac Imaging*. 2009; 24(2):110-114.
- (14) Mata J, Altes T, Knake J et al. Hyperpolarized  $^3\text{He}$  MR imaging of the lung: effect of subject immobilization on the occurrence of ventilation defects. *Acad Radiol*. 2008; 15(2):260-264.
- (15) Woodhouse N, Wild JM, Paley MN et al. Combined helium-3/proton magnetic resonance imaging measurement of ventilated lung volumes in smokers compared to never-smokers. *J Magn Reson Imaging*. 2005; 21(4):365-369.
- (16) Salerno M, de Lange EE, Altes TA et al. Emphysema: hyperpolarized helium 3 diffusion MR imaging of the lungs compared with spirometric indexes--initial experience. *Radiology*. 2002; 222(1):252-260.
- (17) Diaz S, Casselbrant I, Piitulainen E et al. Validity of apparent diffusion coefficient hyperpolarized ( $^3\text{He}$ )-MRI using MSCT and pulmonary function tests as references. *Eur J Radiol*. 2008.
- (18) de Lange EE, Mugler JP, III, Brookeman JR et al. Lung air spaces: MR imaging evaluation with hyperpolarized  $^3\text{He}$  gas. *Radiology*. 1999; 210(3):851-857.
- (19) Shanbhag DD, Altes TA, Miller GW et al. q-Space analysis of lung morphometry in vivo with hyperpolarized  $^3\text{He}$  spectroscopy. *J Magn Reson Imaging*. 2006; 24(1):84-94.
- (20) Hersman FW, Ruset IC, Ketel S et al. Large production system for hyperpolarized  $^{129}\text{Xe}$  for human lung imaging studies. *Acad Radiol*. 2008; 15(6):683-692.
- (21) Patz S, Hersman FW, Muradian I et al. Hyperpolarized ( $^{129}\text{Xe}$ ) MRI: a viable functional lung imaging modality? *Eur J Radiol*. 2007; 64(3):335-344.
- (22) Ruset IC, Ketel S, Hersman FW. Optical pumping system design for large production of hyperpolarized. *Phys Rev Lett*. 2006; 96(5):053002.
- (23) Robnett TJ, Machtay M, Vines EF et al. Factors predicting severe radiation pneumonitis in patients receiving definitive chemoradiation for lung cancer. *Int J Radiat Oncol Biol Phys*. 2000; 48(1):89-94.
- (24) Fain SB, Altes TA, Panth SR et al. Detection of age-dependent changes in healthy adult lungs with diffusion-weighted  $^3\text{He}$  MRI. *Acad Radiol*. 2005; 12(11):1385-1393.
- (25) Yablonskiy DA, Sukstanskii AL, Leawoods JC et al. Quantitative in vivo assessment of lung microstructure at the alveolar level with hyperpolarized  $^3\text{He}$  diffusion MRI. *Proc Natl Acad Sci U S A*. 2002; 99(5):3111-3116.

- (26) Palma DA, van Sornsen dK, Verbakel WF et al. Lung Density Changes After Stereotactic Radiotherapy: A Quantitative Analysis in 50 Patients. *Int J Radiat Oncol Biol Phys*. 2010.
- (27) Tanoli TS, Woods JC, Conradi MS et al. In vivo lung morphometry with hyperpolarized <sup>3</sup>He diffusion MRI in canines with induced emphysema: disease progression and comparison with computed tomography. *J Appl Physiol*. 2007; 102(1):477-484.
- (28) Woods JC, Choong CK, Yablonskiy DA et al. Hyperpolarized <sup>3</sup>He diffusion MRI and histology in pulmonary emphysema. *Magn Reson Med*. 2006; 56(6):1293-1300.
- (29) Hogg JC, Chu F, Utokaparch S et al. The nature of small-airway obstruction in chronic obstructive pulmonary disease. *N Engl J Med*. 2004; 350(26):2645-2653.
- (30) Nakano Y, Muro S, Sakai H et al. Computed tomographic measurements of airway dimensions and emphysema in smokers. Correlation with lung function. *Am J Respir Crit Care Med*. 2000; 162(3 Pt 1):1102-1108.
- (31) Mugler JP, III, Altes TA, Ruset IC et al. Simultaneous magnetic resonance imaging of ventilation distribution and gas uptake in the human lung using hyperpolarized xenon-129. *Proc Natl Acad Sci U S A*. 2010.
- (32) Cleveland ZI, Cofer GP, Metz G et al. Hyperpolarized Xe MR imaging of alveolar gas uptake in humans. *PLoS One*. 2010; 5(8):e12192.
- (33) Patz S, Muradian I, Hrovat MI et al. Human pulmonary imaging and spectroscopy with hyperpolarized <sup>129</sup>Xe at 0.2T. *Acad Radiol*. 2008; 15(6):713-727.

## Appendix – A: Hyperpolarized $^3\text{He}$ Magnetic Resonance Pulmonary Imaging: Image Processing Tools for Clinical Research

The work presented in this chapter has been previously published in *Conference Record on the Forty-Second Asilomar Conference; Signals, Systems and Computers* as follows.

L. Mathew, A. Wheatley, DG McCormack, G. Parraga. “Hyperpolarized  $^3\text{He}$  Magnetic Resonance Pulmonary Imaging: Image Processing Tools for Clinical Research” *Conference record on the Forty-second Asilomar Conference Signals, Systems and Computers, 2008.*

### A.1 Introduction

Chronic obstructive pulmonary disease, (COPD) is a leading cause of death worldwide<sup>1</sup>, and continues to grow in prevalence.<sup>2</sup> The worldwide Burden of Obstructive Lung Disease (BOLD) study recently reported that 10% of the world’s adults 40 years and older have clinically relevant COPD.<sup>3,4</sup> Surprisingly, the world-wide COPD prevalence in never-smokers was between 6 and 15%, only slightly lower than for tobacco smokers.<sup>5</sup>

Despite decades of active research, as well as the staggering and growing societal burden of COPD, therapeutic breakthroughs have not occurred, largely because of: 1) inadequate patient phenotyping of underlying pathology, 2) an incomplete understanding of COPD pathogenesis, and, 3) a scarcity of sensitive tools that can track disease changes. These limitations are critical considerations when treating patients and evaluating clinical trials because the intermediate endpoints currently in use (such as lung function measured using spirometry) are poor surrogates for long-term outcomes -the ultimate target of new treatments. In response to these serious limitations, non-invasive imaging techniques have been recently proposed by Hogg<sup>6</sup> as potential solutions, because they may provide *in vivo* phenotypes of lung pathology and function that can be used for testing new treatments and to personalize patient therapy.

Computed tomography (CT) has emerged as a research and clinical tool because it provides high resolution images of pulmonary anatomy, and quantitative information about lung tissue structure. However, CT is also associated with a small, but potentially significant radiation burden that limits “dynamic” imaging of the lung and longitudinal imaging in certain patients.

Hyperpolarized helium-3 ( $^3\text{He}$ ) magnetic resonance imaging (MRI) has recently emerged as another research approach<sup>7-11</sup> for the non-invasive measurement of lung structure and function, including conduction of gas through airways and into airspaces. Preliminary studies suggest that  $^3\text{He}$  MRI may be ideally suited for longitudinal respiratory research, which is a likely target application of this novel technology.  $^3\text{He}$  MRI *provides a complementary and alternative method for evaluating* respiratory disease and may be superior to CT because it allows simultaneous visualization of both airway and airspace *structure and function* at high spatial and temporal resolution. Two major pathological phenotypes that can be directly measured in respiratory disease involve changes in the airways and airspaces, which in COPD are reflected in *emphysema* and *airways disease*.<sup>12</sup> Emphysema is defined histologically as an abnormal permanent enlargement of the lung parenchyma (or airspace) beyond the terminal bronchioles with destruction of the alveolar walls.<sup>13</sup> Hogg and coworkers<sup>14</sup> have recently identified that pulmonary inflammation is associated with both tissue proliferation in the airways (manifested as *airways disease*) and tissue destruction in the respiratory bronchioles (manifested as *emphysema*), these sites separated by only a few micrometers. In this regard it is important to note that a major goal of COPD research in particular and respiratory research in general is to find a way to differentiate patients with these underlying disease pathological “phenotypes” because the treatments required for the different pathologies are conceptually and practically very different. For decades, the concept of pathology-based respiratory treatments has been explored with the notion that this could result in more efficacious and personalized patient care. However, it remains difficult, if not impossible, to phenotype (i.e. measure the physical or pathological characteristics of) patients *in vivo* based upon underlying disease pathology.

A handful of research centres world-wide have pioneered the use of inhaled hyperpolarized noble gases such as  $^3\text{He}$  for lungs imaging.<sup>7,9-11,15-20</sup> The images acquired provide both anatomical and functional information of the respiratory system that ***have never before been attained***. Of the numerous and novel hyperpolarized  $^3\text{He}$  MRI measurements that can be obtained, the  $^3\text{He}$  ventilation defect and ventilation volume provides an opportunity to visualize (with 1x1mm in-plane resolution and 15-mm slice thickness) and quantify those areas of the lung that participate in ventilation and those that do not. As shown in Figure A-1, in healthy young

adults, a single inhalation of hyperpolarized  $^3\text{He}$  gas results in homogeneous signal suggesting that all areas of the lung are participating equally in ventilation. In contrast, characteristic volumetric “focal” defects are observed in COPD, corresponding to areas of the lung that are not ventilated or are poorly ventilated within the time-course of a typical 8-16s breath hold scan.

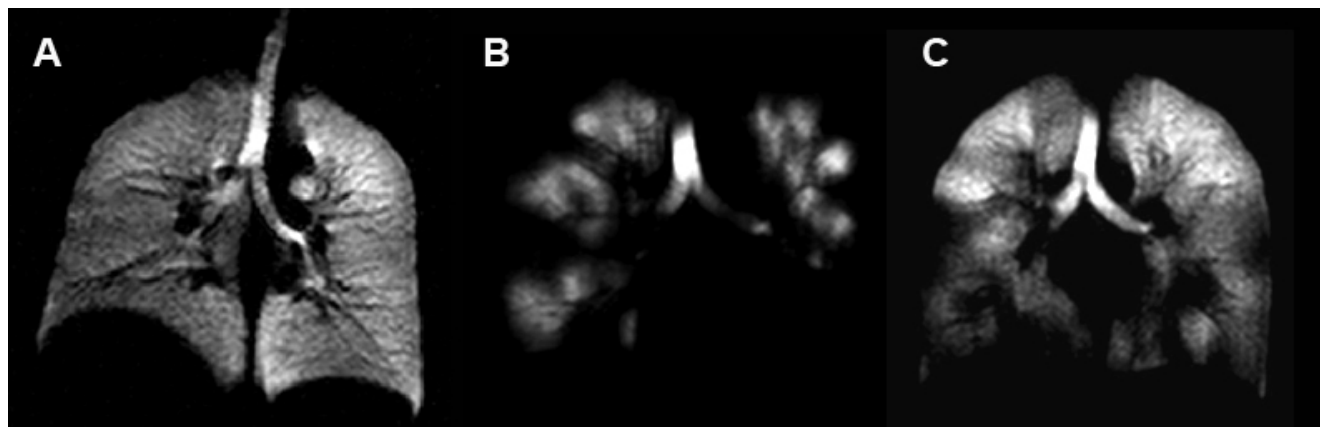


**Figure A-1: Clinical Hyperpolarized  $^3\text{He}$  Magnetic Resonance Imaging.**

A. functional imaging in a healthy volunteer during a 15 second  $^3\text{He}$  breath hold, no ventilation defects are seen B. a subject with stage III COPD with large regions of signal void (ventilation defects), and C. a subject with exercise induced asthma showing focal ventilation defects.

As shown in Figure A-2, scoring methods have been developed and used to provide quantitative regional  $^3\text{He}$  ventilation defect scores<sup>21,22</sup> whereby focal ventilation defects are counted and a defect score/slice is generated. For example, one of the currently used tools for quantifying regions void of  $^3\text{He}$  signal team of radiologists to count them on a slice by slice basis, and dividing by the total number of slices to get the mean number of ventilation defects per slice (VDS).<sup>21,22</sup> Another method shown in Figure A-3 relies on defect scoring by consensus, whereby a group of three radiologists would review all slices of the  $^3\text{He}$  MRI and estimate the percentage of the lung that appears not to be ventilated.<sup>23</sup> These techniques are subject to interpretation, observer bias and potentially less sensitive to the physiological changes that appear to take place in the lung. In addition, in longitudinal studies where focal ventilation defects often change in size as compared to the number of defects, consensus defect and ventilation scoring methods often fail to reveal physiological truth because we and others have observed that ventilation defects often grow in volume as compared to number over time.

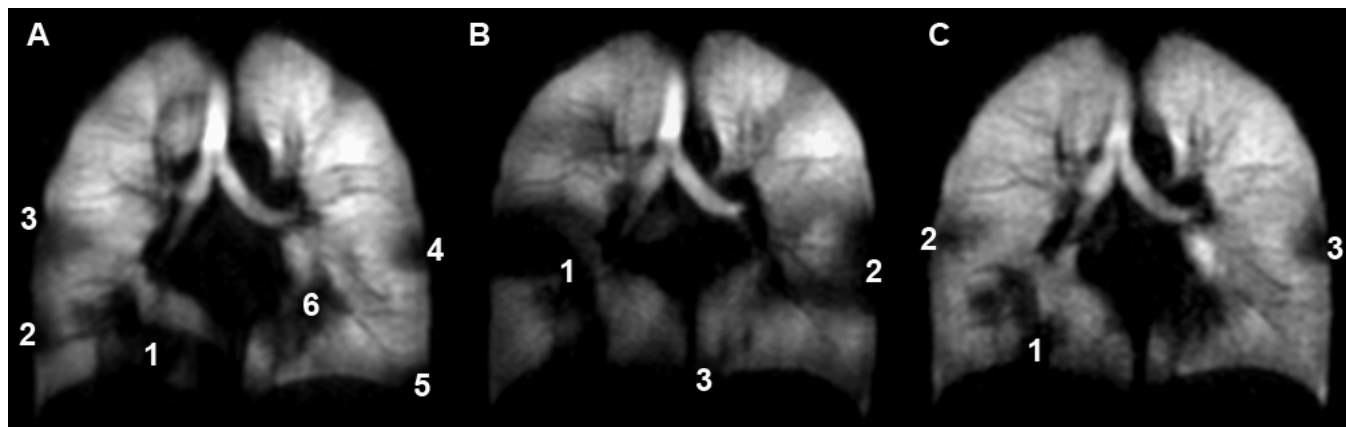


**Figure A-2: Ventilation Defect scoring of  $^3\text{He}$  MRI.**

Ventilation defect scoring of the center slice is shown for A. asthma subject at baseline, B. asthma subject 5 minutes post-exercise, C. asthma subject 55 minutes post-exercise. This demonstrates the lack of information VDS yields- specifically changes in size and location of defects.

Therefore, in order to accelerate the use of  $^3\text{He}$  MRI in clinical longitudinal research, new image analysis, image visualization and processing/segmentation tools are required that account for the physiological changes that potentially can occur and that provide appropriate continuous statistical endpoints. We hypothesize that  $^3\text{He}$  MRI can be analyzed to provide information about how lung regions which are not receiving ventilation change over time, and how potential treatments will affect these unventilated regions. In order to do this, tools that can quantify differences in ventilation are needed, which are both sensitive and specific to regional changes in ventilation over time. These types of tools will have the capability to assess not only regions of signal void, but also regions that are decreasing in ventilation over time- possibly predicting the location of a future ventilation defect. Hyperpolarized  $^3\text{He}$  MR ventilation images contain the information necessary to quantify regional changes in lung function, and thus the aim of this paper is to outline the exact tools needed for this to occur. Here we propose preliminary results of novel image processing tools we have designed to account for these differences and address the outlined image processing needs are described below.

## A.2 Methods

Subjects with asthma and stage II and stage III COPD were recruited for various studies at our site. All subjects provided written informed consent to the study protocols approved by the local

ethics board and Health Canada. Longitudinal time points ranged from same-day rescan to a 2-year follow up study.

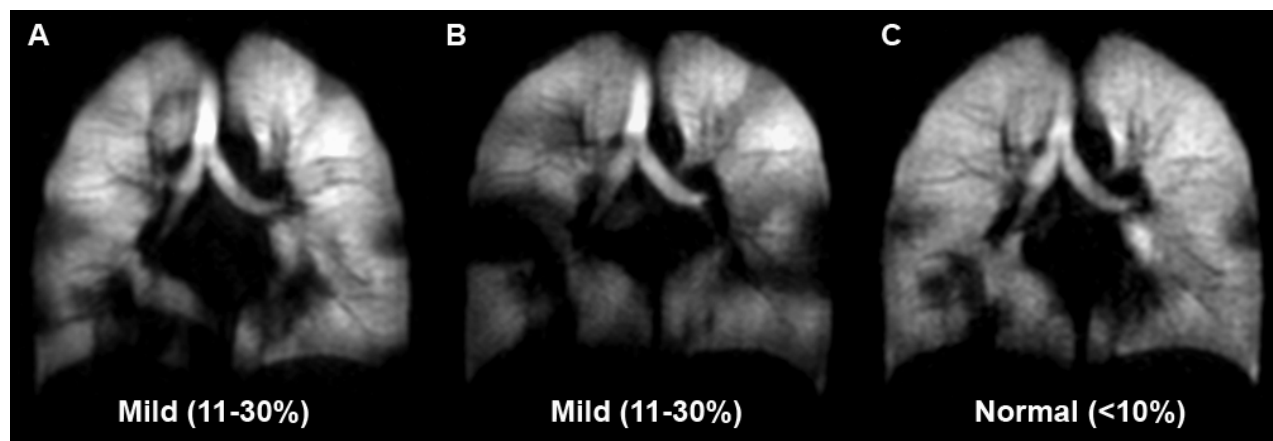


**Figure A-3: Ventilation Defect Evaluation: Estimation by Consensus.**

Ventilation defect estimation by consensus is shown in the centre slice for A. asthma subject at baseline, B. asthma subject 5 minutes post-exercise, C. asthma subject 55 minutes post-exercise. Binning of ventilation abnormalities into groups such as mild-moderate and severe is shown to be an insensitive technique for assessing ventilation and ventilation differences.

## A.3 Results

### A.3.1 Image Visualization

Image analysis was performed in a controlled lighting environment. For the purposes of visualizing and scoring images at baseline and follow-up, images from each visit were compared visually on side-by-side monitors. For direct visualization of differences in signal intensity in baseline and two year follow-up images were changed to red and blue colour scales respectively. These images were previously registered based on main airway anatomy as described below. Red baseline and blue follow-up images were then summed on a pixel-by-pixel basis, with the resulting image showing the contribution of each scan as visualized through the pixel hue.

### A.3.2 Image Registration

Hyperpolarized  $^3\text{He}$  MR images acquired at different time points require image registration before they can be directly compared. This may be possible by rigid registration of points



surrounding the trachea, right and left bronchi, and carina. In order for registration to be successful points used must be present at each time point. Image registration in this preliminary study was performed using a manual image registration of specified points- most consistently the carina, but also points along the perimeter of the trachea. An expert observer selected points in images acquired at each time point and then manually aligned them using in-house software.

### **A.3.3 Signal Normalization**

Following image registration  $^3\text{He}$  signal normalization is necessary. This is due to the fact that there are both physiological and non-physiological reasons for differences in signal intensity of pixels in images from the same subject at different time points. Differences in  $^3\text{He}$  signal intensity due to physiological reasons such as changes in disease should be measured, but prior to this non-physiological reasons for differences in  $^3\text{He}$  signal intensity must be accounted for. These reasons include minor differences in absolute polarization of the  $^3\text{He}$  when it leaves the polarizer, and differences in the amount of time that it takes to get the  $^3\text{He}$  from the polarizer and into the patient. Finally non-physiological differences in signal intensity may be due to the exact amount of gas inhaled, as subjects with severe disease may struggle to inhale the complete 1.0L of gas while in the supine position.

For all images the mean and standard deviation of the background noise was computed from four 30x30 pixel regions of interest. A threshold of the mean background noise plus two standard deviations of the background noise was applied. In this preliminary study, no signal normalization was performed and window and leveling was not changed to account for non-physiological differences in signal intensity.

### **A.3.4 Image Subtraction**

Once image registration was complete image subtraction was performed using two different methods. First, the absolute signal intensity difference was calculated on a pixel-by-pixel basis. Baseline visit images were subtracted from follow-up visit images. Results were displayed in colour showing a full range of differences in intensity from -255 to +255. Second, normalized image subtraction was performed to show the percentage change from baseline as shown in Figure A-4 and Figure A-5 for subjects with COPD and radiation-induced lung injury

respectively. This was done by dividing the absolute subtraction image pixel values by baseline image pixel values. Pixels resulting in the normalized subtraction image were calculated on a pixel-by-pixel basis. If the absolute difference between pixels was zero, normalization values were automatically set to zero. In cases where the follow-up pixel intensity was not equal to zero and the corresponding baseline pixel signal intensity value was equal to zero, the normalized value was set to positive or negative 110% based on the follow-up pixel value. In order to visualize regions of change less than 100%, output image normalization values greater than 110% were scaled to 110%. This enabled visualization of minor ventilation differences.

## **A.4 Conclusion**

<sup>3</sup>He MRI measurement precision, sensitivity and specificity are required in order to translate these surrogates as intermediate endpoints in clinical research. To accomplish this, novel image registration, signal normalization and image subtraction methods are under development for asthma, COPD, cystic fibrosis and radiation-induced lung injury.

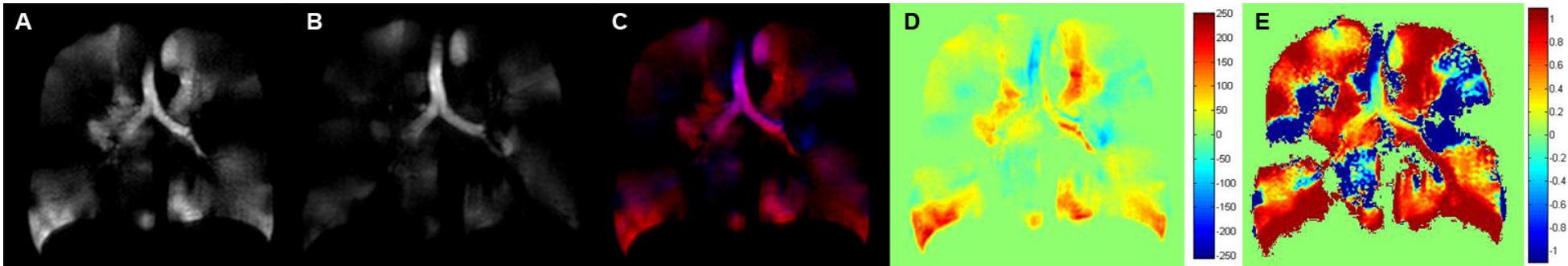


**Figure A-4: Image Processing for a Subject with Stage III COPD.**

A. baseline, B. two-year follow-up, C. image addition – baseline is red and two-year follow-up is blue, D. absolute image subtraction (baseline – follow-up) on a pixel-by-pixel basis, E. normalized image subtraction  $((\text{baseline} - \text{follow-up})/\text{baseline})$  on a pixel-by-pixel basis.

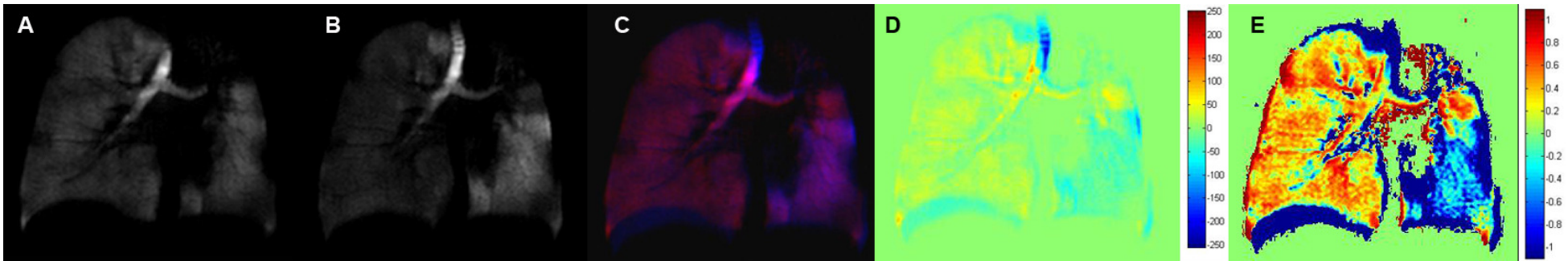


**Figure A-5: Image Processing for a Subject with Radiation-induced lung injury.**

A. baseline, B. five month follow-up, C. image addition – baseline is red and two-year follow-up is blue, D. absolute image subtraction (baseline – follow-up) on a pixel-by-pixel basis, E. normalized image subtraction  $((\text{baseline} - \text{follow-up})/\text{baseline})$  on a pixel-by-pixel basis. Mis-registration is evident in the lower right lobe, suggesting that registration based on points beyond the trachea and main bronchi may be necessary.

## A.5 References

- (1) Murray CJ, Lopez AD. Alternative projections of mortality and disability by cause 1990-2020: Global Burden of Disease Study. *Lancet*. 1997; 349(9064):1498-1504.
- (2) Global strategy for the diagnosis, management, and prevention of chronic obstructive pulmonary disease. NHLBI/WHO Workshop Report Update. 2701. 2003.
- (3) Buist AS, McBurnie MA, Vollmer WM et al. International variation in the prevalence of COPD (the BOLD Study): a population-based prevalence study. *Lancet*. 2007; 370(9589):741-750.
- (4) Menezes AM, Perez-Padilla R, Jardim JR et al. Chronic obstructive pulmonary disease in five Latin American cities (the PLATINO study): a prevalence study. *Lancet*. 2005; 366(9500):1875-1881.
- (5) Menezes AM, Perez-Padilla R, Jardim JR et al. Chronic obstructive pulmonary disease in five Latin American cities (the PLATINO study): a prevalence study. *Lancet*. 2005; 366(9500):1875-1881.
- (6) Hogg JC, Chu F, Utokaparch S et al. The nature of small-airway obstruction in chronic obstructive pulmonary disease. *N Engl J Med*. 2004; 350(26):2645-2653.
- (7) Albert MS, Cates GD, Driehuys B et al. Biological magnetic resonance imaging using laser-polarized  $^{129}\text{Xe}$ . *Nature*. 1994; 370(6486):199-201.
- (8) Yablonskiy DA, Sukstanskii AL, Leawoods JC et al. Quantitative in vivo assessment of lung microstructure at the alveolar level with hyperpolarized  $^3\text{He}$  diffusion MRI. *Proc Natl Acad Sci U S A*. 2002; 99(5):3111-3116.
- (9) Mills GH, Wild JM, Eberle B et al. Functional magnetic resonance imaging of the lung. *Br J Anaesth*. 2003; 91(1):16-30.
- (10) Kauczor HU, Hofmann D, Kreitner KF et al. Normal and abnormal pulmonary ventilation: visualization at hyperpolarized He-3 MR imaging. *Radiology*. 1996; 201(2):564-568.
- (11) de Lange EE, Mugler JP, III, Brookeman JR et al. Lung air spaces: MR imaging evaluation with hyperpolarized  $^3\text{He}$  gas. *Radiology*. 1999; 210(3):851-857.
- (12) Hogg JC, Chu F, Utokaparch S et al. The nature of small-airway obstruction in chronic obstructive pulmonary disease. *N Engl J Med*. 2004; 350(26):2645-2653.
- (13) Fabbri LM, Hurd SS. Global Strategy for the Diagnosis, Management and Prevention of COPD: 2003 update. *Eur Respir J*. 2003; 22(1):1-2.

- (14) Hogg JC. Pathophysiology of airflow limitation in chronic obstructive pulmonary disease. *Lancet*. 2004; 364(9435):709-721.
- (15) Kauczor HU, Ebert M, Kreitner KF et al. Imaging of the lungs using <sup>3</sup>He MRI: preliminary clinical experience in 18 patients with and without lung disease. *J Magn Reson Imaging*. 1997; 7(3):538-543.
- (16) MacFall JR, Charles HC, Black RD et al. Human lung air spaces: potential for MR imaging with hyperpolarized He-3. *Radiology*. 1996; 200(2):553-558.
- (17) Tooker AC, Hong KS, McKinstry EL et al. Distal airways in humans: dynamic hyperpolarized <sup>3</sup>He MR imaging--feasibility. *Radiology*. 2003; 227(2):575-579.
- (18) Wild JM, Paley MN, Viallon M et al. k-space filtering in 2D gradient-echo breath-hold hyperpolarized <sup>3</sup>He MRI: spatial resolution and signal-to-noise ratio considerations. *Magn Reson Med*. 2002; 47(4):687-695.
- (19) Van Beek EJ, Wild JM, Kauczor HU et al. Functional MRI of the lung using hyperpolarized 3-helium gas. *J Magn Reson Imaging*. 2004; 20(4):540-554.
- (20) Van Beek EJ, Wild JM. Hyperpolarized 3-helium magnetic resonance imaging to probe lung function. *Proc Am Thorac Soc*. 2005; 2(6):528-532.
- (21) de Lange EE, Altes TA, Patrie JT et al. The variability of regional airflow obstruction within the lungs of patients with asthma: assessment with hyperpolarized helium-3 magnetic resonance imaging. *J Allergy Clin Immunol*. 2007; 119(5):1072-1078.
- (22) de Lange EE, Altes TA, Patrie JT et al. Evaluation of asthma with hyperpolarized helium-3 MRI: correlation with clinical severity and spirometry. *Chest*. 2006; 130(4):1055-1062.
- (23) van Beek EJ, Hill C, Woodhouse N et al. Assessment of lung disease in children with cystic fibrosis using hyperpolarized 3-Helium MRI: comparison with Shwachman score, Crispin-Norman score and spirometry. *Eur Radiol*. 2007; 17(4):1018-1024.

## **Appendix – B: Hyperpolarized $^3\text{He}$ Magnetic Resonance Imaging Biomarkers of Bronchoscopic Airway Bypass in COPD**

The work presented in this chapter has been submitted to *Journal of Magnetic Resonance Imaging* for publication (submission # JMRI-10-0886).

*L. Mathew, M. Kirby, D. Farquhar, C. Licskai, R. Etemad-Rezai, DG McCormack, G. Parraga*  
“Hyperpolarized  $^3\text{He}$  Magnetic Resonance Imaging Biomarkers of Bronchoscopic Airway Bypass in COPD” Submitted to *J Magn Reson Imaging*, January 2011.

### **B.1 Introduction**

Pulmonary functional imaging using hyperpolarized helium-3 magnetic resonance imaging ( $^3\text{He}$  MRI) provides quantitative regional pulmonary functional information with high sensitivity to longitudinal changes in chronic obstructive pulmonary disease (COPD).<sup>1</sup> In the case of lung functional changes in COPD after drug<sup>2</sup> or direct airway interventions<sup>3</sup> a discordant relationship has been previously reported between symptomatic improvements measured using quality of life scores, and pulmonary function tests.<sup>4</sup> Until very recently, the use of pulmonary imaging methods has been limited to the evaluation of structural lung changes. Here, we report the first case of an elderly ex-smoker with severe emphysema who was monitored longitudinally for 2 years before, and 1 year after bronchoscopic Airway Bypass (AB) using  $^3\text{He}$  MRI for the quantitative evaluation of functional lung changes.

### **B.2 Case Report**

A 73-year old male ex-smoker with GOLD stage III COPD underwent AB in February 2009 as part of the Exhale Airway Stents for Emphysema (EASE) Trial. AB is an investigational procedure that involves Doppler-guided transbronchial delivery and airway insertion of drug-eluting stents (Exhale® Drug-Eluting Stent, Broncus Technologies, Inc., USA) with the aim being connection of the segmental airways to adjacent lung tissue allowing trapped gas to be exhaled. Written informed consent was provided to a Health Insurance Portability and Accountability Act (HIPAA) compliant protocol approved by a local ethics board, and Health Canada. Thirty-two months prior to AB (June 2006), he reported a 70-pack-year smoking history, having ceased smoking

approximately 13 years earlier, and was enrolled in a longitudinal hyperpolarized  $^3\text{He}$  MRI study that also included same day spirometry and plethysmography. As shown in Table B-1, at 32 months pre-AB forced expiratory volume in one second ( $\text{FEV}_1$ ) was 1.2L ( $32\%_{\text{pred}}$ ), and residual volume (RV) to total lung capacity (TLC) ratio was 0.62. Hyperpolarized  $^3\text{He}$  ventilation and diffusion-weighted MRI was performed on a 3.0T scanner (Excite 12.0, GEHC, Milwaukee, WI) as previously described<sup>5</sup> in a breath-hold, after inspiration of 1.0L of 5mL/kg  $^3\text{He}$  mixed with  $\text{N}_2$  gas from functional residual capacity (FRC). Proton images were also acquired as previously described<sup>6</sup> within 3 minutes of  $^3\text{He}$  MRI, with the same breath-hold volume from functional residual capacity (FRC) (1.0L of  $^4\text{He}/\text{N}_2$  mixture) to obtain a structural image of the thorax allowing for clear delineation of the thoracic cavity.  $^3\text{He}$  ventilation MRI (Figure B-1A, 32 months pre-AB) shows a heterogeneous distribution of gas with large ventilation defects, and in regions of gas distribution, heterogeneous signal intensity - both of which are the hallmark of COPD. Upon returning for follow-up imaging 24 months later in June 2008 (8 months pre-AB Figure B-1B)  $^3\text{He}$  MR images showed a decrease in ventilation of the right upper and lower and left upper lung regions (Figure B-1B). Quantitative analysis of the  $^3\text{He}$  ventilation distribution (Table B-1) resulted in a  $^3\text{He}$  MRI ventilation volume (VV) decrease of 3.8L over the two year period, corresponding to a decrease in the percentage of ventilated lung volume (PVV) from 73% to 26% and an increased ventilation defect percent (VDP). The functional imaging changes observed were concomitant with a decrease in  $\text{FEV}_1$  and FVC and an increase in RV/TLC (Table B-1) during the follow-up period. There were no exacerbations or hospitalizations reported during the follow-up period.

At this time the subject was enrolled in a randomized double-blind study evaluating the safety and efficacy of AB in subjects with homogeneous emphysema and severe hyperinflation ( $\text{RV}/\text{TLC} \geq 0.65$ ). For 6 weeks prior to AB, the subject underwent pulmonary rehabilitation, and four days prior to AB his self-reported dyspnea rating was 2 on the modified Medical Research Council (mMRC) scale and his St George's Respiratory Questionnaire (SGRQ) score was 65. In February 2009 four stents were placed; two in the right lower and two in the left upper lung. The subject returned for follow-up evaluation one, three, six and twelve months post-stent, with  $^3\text{He}$  MRI at the

six month (Figure B-2A) and twelve month (Figure B-2B) time points. At 6 months post-AB, the subject reported an increase in forced vital capacity (FVC)  $\geq 12\%$  and therefore failed to achieve responder status and was subsequently categorized as an AB non-responder.

**Table B-1: Pulmonary function test and  $^3\text{He}$  MRI results pre- and post-AB.**

	Months							
	Pre-Airway Bypass				Post-Airway Bypass			
	32	8	2	0.1	1	3	6	12
FEV <sub>1</sub> (L)	1.2	0.8	0.9	1.1	1.2	1.2	1.1	1.2
FEV <sub>1</sub> (% <sub>pred</sub> )	32	23	27	32	34	35	33	35
FVC (L)	3.2	2.3	2.6	3.2	3.6	3.6	3.5	3.8
FVC (% <sub>pred</sub> )	66	49	57	68	77	78	76	81
FEV <sub>1</sub> /FVC (%)	37	34	35	35	32	33	32	31
RV (L)	5.2	5.2	5.6	4.4	5.0	4.5	4.7	5.0
RV (% <sub>pred</sub> )	193	200	213	169	190	169	169	189
TLC (L)	8.4	8.0	8.6	7.8	8.2	8.2	8.3	8.5
TLC (% <sub>pred</sub> )	111	107	115	104	114	110	108	114
RV/TLC	0.62	0.65	0.65	0.57	0.60	0.55	0.56	0.58
IC (L)	1.8	1.6	1.6	2.1	2.3	2.3	1.8	2.8
DLCO (ml/min/mmHg)			9.2	9.9	14.6	16.9	14.6	18.7
DL <sub>CO</sub> (% <sub>pred</sub> )			26	28	42	48	42	53
mMRC				2	1	0	1	1
6MWD (m)				288	315	330	366	330
SGRQ				65	27	27	27	31
CE (s)				750			1084	
WL TCV (L)	7.3	6.3					8.5	8.1
WL VV(L)	5.4	1.6					4.8	5.8
WL PVV (%)	73	26					57	72
WL VDV (L)	2.0	4.7					3.6	2.4
WL VDP (%)	27	74					43	28
WL ADC (cm <sup>2</sup> /s)	0.47	0.49					0.48	0.49

Note: the dashed line separates pre- and post-AB results

FEV<sub>1</sub> = forced expiratory volume in one second, FVC = forced vital capacity, RV = residual volume, TLC = total lung capacity, IC=Inspiratory Capacity, DL<sub>CO</sub>=Carbon Monoxide Diffusion Capacity of the lung, mMRC = modified medical research council, 6MWD = six minute walk distance, SGRQ = St. George's research questionnaire, CE = cycle ergometry, TCV = thoracic cavity volume, VV = ventilated volume, PVV = percent ventilated volume, VDV = ventilation defect volume, VDP = ventilation defect percent, ADC = apparent diffusion coefficient.

In contrast, at 6 months post-AB, very obvious changes in  $^3\text{He}$  MRI were observed throughout the right lung and in the left upper lobe at six months (Figure 2A) with further



improvements, specifically in the right lower lung observed at twelve months (Figure 2B) post AB. Such visual changes did appear to generally correspond with stent placements in the right lower and left upper lung lobes. These gas distribution improvements that occurred after stent placement corresponded to  $^3\text{He}$  MRI VV increases of 3.2L at 6 months and 4.2L, 1 year after the AB procedure. As noted in Table B-1, the thoracic cavity volume (TCV) measured using  $^1\text{H}$  MRI increased approximately 2.0L between the 8 month pre-stent visit and the 6 and 12 month post-stent visits. Taken together, the increase in VV and TCV resulted in an improved PVV 6 months post-stent that persisted at the 1 year post AB time-point. At the same time, other surrogate measures of lung functional capacity including the six minute walk distance (6MWD), SGRQ score and cycle ergometry (CE) time showed improvements post-AB 6MWD increased by 78m, SGRQ score decreased by 38, and CE time improved by 334s. During this same time period an increased diffusing capacity of carbon monoxide ( $\text{DL}_{\text{CO}}$ ) was measured with  $^3\text{He}$  MRI whole lung ADC remaining unchanged.

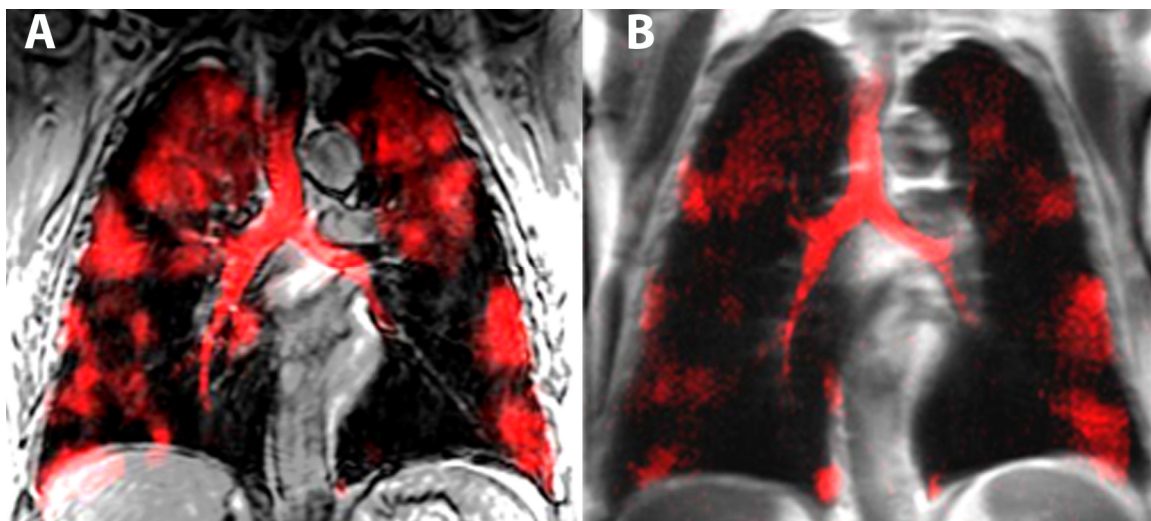


**Figure B-1:  $^3\text{He}$  MRI registered to  $^1\text{H}$  MRI Prior to Airway Bypass.**

$^3\text{He}$  MRI registered to  $^1\text{H}$  MRI of GOLD stage III COPD ex-smoker A) 32 months prior to AB and B) 8 months prior to AB. Heterogeneous  $^3\text{He}$  signal intensity and large ventilation defects are visualized in both scans, with  $^3\text{He}$  MRI VV decreased by 3.8L during this two year time period.

### B.3 Discussion

Bronchoscopic lung volume reduction methods provide a minimally invasive alternative to lung volume reduction surgery with the goal of improving COPD quality of life, pulmonary function and survival.<sup>7-9</sup> Unfortunately, for many of these approaches, including AB<sup>10</sup>, significant improvements in the established intermediate endpoints such as FEV<sub>1</sub> and RV/TLC have not been realized post-intervention<sup>3,4</sup> and sometimes these results are discordant with measures of symptoms or functional improvements. In these studies lung imaging has been used only as a structural tool to capture lung volumes using CT.

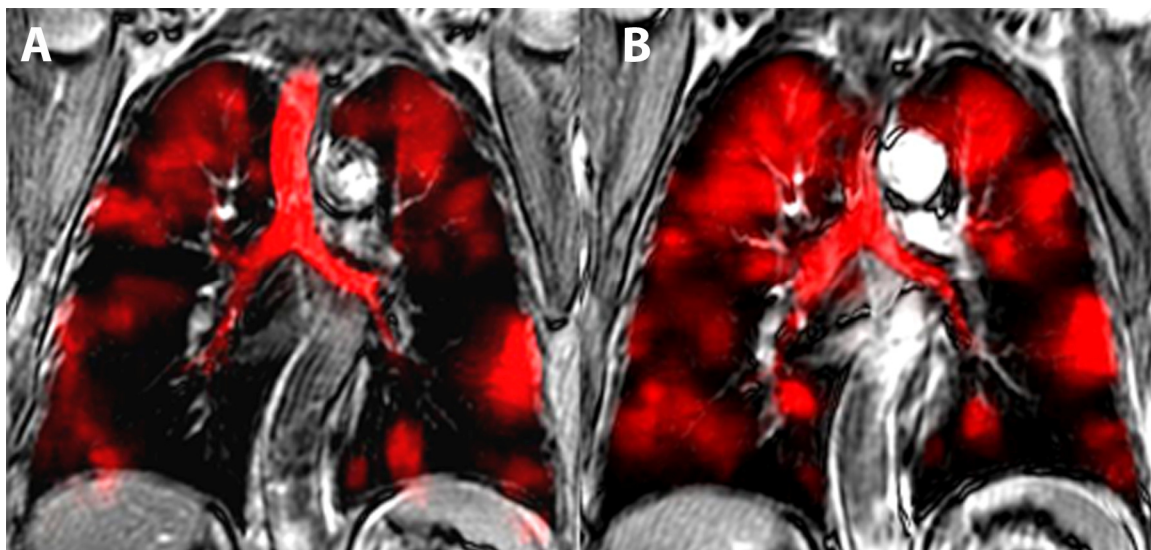


**Figure B-2: <sup>3</sup>He MRI registered to <sup>1</sup>H MRI Following Airway Bypass.**

<sup>3</sup>He MRI registered to <sup>1</sup>H MRI of GOLD stage III COPD ex-smoker A) 6 months post-AB and B) 12 months post-AB after insertion of two stents left upper lung and two stents right lower lung. Improved gas distribution post-AB is suggested with new regions of <sup>3</sup>He ventilation and increased <sup>3</sup>He signal intensity and VV at both time points post-AB.

<sup>3</sup>He MRI has emerged over the last 10 years as a highly reproducible and sensitive research tool for the evaluation of COPD in cross-sectional and longitudinal studies<sup>1,5,11,12</sup>. Here we show hyperpolarized <sup>3</sup>He MRI in a COPD ex-smoker on 4 occasions – twice before AB (32 and 8 months prior) and twice after AB (6 and 12 months post) and the results suggest significant improvements in gas distribution (<sup>3</sup>He

VV increase of over 3L) 6 months and 12 months after AB. These imaging results cannot be explained by the small changes in spirometry and plethysmography results but they are in agreement with post-AB changes (improvements) in the 6MWD, SGRQ and mMRC.

In summary, we report changes in  $^3\text{He}$  MRI VV for a COPD ex-smoker following AB that are similar to changes in quality of life measurements but not reflected in FEV<sub>1</sub>, FVC, IC or RV/TLC. Potential explanations for these findings include higher sensitivity of  $^3\text{He}$  MRI to functional lung changes than traditional pulmonary function tests. This discordance in outcome measures, in the only EASE Trial subject for whom  $^3\text{He}$  MRI was performed, highlights the utility of functional lung imaging in COPD interventional trials, and suggests this high resolution functional imaging method may offer insight into underlying regional physiologic changes in COPD patients following treatment.

## B.4 References

- (1) Kirby M, Mathew L, Wheatley A et al. Chronic obstructive pulmonary disease: longitudinal hyperpolarized (3)He MR imaging. *Radiology*. 2010; 256(1):280-289.
- (2) Tashkin D, Kesten S. Long-term Treatment Benefits With Tiotropium in COPD Patients With and Without Short-term Bronchodilator Responses\*. *Chest*. 2003; 123(5):1441-1449.
- (3) Sterman DH, Mehta AC, Wood DE et al. A Multicenter Pilot Study of a Bronchial Valve for the Treatment of Severe Emphysema. *Respiration*. 2010; 79(3):222-233.
- (4) Berger RL, Decamp MM, Criner GJ et al. Lung volume reduction therapies for advanced emphysema: an update. *Chest*. 2010; 138(2):407-417.
- (5) Mathew L, Evans A, Ouriadov A et al. Hyperpolarized (3)He magnetic resonance imaging of chronic obstructive pulmonary disease reproducibility at 3.0 tesla. *Acad Radiol*. 2008; 15(10):1298-1311.
- (6) Mathew L, Gaede S, Wheatley A et al. Detection of longitudinal lung structural and functional changes after diagnosis of radiation-induced lung injury using hyperpolarized 3He magnetic resonance imaging. *Med Phys*. 2010; 37(1):22-31.
- (7) Yim APC, Hwong TMT, Lee TW et al. Early results of endoscopic lung volume reduction for emphysema. *The Journal of Thoracic and Cardiovascular Surgery*. 2004; 127(6):1564-1573.
- (8) Wood DE, McKenna J, Yusef RD et al. A multicenter trial of an intrabronchial valve for treatment of severe emphysema. *The Journal of Thoracic and Cardiovascular Surgery*. 2007; 133(1):65-73.
- (9) Choong CK, Macklem PT, Pierce JA et al. Airway Bypass Improves the Mechanical Properties of Explanted Emphysematous Lungs. *Am J Respir Crit Care Med*. 2008; 178(9):902-905.
- (10) Broncus Reports Early EASE Trial Results for Airway Bypass With Exhale(R) Drug-Eluting Stents.  
<http://www.broncus.com/PDFS/Early%20EASE%20Trial%20results.pdf>.  
Accessed September 30, 2010
- (11) Diaz S, Casselbrant I, Piitulainen E et al. Validity of apparent diffusion coefficient hyperpolarized (3)He-MRI using MSCT and pulmonary function tests as references. *Eur J Radiol*. 2008.

- (12) Swift AJ, Wild JM, Fischele S et al. Emphysematous changes and normal variation in smokers and COPD patients using diffusion 3He MRI. *Eur J Radiol.* 2005; 54(3):352-358.

## Appendix – C: Permissions for Reproduction of Scientific Articles

### ELSEVIER LICENSE TERMS AND CONDITIONS

Dec 20, 2010

---



---

This is a License Agreement between Lindsay Mathew ("You") and Elsevier ("Elsevier") provided by Copyright Clearance Center ("CCC"). The license consists of your order details, the terms and conditions provided by Elsevier, and the payment terms and conditions.

**All payments must be made in full to CCC. For payment instructions, please see information listed at the bottom of this form.**

Supplier	Elsevier Limited The Boulevard, Langford Lane Kidlington, Oxford, OX5 1GB, UK
Registered Company Number	1982084
Customer name	Lindsay Mathew
Customer address	100 Perth Drive London, ON N6A5K8
License number	2554800163257
License date	Nov 23, 2010
Licensed content publisher	Elsevier
Licensed content publication	Academic Radiology
Licensed content title	Hyperpolarized <sup>3</sup> He Magnetic Resonance Imaging of Chronic Obstructive Pulmonary Disease: Reproducibility at 3.0 Tesla
Licensed content author	Lindsay Mathew, Andrea Evans, Alexei Ouriadov, Roya Etemad-Rezai, Robert Fogel, Giles Santyr, David G. McCormack, Grace Parraga
Licensed content date	October 2008
Licensed content volume number	15
Licensed content issue	10

number	
Number of pages	14
Start Page	1298
End Page	1311
Type of Use	reuse in a thesis/dissertation
Intended publisher of new work	other
Portion	full article
Format	both print and electronic
Are you the author of this Elsevier article?	Yes
Will you be translating?	No
Order reference number	
Title of your thesis/dissertation	Quantification of Pulmonary Ventilation using Hyperpolarized <sup>3</sup> He Magnetic Resonance Imaging
Expected completion date	Jan 2011
Estimated size (number of pages)	200
Elsevier VAT number	GB 494 6272 12
Permissions price	0.00 USD
Value added tax 0.0%	0.00 USD / GBP
Total	0.00 USD
Terms and Conditions	

**ELSEVIER LICENSE  
TERMS AND CONDITIONS**

Dec 20, 2010

This is a License Agreement between Lindsay Mathew ("You") and Elsevier ("Elsevier") provided by Copyright Clearance Center ("CCC"). The license consists of your order details, the terms and conditions provided by Elsevier, and the payment terms and conditions.

**All payments must be made in full to CCC. For payment instructions, please see information listed at the bottom of this form.**

Supplier	Elsevier Limited The Boulevard, Langford Lane Kidlington, Oxford, OX5 1GB, UK
Registered Company Number	1982084
Customer name	Lindsay Mathew
Customer address	100 Perth Drive London, ON N6A5K8
License number	2554800239319
License date	Nov 23, 2010
Licensed content publisher	Elsevier
Licensed content publication	Academic Radiology
Licensed content title	Hyperpolarized <sup>3</sup> He Magnetic Resonance Imaging of Ventilation Defects in Healthy Elderly Volunteers: Initial Findings at 3.0 Tesla
Licensed content author	Grace Parraga, Lindsay Mathew, Roya Etemad-Rezai, David G. McCormack, Giles E. Santyr
Licensed content date	June 2008
Licensed content volume number	15
Licensed content issue number	6
Number of pages	10
Start Page	776



End Page	785
Type of Use	reuse in a thesis/dissertation
Intended publisher of new work	other
Portion	full article
Format	both print and electronic
Are you the author of this Elsevier article?	Yes
Will you be translating?	No
Order reference number	
Title of your thesis/dissertation	Quantification of Pulmonary Ventilation using Hyperpolarized 3He Magnetic Resonance Imaging
Expected completion date	Jan 2011
Estimated size (number of pages)	200
Elsevier VAT number	GB 494 6272 12
Permissions price	0.00 USD
Value added tax 0.0%	0.00 USD / GBP
Total	0.00 USD
Terms and Conditions	

## ELSEVIER LICENSE TERMS AND CONDITIONS

Dec 20, 2010

---

This is a License Agreement between Lindsay Mathew ("You") and Elsevier ("Elsevier") provided by Copyright Clearance Center ("CCC"). The license consists of your order details, the terms and conditions provided by Elsevier, and the payment terms and conditions.

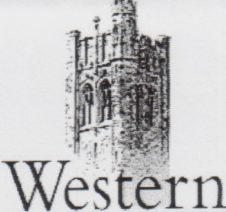
**All payments must be made in full to CCC. For payment instructions, please see information listed at the bottom of this form.**

Supplier	Elsevier Limited The Boulevard, Langford Lane Kidlington, Oxford, OX5 1GB, UK
Registered Company Number	1982084
Customer name	Lindsay Mathew
Customer address	100 Perth Drive London, ON N6A5K8
License number	2554800284475
License date	Nov 23, 2010
Licensed content publisher	Elsevier
Licensed content publication	European Journal of Radiology
Licensed content title	Hyperpolarized <sup>3</sup> He magnetic resonance imaging: Preliminary evaluation of phenotyping potential in chronic obstructive pulmonary disease
Licensed content author	Lindsay Mathew, Miranda Kirby, Roya Etemad-Rezai, Andrew Wheatley, David G. McCormack, Grace Parraga
Licensed content date	22 November 2009
Licensed content volume number	n/a
Licensed content issue number	n/a
Number of pages	1
Start Page	

End Page	
Type of Use	reuse in a thesis/dissertation
Portion	full article
Format	both print and electronic
Are you the author of this Elsevier article?	Yes
Will you be translating?	No
Order reference number	
Title of your thesis/dissertation	Quantification of Pulmonary Ventilation using Hyperpolarized 3He Magnetic Resonance Imaging
Expected completion date	Jan 2011
Estimated size (number of pages)	200
Elsevier VAT number	GB 494 6272 12
Permissions price	0.00 USD
Value added tax 0.0%	0.00 USD / GBP
Total	0.00 USD
Terms and Conditions	

# Appendix – D: Health Science Research Ethics Board Approval Notices

K030008



**Office of Research Ethics**

The University of Western Ontario  
 Room 00045 Dental Sciences Building, London, ON, Canada N6A 5C1  
 Telephone: (519) 661-3036 Fax: (519) 850-2466 Email: ethics@uwo.ca  
 Website: www.uwo.ca/research/ethics

---

**Use of Human Subjects - Ethics Approval Notice**

---

**Principal Investigator:** Dr. G. Parraga

**Review Number:** 13534

**Review Date:** August 14, 2007

**Review Level:** Full Board

**Protocol Title:** Assessment of Radiation-Induced Pneumonitis in Breast and Lung Cancer Patients

**Department and Institution:** Diagnostic Radiology & Nuclear Medicine, Robarts Research Institute

**Sponsor:**

**Ethics Approval Date:** September 19, 2007

**Expiry Date:** December 31, 2010

**Documents Reviewed and Approved:** UWO Protocol, Letter of Information and Consent dated September 7, 2007,

**Documents Received for Information:** Protocol, 30 July 2007; IB, ed 6, 09 Sept 2005

---

This is to notify you that The University of Western Ontario Research Ethics Board for Health Sciences Research Involving Human Subjects (HSREB) which is organized and operates according to the Tri-Council Policy Statement: Ethical Conduct of Research Involving Humans and the Health Canada/ICH Good Clinical Practice Practices: Consolidated Guidelines; and the applicable laws and regulations of Ontario has reviewed and granted approval to the above referenced study on the approval date noted above. The membership of this REB also complies with the membership requirements for REB's as defined in Division 5 of the Food and Drug Regulations.

The ethics approval for this study shall remain valid until the expiry date noted above assuming timely and acceptable responses to the HSREB's periodic requests for surveillance and monitoring information. If you require an updated approval notice prior to that time you must request it using the UWO Updated Approval Request Form.

During the course of the research, no deviations from, or changes to, the protocol or consent form may be initiated without prior written approval from the HSREB except when necessary to eliminate immediate hazards to the subject or when the change(s) involve only logistical or administrative aspects of the study (e.g. change of monitor, telephone number). Expedited review of minor change(s) in ongoing studies will be considered. Subjects must receive a copy of the signed information/consent documentation.

Investigators must promptly also report to the HSREB:

- a) changes increasing the risk to the participant(s) and/or affecting significantly the conduct of the study;
- b) all adverse and unexpected experiences or events that are both serious and unexpected;
- c) new information that may adversely affect the safety of the subjects or the conduct of the study.

If these changes/adverse events require a change to the information/consent documentation, and/or recruitment advertisement, the newly revised information/consent documentation, and/or advertisement, must be submitted to this office for approval.

Members of the HSREB who are named as investigators in research studies, or declare a conflict of interest, do not participate in discussion related to, nor vote on, such studies when they are presented to the HSREB.

Chair of HSREB: Dr. John W. McDonald

---

Ethics Officer to Contact for Further Information		
<input checked="" type="checkbox"/> Jennifer McEwen (jmcewen4@uwo.ca)	<input type="checkbox"/> Denise Grafton (dgrafton@uwo.ca)	<input type="checkbox"/> Grace Kelly (gkelly2@uwo.ca)

*This is an official document. Please retain the original in your files.*

cc: ORE File  
LHRI

Rob 0016



**Office of Research Ethics**

The University of Western Ontario  
 Room 4180 Support Services Building, London, ON, Canada N6A 5C1  
 Telephone: (519) 661-3036 Fax: (519) 850-2466 Email: ethics@uwo.ca  
 Website: www.uwo.ca/research/ethics

**Use of Human Subjects - Ethics Approval Notice**

**Principal Investigator:** Dr. G. Parraga

**Review Number:** 15929

**Review Level:** Full Board

**Review Date:** February 10, 2009

**Protocol Title:** Predictors of Radiation Induced Lung Injury using 3He Magnetic Resonance Imaging

**Department and Institution:** Imaging, Roberts Research Institute

INTERNAL RESEARCH FUNDING PROGRAM

HSREB's periodic requests for surveillance and monitoring information. If you require an updated approval notice prior to that time you must request it using the UWO Updated Approval Request Form.

During the course of the research, no deviations from, or changes to, the protocol or consent form may be initiated without prior written approval from the HSREB except when necessary to eliminate immediate hazards to the subject or when the change(s) involve only logistical or administrative aspects of the study (e.g. change of monitor, telephone number). Expedited review of minor change(s) in ongoing studies will be considered. Subjects must receive a copy of the signed information/consent documentation.

Investigators must promptly also report to the HSREB:

- a) changes increasing the risk to the participant(s) and/or affecting significantly the conduct of the study;
- b) all adverse and unexpected experiences or events that are both serious and unexpected;
- c) new information that may adversely affect the safety of the subjects or the conduct of the study.

If these changes/adverse events require a change to the information/consent documentation, and/or recruitment advertisement, the newly revised information/consent documentation, and/or advertisement, must be submitted to this office for approval.

Members of the HSREB who are named as investigators in research studies, or declare a conflict of interest, do not participate in discussion related to, nor vote on, such studies when they are presented to the HSREB.

Chair of HSREB: Dr. Joseph Gilbert

**Ethics Officer to Contact for Further Information**

<input checked="" type="checkbox"/> Janice Sutherland (jsutherf@uwo.ca)	<input type="checkbox"/> Elizabeth Wambolt (ewambolt@uwo.ca)	<input type="checkbox"/> Grace Kelly (grace.kelly@uwo.ca)	<input type="checkbox"/> Denise Grafton (dgrafton@uwo.ca)
--	---	--	--

*This is an official document. Please retain the original in your files.*

cc: ORE File  
LHRI

Curriculum Vitae  
**Lindsay Mathew BMSc.**

---

**EDUCATION and TRAINING**

- PhD.** Defense date March 11, 2011. University of Western Ontario (UWO), Department of Medical Biophysics  
*Thesis:* 'Quantification of Pulmonary Ventilation using Hyperpolarized  $^3\text{He}$  Magnetic Resonance Imaging'  
*Supervisor:* Dr. Grace Parraga
- BMSc.** 2003-2007. University of Western Ontario, Honors Medical Biophysics

**RESEARCH EXPERIENCE**

- 2007 **Summer Research Student**, Robarts Research Institute  
*Supervisor:* Dr. Grace Parraga  
*Project:* 'Reproducibility of Ventilation Defect Volume in a population with Chronic Obstructive Pulmonary Disease and Healthy Volunteers'  
  - Evaluated the reproducibility of ventilation defect volume for its potential use as a novel phenotype in the assessment of COPD
  - Investigated the effects of age on ventilation defect volume in a cohort of healthy volunteers
- 2006-2007 **4<sup>th</sup> Year Thesis Student**, Department of Medical Biophysics  
*Supervisor:* Dr. Grace Parraga, Robarts Research Institute  
*Thesis:* 'Ventilation Volumes of Chronic Obstructive Pulmonary Disease Patients Using  $^3\text{He}$ '  
  - Assessed percent ventilated volume through analysis of MR images for disease and healthy volunteer subject groups
  - Analyzed results of percent ventilation volume as a biomarker compared to the gold standard (pulmonary function tests)
- 2006 **Summer Research Student**, Robarts Research Institute  
*Supervisor:* Dr. Grace Parraga  
*Project:* '3D Histology and MRI of Phantom Elastase and Wildtype Mouse Lung'  
  - Prepared, Sectioned and Digitized elastase and wildtype mouse lungs for reconstruction
- 2006 **3<sup>rd</sup> Year Research Project**, Department of Medical Biophysics  
*Supervisor:* Dr. Neil Gelman, Lawson Health Research Institute  
*Project:* 'Testing Parameters for Detecting Hypoxic Ischemic Encephalopathy in Neonates'  
  - Performed regional analysis of apparent diffusion coefficient in neonates having suffered hypoxic ischemic injury at birth

## PUBLICATIONS and PRESENTATIONS

### Scientific Papers (6 published, 2 submitted, 2 in preparation)

#### Published Refereed Papers

1. **L. Mathew**, A. Evans, A. Ouriadov, R. Etemad-Rezai, R. Fogel, G. Santyr, D.G. McCormack, G. Parraga. "Hyperpolarized  $^3\text{He}$  Magnetic Resonance Imaging of Chronic Obstructive Pulmonary Disease at 3.0 Tesla: Reproducibility at 3.0 Tesla" *Acad Radiol.* 2008 Oct;15(10):1298-311
2. G. Parraga, **L. Mathew**, R. Etemad-Rezai, D.G. McCormack, G. Santyr. "Hyperpolarized  $^3\text{He}$  Magnetic Resonance Imaging Ventilation Defects in Healthy Elderly Volunteers: Initial Findings at 3.0 Tesla" *Acad Radiol.* 2008 Jun;15(6):776-85
3. **L. Mathew**, A. Wheatley, DG McCormack, G. Parraga. "Hyperpolarized  $^3\text{He}$  Magnetic Resonance Pulmonary Imaging: Image Processing Tools for Clinical Research" *Conference record on the Forty-second Asilomar Conference Signals, Systems and Computers, 2008.*
4. **L. Mathew**, S. Gaede, A. Wheatley, R. Etemad-Rezai, G.B. Rodrigues G. Parraga "Detection of Longitudinal Lung Structural and Functional Changes after Diagnosis of Radiation-induced lung injury using Hyperpolarized  $^3\text{He}$  Magnetic Resonance Imaging" *Med Phys.* 2010 Jan;37(1):22-31
5. **L. Mathew**, M Kirby, A. Wheatley, DG McCormack, G. Parraga. "Hyperpolarized  $^3\text{He}$  Magnetic Resonance Imaging: Preliminary Evaluation of Phenotyping Potential in Chronic Obstructive Pulmonary Disease" *Eur J Radiol.* 2009 Nov 20. [Epub ahead of print]
6. M. Kirby, **L. Mathew**, A. Wheatley, GE Santyr, DG McCormack, G. Parraga "Longitudinal Hyperpolarized  $^3\text{He}$  Magnetic Resonance Imaging of Chronic Obstructive Pulmonary Disease" *Radiology.* 2010 Jul;256(1):280-9

#### Submitted Manuscripts

7. **L. Mathew**, M. Kirby, D. Farquhar, C. Licskai, R. Etemad-Rezai, DG McCormack, G. Parraga "Hyperpolarized  $^3\text{He}$  Magnetic Resonance Imaging Biomarkers of Bronchoscopic Airway Bypass in COPD" *Submitted to J Magn Reson Imaging, November 2010, submission # JMRI-11-0085*
8. M. Kirby, **L. Mathew**, R. Etemad-Rezai, D.G. McCormack, G. Parraga. "Evaluating Bronchodilator Effects in Chronic Obstructive Pulmonary Disease using Hyperpolarized Helium-3 Magnetic Resonance Imaging" *Submitted to Radiology, February 2011, submission # RAD-11-0403*

#### Papers in Preparation

9. **L. Mathew**, R Castillo, E. Castillo, M. Kirby, B. Yaremko, R. Etemad-Rezai, GB Rodrigues, T. Guerrero, G. Parraga "Lung Ventilation Imaging for use in Radiation Treatment Planning: A comparison of  $^3\text{He}$  Magnetic Resonance Imaging and 4-dimensional Computed Tomography" *In preparation for submission to Int J Radiat Oncol Biol Phys*
10. **L. Mathew**, R. Etemad-Rezai, A. Wheatley, B Yaremko, GB Rodrigues, G. Parraga "Novel *In vivo* Imaging Predictors of Radiation Induced Lung Injury: Measuring Airway Function and Tissue Destruction in Lung Cancer Patients before Radiation Treatment" *In preparation for submission to Int J Radiat Oncol Biol Phys*

**Published Refereed Abstracts (12)**

1. **L. Mathew**, G Rodrigues, R Etemad-Rezai, DG. McCormack, G Parraga Detecting Regional Differences In Hyperpolarized Helium-3 Magnetic Resonance Imaging Measurements In Lung Cancer Prior To Radiation Treatment *Am. J. Respir. Crit. Care Med. Suppl. 2010 May;181: A3659*
2. **L. Mathew**, M. Kirby, R. Etemad-Rezai, D.G. McCormack, and G Parraga Characterization Of Hyperpolarized Helium-3 Magnetic Resonance Imaging Phenotype Dominant COPD *Am. J. Respir. Crit. Care Med. Suppl. 2010 May;181: A1562.*
3. **L. Mathew**, S. Gaede, A. Wheatley, R. Etemad-Rezai, G.B. Rodrigues, G. Parraga. "Detection of Lung Remodeling following Radiation Therapy using Hyperpolarized <sup>3</sup>He Magnetic Resonance Imaging", *Interactions: Canadian Medical Physics Newsletter Volume 56, Issue 3 (July 2010), pp. 77-79.*
4. M Kirby, **L. Mathew**, A Wheatley, DG McCormack and G Parraga. "Longitudinal Hyperpolarized <sup>3</sup>He Magnetic Resonance Imaging of Chronic Obstructive Pulmonary Disease", *Interactions: Canadian Medical Physics Newsletter Volume 56, Issue 1 (January 2010), pp. 13-22.*
5. **L. Mathew**, S. Gaede, R. Etemad-Rezai, et al. "Detection of Longitudinal Structural and Functional Changes after Diagnosis of Radiation Induced Lung Injury using Hyperpolarized <sup>3</sup>He Magnetic Resonance Imaging", *Am. J. Respir. Crit. Care Med. Suppl. 2009 Apr;179: A3549.*
6. M Kirby, **L. Mathew**, A Wheatley, DG McCormack and G Parraga. "Longitudinal Hyperpolarized Helium-3 Magnetic Resonance Imaging of Chronic Obstructive Pulmonary Disease: Two year Follow-up Evaluation", *Am. J. Respir. Crit. Care Med. Suppl. 2009 Apr;179: A6203.*
7. **L. Mathew**, DG McCormack, G. Santyr, G. Parraga, "Discriminating between Airways Disease and Emphysema in Severe COPD Using Hyperpolarized <sup>3</sup>He Magnetic Resonance Imaging", *Int J Comput Assist Radiol Surg Suppl. 2008 June;3(1):S357*
8. **L. Mathew**, G.B. Rodrigues, R. Etemad-Rezai, G. Santyr, DG. McCormack, G. Parraga, "Hyperpolarized <sup>3</sup>He Magnetic Resonance Imaging of Radiation Pneumonitis and Fibrosis and Comparison with Computed Tomography and Pulmonary Function Measurements: Initial Findings", *Am. J. Respir. Crit. Care Med Suppl. 2008 Apr;177:A758*
9. **L. Mathew**, G. Parraga, DG McCormack, G. Santyr, "Hyperpolarized <sup>3</sup>He Magnetic Resonance Imaging Detection of Airway Disease and Emphysema in Severe COPD". *Am. J. Respir. Crit. Care Med Suppl. 2008 Apr;177:A564*
10. **L. Mathew**, A. Wheatley, GE Santyr, NA Paterson, G. Parraga. "Hyperpolarized <sup>3</sup>He Magnetic Resonance Imaging of Cystic Fibrosis: Initial Findings in Adults with Moderate and Good Lung Function and Comparison to Spirometry". *Proc. Intl. Soc. Mag. Reson. Med. 2008;16:2672.*
11. A. Wheatley, S. McKay, **L. Mathew**, G. Santyr, D.G. McCormack and G. Parraga. "Hyperpolarized Helium-3 Magnetic Resonance Imaging of Asthma: Short-term Reproducibility". *Proc. SPIE. 2008 Mar;6916(1):69161X*
12. **L. Mathew**, J. McCallum, S. McKay, G. Santyr, R. Etemad-Rezai, D. McCormack, G. Parraga, "Hyperpolarized <sup>3</sup>He Magnetic Resonance Imaging of Ventilation Volume and Ventilation Defect Volume Variability in COPD", *Proc. Intl. Soc. Mag. Reson. Med. 2007;15:1304*



### Invited Peer-Reviewed Talks (7)

1. **L. Mathew**, S. Gaede, A. Wheatley, R. Etemad-Rezai, G.B. Rodrigues, G. Parraga. "Detection of Lung Remodeling following Radiation Therapy using Hyperpolarized  $^3\text{He}$  Magnetic Resonance Imaging", Canadian Organization of Medical Physics Annual Conference. Victoria, Canada (07/2009)
2. M Kirby, **L. Mathew**, A Wheatley, DG McCormack and G Parraga. Longitudinal Hyperpolarized  $^3\text{He}$  Magnetic Resonance Imaging of Chronic Obstructive Pulmonary Disease, The Canadian Organization of Medical Physicists, Victoria, British Columbia, Canada (07/09)
3. **L. Mathew**, DG McCormack, G. Parraga, "Hyperpolarized  $^3\text{He}$  Magnetic Resonance Imaging: Tools for Longitudinal, In vivo analysis of Lung Diseases", Asilomar Conference on Signals, Systems and Computers, Monterey Bay, USA (08/2008)
4. A. Rozik, U. Adladi, **L. Mathew**, J. McCallum, D. Slipetz, A. Fenster and G. Parraga. Three-dimensional Histology for the Evaluation of Elastase-induced emphysema in Mice. The Future of Quantitative and Functional Lung Imaging, Iowa Comprehensive Lung Imaging Center, Coralville, USA (08/2008)
5. **L. Mathew**, G. Parraga, DG McCormack, G. Santyr, "Hyperpolarized  $^3\text{He}$  Magnetic Resonance Imaging Detection of Airway Disease and Emphysema in Severe COPD". American Thoracic Society, Toronto, Canada, (05/2008).
6. G. Parraga, **L. Mathew**, A. Evans, R. Etemad-Rezai, D. McCormack, G. Santyr. "Hyperpolarized  $^3\text{He}$  Magnetic Resonance Imaging of Chronic Obstructive Pulmonary Disease: Same-day and 7-day Reproducibility of Apparent Diffusion Coefficients, Ventilation Defect volume and Ventilation Volumes" Radiological Society of North America, Chicago, USA, (11/2007).
7. G.B. Rodrigues, **L. Mathew**, G. Parraga. B. Yaremko. Hyperpolarized Helium-3 Magnetic Resonance Imaging for the Prediction, Reduction, and Assessment of Radiation-Induced Lung Injury. Canadian Organization of Medical Physicists, Toronto, Canada, (10/2007).

### Invited Oral Presentations (1)

8. **L. Mathew**, G. Rodrigues, G. Parraga. "Hyperpolarized  $^3\text{He}$  MRI of Radiation-induced Lung Injury" Department of Oncology Grand Rounds, London Regional Cancer Program, London, Canada, (01/2010)

### Poster Presentations (27)

1. **L. Mathew**, G. Rodrigues, R. Etemad-Rezai, D.G. McCormack, G. Parraga. "Detecting Regional Differences in Hyperpolarized  $^3\text{He}$  Magnetic Resonance Imaging Measurements in Subjects with Lung Cancer Prior to Radiation Therapy" Oncology Research and Education Day. London, Canada (06/2010)
2. **L. Mathew**, G. Rodrigues, R. Etemad-Rezai, D.G. McCormack, G. Parraga. "Detecting Regional Differences in Hyperpolarized  $^3\text{He}$  Magnetic Resonance Imaging Measurements in Subjects with Lung Cancer Prior to Radiation Therapy", London Imaging Discovery Day. London, Canada (06/2009)
3. **L. Mathew**, M. Kirby, R. Etemad-Rezai, DG. McCormack, G. Parraga. "Characterization of Hyperpolarized  $^3\text{He}$  Magnetic Resonance Imaging Phenotype Dominant COPD" American Thoracic Society. New Orleans, USA (05/2010)
4. **L. Mathew**, G. Rodrigues, R. Etemad-Rezai, D.G. McCormack, G. Parraga. "Detecting Regional Differences in Hyperpolarized  $^3\text{He}$  Magnetic Resonance Imaging Measurements in Subjects with Lung Cancer Prior to Radiation Therapy", American Thoracic Society. New Orleans, USA (05/2010)

5. **L. Mathew**, U. Aladl, A. Fenster, G. Parraga. "Hyperpolarized  $^3\text{He}$  Magnetic Resonance Imaging Tools for Longitudinal and Multi-Modality Studies", International Society for Magnetic Resonance in Medicine, Stockholm, Sweden (05/2010)
6. M Kirby, **L. Mathew**, A Wheatley, DG McCormack and G Parraga. "Inter-Observer Reproducibility of Longitudinal Hyperpolarized Helium-3 Magnetic Resonance Imaging of Chronic Obstructive Pulmonary Disease" International Society for Magnetic Resonance in Medicine, Stockholm, Sweden (05/2010)
7. **L. Mathew**, G. Rodrigues, R. Etemad-Rezai, D.G. McCormack, G. Parraga. "Regional Differences in Hyperpolarized  $^3\text{He}$  Magnetic Resonance Imaging Measurements in Subjects with Lung Cancer Prior to Radiation Therapy", Margaret Moffat Research Day. London, Canada (03/2010)
8. M Kirby, **L. Mathew**, A Wheatley, DG McCormack and G Parraga. "Inter-Observer Reproducibility of Longitudinal Hyperpolarized Helium-3 Magnetic Resonance Imaging of Chronic Obstructive Pulmonary Disease" Margaret Moffat Research Day, London, Ontario, Canada (03/2010)
9. **L. Mathew**, G. Rodrigues, R. Etemad-Rezai, D.G. McCormack, G. Parraga. "Regional Differences in Hyperpolarized  $^3\text{He}$  Magnetic Resonance Imaging Measurements in Subjects with Lung Cancer Prior to Radiation Therapy", Lawson Research Day, London, Canada, (03/2010)
10. **L. Mathew**, S. Gaede, R. Etemad-Rezai, G. Rodrigues, G. Parraga. "Detection of Lung Remodelling following Radiation Therapy using Hyperpolarized  $^3\text{He}$  Magnetic Resonance Imaging" London Imaging Discovery Day. London, Canada (06/2009)
11. **L. Mathew**, G. Rodrigues, R. Etemad-Rezai, G. Parraga. "Longitudinal Evaluation of Radiation Induced Lung Injury using Hyperpolarized  $^3\text{He}$  Magnetic Resonance Imaging" Oncology Research and Education Day. London, Canada (06/2009)
12. **L. Mathew**, S. Gaede, R. Etemad-Rezai, G. Rodrigues, G. Parraga. "Detection of Lung Remodelling following Radiation Therapy using Hyperpolarized  $^3\text{He}$  Magnetic Resonance Imaging" American Thoracic Society International Conference. San Diego, USA (05/2009)
13. **L. Mathew**, M. Kirby, H. Ahmed, A. Wheatley, C. Licskai, N. Paterson, DG McCormack, G. Parraga. "Quantification of Pulmonary Ventilation Heterogeneity in Sickness and Health: Generation of Hyperpolarized  $^3\text{He}$  Magnetic Resonance Imaging Ventilation Gradient Vector Maps" Canadian Respiratory Conference. Toronto, Canada (04/2009)
14. **L. Mathew**, G. Rodrigues, R. Etemad-Rezai, G. Parraga. "Longitudinal Evaluation of Radiation Induced Lung Injury using Hyperpolarized  $^3\text{He}$  Magnetic Resonance Imaging" Margaret Moffat Research Day. London, Canada (03/2009)
15. M. Kirby, **L. Mathew**, A. Wheatley, DG. McCormack, G. Parraga. "Chronic Obstructive Pulmonary Disease Progression Detected by Hyperpolarized Helium-3 Magnetic Resonance Imaging" Margaret Moffat Research Day. London, Canada (03/2009)
16. **L. Mathew**, DG McCormack, G. Parraga, "The Future of Hyperpolarized  $^3\text{He}$  MRI: Image Processing Requirements for Longitudinal Studies", Future of Quantitative and Functional Lung Imaging, Coralville, USA (08/2008).
17. **L. Mathew**, DG McCormack, G. Santyr, G. Parraga, "Discriminating between Airways Disease and Emphysema in Severe COPD Using Hyperpolarized  $^3\text{He}$  Magnetic Resonance Imaging", Computer Assisted Radiology and Surgery, Barcelona, Spain. (06/2008).
18. **L. Mathew**, G. Rodrigues, R. Etemad-Rezai, G. Santyr, DG. McCormack, G. Parraga, "Hyperpolarized  $^3\text{He}$  Magnetic Resonance Imaging of Radiation Pneumonitis and Fibrosis and Comparison with Computed Tomography and Pulmonary Function Measurements: Initial Findings", American Thoracic Society, Toronto, Canada, (05/2008).

19. **L. Mathew**, A. Wheatley, GE Santyr, NA Paterson, G. Parraga. "Hyperpolarized  $^3\text{He}$  Magnetic Resonance Imaging of Cystic Fibrosis: Initial Findings in Adults with Moderate and Good Lung Function and Comparison to Spirometry". International Society of Magnetic Resonance in Medicine, Toronto, Canada, (05/2008).
20. R. Etemad-Rezai, Y. Hosein, **L. Mathew**, DG McCormack, N. Paterson, G. Parraga. "Hyperpolarized  $^3\text{He}$  Magnetic Resonance Imaging of Adult Cystic Fibrosis and Asthma: Reproducibility of Ventilation Defects, Ventilation Volume and Pulmonary Function Measurements". Canadian Association of Radiologists, Ottawa, Canada, (05/2008).
21. **L. Mathew**, G. Rodrigues, G. Parraga, "Hyperpolarized  $^3\text{He}$  Magnetic Resonance Imaging of Radiation Pneumonitis: Initial Findings at 3.0 Tesla", Ontario Thoracic Cancer Conference, Niagara-on-the-Lake, Canada, (03/2008).
22. **L. Mathew**, G. Rodrigues, R. Etemad-Rezai, G. Parraga, "Hyperpolarized  $^3\text{He}$  Magnetic Resonance Imaging of Radiation Pneumonitis: Initial Findings at 3.0 Tesla", Robarts Research Day, London, Canada, (03/2008).
23. **L. Mathew**, G. Rodrigues, R. Etemad-Rezai, G. Parraga, "Hyperpolarized  $^3\text{He}$  Magnetic Resonance Imaging of Radiation Pneumonitis: Initial Findings at 3.0 Tesla", Lawson Research Day, London, Canada, (03/2008).
24. **L. Mathew**, G. Rodrigues, R. Etemad-Rezai, G. Parraga, "Hyperpolarized  $^3\text{He}$  Magnetic Resonance Imaging of Radiation Pneumonitis". Margaret Moffat Research Day, London, Canada, (03/2008)
25. A. Wheatley, S. McKay, **L. Mathew**, G. Santyr, D.G. McCormack and G. Parraga. Hyperpolarized Helium-3 Magnetic Resonance Imaging of Asthma: Short-term Reproducibility. Society for Photonics and Instrumentation Engineers (SPIE): Medical Imaging, San Diego, California (02/2008)
26. R. Etemad-Rezai, **L. Mathew**, A. Evans, S. McKay, D. McCormack, A. Ouriadov, G. Santyr, G. Parraga. "Hyperpolarized  $^3\text{He}$  Magnetic Resonance Imaging: New Radiological Biomarkers of Chronic Obstructive Pulmonary Disease" Canadian Association of Radiologists, St. John's, Canada, (06/2007)
27. **L. Mathew**, J. McCallum, S. McKay, G. Santyr, R. Etemad-Rezai, D. McCormack, G. Parraga, "Hyperpolarized  $^3\text{He}$  Magnetic Resonance Imaging of Ventilation Volume and Ventilation Defect Volume Variability in COPD", International Society for Magnetic Resonance in Medicine, Berlin, Germany, (05/2007)

## GRANTS

1. **L. Mathew**, GB Rodrigues, G Parraga “Novel *In vivo* Imaging Predictors of Radiation Induced Lung Injury: Measuring Airway Function and Tissue Destruction in Lung Cancer Patients before Radiation Treatment”, London Regional Cancer Program Small Grants for Cancer Research and Training. January 2009. **\$25,000**

## SCHOLARSHIPS and AWARDS

- |      |   |
|------|---|
| 2010 | Vanier Canadian Graduate Scholarship <b>\$50,000/year</b> (National) <ul style="list-style-type: none"> <li>▪ PhD research, stipend support for <b>3 years</b></li> </ul>   |
| 2010 | Ontario Graduate Scholarship <b>\$15,000</b> (Provincial) <i>declined</i>   |
| 2010 | CIHR- Strategic Training Program in Cancer Research and Technology Transfer <b>\$26,700/year</b> (Institutional, UWO) <i>declined</i> <ul style="list-style-type: none"> <li>▪ PhD research, stipend support for 2 years (year 2 of 2)</li> </ul>   |
| 2009 | JR Cunningham Young Investigator Award <b>\$200</b> (National) <ul style="list-style-type: none"> <li>▪ 3<sup>rd</sup> place talk at Young Investigator Symposium, Canadian Organization of Medical Physicists</li> </ul>   |
| 2009 | CIHR- Strategic Training Program in Cancer Research and Technology Transfer <b>\$26,700/year</b> (Institutional, UWO) <ul style="list-style-type: none"> <li>▪ PhD research, stipend support for 2 years (year 1 of 2)</li> </ul>   |
| 2009 | London Imaging Discovery Day <b>\$150</b> (Institutional, UWO) <ul style="list-style-type: none"> <li>▪ Second place for scientific poster: “Detection of Lung Remodelling following Radiation Therapy using Hyperpolarized <sup>3</sup>He Magnetic Resonance Imaging”</li> </ul>                   |
| 2009 | JR Cunningham Young Investigator Finalist <b>\$175</b> (National) <ul style="list-style-type: none"> <li>▪ Canadian Organization of Medical Physics Annual Conference Top 10 Finalist 2009</li> </ul>   |
| 2009 | Ontario Graduate Scholarship <b>\$15,000</b> (Provincial) <ul style="list-style-type: none"> <li>▪ Doctoral level research, stipend support</li> </ul>  |
| 2009 | Schulich Graduate Scholarship, <b>\$6,484</b> (Institutional, UWO) <ul style="list-style-type: none"> <li>▪ For over 80% cumulative average in graduated and undergraduate studies</li> </ul>   |
| 2009 | Margaret Moffat Research Day Award, <b>\$500</b> (Institutional, UWO) <ul style="list-style-type: none"> <li>▪ Awarded for top poster presentation in Imaging: “Longitudinal Evaluation of Radiation Induced Lung Injury using Hyperpolarized <sup>3</sup>He Magnetic Resonance Imaging”</li> </ul> |
| 2008 | Ontario Graduate Scholarship in Science and Technology, <b>\$15,000</b> (Provincial) <ul style="list-style-type: none"> <li>▪ Masters level research, stipend support</li> </ul>  |
| 2008 | Schulich Graduate Scholarship, <b>\$6,484</b> (Institutional, UWO) <ul style="list-style-type: none"> <li>▪ For over 80% cumulative average in graduated and undergraduate studies</li> </ul>   |

- 2008 Margaret Moffat Research Day Award, **\$500** (Institutional, UWO)
- Awarded for top poster presentation in Imaging: “Hyperpolarized  $^3\text{He}$  Magnetic Resonance Imaging of Radiation Pneumonitis”
- 2007 CIHR- Strategic Training Program in Cancer Research & Technology Transfer, **\$24,100** (Institutional, UWO)
- Masters level research project support
- 2007 Graduate Thesis Research Award, **\$1,327** (Institutional, UWO)
- Awarded for travel to scientific meetings
- 2007 Schulich Graduate Scholarship, **\$6,484** (Institutional, UWO)
- For over 80% cumulative average in undergraduate studies
- 2003 UWO Entrance Scholarship, **\$2,000** (Institutional, UWO)
- For cumulative average over 80% in high school

### POST-GRADUATE EDUCATION DEVELOPMENT

- 2010 **Teaching Assistantship**, The Department of Medical Biophysics
- Organizing Seminar Course for all graduate students in department
  - Recruitment of potential graduate students: writing and distribution of department literature, speaking with students at recruitment fairs/lectures

### RELEVANT COURSE WORK

NMR Physics, MRI Physics, Imaging Principles, Scientific Communications, Research Ethics and Biostatistics, Biology of Human Cancer, Public and Private Partnerships in Cancer Research, Medical Imaging, Radiobiology and Radionuclides, Hemodynamics, Introduction to Biophysics, Biophysical Analysis, Human and Animal Biomechanics,

### PROFESSIONAL MEMBERSHIPS

1. Canadian Thoracic Society. **Student Member** (since September 2008)
2. American Association of Physicists in Medicine. **Student Member** (October 2008)
3. Canadian Organization of Physicists in Medicine **Student Member** (January 2009)

### LEADERSHIP and VOLUNTEER ACTIVITIES

- 2010 **Past-President**, Network of Imaging Students (NOISe)  
**Event Chair**, Great Ride ‘n’ Stride 2010, Canadian Cancer Society  
**Coach**, University of Western Ontario Synchronized Swimming Team
- 2009 **President**, Network of Imaging Students (NOISe)  
**Event Chair**, Great Ride ‘n’ Stride 2009, Canadian Cancer Society  
**Coach**, University of Western Ontario Synchronized Swimming Team  
**Research tour guide**, Doors Open London, Robarts Research Institute  
**Fundraiser**, Light the Night, Leukemia and Lymphoma Society
- 2008 **Invited Speaker**, Canadian Cancer Society’s Volunteer Leadership Conference

- Event Volunteer Coordinator**, Great Ride 'n' Stride 2008, Canadian Cancer Society  
**Coach**, University of Western Ontario Synchronized Swimming Team  
**Member**, Network of Imaging Students (NOISe)  
**Fundraiser**, Light the Night, Leukemia and Lymphoma Society
- 2007 **Team member**, University of Western Ontario Synchronized Swimming Team  
**Duet Member**, University of Western Ontario Synchronized Swimming Team  
**Recipient**, All Canadian Synchronized Swimmer Award (Academic Excellence)  
**Fundraiser**, Light the Night, Leukemia and Lymphoma Society  
**Member**, Biophysics and You Club
- 2006 **Team member**, University of Western Ontario Synchronized Swimming Team  
**Member**, Biophysics and You Club
- 2005 **Team member**, University of Western Ontario Synchronized Swimming Team  
**Member**, Biophysics and You Club
- 2004 **Team member**, University of Western Ontario Synchronized Swimming Team